Reconstructing the Pleistocene connectivity history of the Black Sea and the Caspian Sea using strontium isotopes

By

Diksha Bista

School of Geographical Sciences

University of Bristol

A thesis submitted to the University of Bristol in

accordance with the requirements of the degree of

Doctor of Philosophy

in the

Faculty of Sciences

September 2019

Word Count: 48,322

Abstract

Quantifying the timing and nature of the connection between two hydrographic systems is critical to understanding the impact of different drivers on basin hydrology. The evolution of the Black Sea and the Caspian Sea is driven by a complex combination of tectonics and climate, resulting in extreme water level fluctuations in these two basins and multiple connection and isolation events between each other and the open ocean throughout their geological history.

The Quaternary connectivity history between the Black Sea and the Caspian Sea has previously been reconstructed using palaeontological, phylogenetic and geochemical studies. However, these records are often contradictory, lack precision, are rarely continuous and are commonly qualitative. Strontium isotopic ratios ($^{87}Sr/^{86}Sr$), by contrast, can provide a direct and quantitative means of reconstructing the connectivity history between the two basins and the open ocean. The $^{87}Sr/^{86}Sr$ of non-marine systems is sensitive to changing water sources and is incorporated and preserved in the calcitic shells of aquatic organisms. The $^{87}Sr/^{86}Sr$ measured on well-preserved fossil carbonates can therefore be used to obtain past $^{87}Sr/^{86}Sr$ of the basin and, consequently, to identify possible water sources as the connectivity of the basin changes.

This study adds substantial new data to the very sparse Sr isotopic dataset that exists in the modern Black Sea, Caspian Sea and the rivers that drain into them. A numerical box model parameterized with these fluvial data is used to constrain the past hydrological budget of each basin and to reconstruct the inter-basin connectivity required to produce palaeo salinity estimates and the $^{87}Sr/^{86}Sr$ measured on fossil ostracods collected from sedimentological sections and deep sea cores across the Black and Caspian Sea region.

The new $^{87}Sr/^{86}Sr$ records show that the Caspian Sea, in addition to present-day fluvial sources, also received significant amount of water from the Amu Darya river throughout most of the Pleistocene. The Caspian Sea also sustained a connection with the Arctic ocean in the earliest part of the Pleistocene between 2.7 to ~2 Ma. The overlapping $^{87}Sr/^{86}Sr$ values of the coeval Black and Caspian seas during the early Pleistocene indicate that the two basins were connected during the time, via both one way flow from the Caspian Sea into the Black Sea, as well as a two way exchange between them. This Black- Caspian Sea connection was persistent until ~380 ka, after which Mediterranean input into the Black Sea began to dominate the $^{87}Sr/^{86}Sr$ signal of Black Sea water. Although, the Caspian Sea may have continued to flow into the Black Sea until ~150 ka, divergence of the Caspian Sea and the Black Sea $^{87}Sr/^{86}Sr$ record suggests progressive isolation of these basins from each other, while the Black Sea experienced increasing frequency of connection with the Mediterranean Sea.

The timing of connection between the Black and the Caspian seas throughout the Pleistocene and between Black and the Mediterranean seas prior to 500 ka appears to be unrelated to the glacial - interglacial cyclicity, suggesting that tectonics was the primary control on the basin connectivity. However, over the last 500 ka, the Black Sea connection to the Mediterranean Sea was mainly driven by eustatic sea level changes at the Bosporus and the Black Sea connection to the Caspian Sea was impacted by additional meltwater fuelled discharge, reflecting the glacial interglacial cycle. This new connectivity record of the Black Sea and the Caspian Sea to each other and the open ocean therefore provides new insight into the relative impact of climate and tectonics on the evolution of these basins.

Acknowledgements

In the course of this work I have become indebted to vast number of people who have made this journey possible. First and foremost, I owe a huge thank you to my supervisors Rachel Flecker and David Richards. Without your invaluable advice, guidance and constant support, I am not sure I would have made it through this PhD. I am particularly grateful for your patience and encouragement when I was feeling lost. Your contagious enthusiasm and your words of wisdom gave me the clarity and focus needed to reach the finish line. In addition to the academic expertise, I have learned so much more from you both, so thank you for everything.

I am deeply grateful to Dr. Chris Coath and Dr. Jamie Lewis for sharing their expertise on mass spectrometry and Sr chemistry, respectively, and to Dirk Simon for showing me the rope regarding box modelling. A huge thanks to Arjen Grothe, Sevi Modestou, and Vanessa Fairbank for providing the initial help and guidance regarding the column chemistry and answering all my (sometime nonsense) queries. Thanks to Bristol Isotope Group members for making the late nights in the lab bearable.

A special mention goes to all the PRIDE team members for the insightful scientific discussions, and their help along the way (and not to mention crazy ITNS). In particular, thanks to Dr. Frank Wesselingh for his dedication and enthusiasms for the project. I also owe special thanks to all the PRIDE ESRs. Thank you for the laughs, good times and your friendships during last 4 years. The training events and field trips would have been a lot less enjoyable experience without you there. Special thanks to the biologists, Manuel, Alberto, Matteo, and Arthur (Scotty) for taking my water samples in Azerbaijan, Ukraine and Russia, even though you hated doing it. Similarly, thanks to the geologists of the group, Sergei (Serjay), Liesbeth, for taking sediment samples for me when I could not be there in Azerbaijan. Thank you, Sabrina and Anouk for taking samples from the Caspian Sea. Tom and Justine for sharing your expertise (and for always being up for a drink), Sifan and Sri for teaching me more about modelling, Aleksandre (Aleko) for being there in Georgia 2016 to help us during the fieldtrip (but mostly for being himself). Last but not the least, thank you Lea for sharing your ostracod expertise, always being there at the other end of the line when I needed your help but finally, for all the encouraging texts and messages over the last few months. Your support has been a great help during this writing process.

Shout out to all my colleagues and friends in Bristol. Ali Marzocchi, I will be forever grateful to you for taking me under your wings when I first moved to Bristol (and to Utrecht). Special thanks to Louise Griffth for being an amazing flat mate, for listening rants and for being there with a hug when I was having a bad day. James Dunne, Amy Waterson, Gareth Griffith, Philip Pika, and Bea Gill Olivas, thank you for all the hugs, chats, laughs and generally keeping me sane these last four years. Thank you Mike Cooper, Tim Morris, Moya McDonald, Gwil Owen, Nina Zang, Helena Pryer, Markus Adloff , Hazel Vallack for your friendship. I am sure I have forgotten a lot of you but thanks to all the Browns crowd for making it a fun working place. Special thanks to Bea and Guillaume for proofreading some of my chapters.

I want to thank my family for their never ending love and support. To my mom, thank you for always trusting and believing in me. To my siblings, thank you for all the laughs over skype, for all your encouraging words, and for your listening ears when I needed one. And finally, special thanks to my dad, who thought I could achieve anything I wanted to and who taught me to believe in myself.

This research was funded by the PRIDE project, which received funding from the European Union's Horizon 2020 research and innovation programme under the Marie Sklodowska-Curie grant agreement No 642973.

Declaration of Authorship

I declare that the work in this dissertation was carried out in accordance with the requirements of the University's Regulations and Code of Practice for Research Degree Programmes and that it has not been submitted for any other academic award. Except where indicated by specific reference in the text, the work is the candidate's own work. Work done in collaboration with, or with the assistance of, others, is indicated as such. Any views expressed in the dissertation are those of the author.

Signed:

_____

Date:

_____

"*Well, I must endure the presence of a few caterpillars if I wish to become acquainted with the butterflies.*"

Antoine de Saint-Exupéry

- The Little Prince

Contents

List of Figures

List of Tables

List of Abbreviations

Abbreviation	Description
NAF	North Anatolian Fault
NAFZ	North Anatolian Fault Zone
MSC	Messinian Salinity Crisis
PLG	Primary Lower Gypsum
$^{87}Sr/^{86}Sr$	Strontium isotopic ratio
BS	Black Sea
CS	Caspian Sea
GC	Greater Caucasus
LG	Lesser Caucasus
NHG	Northern Hemisphere Glaciation
LGM	Last Glacial Maximum
GTS	Geological Time Scale
GPTS	Geomagnetic Polarity Time Scale
DSDP	Deep Sea Drilling Project
TIMS	Thermal Ionization Mass Spectrometry
KFTB	Kura Fold Thrust Belt

AJgloe (2018)

Chapter 1

Introduction

Section 1.5.3 of this introductory chapter is adapted from part of a published paper (Krijgsman et al., 2019), on which I am a co-author. My contribution to the paper was Section 4.4 "Geochemical proxies of inter-basinal connectivity". The version presented here differs from the published copy as, in addition to the Quaternary, it includes a review of the Miocene connectivity history of the region using Sr isotopic ratios.

Krijgsman W.,Tesakov A., Yanina T., Lazarev S., Danukalova G., Van Baak C., Agustí J., Alçiçek M., Aliyeva E., ***Bista D.****, Bruch A., Büyükmeriç Y., Bukhsianidze M., Flecker R., Frolov P., Hoyle T., Jorissen E., Kirscher U., Koriche S., Kroonenberg S., Lordkipanidze D., Oms O., Rausch L., Singarayer J., Stoica M., van de Velde S., Titov V., Wesselingh F., 2019,* ***Quaternary time scales for the Pontocaspian domain: Interbasinal connectivity and faunal evolution****, Earth-Science Reviews, 188 (1- 40).*

1.1 Thesis motivation

Marginal basins are large bodies of water along the edges of continents that have a restricted connection to the open ocean. Their close proximity to a continental landmass means that a significant portion of the water in these basins comes from fluvial run-off. As such, the hydrology of these basins is responsive both, to any changes in continental climatic conditions as well as tectonic changes that influence the fluvial discharge they receive. Because of their restricted communication with the global ocean, its buffering capacity is reduced. A marginal basin where

the ocean buffering is either reduced or lacking, a clear continental drainage signal is recorded and may, therefore provide a unique opportunity to study Earth history.

Marginal basins also provide a convenient platform on which to study biotic adaptability and ecosystem stability. The presence and distribution of organisms within a basin is governed by environmental parameters such as temperature, nutrients, oxygen and salt content, light availability (Chapin III et al., 2011; Mudie et al., 2017). Marginal basins often experience rapid and extreme changes in these parameters as a result of changing climatic and tectonic configuration (Krijgsman et al., 2019; van Baak et al., 2017). Consequently, organisms residing within the basins are often subjected to changing conditions and as such, usually develop wider environmental tolerance as they adapt to the new environmental conditions (Chapin III et al., 2011). The evolution of biota within these basins are rapid resulting in quick turnover events with new species colonizing the basin while some species become extinct (Kideys, 2002; Reid and Orlova, 2002; Selifonova, 2008). Therefore, biodiversity of marginal basins can provide key insights into biotic evolution and ecosystem functioning in a rapidly changing world like today.

The Black Sea, Caspian Sea, Sea of Azov and Aral Sea (Figure 1.1), collectively known as the Pontocaspian basin, are relict of the ancient Paratethys Sea. Although today, some of these are endorheic basins, all have been connected to the global ocean over the last few million years. Consequently, the Pontocaspian basin is considered to be the last remnant of a marginal basin system sandwiched between Eastern Europe and Western Asia. These basins contain rich sedimentary archives in which to study long-term climatic and tectonic variation as well as biodiversity fluctuations of the region.

1.1.1 Disentangling the climatic and tectonic signal

The catchment area of the Black and Caspian seas is ~5 times (Kosarev and Kostianoy, 2008) and ~10 times (Kosarev and Yablonskaya, 1994), respectively, larger than the basin itself (Figure 1.1). As such, climate or tectonic changes over the catchment area have discernable impacts on the fluvial discharge received by these basins and results in about two order of magnitude water-level fluctuations (Krijgsman et al., 2019 and references therein). In addition, the hydrology of these basins is also sensitive to the eustatic sea level variation and/or tectonics of the area as they influence the connection to the open ocean (e.g., Esin et al., 2010; Le Pichon et al., 2001;

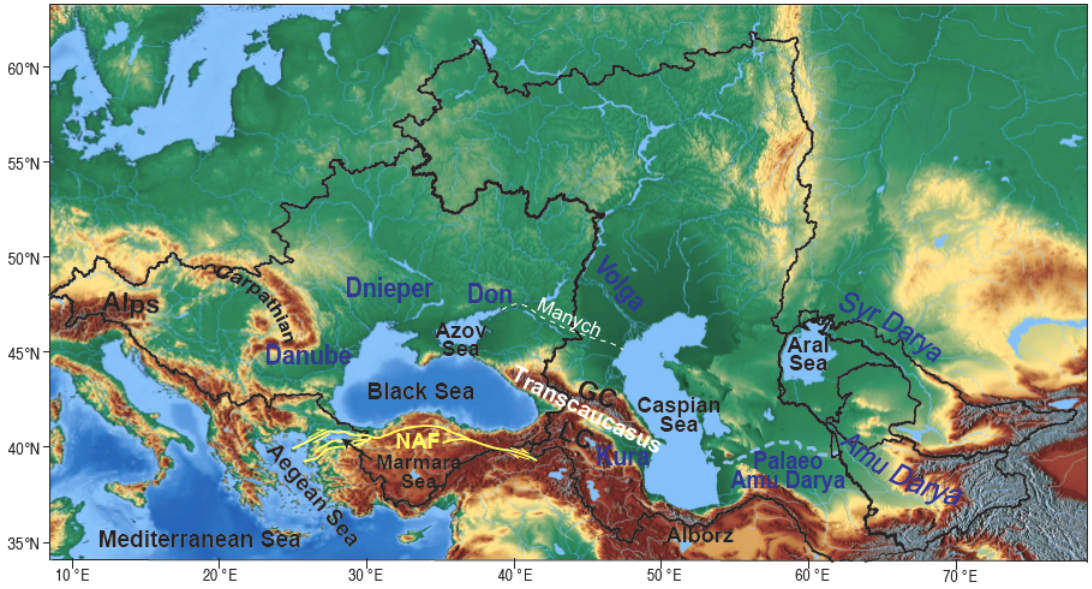

FIGURE 1.1: Topographic map of the present-day Black and the Caspian seas with the extent of their drainage area indicated by the solid black line. Topographic highs are shown in black and lows are shown in white. Dashed white line indicates the Manych spillway that connected the Black Sea and the Caspian Sea in the past (Yanina, 2014). Dashed blue line indicates the former course of the Amu Darya river when it drained into the Caspian Sea (Boomer et al., 2000). North Anatolian Fault (NAF) is indicated by yellow line. GC: Greater Caucasus and LC: Lesser Caucasus.

Ryan et al., 2003; Yanina et al., 2017). Consequently, the connection between both these basins and the open ocean are governed by either eustatic sea level changes during glacial interglacial cycles, climatic variation over the catchment area, tectonics in the region, or a combination of all three (e.g. Kislov and Toropov, 2007; Kwiecien et al., 2009; Le Pichon et al., 2015; Rodionov, 1994; Yanina, 2014). The Pleistocene time scale consists of large changes in global climate with amplified glacial - interglacial cycles (Lisiecki and Raymo, 2005) and in regional tectonics (McHugh et al., 2008). Reconstructing the connectivity history of these basins during this period can, therefore help disentangle the climatic and tectonic signal impacting the basins' hydrology in order to understand the long-term variation in these drivers.

1.1.2 Understanding the biodiversity fluctuations

The Black Sea and Caspian Sea are considered to be biodiversity hotspots (Reid and Orlova, 2002). The complex history of connection and isolation of the Black Sea, Caspian Sea and the open ocean has resulted in unique endemic faunal assemblages in the region that are derived from Paratethyan species, marine Mediterranean species and freshwater species (Zenkevitch, 1963). The palaeontological evidence from the Black and Caspian seas show that the endemic faunal

communities have waxed and waned since the Miocene (e.g. Dumont, 1998; Harzhauser et al., 2002; Reid and Orlova, 2002), but have experienced rapid turnover events during the Quaternary (Grigorovich et al., 2002). These faunal events are inherently linked to the connectivity history of the basins, as connection of basins facilitates faunal exchange, while isolation promotes faunal endemism. One of the motivations of this research is therefore to reconstruct the Pontocaspian's connectivity history and thereby, constrain one of the key abiotic drivers of faunal evolution in the Black and Caspian seas.

1.2 PRIDE

This research was funded through the PRIDE Project, a European Union Marie Curie Initial Training Network. PRIDE (drivers of Pontocaspian RIse and DEmise) brings together sedimentology, geochemistry, micropalaeontology, and molecular biology to study the changes in palaeoenvironment and past faunal biodiversity in the Pontocaspian basins. PRIDE also involves climate as well as lake level modelling to understand the abiotic causes and controls on these changes. The PRIDE project also includes research on biodiversity modelling, heavy metal, and microplastic distribution to evaluate the anthropogenic impact on the current biodiversity of the region. The overarching goal of the PRIDE project is to understand the causes of natural biodiversity fluctuations recorded in the recent geological archive in order to develop strategies that support and promote the preservation of the current biodiversity in the area. Given that the connection between two basins is one of the key abiotic controls on the evolution of the biota, as part of the PRIDE project, this PhD focused on reconstructing the connectivity history of the Black Sea and the Caspian Sea during the Pleistocene. This can then be used as a framework to understand the natural biodiversity fluctuation and to establish faunal evolutionary rates in the region.

PRIDE research was carried out by 15 doctoral students, based in four different European countries, working in various sub-disciplines of geology, biology and climate science. Experienced researchers, acting as supervisors, and project partners based in countries surrounding the Black Sea and the Caspian Sea provided the necessary support and additional expertise in the area. To achieve a holistic research, results from different sub-disciplines were shared and combined together. As such, this thesis incorporates data generated by or in concert with co-researchers within

the PRIDE project. Contributions from other individuals to this thesis are clearly indicated at the beginning of each chapter.

1.3 Geological evolution of the Black Sea and the Caspian Sea

The Black and Caspian seas are relict basins of the Tethys Ocean (Figure 1.2). The geological evolution and the palaeogeographical reconfiguration during Mesozoic and Cenozoic (Rögl, 1998) have placed these basins along plate margins and surrounded by active faults and rapidly rising mountain ranges (Allen et al., 2004). The ongoing tectonics of the region, therefore controls the gateway connecting these basins to each other and the open ocean.

FIGURE 1.2: Palaeogeographic map showing the progressive evolution of the Tethys Ocean into the Mediterranean and the Paratethys. Palaeomaps are adapted from Scotese (2016).

The Tethys was a vast ocean that divided Laurasia from Gondwana during the Jurassic and Cretaceous period providing a route for a circum-equatorial current (Figure 1.2A and 1.2B; Ricou 1995). Tectonic movements during the early Eocene restricted the Tethys Ocean (Figure 1.2C, Steininger and Rögl, 1984) which eventually split into two marine realms separated by an orogenic belt that stretched along the Alpine, Caucasus and Pontide Mountain range by the end of the Eocene and the beginning of the Oligocene (Rögl, 1999). A southern Mediterranean branch was created at the western end of the Tethys and a vast Paratethys Sea was formed in central Eurasia to the east (Figure 1.2D, Rögl, 1997).

Accelerated tectonic movement during the Miocene caused initial uplift of the Caucasus ~15 Ma and progressive restriction of the Paratethys Sea, which eventually reorganized into Central and Eastern Paratethys (Figure 1.3A, Rögl, 1998; Steininger and Rögl, 1984). Continued plate movement and orogenic phases during the Late Miocene–early Pliocene significantly re-shaped the palaeogeography of the Pontocaspian area (Figure 1.3B and C). While, the Mediterranean Sea experienced a dramatic salinity crisis in the Messinian (MSC; 5.97 – 5.33 Ma), the Black and Caspian seas showed a general trend of decreasing salinity indicating progressive disconnection between the Paratethys realm and the Mediterranean Sea (van Baak et al., 2017, and references therein). The fragmentation of the Eastern Paratethys into the Black Sea and the Caspian Sea occurred when the strait connecting the two basins north of the Caucasian mountains (Figure 1.3B) closed due to uplift of the Caucasus (Figure 1.3C, Popov et al., 2006).

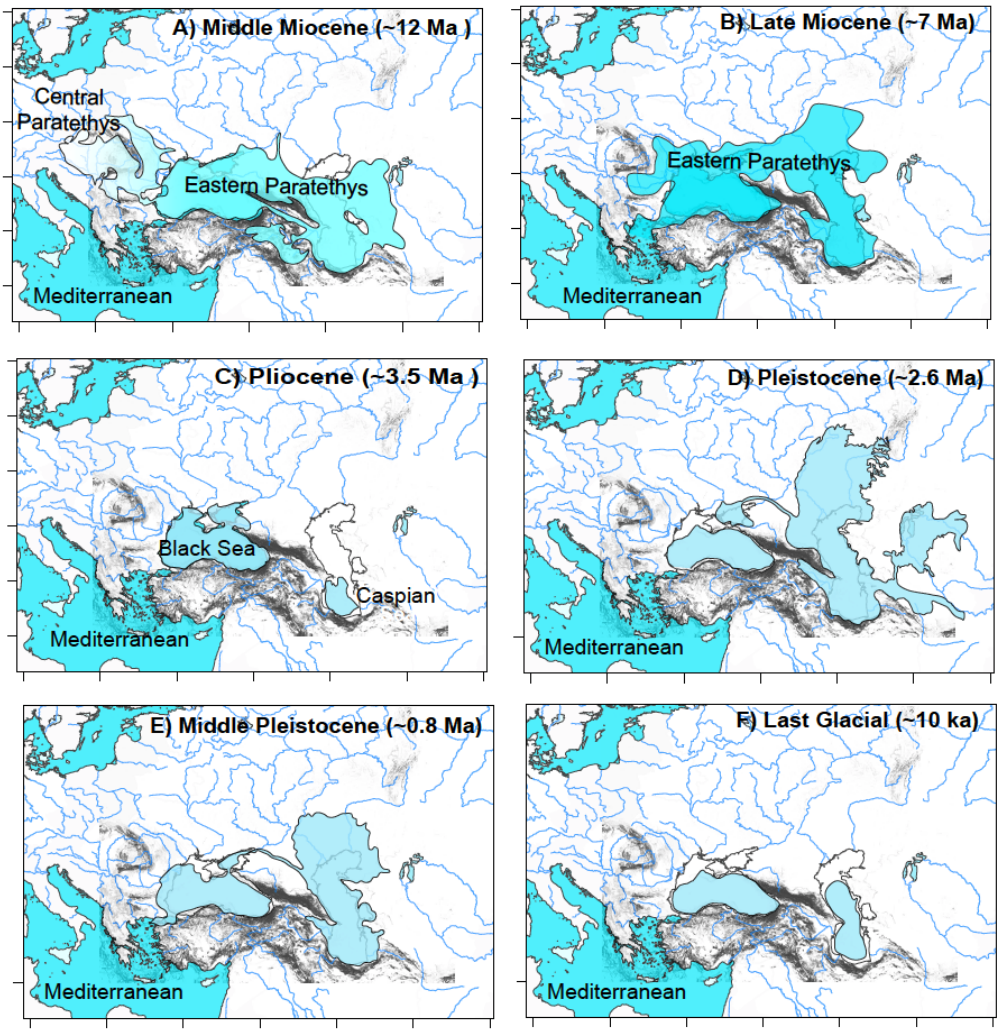

FIGURE 1.3: Palaeogeographic map showing evolution of the Black Sea and the Caspian Sea since the Middle Miocene until the last glacial period, adapted from Popov et al., 2006; Yanina, 2012. Darker blue indicates saline conditions and pale blue indicates brackish and freshwater conditions.

During the Early Pliocene, both the Black and Caspian seas experienced a sea level drop (Figure 1.3C, Jones and Simmons, 1997; Popov et al., 2006). The Black Sea transformed into a lake but the water level drop in the Caspian Sea was comparatively more dramatic and resulted in the entire basin occupying a much smaller area in the southern Caspian basin (Figure 1.3C, Popov et al., 2006). Three major rivers that fed the Caspian during the Pliocene (Volga, Kura and Amu Darya; Figure 1.1) formed deeply incised river valleys (Kroonenberg and Park, 2005) and deposited fluvial and deltaic sediment in the Caspian basin (Abdullayev et al., 2012; Hinds et al., 2004; Reynolds et al., 1998). This deltaic deposit is referred to as Pliocene Productive Series, which is the main hydrocarbon reservoir unit (e.g., Hinds et al., 2004). During the Late Pliocene – early Pleistocene, the Caspian Sea experienced another dramatic event as the surface area of the Caspian Sea increased five fold (Figure 1.3D, Andrusov, 1912). This event is known as Akchagylian transgression in the Caspian Sea. The Caspian Sea reached as far east as the Aral Sea (Boomer et al., 2000; Popov et al., 2006), and is likely to have had ephemeral connections to the Black Sea (Figure 1.1D, Danukalova, 1996). Drivers for this extreme sea level rise has been linked to overflow of marine water in the Caspian Sea (Nevesskaya et al., 2003). The exact location of this marine connection (Mediterranean Sea via the Black Sea, Arctic Ocean or Indian Ocean), however is still debated (Grothe et al., 2018; van Baak et al., 2016b, 2019).

The Quaternary evolution of the Black and Caspian Sea shows large water level variation over short periods (Figure 1.3E and F, Krijgsman et al., 2019). The Caspian Sea, in particular, has experienced water level fall of ~2 m from 1929 to 1978 and a subsequent rise of ~2.7 m from 1978 to 1995, a rate significantly faster than the present-day global sea level rise (Figure 1.4, Beni et al., 2013; Kroonenberg et al., 2000). The rapid change in the water level has mostly been linked to global and regional climatic variation, resulting in periods of isolation with intermittent connection between the two basins and the open ocean (Section 1.5, Krijgsman et al., 2019, and references therein). However, the gateway connecting the Caspian Sea to the Black Sea (Manych strait, Figure 1.1) and the Black Sea to the Mediterranean (Bosporus) are also affected by the Caucasus uplift and active tectonics along the North Anatolian Fault (NAF, Figure 1.1), respectively (e.g., Le Pichon et al., 2015; Ryan et al., 2003; Svitoch, 2013). As such, the Black and Caspian seas' evolution and the resultant connection between them and the open ocean during the Quaternary are governed by a combination of climatic and tectonic drivers.

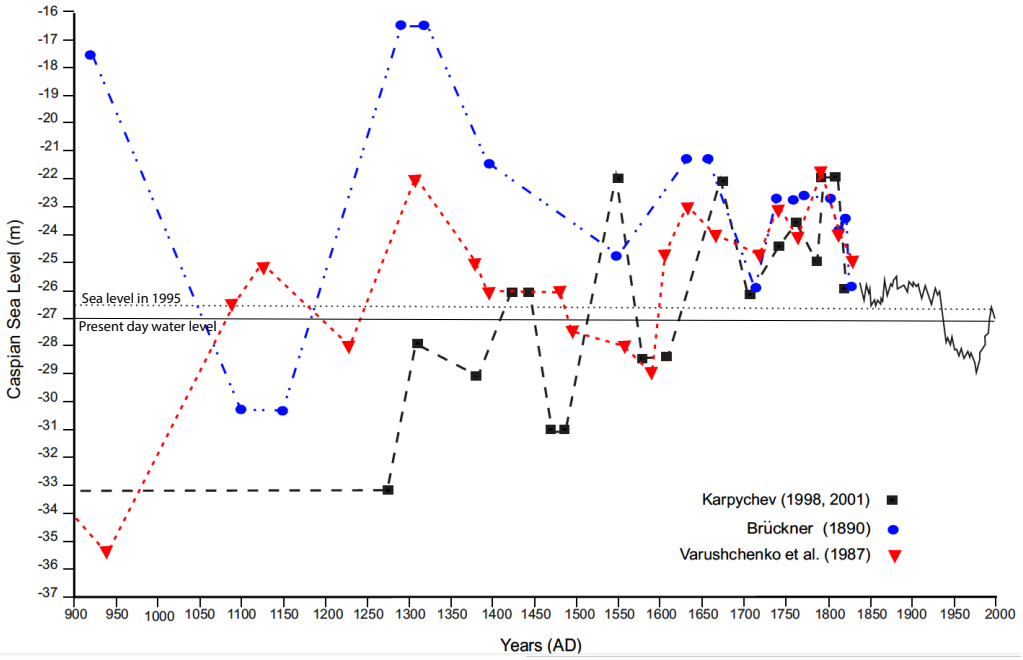

FIGURE 1.4: The Caspian Sea water level curve based on Brückner (1890), Karpychev (1998, 2001), and Varushchenko et al. (1890). The dashed lines connecting the filled symbols are interpolations. The continuous line from 1850 to 2000 show instrumental observations. The two horizontal lines are Caspian Sea level in 1995 (dashed; -26.5 m) and today (solid; -27 m). Plot taken from Beni et al. (2013).

1.4 Present-day configuration and hydrography

1.4.1 Black Sea

The Black Sea is a Mesozoic–Early Cenozoic marginal back-arc basin generated by the northwards subduction of the Tethys Ocean (Nikishin et al., 2003; Okay et al., 1994). It stretches ~1175 km E - W (27°27' - 41°42'E) and ~800 km N - S (46°33' - 40°56' N) and has a total area of ~436,400 km^2 (Figure 1.5). The Black Sea is connected to the Marmara Sea in the west via the 30 km long and 0.7 - 3.6 km wide Bosporus Strait, which has a depth of ~35 m. The morphology of this strait is controlled by the North Anatolian Fault (NAF; Figure 1.1), which runs through the Marmara Sea and into the Aegean Sea (Armijo and Hubert, 1999; Şengör and Canitez, 1982; Şengör et al., 2005). To the north, the Black Sea is connected to the Sea of Azov via the Kerch Strait (Figure 1.5), which is 41 km long and 4.5 to 15 km wide with a maximum depth of 15 m. The Black Sea has a wide continental shelf with depth less than 200 m along the north and west coasts. This flat bathymetric area is substantially narrower along the east and south coasts, where it rarely exceeds

a width of 20 km. The Black Sea has a mean water depth of 1315 m and a maximum depth of 2258 m.

At present, the Black Sea has a restricted connection to the Mediterranean through the intermediate Marmara Sea (Figure 1.5). The Mediterranean water with salinity of ~38 g/kg enters the Marmara Sea at depths and mixing of this dense water with fresher surface water results in Marmara Sea surface salinity of ~22 g/kg (Beşiktepe et al., 1994). This Marmara Sea water with salinity of ~22 g/kg then enters the Black Sea at greater depths. The Black Sea's drainage area stretches from eastern Europe to western Asia (Figure 1.1). Substantial run-off from major rivers like the Danube, Don, and Dnieper creates a surface freshwater cap above the saline water and mixing between the two occurs to a depth of 200 m induced by winds and winter circulation (Kosarev and Kostianoy, 2008). Consequently, the salinity of the basin changes from ~17 – 18 g/kg at the surface to ~22 - 24 g/kg at deeper depths (Cagatay et al., 2006; Cox and Faure, 1974). A strong vertical stratification is maintained due to this density difference, limiting the exchange between the surface and deep water and resulting in an anoxic environment below 100 -200 m water depth (Figure 1.5, Kosarev and Kostianoy, 2008).

Currently, the Black Sea has a positive hydrological balance with freshwater input of ~338 km^3/yr from fluvial sources, ~300 km^3/yr from precipitation and evaporative loss of ~350 km^3/yr (Özsoy and Ünlüata, 1997). Although a positive hydrological budget results in an outflow from the Black Sea, the exchange with the Mediterranean Sea via the Marmara Sea is largely driven by the differences in density of each water body. The large freshwater influx in the Black Sea and a narrow opening to the Marmara Sea result in an asymmetric exchange between them, with outflow of the less saline water at the surface twice as much than the inflow of more saline water at deeper depths (Esin et al., 2010). Because salinity of the Black Sea have varied through time (Schrader, 1978), this density driven exchange and hence the connection with the adjacent basins can be expected to change substantially as well. This has been observed in the Mediterranean Sea (Modestou et al., 2017). Although the exchange between the Mediterranean and Atlantic Ocean today is driven by density contrast between the two, salinity change in the Mediterranean Sea during Late Miocene has prevented the exchange with Atlantic ocean even when these basins were fully connected (Modestou et al., 2017).

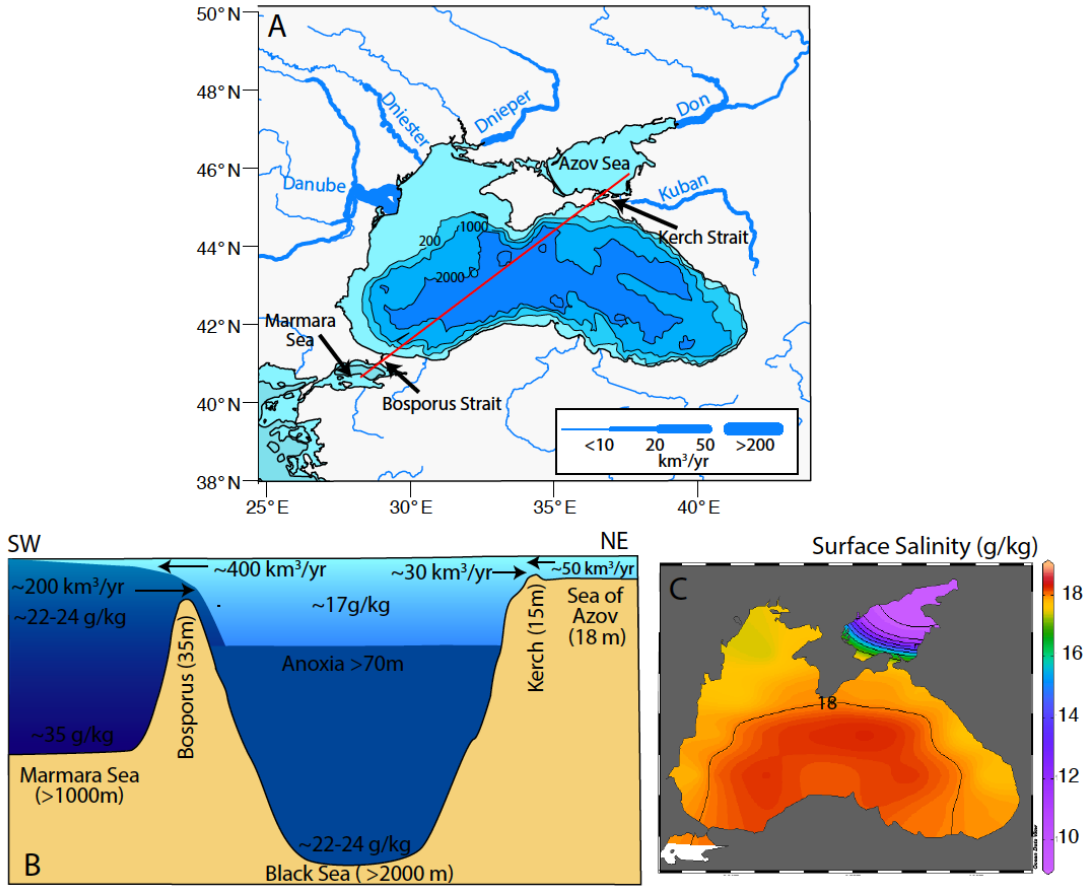

FIGURE 1.5: A) Bathymetric map of the Black Sea with fluvial sources. The thickness of the river is proportional to the magnitude of the river discharge. B) Cross sectional schematic (not to scale) of the Black Sea along the red line indicated in A showing inflow and outflow to the Mediterranean via Marmara Sea and Sea of Azov and vertical salinity stratification. C) Mean annual surface salinity of the Black Sea. Salinity data from *WOA 2013 V2*.

1.4.2 Caspian Sea

The Caspian Sea is the world's largest inland body of water with a present-day surface area of about 374 x 10^3 km^2 and a lake level of ~27 m below global sea level. The sea stretches ~1200 km N - S (36° - 47°N) and ~195 - 435 km (46° - 56°E). The basin is divided into three parts; North, Middle and South basin (Figure 1.6A). These three basins are about the same size, but vary significantly in depth and volume (0.5, 33.9 and 65.6%, respectively; Baidin and Kosarev, 1986). The northern basin is very shallow with a maximum depth of only about 20 m. There is a gradual increase in depth from north to south, reaching a maximum depth of 788 m in the Middle Caspian. The South Caspian basin is the deepest part of the Caspian Sea reaching a maximum depth of 1024 m (averages ~330 m). The Middle and South Caspian basins are separated by the Apsheron sill, a structural high created during the regional convergence of Arabia and Eurasia plate (Allen et al.,

2004). The Apsheron sill has a maximum water depth of about 160 – 180 m (Figure 1.6C) and extends onshore from the eastern Greater Caucasus, through the Apsheron Peninsula to the Kopet Dagh.

The basement of the South Caspian Basin is not exposed as it is covered by ~ 20 km of sediments (Allen et al., 2004), about half of which are fluvial and deltaic deposits of Pliocene – Quaternary age (Ali-Zade et al., 1985). Deposition of large amounts of sediment in this basin has been interpreted as both cause and effect of the high subsidence rate observed in the South Caspian Basin since ~5.5 Ma (Allen et al., 2002; Brunet et al., 2003; Green et al., 2009). Consequently, even when the Caspian Sea experiences major regression, such as during the Pliocene (Popov et al., 2006), the South Caspian basin always remains subaqueous.

Today, the drainage basin of the Caspian Sea is about 10 times larger than the basin itself and covers a large part of southern Russia (Figure 1.1). During parts of the Pleistocene, the drainage area of the Caspian Sea also included the Amu Darya River, which flowed south-westward into the Caspian (Boomer et al., 2000; Brunet et al., 2017) until early Holocene and today feeds the Aral Sea. Currently, the Caspian Sea receives a total continental run-off of about 3.4 x 10^{11} m^3/yr (Shiklomanov et al., 1995) of which 82% is from the Volga river, 11.5% is from the western rivers, including the Sulak, Samur, Kura, and Terek rivers, 3.5% is from the Iranian rivers and 3% is from the Ural River (Figure 1.6A, Shiklomanov et al., 1995). Additional sources of water to the Caspian Sea are from direct precipitation over the basin (1.3 x 10^{11} m^3/yr) and shallow ground water discharge (0.03 – 0.05 x 10^{11} m^3/yr, Clauer et al., 2000). The Caspian Sea also loses about 4.3 x 10^{11} m^3/yr of water by evaporation. Overall, the Caspian Sea today, has a positive hydrological budget of 0.43 – 0.45 x 10^{11} m^3/yr. However, the water balance of the Caspian Sea is extremely sensitive to continental run-off and evaporation; relations between their intensities mostly control the inter-annual changes in the water volume and the sea level of the basin (Figure 1.4).

Even though it is an isolated basin, the Caspian Sea has the average salinity of 12 g/kg. The high fresh water discharge from the Volga produces water with a salinity less than 1 g/kg in the North Caspian (Figure 1.6B). There is a steep salinity gradient from north to south where the salinity changes from 1 - 2 to 9 - 10 g/kg in the Middle Caspian and reaches a salinity of ~12 g/kg and more in the South Caspian basin (Figure 1.6B). This salinity gradient depends upon the volume of Volga discharge, its distribution, and water exchange between the North and Middle Caspian. Compared to the surface salinity distribution, there is no vertical salinity gradient and salinity

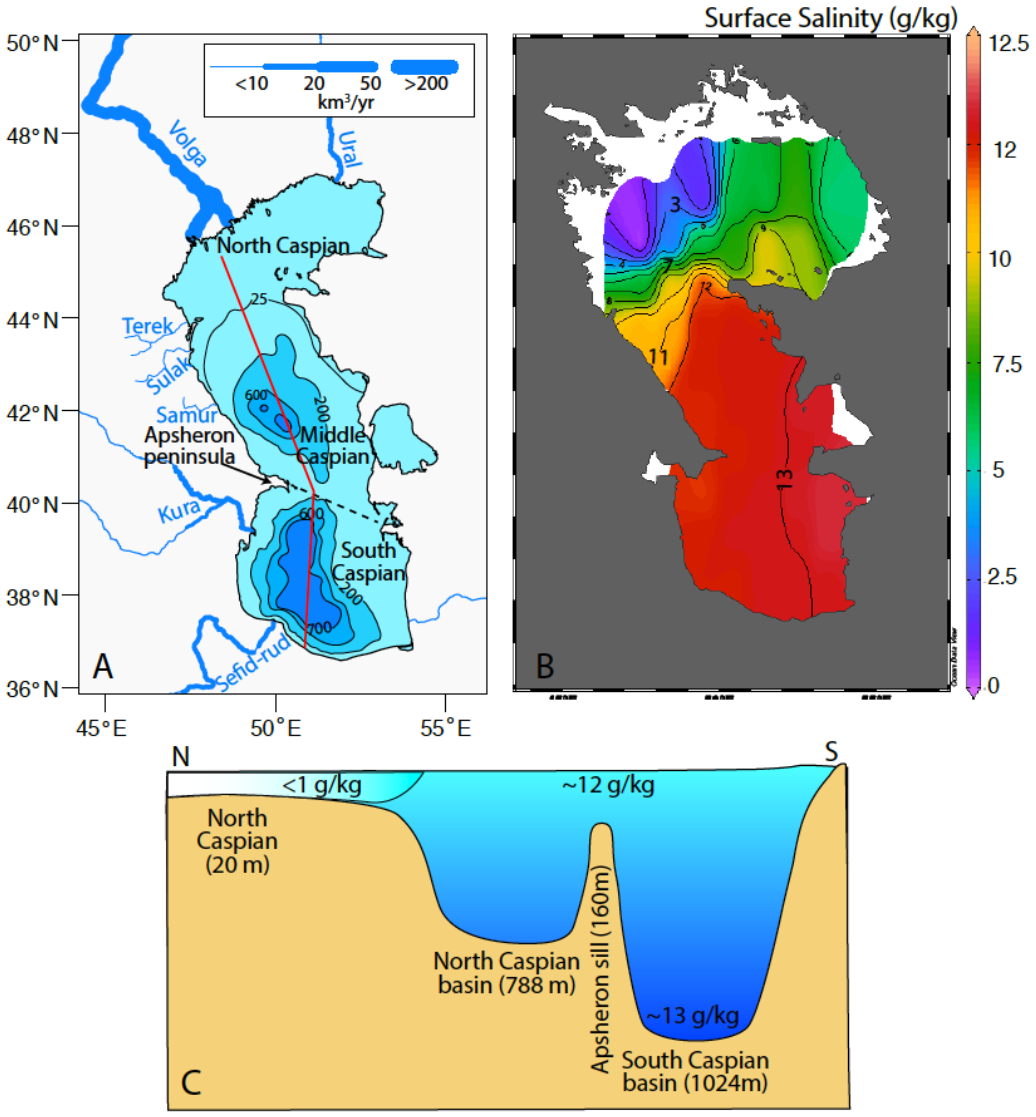

FIGURE 1.6: A) Bathymetric map of the Caspian Sea with fluvial sources. The thickness of the river represents magnitude of the river discharge. B) Mean annual surface salinity of the Caspian Sea. Salinity data from *WOA 2013 V2*. C) Cross sectional schematic (not to scale) along the red line indicated in A and showing vertical salinity gradient.

below 100 m does not exceed 13 g/kg (Figure 1.6C). Because of the isolated nature of the basin, there is no advection from other water bodies and the hydrological structure is controlled by winds, heat exchanges at the sea surface and the resulting changes in density.

1.5 Published connectivity record of the Pontocaspian region

The history of Pontocaspian connectivity and isolation events have previously been identified on the basis of faunal assemblages (e.g., Dumont, 1998; Grigorovich et al., 2003; Nevesskaya, 1965;

Yanina, 2012, 2014; Yanko-Hombach et al., 2014; Yanko-Hombach et al., 2007), phylogenetic studies (e.g., Audzijonyte, 2005; Fulton and Strobeck, 2010; Kvach, 2009; Palo and Väinölä, 2006; Väinölä et al., 2001) and geochemical studies (e.g., Badertscher et al., 2011; Bahr et al., 2006; Grothe, 2016; Major et al., 2006; van Baak et al., 2019; Wegwerth et al., 2014). These records are rather fragmented and the resulting connectivity reconstruction is discontinuous. Additionally, connectivity reconstructions by different authors and studies based on different proxy methods generally provide contradictory results.

1.5.1 Palaeontological studies

Palaeontological studies investigating the connectivity history of the Black Sea and the Caspian Sea have mainly used mollusc and bivalve assemblages (e.g., Buyukmeric and Wesselingh, 2016; Svitoch, 2008; Yanina, 2012, 2014) but few studies have also used ostracod (e.g., Richards et al., 2018; Stoica et al., 2013), foraminifera (e.g., Richards et al., 2014; Yanko-Hombach et al., 2014), diatoms (Schrader, 1979), and dinocyst assemblages (Hoyle, 2019; Ivanova et al., 2014). All faunal studies are based on the concurrent occurrence of similar or identical faunal assemblages in adjacent basins. Theoretically, when connected, adjacent basins will develop similar ecological conditions and will have similar biota because of the faunal exchange between them, but will develop endemic fauna when separated for long enough periods of time (Reid and Orlova, 2002). However, ecological conditions suitable for faunal evolution (e.g. salinity, nutrient etc.) are primarily determined by the hydrology of the basin and therefore, even when connected, two basins could have ecological differences resulting in different faunal assemblages. It is probably for this reason that there is disagreement between connectivity reconstruction based on different faunal groups (e.g. mollusc and ostracods Nevesskaya et al., 1986; van Baak et al., 2013; Yanko-Hombach et al., 2013).

In addition, contradictory connectivity reconstruction also arises from lack of reliable stratigraphic correlations between the Black Sea and Caspian Sea and the open ocean. In an open ocean setting, faunal assemblages are typically used to constrain the age of the sediments. In the Black and Caspian Sea, because of their complex geological evolution, faunal assemblages typically consist of endemic faunas, which have been used to construct local and regional time scales for individual basins (Krijgsman et al., 2019). Cross correlation between these basins without any additional independent age constraints are difficult. The precise timing of these regional stages and their correlation to the standard geological time scale (Hilgen et al., 2012), therefore vary from author

to author (Krijgsman et al., 2019, and references therein). The connectivity reconstruction of the Black and Caspian seas, which are conducted relative to these regional stages, generally show different results (e.g., Nevesskaya, 2007; Yanina, 2012). Here, I provide a summary of faunal based connectivity using the framework of regional stages by Krijgsman et al. (2019) and correlate them broadly to the standard geological time scale (Figure 1.7E).

Prior to the fragmentation of the Eastern Paratethys in the Late Miocene - early Pliocene (Figure 1.3), the occurrence of marine fauna across the region suggests an enduring Mediterranean - Paratethys connection until early Maeotian (Late Miocene) times (Nevesskaya et al., 2003). During late Maeotian, the marine fauna in the Eastern Paratethys was replaced by brackish and freshwater species indicating disconnection from the Mediterranean Sea during the time (Figure 1.7E, Popov et al., 2006, 2010). The base of the Pontian (at ~6.1 Ma; van Baak et al., 2016b) was marked by reappearance of marine planktonic and benthic foraminifera, and marine diatom assemblages indicating the reestablishment of a marine connection to Eastern Paratethys (Krijgsman et al., 2010; Popov et al., 2006; Radionova et al., 2012; Stoica et al., 2013, Figure 1.7E). The Pontian regional stage is tentatively correlated to the MSC of the Mediterranean (van Baak et al., 2017). During most of the MSC, similar mollusc and ostracod species suggest that connection existed between the Eastern Paratethys and the Mediterranean Sea, which was not connected to the open ocean (Nevesskaya et al., 1986; Popov et al., 2006). The connection to the Mediterranean was however, severed during the Stage 2 of the MSC (5.5 - 5.55 Ma) but presence of the Pontian Black Sea species in the time equivalent of the Caspian Sea implies that the two basins were connected at that time (Nevesskaya et al., 1986).

Freshwater taxa completely replaced previous Pontian fauna during the deposition of the Productive Series (early Pliocene) in the Caspian Sea (Nevesskaya et al., 2003). However, in the Black Sea basin "Pontian" type fauna and their descendants dominated throughout the Kimmerian (Figure 1.7E). This has been interpreted as evidence for a prolonged period of separation of the two basins and isolation from the open ocean (Nevesskaya et al., 2003). The base of the Akchagylian (Pliocene) in the Caspian Sea was marked by the abrupt occurrence of marine foraminifera and ostracod assemblages indicative of marine influx, suggesting a Caspian connection to the open ocean (Richards et al., 2018). However, source of this marine water is much debated and could be either Arctic Ocean or Mediterranean Sea (Krijgsman et al., 2019; Richards et al., 2018, and references therein). After this short marine interval, the faunal assemblage of the upper Akchagylian Caspian

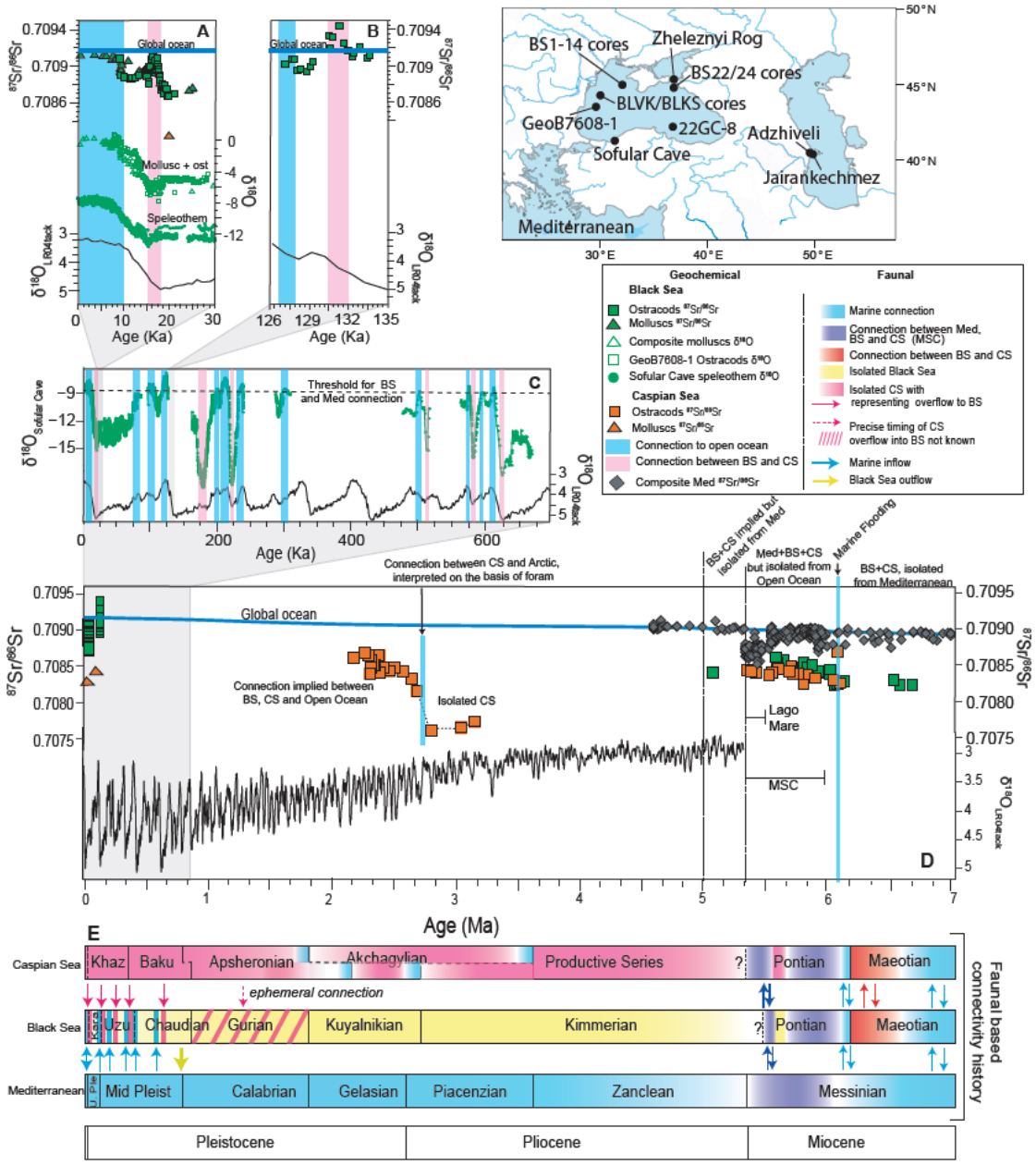

FIGURE 1.7: The $^{87}Sr/^{86}Sr$ and $\delta^{18}O$ data from the Black Sea (green), Caspian Sea (red) and Mediterranean Sea (grey) for different time slices (A - D). Different symbols represent different archives; ostracods (squares), mollusc (triangles), speleothem (circles), composite of carbonate precipitates (diamonds). The $^{87}Sr/^{86}Sr$ of the global ocean is from McArthur et al. (2012) and the global benthic $\delta^{18}O$ is from Lisiecki and Raymo (2005). The $^{87}Sr/^{86}Sr$ of the Mediterranean Sea is from Flecker et al. (2015), of the Black Sea is from Grothe (2016), Major et al. (2006), and Wegwerth et al. (2014), of the Caspian Sea is from Page (2004) and van Baak et al. (2019). The Sofular Cave $\delta^{18}O$ record is from Badertscher et al. (2011) and $\delta^{18}O$ of the Black Sea over the last 30 ka are from Bahr et al. (2006) and Major et al. (2006). E) Faunal based connectivity history between the Caspian Sea, Black Sea and the Mediterranean Sea. Regional stages for the Black and Caspian seas are from Krijgsman et al. (2019). Colour and direction of the arrow indicate the source water and direction of the input. Dashed arrow represent ephemeral connection between the Caspian Sea and the Black Sea without any precise timing. (Modified after Krijgsman et al., 2019).

Sea suggests mostly an isolated basin (Nevesskaya et al., 2003). The presence of Akchagylian molluscs in the northern coast of the Sea of Azov implies Caspian connections with the Sea of Azov. However, the absence of Akchagylian molluscs in similar aged Kuyalnikian Black Sea sediment, which hosted bivalves endemic to the Black Sea suggests a Black Sea isolated from both the Mediterranean Sea and the Caspian-Azov during this time (Figure 1.7E, Nevesskaya et al., 1986).

Sediment at the base of the Caspian's Apsheronian succession (Calabrian) contains euryhaline foraminifera *Ammonia spp.*, suggesting the existence of another minor marine connection event (Richards et al., 2018). Similar aged, Gurian fauna in the Black Sea are completely dissimilar with only very limited species in common (e.g, one bivalve genus is thought to have migrated in the Caspian Sea from the Black Sea during this interval; Nevesskaya, 2007). This has been interpreted as indicating another prolonged isolation event both between the two basins and the open ocean but with perhaps ephemeral connections between the Black and Caspian seas (Nevesskaya, 2007).

Middle and Late Pleistocene faunal records indicate multiple connectivity events between the Black Sea, Caspian Sea and Mediterranean Sea (Figure 1.7E). The driver for this connectivity is thought to have been the Pleistocene glacial- interglacial cycles (Svitoch, 2010; Yanina, 2014). Consequently, connection between the Mediterranean Sea and the Black Sea have been suggested during the interglacials due to eustatic sea level highs whereas connections between the Caspian Sea and the Black Sea have been suggested during glacial periods due to sea level rise in the Caspian Sea driven by input of glacial meltwater, resulting in overflow events to the Black Sea (Yanina, 2014). However, without absolute independent age constraints, the resolution of these studies maybe insufficient to support this hypothesis.

1.5.2 Phylogenetic studies

Endemic faunas in the Black and Caspian basins have both Paratethyan and open ocean lineages. Commonly, these oceanic ancestors are thought to have reached the Pontocaspian basin via the Mediterranean Sea. However, the Caspian Sea currently, also harbours some species (e.g. *Pusa Caspia* - Caspian Seal, some genera of crustacean that have closest living relatives in the coastal and estuarine waters of the Arctic Ocean (e.g. Davies, 1958; Holmquist, 1959; Mclaren, 1960; Zenkevitch, 1963). This suggests that a connection between the Caspian Sea and the Arctic Ocean

existed in the past which allowed for the transfer of these Arctic elements to the Caspian Sea. Although phylogenetic studies largely agree on the Caspian-Arctic connection that resulted in dispersal and subsequent diversification of Arctic taxa in the Caspian Sea, the timing and number of these biologically determined connection episodes are keenly debated. Initially, based on fossil morphology and identification, Mclaren (1960) suggested that the connection between the Arctic Ocean and the Caspian Sea occurred during the Late Miocene. This idea was subsequently revised using phylogenetic studies of Arctic taxa by various authors. Based on seal phylogeny, Árnason et al. (2006) suggested a Pliocene connection whereas Árnason et al. (1995) and Palo and Väinölä (2006) suggests a late Pliocene - early Pleistocene (2 – 3 Ma) connection and Fulton and Strobeck (2010) suggested a more recent (~1 Ma) connection. Studies of crustacean (*Mysis* and *Gammaracanthus*) by Dooh et al. (2006) suggested a Pre-Pleistocene connection (3.5 - 2 Ma) consistent with studies by Árnason et al. (1995) and Palo and Väinölä (2006). This diverse timing of the connection could be because these studies used different DNA markers (e.g. nuclear DNA and mitochondrial DNA) that have variable mutation rate (e.g., Árnason et al., 2006; Palo and Väinölä, 2006). Additionally, dated phylogenetic studies may use external calibration points to constrain the timing of the divergence. These external calibration points can include geological events like Messinian Salinity Crisis or biogeographic separation events of other taxa, such as cat and dog divergence at 55 (50–60) Ma or odontocetes and mysticetes divergence at 33 - 35 Ma (Árnason et al., 1995, 2006; Fulton and Strobeck, 2010; Palo and Väinölä, 2006), which themselves have age uncertainties. Consequently, resulting age error associated with a molecular clock is usually counted in hundreds of thousands of years. This means that the ages suggested by these authors should be treated as estimations and not as exact ages or time range.

1.5.3 Geochemical studies

Compared to the palaeontological and phylogenetic studies, the hydrochemistry of a basin is directly controlled by changing environmental conditions as the connectivity between basins changes. Geochemical studies can, therefore give a more accurate record of the timing of the connection and isolation between basins, providing sections are well dated by non-faunal methods and well preserved archives are available.

1.5.3.1 Proxy archives

Proxy archives used for connectivity reconstruction in the Pontocaspian include cave speleothems (Badertscher et al., 2011), organic matter (Vasiliev et al., 2013, 2017) and biogenic carbonates preserved in the sedimentary succession (e.g. Bahr et al., 2006; Major et al., 2006; Vasiliev et al., 2010). Calcareous organisms like molluscs, ostracods, foraminifera, corals etc are most suitable for geochemical studies because they precipitate their carbonate shell in equilibrium with the surrounding water (Rosenthal and Katz, 1989; Turpen and Angell, 1971). The diversity of these organisms mean that they can be found in various aquatic settings and are therefore usually present in fossil records making them an ideal archive for past environmental changes. The most environmentally and geographically diverse species that precipitate calcium carbonate in both fresh and marine environment are ostracods.

Ostracods (Figure 1.8) are bivalved micro-crustaceans with an exoskeleton composed of low-magnesium calcite. They are generally 0.2 to 1 mm in length and weigh between 20 and 200 mg (Rosenthal et al., 2006). Unlike other shell forming microorganisms, ostracods have up-to 8 moulting stages during their life cycle until they reach maturity. During moulting, they shed their previous calcitic exoskeleton and form a new one very quickly within a few hours to several days. Once calcification of the valve is complete, there are no changes in valve chemistry, preserving the geochemical signal of the ambient water (Chivas et al., 1985; Holmes, 1996; Holmes et al., 1992).

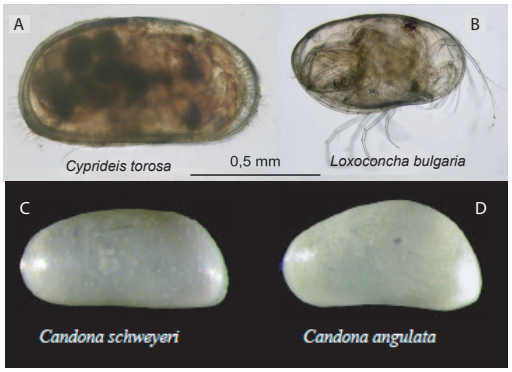

FIGURE 1.8: Side view of two different species of living ostracods from Sea of Azov (A and B; Drapun et al., 2017) and of fossil ostracods from the Black Sea (C and D).

Ostracods occupy virtually all the known aquatic ecosystems from fresh water to highly saline water and even occur in semi-terrestrial habitats such as soils with leaf litter (de Deckker and Forester, 1988; Delorme, 1989; Viehberg and Mesquita-Joanes, 2012). Their carapace has a

high preservation potential because they are formed of a stable carbonate phase. Consequently, compared to other biogenic carbonates, ostracods have the most complete fossil record extending back to Ordovician (at least 450 Ma) and are ideal as a biostratigraphy tool, palaeoenvironment and palaeoclimate proxies (Boerner et al., 2013; Boomer et al., 2003; Chivas et al., 1985; Decrouy et al., 2011a,b; Holmes, 1996; Holmes et al., 1992, and references therein).

1.5.3.2 Isotopic systems that monitor connectivity

There are three main geochemical proxies that have been used to reconstruct the past hydrography of the Black Sea and the Caspian Sea; oxygen isotopes ($\delta^{18}O$), Sr isotopes ($^{87}Sr/^{86}Sr$) and hydrogen isotopes (δD). A brief summary of the background is described below along with the synthesis of the published data for the Pontocaspian region.

1.5.3.2.1 Oxygen isotopes

The oxygen isotopic composition ($\delta^{18}O$) of a marginal marine or lacustrine basin depends on several factors, such as, the isotopic composition of precipitated and evaporated water, as well as the isotopic composition of different source waters entering the basin i.e river run-off and ocean inflow (Craig, 1965; Craig et al., 1963; Dansgaard, 1964; Gat and Gonfiantini, 1981; Stuiver, 1970). In principle, higher $\delta^{18}O$ of the basin water indicates input and mixing with isotopically heavy marine water (enriched in ^{18}O), whereas lower $\delta^{18}O$ of the basin water indicates increased input of isotopically light freshwater (depleted in ^{18}O, Gilfillan, 1934). The sources of isotopically depleted freshwater in marginal basins include precipitation derived from high latitudes and high altitudes, glacial run-off, and inland river discharge, and reflect the broad latitudinal change in $\delta^{18}O$ driven by the global hydrological cycle (Dansgaard, 1964). Biogenic carbonates from foraminifera are commonly used archives for $\delta^{18}O$ in the open ocean (Shackleton, 1967). However, because species-specific vital effects fractionate the two main stable isotopes of oxygen (^{18}O and ^{16}O) differently (Rohling and De Rijk, 1999), teasing apart the individual signals that impact the $\delta^{18}O$ of a basin is quantitatively complex and open to interpretation. This is particularly problematic when trying to reconstruct past connectivity in basins where fossil fauna are extinct today, forcing reliance on the untestable assumption that nearest living relatives will have the same vital effect fractionation. No $\delta^{18}O$ from biogenic archives are available for the Pontocaspian over the last 3 Ma.

An alternative archive for $\delta^{18}O$ is calcareous speleothems. During calcite precipitation, speleothems capture the oxygen isotopic signature of the cave drip-waters with a temperature dependent fractionation between the drip-waters and the deposited calcite (McDermott, 2004). In a carefully chosen site, cave moisture is derived from the local precipitation sourced from an adjacent water bodies and consequently, speleothems of such caves can record and preserve the isotopic signal of the basin water. However, the original signal of the basin water is affected by kinetic fractionation (evaporation/condensation), cave temperature, atmospheric circulation, and temperature dependent fractionation during calcite precipitation (Fairchild et al., 2006; McDermott, 2004). The $\delta^{18}O$ record from the cave at the southern coast of Black Sea has been used to reconstruct the connectivity of the Black Sea with Mediterranean Sea and the Caspian Sea for the last 700 ka (Badertscher et al., 2011).

1.5.3.2.2 Compound specific hydrogen isotopes

Plant biomarkers retain the hydrogen isotopic composition of the water (δD) used at the time of biosynthesis with additional physical and biosynthetic fractionations (Leaney et al., 1985; Luo and Sternberg, 1992; Roden and Ehleringer, 1999). In a continental setting, the δD value of long-chain n-alkanes, which form part of the protective layers on higher plant leaves (Eglinton and Hamilton, 1967) can, therefore provide information about the terrestrial precipitation and evaporation conditions (e.g. Sachse et al., 2006). Similarly, in aquatic settings, unicellular eukaryotic haptophyte algae synthesise alkenones (long strait chain ketones), recording the hydrogen isotopic composition of the water. The δD of the alkenones can reflect the variability of the basin hydrology and has been used to investigate the changes in hydrology of the Black Sea during the Late Miocene (Vasiliev et al., 2013).

1.5.3.2.3 Strontium isotopes

Strontium (Sr) has four naturally occurring isotopes; ^{84}Sr (0.56%),^{86}Sr (9.87%), ^{87}Sr (7.04%) and ^{88}Sr (82.53%). Of these four isotopes, ^{84}Sr, ^{86}Sr, ^{88}Sr are stable whereas ^{87}Sr is produced due to radioactive decay of rubidium-87 (^{87}Rb). Minerals incorporate Rb and Sr during their formation and if the system remains closed with respect to these elements, then the amount of ^{87}Sr increases over time as radioactive ^{87}Rb decays, changing the abundance of ^{87}Sr relative to the abundance of stable ^{86}Sr.

Strontium is an alkali earth element with ionic radius of 1.18 Å, similar to that of Calcium (1 Å) and partition preferentially into plagioclase feldspar. Comparatively, Rb is an alkali metal with a larger ionic radius (1.52 Å), similar to that of the potassium (1.38 Å) and hence, readily incorporates into K-bearing minerals including muscovite, biotite, and alkali feldspars. During the fractional crystallization of mantle derived magma, Sr is removed from the liquid phase and is concentrated primarily in early-formed calcic plagioclase, while Rb is concentrated in the residual magma and eventually enters potassium-rich minerals. The continental crust, which accumulated from the magma produced by differentiation of the Earth's mantle via partial melting and crystal fractionation processes, therefore largely consists of minerals enriched in Rb. The crust developed a higher Rb/Sr ratio than the upper mantle which in time led to a higher $^{87}Sr/^{86}Sr$ ratios in the continental crust than the upper mantle (e.g., Elderfield, 1986; Faure and Powell, 1972b). As such, the older crustal rocks have evolved to a higher present-day $^{87}Sr/^{86}Sr$ values than the recently formed crustal rocks (Figure 1.9A).

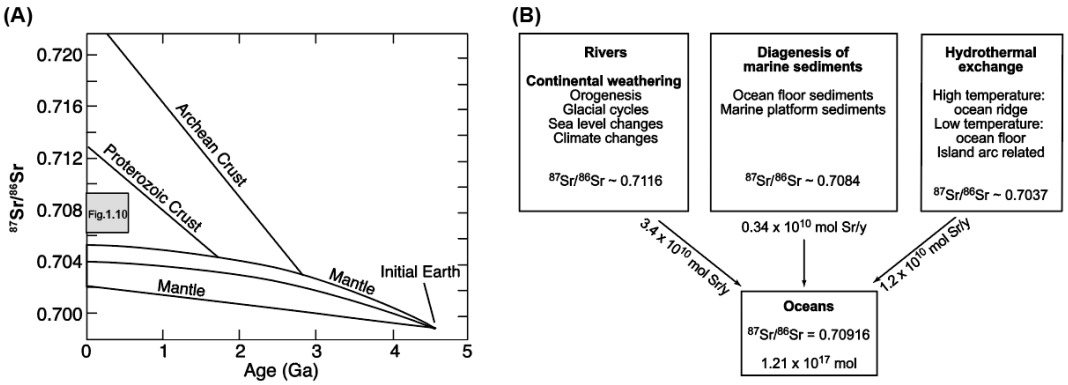

FIGURE 1.9: A) Sr isotopic evolution of the Earth over geologic time. The crust evolution lines shown in the figure represent only two representation of evolution lines. The $^{87}Sr/^{86}Sr$ evolution of the continental crust, in fact, corresponds to a wide range of Rb–Sr ratios and ages found in different parts of the continental crust. The shaded area shows the space occupied by Figure 1.10, which contains Phanerozoic seawater Sr isotope curve. B) The modern isotopic composition and flux of Sr from different input sources into the ocean (after Davis et al., 2003; Holland, 1984; Palmer and Edmond, 1989). Figures modified from Banner (2004).

The continental crust and the upper mantle are the two primary sources of Sr and therefore, the input from both these two main Sr reservoirs influences the isotopic composition of Sr in the ocean (Figure 1.9B). Continental crustal rocks provide dissolved Sr to the ocean through chemical weathering of old silicate lithologies and supplies waters with typically a high $^{87}Sr/^{86}Sr$ ratios (~0.711), but with low strontium concentrations delivered via river input (Palmer and Edmond, 1989). The upper mantle supplies low $^{87}Sr/^{86}Sr$ to the ocean primarily via hydrothermal activity at mid ocean ridges, submarine weathering of basalts, and chemical weathering of continental basalts

(e.g., Elderfield, 1986; Faure and Powell, 1972a). Changes in the balance between these two major input sources have resulted in a varying budget of dissolved strontium in ocean water through time (Figure 1.10).

At any given time however, the global ocean is homogeneous with respect to strontium isotopic ratio ($^{87}Sr/^{86}Sr$) because it has a long residence time (~10^6 years) relative to the ocean mixing time of 3000 yrs (McArthur et al., 2012; Veizer, 1989). As a result, long term variation in oceanic $^{87}Sr/^{86}Sr$ has been used as a stratigraphic tool for carbonates formed in open marine settings (Figure 1.10, Elderfield, 1986; McArthur et al., 2012) and can provide open ocean age with a precision of up to ±3 Ma (El Meknassi et al., 2018).

However, oceanic $^{87}Sr/^{86}Sr$ cannot be used as a stratigraphic tool in isolated or semi-isolated basins like the Black and Caspian seas. In these basins, the $^{87}Sr/^{86}Sr$ can deviate from the global ocean curve (e.g., El Meknassi et al., 2018; Ingram and Sloan, 1992) reflecting substantial input from continental sources (e.g., fluvial run-off and groundwater), which generally have $^{87}Sr/^{86}Sr$ significantly different from the oceanic ratio (Palmer and Edmond, 1989). While $^{87}Sr/^{86}Sr$ may not be useful as a dating tool in the Black and Caspian seas, it can be used to assess the relative input of different source water into the basin, if the isotopic signature (Sr concentration and $^{87}Sr/^{86}Sr$) of those sources are known.

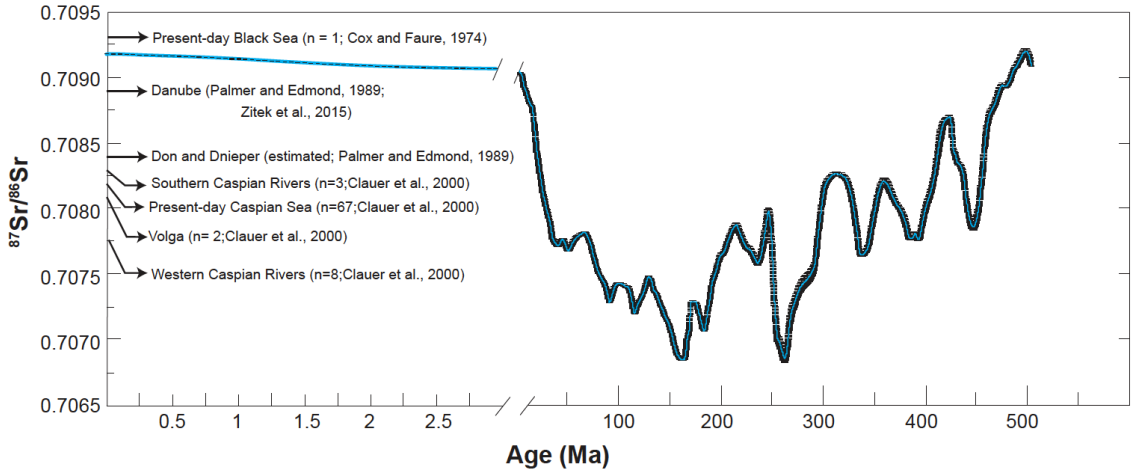

FIGURE 1.10: Oceanic Sr isotopic ratio (McArthur et al., 2012) over time with the isotopic ratio of the present-day Black Sea and the Caspian Sea and their fluvial sources (Clauer et al., 2000; Palmer and Edmond, 1989). Note the x-axis scale change.

The Sr concentration and isotopic ratio of a river depends on its catchment geology and therefore usually varies between drainage basins (Krom et al., 1999; Stein et al., 1997). Although the data are limited, the fluvial Sr concentration and ratios in the Black Sea and the Caspian Sea appear to

be substantially lower than the modern to Pleistocene oceanic values (Figure 1.10). The $^{87}Sr/^{86}Sr$ of three major fluvial sources of the Black Sea, measured for the Danube, and estimated for the Don and Dnieper (Palmer and Edmond, 1989), have values lower than both, the oceanic ratio and one existing measurement of modern Black Sea water (Cox and Faure, 1974). The Caspian Sea has main fluvial discharge from Volga, Kura, and Ural. Although dominated by Volga river signal, the Caspian Sea has a $^{87}Sr/^{86}Sr$ reflecting a mixture of all these fluvial sources (Clauer et al., 2000). Given that the $^{87}Sr/^{86}Sr$ of a basin is simply a product of the input and mixing of different water sources (Albarède and Michard, 1987; Ingram and Sloan, 1992; Reinhardt et al., 1998), the variation in $^{87}Sr/^{86}Sr$ of the basin reflects the variation in its water sources. These changes can be preserved in the shells of calcareous organisms living in the water.

Strontium is chemically similar to calcium and is therefore easily incorporated in the carbonate crystal lattice. Unlike oxygen and hydrogen isotopes, the uptake of Sr by biogenic precipitates occurs at geochemical equilibrium with the water, as such they preserve the $^{87}Sr/^{86}Sr$ of the basin water unaltered by phase change, any local temperature variation or biological processes (Banner, 2004; Reinhardt et al., 1999). Consequently, the $^{87}Sr/^{86}Sr$ measured on fossil carbonate from two (or more) sub-basins can be used to trace changes in input sources as the connectivity between basins changes. At its simplest, the $^{87}Sr/^{86}Sr$ record of the basins will show similar values during periods of connectivity, whereas the $^{87}Sr/^{86}Sr$ record of the two basins will diverge from each other and adjust to their cumulative fluvial signal during periods of isolation. It is this direct response to connectivity and isolation that makes Sr isotopes a powerful connectivity tool. This, however, requires an independent age model for each basin to constrain the timing and duration of these events.

1.5.3.3 Existing geochemical records of connectivity

The geochemical evidence of the connectivity between the Black Sea, the Caspian Sea and the open ocean is limited. The only high-resolution and continuous record is from the Black Sea for the last 30 ka (Bahr et al., 2008; Major et al., 2006). Very few data are available for strontium, oxygen and hydrogen isotopes prior to the last glacial period. Where these recods are available, they are fragmented, focus on very short time frames and are mostly from the Black Sea. Here, I synthesise the available geochemical data that underpins the existing connectivity history of the Black and Caspian seas since the Miocene.

1.5.3.3.1 Connectivity record during the Miocene

Grothe (2016) produced an $^{87}Sr/^{86}Sr$ record for the Black Sea and the Caspian Sea between 6.2 - 5 Ma to investigate the connection between the Black Sea, Caspian Sea and the Mediterranean prior to and during the Messinian Salinity Crisis (MSC; Figure 1.7D). Before 6.1 Ma, measured Sr isotopic ratios from the Black Sea and the Caspian Sea are similar but are substantially lower than Mediterranean Sea ratios which are close to or within error of coeval ocean water values (Figure 1.7, Flecker et al., 2015, and references therein). Similarity in the $^{87}Sr/^{86}Sr$ indicates the Black and Caspian seas were a single basin prior to 6.1 Ma and their dissimilarity with the coeval ocean water value suggests that Pontocaspian region was not connected to the Mediterranean Sea and the open ocean (Grothe, 2016). One high $^{87}Sr/^{86}Sr$ data only from the Caspian Sea 6.1 Ma may indicates a brief connection to the open ocean (Figure 1.7D). This geochemical evidence of marine influx is supported by ostracod biostratigraphy (Krijgsman et al., 2010; Stoica et al., 2013). There are no $^{87}Sr/^{86}Sr$ data from the Black Sea at the time to ascertain whether the Caspian Sea's connection to the open ocean was via the Black Sea. The Black Sea connection to the Mediterranean at about 6.1 Ma, however, is supported by compound specific hydrogen isotopes measured in the aquatic biomarkers (Vasiliev et al., 2015) collected from the Black Sea. The hydrogen isotope record in the Black Sea decreases sharply and reaches the typical present-day ocean values at ~6.1 Ma, indicating an influx of marine water with lower hydrogen isotopic composition into the Black Sea (Vasiliev et al., 2015).

The decreasing $^{87}Sr/^{86}Sr$ of the Mediterranean Sea (Figure 1.7D, Flecker et al., 2015; Roveri et al., 2014) during the MSC indicate progressive disconnection from the open ocean. Based on the concurrent increasing trend observed in the $^{87}Sr/^{86}Sr$ record of the Black Sea and the Caspian Sea, Grothe (2016) suggests progressive connectivity between the Mediterranean and the combined Black-Caspian Sea basin throughout the MSC. However, time equivalence of the MSC stage 2 and 3 is not available in the Black Sea due to hiatus in the key Black Sea section.

The $^{87}Sr/^{86}Sr$ data available during the Lago Mare period at the end of the MSC are only from the Caspian Sea (Figure 1.7D, Grothe, 2016). The Caspian data show values similar to those of the Mediterranean, which had brackish - freshwater salinities during this time (McCulloch and De Deckker, 1989; Müller and Mueller, 1991). There is also evidence of faunal exchange between the sub-basins of Paratethys and the Mediterranean (Cosentino et al., 2007; Londeix et al., 2007; Rouchy et al., 2001; Stoica et al., 2016), therefore implying a connection between the

Mediterranean, Black and Caspian seas during the Lago Mare. Finally at the onset of Pliocene, the Mediterranean Sr isotopic values adjusted back to the ocean water values indicating its reconnection to the open ocean. The Black Sea value suggests that its connection to the Mediterranean Sea was severed at approximately the same time (Figure 1.7D). No data are available for the Caspian Sea.

1.5.3.3.2 Connectivity record over the last 3 Ma

van Baak et al. (2019) generated a Caspian Sea $^{87}Sr/^{86}Sr$ record (Figure 1.7D) for the Pliocene - Pleistocene boundary (3.2 - 2 Ma). There are no coeval data from the Black Sea for this period. Based on the low values prior to 2.7 Ma, van Baak et al. (2019) suggested that the Caspian Sea was an isolated basin dominated by local rivers. The rapid increase in Sr isotopic ratios at 2.7 Ma and subsequent stabilisation of Sr isotopic ratios that are consistent with LGM Black Sea has been attributed to progressively connection between the Black Sea and the Caspian Sea during this period with an additional source of radiogenic $^{87}Sr/^{86}Sr$ from the open ocean (van Baak et al., 2019). Given that sediments of this age also contains cold water foraminifera, these authors suggests that the ocean water derived from the Arctic via a marine connection with the Caspian Sea, consistent with genetic studies of Caspian Seals and crustaceans (Palo and Väinölä, 2006).

The only long connectivity record in the region is a speleothem oxygen isotopic covering the last 700 ka (Badertscher et al., 2011). The speleothem was obtained from the Sofular Cave, located 10 km from the southern coast of the Black Sea (Figure 1.7C). Badertscher et al. (2011) correlated the evolution of the $\delta^{18}O$ of the Sofular Cave with the $\delta^{18}O$ of the Black Sea and suggest that -8.5‰ is the characteristic $\delta^{18}O$ value for the Black Sea when it is connected to the Mediterranean Sea. The Sofular Cave $\delta^{18}O$ record shows twelve episodes when the values are close to or surpasses $\delta^{18}O$ of -8.5 ±1‰ (Figure 1.7C), interpreted as twelve separate connectivity episodes between the Black Sea and the Mediterranean Sea (Badertscher et al., 2011). These authors also interpret $\delta^{18}O$ excursions towards isotopically depleted values of -15‰ or lower as reflecting inflow from the Caspian Sea and identify six separate episodes of Caspian overspill into the Black Sea (Badertscher et al., 2011).

A $^{87}Sr/^{86}Sr$ record from the Black Sea between 133.5 and 122.5 ka shows that the Black Sea connection to the Mediterranean Sea during the Eemian was most likely at 128.1 ± 0.7 ka based on the deviation of the Black Sea's $^{87}Sr/^{86}Sr$ towards coeval oceanic value (Figure 1.7B, Wegwerth et al., 2014). These authors suggest that the increased $^{87}Sr/^{86}Sr$ observed in the Black Sea during

the 131.5–130.5 ka reflects an increased influx from the Amu Darya river during the deglaciation entering the Caspian Sea and finally connecting the Black Sea with the Caspian Sea via Manych depression. This interpretation assumes that the Amu Darya has a radiogenic $^{87}Sr/^{86}Sr$ as a result of its source catchment in the Himalayas (Palmer and Edmond, 1989). However, there are no Caspian Sea $^{87}Sr/^{86}Sr$ from this time period or $^{87}Sr/^{86}Sr$ data for the Amu Darya to test this hypothesis.

Currently, the Black Sea is connected to the Mediterranean Sea via the Marmara Sea and the strontium isotopic ratio of the present-day Black Sea is 0.7093 (Cox and Faure, 1974), much higher than the oceanic ratio (0.709175, McArthur et al., 2012). However, this value is based on only one measurement. The strontium isotopic record for the last 30 ka shows that the Black Sea was an isolated basin during the Last Glacial Maximum (Figure 1.7A, Major et al., 2006). This is consistent with the oxygen isotopic record from the western Black Sea (Bahr et al., 2006, 2008; Major et al., 2006) during the time. Increased $^{87}Sr/^{86}Sr$ along with the depleted (negative) $\delta^{18}O$ during the last termination (18 – 16 ka) has been suggested to result from increased freshwater input into the Black Sea, either from the northern Black Sea rivers or Caspian Sea overspill caused by high melt water delivered via the Volga or northern Black Sea rivers (Bahr et al., 2006, 2008; Major et al., 2006). The final shift of the $^{87}Sr/^{86}Sr$ and $\delta^{18}O$ in the Black Sea towards the present-day values at 9.4 ka marks the most recent connection of the Black Sea to the open ocean. However, there are studies conducted in the Black Sea that provide slightly different timings for the last Black Sea-Mediterranean connection. For example, Ryan (1997) suggests ~7.1 ka for Black Sea - Mediterranean connection based on erosional surfaces in the Black Sea, Aksu et al. (2002) suggests ~10.5 ka based on micropaleontology and stable isotope data from the Aegean Sea, Marmara Sea, and south-western Black Sea, Bahr et al. (2006, 2008) suggests 8 – 9 ka based on stable isotope and XRF data from the western Black Sea (Figure 1.7A) and Piper and Calvert (2011) suggests ~9.3 ka connection based on elemental geochemistry. These disagreements between the studies arise due to the use of different age models (Krijgsman et al., 2019, and references therein).

Although, there is a clear scientific interest in reconstructing the connectivity history of the Black Sea and the Caspian Sea, the available geochemical records are fragmented and often contradictory as a result of both, methods and age models. In addition, these record are usually only available for one basin. The interpretation of these records is further hampered by the poor constraints on the modern hydrologic and geochemical system. Very little is known regarding the spatial variability of the modern water (for example there is only one $^{87}Sr/^{86}Sr$ for the modern Black Sea water)

and there are no isotopic measurements of the key rivers (e.g. Don, Dnieper and Amu Darya). Consequently, to understand the connectivity history in the region, better constraints on modern water and rivers, complete record from both Black and Caspian seas with independent age model and better quantification on the nature of the connection between the Black Sea, Caspian Sea and the open ocean is required.

1.6 Research questions

There are two main aims of this thesis; 1) constraining the Sr isotopic characteristic of modern inputs to the Black Sea and the Caspian Sea to test the existing assumptions and 2) reconstructing the connectivity history of the Black and the Caspian Sea for the last 3 million years.

1.6.1 Constraining modern input sources of Sr in the Black and Caspian seas and testing existing assumptions about Sr isotopes in marginal and freshwater basins

Although there have been several previous studies that used $^{87}Sr/^{86}Sr$ on fossil ostracods as a palaeoenvireonmental proxy and to reconstruct the connectivity history, the effectiveness of the methodology depends on the basin water being homogeneous with respect to Sr isotopic ratio. This is particularly important for marginal basin settings with significant continental run-off. At present, the Black and Caspian seas have complex hydrodynamic settings (Section 1.4.1 and 1.4.2). However, there are no empirical studies demonstrating homogeneous behaviour of Sr isotopes in either of these basins or the reliability of ostracods for incorporating and preserving the primary water signal in such settings. The first aim of this thesis is, therefore to test existing assumptions about Sr isotopic ratio in the Black and Caspian seas by generating more Sr isotopic data for the region. This allows me to examine the spatial distribution of Sr isotopic ratio in these basins as well as their fluvial sources. More explicitly, this thesis will try to answer the following questions;

1. Is the strontium isotopic signal in the Black and Caspian seas spatially homogeneous?
2. Does the strontium isotopic signal in the Black and Caspian seas vary with water depth? What influence does the density stratification have on Sr isotopic variability in the water column?

3. Are fossil ostracods a robust archive for preserving the primary $^{87}Sr/^{86}Sr$ of ambient water in the Black and Caspian seas?

1.6.2 Reconstruction of the connectivity history between the Black Sea, Caspian Sea and the open ocean for the last 3 Ma

Evidence for connectivity and isolation of the Black Sea, Caspian Sea and the open ocean are fragmented, sparse and often contradictory (Section 1.5). The available palaeontological evidence of the connectivity between the Black Sea and the Caspian Sea is typically low resolution and provides no clear boundary between connection and isolation events (Section 1.5.1). Similarly, the timings of the connection between the Caspian Sea and the Arctic Ocean, which resulted in the presence of several Arctic sister species in the Caspian Sea is highly debated. Although Sr isotopic data are a more direct means of reconstructing connectivity of basins like today's Pontocaspian system, there are no Sr isotopic data available for most of the Pleistocene (Figure 1.7), during which there were large climatic variations associated with high amplitude glacial interglacial cycles and the active uplift of the Caucasus Mountains. Without records that allows us to disentangle both the drivers and timing of the connection and isolation events, it is not possible to determine the rate of faunal evolutionary response (Section 1.5.2). This thesis will try to address the following questions.

4. Does the geochemical system suggest a Caspian connection to the Arctic Ocean and if so, when did this connection occur?

5. How did the Sr isotopic ratio evolve in the Black and Caspian seas over the last 3 million years and what is its implication for the Quaternary connectivity history of the two basins to each other and the open ocean?

6. What was the nature of connection (one way flow or two way exchange) between the Black Sea, Caspian Sea and the open ocean during the Pleistocene?

7. Does the geochemical evidence of the connectivity and isolation between the Black Sea, Caspian Sea and the open ocean match the faunal evidence?

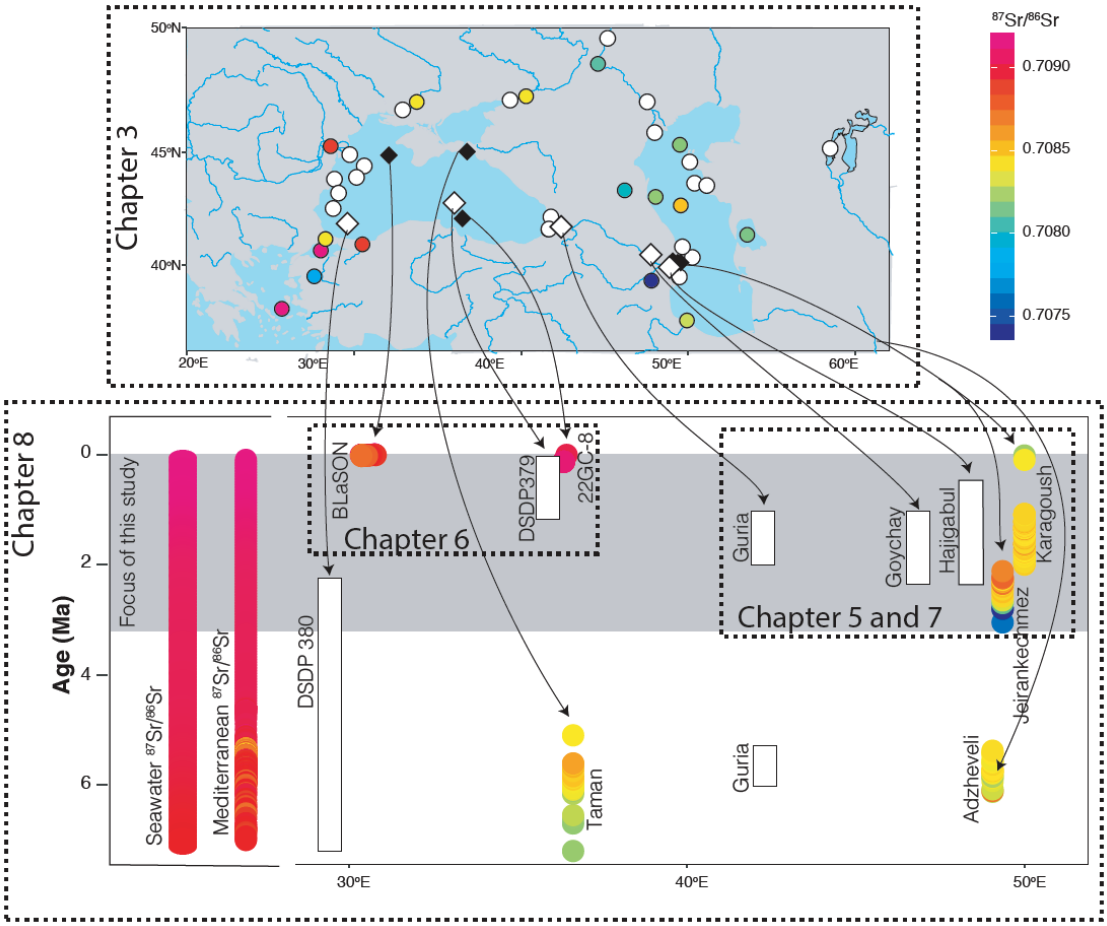

FIGURE 1.11: Map of the Black Sea and the Caspian Sea showing location of previously published Sr isotopic ratio of water (coloured dots) and fossil carbonates (black diamonds). White dots (water) and white diamonds (fossil ostracods) represent the sampling locations for this study. Bottom panel shows the previously published Sr isotopic record for the open ocean, Mediterranean Sea, Black Sea and the Caspian Sea over the last 7 Ma. Grey shaded area shows the time slices focused in this study. Colour gradient at the top right hand side of the diagram indicates the range of $^{87}Sr/^{86}Sr$ measured to date.

1.7 Thesis outline

This thesis consists of eight chapters. The general background, thesis motivation and the research questions are presented here as Chapter 1. Chapter 2 provides information regarding samples, sampling locations, and the analytical method used during the project to produce Sr isotopic data.

Chapter 3 explores the assumption of basin homogeneity with respect to strontium isotopes in highly stratified, marginal marine or isolated lacustrine systems. This chapter will include the Sr isotopic analysis of the Black and Caspian seas and river water samples from across the region (Figure 1.11). This chapter also explores the robustness of ostracods as palaeo archives of the $^{87}Sr/^{86}Sr$ by comparing $^{87}Sr/^{86}Sr$ measured in ostracods collected from modern sediment with the

$^{87}Sr/^{86}Sr$ of the bottom water at the same sites in both Black Sea and the Caspian Sea. The new $^{87}Sr/^{86}Sr$ measurements from the modern water is then incorporated in the numerical box model to constrain the fluvial signal of the region.

Chapter 4 provides descriptions of the numerical model used in this study and of Sr source end members in the region. This chapter also tests the validity of the model for the present-day configuration. The model described in this chapter is then adapted in subsequent results chapters to constrain the past hydrological budget of the Black Sea and the Caspian Sea and to explain the $^{87}Sr/^{86}Sr$ measured on fossil ostracods.

Chapter 5 presents $^{87}Sr/^{86}Sr$ records of the Caspian Sea during the early Pleistocene (Figure 1.11) and discusses their implications for the connectivity between the Caspian Sea and the Arctic Ocean.

Chapter 6 presents the $^{87}Sr/^{86}Sr$ record of the Black Sea during the last 1.2 Ma (Figure 1.11) and discusses the connectivity history between the Black Sea, the Mediterranean Sea, and the Caspian Sea during this interval.

Chapter 7 presents additional new Sr isotopic record from the Caspian Sea between 2.2 Ma to ~200 ka and together with the $^{87}Sr/^{86}Sr$ record from Chapter 6 discusses the Pleistocene evolution of the Black and Caspian seas.

Chapter 8 provides a synthesis of the all $^{87}Sr/^{86}Sr$ records produced during this project (including data used in Chapter 5, 6 and 7) together with the previously published geochemical, faunal, phylogenetic data (Section 1.5) to reconstruct the connectivity history of the Pontocaspian region over the last 3 Ma. This chapter also provides the key findings from this study and answers the research questions posed in Section 1.6.1 and 1.6.2.

Chapter 2

Methodology

This chapter describes the sampling locations, materials and methods used in this study. First I focus on the sampling sites and methodology for collecting both present-day water samples and modern and fossil ostracods. Detailed descriptions of the chemical procedures and measurement techniques employed to obtain the results is described next. Finally, this chapter concludes with a table that lists additional datasets used in the result chapters.

2.1 Sampling sites and sample collection

In order to constrain the $^{87}Sr/^{86}Sr$ of modern water and to test spatial variability (Section 1.6.1) water samples from across the Black and Caspian seas region and within the basins were required (Figure 1.11). Sampling locations were selected to cover a wide horizontal and vertical range within the basin. This was however restricted by availability of offshore cruises as well as cruise tracks. When possible, river water samples were collected at both, the mouth as well as upstream of the river. Logistical difficulties prevented sampling full length of the rivers.

In order to reconstruct the connectivity history of the Black and the Caspian seas during the Pleistocene (Section 1.6.2), well-dated fossil samples from both basins were required (Figure 1.11). It was not in the scope of this project to generate age models. Sedimentary sections/cores from the region were therefore, only selected for sampling if an age model independent of faunal dating method was available or would be generated during the course of the PRIDE project. Given the complex connectivity history of the Black Sea and the Caspian Sea, a high resolution study is required. However, the scope of this study was to generate longer time scale connectivity history

and as such compromise was made regarding the resolution of the data. It is acknowledged that in doing so, finer details of the Black Sea, Caspian Sea connectivity history will be missed.

2.1.1 Present-day water and modern sediment

2.1.1.1 Sampling locations

Black Sea river-water samples were collected from the Dnieper, Don, Rioni and other minor rivers along the coast of Georgia (Figure 2.1, Table 2.1). Black Sea water samples were collected in the eastern Black Sea along the coast of Georgia from the beach. Water samples were also collected offshore along the coast of Romania and Bulgaria in the western Black Sea (Figure 2.1) during the GeoEcoMar cruise MN167 on the *Mare Nigrum* in May 2017. Caspian river water samples were collected from Kura and Volga (Figure 2.1). Offshore Caspian Sea water samples were collected during a cruise off the Kazakhstan coast onboard the KAPE research vessel, *Elen*, in June 2017. The Aral Sea water samples were collected by Dr. Georg Schettler, GFZ, Germany in 2009 (for sampling method see Schettler et al., 2013).

Wherever possible, surface sediment samples were collected from the same Black and Caspian sea locations as the water samples. These sediment samples were collected for modern ostracods.

2.1.1.2 Water samples

All river surface water samples were collected within a few metres of the riverbank. During the *Mare Nigrum* cruise, Black Sea water samples were collected from the surface and, in some cases, intermediate depths using CTD rosette. Bottom water was collected immediately above the sediment surface using a multi corer (Mark II-400). In the Caspian Sea, surface water samples and samples from ~20 m depths were collected using a single Niskin bottle. Logistical difficulties prevented from collecting water sample more than 20 m water depth. *In situ* temperature and conductivity measurements were obtained when suitable meters were available. This was possible for the offshore water samples collected from research vessels. However, hand held probes were not available during most of the river water sampling.

Prior to the fieldwork, all equipment was acid cleaned and wrapped securely with parafilm and/or cling film for transportation to the field site. At the sampling site, beakers used for sample collection

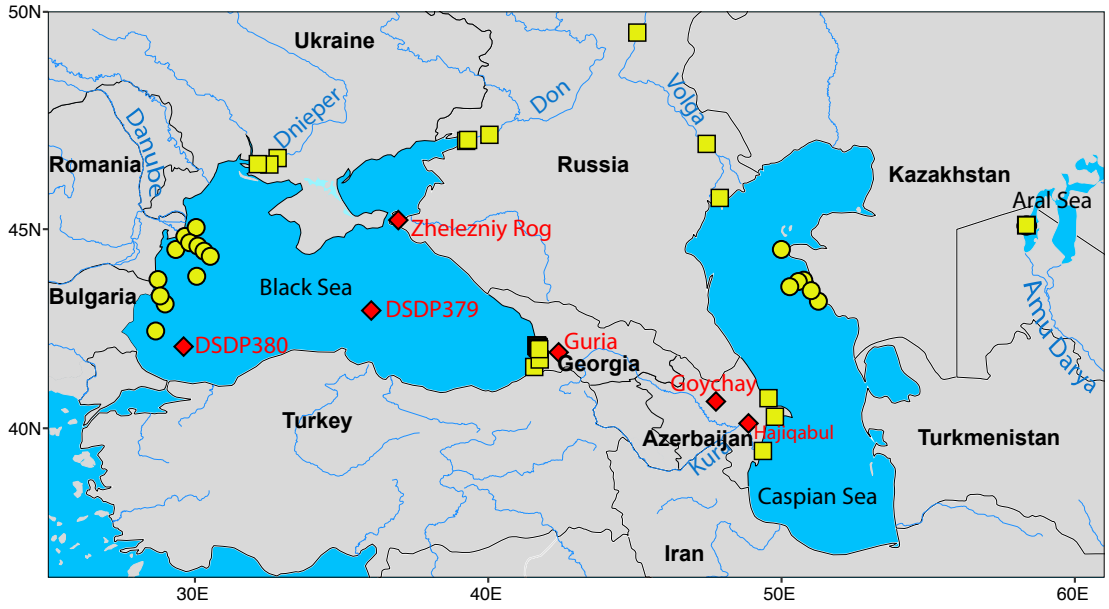

FIGURE 2.1: Location map of the sampling sites in the Black Sea and the Caspian Sea with major river represented by blue lines. Yellow dots show offshore locations for water and modern sediment samples (Table 2.1), yellow boxes show locations where only water samples were collected and red diamonds show section and core locations studied in this project (Table 2.2). Black lines define the country boundaries.

were rinsed multiple times with the sample water prior to sample collection. Syringes and filter tips were also rinsed three times with pure deionized water (>18.2 MΩ) and once with the sample water, prior to collection. For water sample filtration, 0.45 μm pore size filters were used.

At each location, 50 ml of water was filtered through the 0.45 μm pore size sterile MCE (mixed cellulose ester) filter and was collected in an acid-cleaned HDPE centrifuge tube. The samples were acidified with a few drops of high purity nitric acid, gently shaken to homogenize and sealed with parafilm before transportation. Once in the laboratory, the water samples were stored at 4°C until further analysis.

2.1.1.3 Modern sediment samples

A Van Veen Grab Sampler was used to collect sediment from offshore Black Sea and the Caspian Sea water sampling sites. Once onboard the research vessel, about 50 g of sediment was taken from the top 2 cm at each location and collected in pre-labelled zip-lock plastic bags for transportation. Sediment samples were stored at 4°C until further analysis.

TABLE 2.1: Latitude and Longitude of all the sampling sites for water and modern ostracod samples shown in Figure 2.1. Location, water depths, temperature and salinity for each samples are included in Appendix G.

Sample type	**Location**	**Country**	**Latitude [N]**	**Longitude [E]**	**No. of samples collected**	**No. of samples analyzed**
Water	Black Sea	Along the coast of Romania & Bulgaria			66	30
Modern ostracod	Black Sea	Along the coast of Romania & Bulgaria			24	10 (6 locations)
Water	Black Sea	Along the coast of Georgia			8	8
Water	Caspian Sea	Along the coast of Kazakhstan			43	12
Modern ostracod	Caspian Sea	Along the coast of Kazakhstan			26	12 (6 locations)
Water	Caspian Sea	Along Absheron peninsula in Azerbaijan			3	3
Water	Azov Sea	Russia	47.08833	39.24778	3	1
Water	Aral Sea		45.08334	58.33631	20	5
Water	Dnieper River	Ukraine	46.53733	32.53658	4	3
Water	Don River	Russia	47.11027	39.31222	4	2
Water	Chorokhi River	Georgia	41.60472	41.57611	2	2
Water	Natanebi River	Georgia	41.91167	41.77833	2	2
Water	Rioni River	Georgia	42.1975	41.6622	1	1
Water	Enguri River	Georgia	42.39319	41.56089	1	1
Water	Pichori River	Georgia	42.13711	41.75948	1	1
Water	Palliastomi Lake	Georgia	42.0929	41.70799	2	2
Water	Supsa River	Georgia	42.02139	41.75333	1	0
Water	Kura River	Azerbaijan	40.1203	48.0853	2	1
Water	Volga River	Russia	45.59962	47.90989	9	3

2.1.2 Fossil ostracods

In order to reconstruct the connectivity history of the Black Sea and the Caspian Sea over the last 3 Ma, sediment samples were obtained from four different locations in the Black Sea; two sections in Guria, Georgia and two DSDP cores (Figure 2.1). For the Caspian Sea, sediment samples were collected from the Goychay and Hajigabul sections in Azerbaijan. Sampling location are provided

in Figure 2.1 and Table 2.2.

TABLE 2.2: Latitude and Longitude of all the geological sections from which fossil ostracods were picked. Location are shown in Figure 2.1.

Location	**Section**	**Latitude [N]**	**Longitude [E]**	**No. of samples collected**	**No. of samples analyzed**
Guria, Georgia	Khaverbeti	41.95361	41.91417	37	16
Guria, Georgia	Tsikhisperdi	41.960	41.94083	12	8
Black Sea	DSDP 379	43.00483	36.01133	93	72
Black Sea	DSDP 380	42.0990	29.61367	17	3
Taman	Zhelezniy Rog	45.11513	36.76076	12	12
Azerbaijan	Goychay	40.69628	47.76239	107	78
Azerbaijan	Hajigabul	40.12703	48.87269	200	23

2.1.2.1 Guria (Khaverbeti and Tsikhisperdi sections), Black Sea

Two lithological sections in the Guria region, which is located in the western part of Georgia within the Rioni basin, were studied in this project; Khaverbeti section and Tsikhisperdi section (Figure 2.1, Table 2.2). The Khaverbeti section spans about 166 m and is divided into three main parts (Figure 2.2, Kirscher et al., 2017). The bottom of the section consists of fine grained sandstones with calcareous fossils, the middle part consists of marly intervals with rare fine grained sandstone levels and is overlaid by calcarenitic sandstones with abundant microfauna at the top (Figure 2.2). The Tsikhisperdi section, which lies stratigraphically below Khaverbeti section, is about 10 m thick and is a succession of calcarenites and mudstones with abundant fauna (Figure 2.2).

Sampling fieldwork was conducted in October 2016 but showed that parts of the Khaverbeti section were difficult to access as they were covered with heavy vegetation of Gurian lowlands. A fragmented sedimentary log was constructed and samples were selected on the basis of fine grained lithology and/or presence of macro fauna (e.g. molluscs and gastropods). For the correct correlation with existing log, samples were also taken close to previously sampled sites for palaeomagnetic measurements (Kirscher et al., 2017). A total of 49 sediment samples were collected in Guria (Khaverbeti and Tsikhisperdi sections) and of these, 24 samples were analysed for Sr isotopic ratio (Figure 2.2).

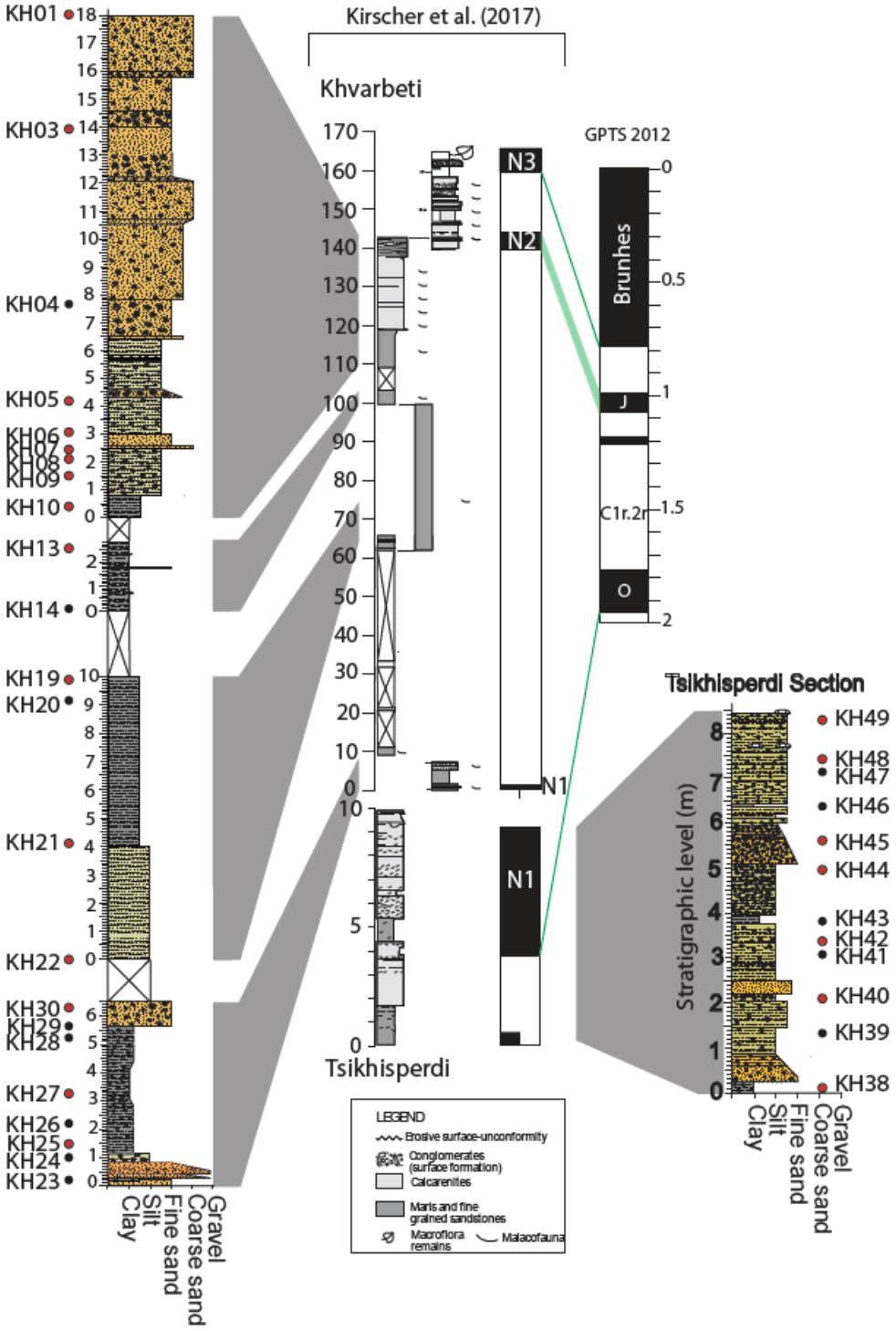

FIGURE 2.2: Correlation of sedimentary log generated in this study with Kirscher et al. (2017) for the Guria sections. Sampled stratigraphic levels are indicated by dots (red: analysed for $^{87}Sr/^{86}Sr$ and black: not analysed). B: Brunhes, J: Jaramillo, O: Olduvai.

The palaeomagnetic age model for the Guria section was produced by Kirscher et al., 2017. The sections were interpreted as indicating Pleistocene age that includes the lower most part of the Brunhes chron as well as the Matuyama chron including the Jaramillo and Olduvai normal

polarity subchrons. Ages of the samples picked for ostracods were calculated assuming constant sedimentation rate between chron boundaries. The upper boundary of the Olduvai was not reached in the Tsikhisperdi section and as such age estimation for individual samples based on sedimentation rate was not possible for this section. Samples taken from the stratigraphic level that correlates with the base of the Olduvai subchron, allows for tentative age estimation of around 2 Ma for samples collected from this section.

The Pleistocene age interpretation of the Guria section based on the palaeomagnetic data has been recently cast into doubt by unpublished data based on ostracod assemblages, which suggests that the this sedimentary succession may be as old as the Late Miocene age (see Chapter 8 for details).

2.1.2.2 DSDP 379A and 380/380A, Black Sea

Deep Sea Drilling Project (DSDP) samples used in this study are from two cores (379A and 380/380A) collected during DSDP Leg42B in 1975. DSDP site 379A was drilled on the abyssal plain of the central Black Sea, at a water depth 2165 m (Figure 2.1, Table 2.2). The drilling recovered 624.5 m of sediment mainly composed of dark greenish-grey to dark grey terrigenous mud with intercalations of thin sandy silt to sand laminae (Ross et al., 1978a). The core is divided in nine units (Figure 2.3). Subunit 1 (0 - 0.3 m) consists of nannofossil ooze principally composed of the coccolith *Emiliania huxleyi*. Unit 1 was dated as Holocene on the basis of ^{14}C dating and presence of coccolith ooze (Ross, 1978). Unit 2 (0.3 – 0.7 m) is a sapropel that consists of ~40 - 50% organic matter by dry weight with occasional thin nannofossil beds and fine layers of aragonite. Unit 3 (0.7 – 65m) is dark greenish grey detrital silty clay to clayey silt (Figure 2.3). Streaks and patches of silt and fine sand and coarser sediment layers with graded bedding within unit 3 suggests occurrence of turbidity current deposits. Unit 4 (65 – 100 m) consists of a dark greenish grey to medium grey mud characterized by the first appearance of marine diatoms, foraminifera, and nannofossils after the Holocene deposits. This unit is linked to MIS 5 (Ross, 1978; Schrader, 1978). A thin layer of fresh-water diatoms during this marine period indicates a brief freshwater interval. Unit 5 consists of a 0.3 m of intensely compact sapropel layer. Unit 6 (100 - 225 m) is a dark greenish-gray terrigenous mud that resembles unit 3 with high content of clay, quartz, and detrital carbonates (Ross et al., 1978a). Diatom assemblages within this subunit suggest that the sediment was deposited in a fresh-water environment with one brief marine invasion (Schrader, 1978). Cold climate was indicated by pollen analyses, and the marine invasion is interpreted as a

short interstadial period (Ross, 1978). Unit 7 (225 – 273 m) is a diatomaceous nannofossil-rich terrigenous mud deposited under brackish marine condition in a warm climate indicated by pollen and has been linked to MIS 11 (Ross, 1978). Unit 8 (275 -553 m) and unit 9 (453 – 625.6 m) are terrigeneous mud with common occurrences of turbidities and intercalations of carbonate rich layers, respectively (Ross et al., 1978a). The palaeomagnetic measurement on core 379A together with the biostratigraphic tie points for MIS 5 and MIS 11 showed that the entire core spans around 1.2 Ma (Figure 2.3, van Baak et al., 2016a).

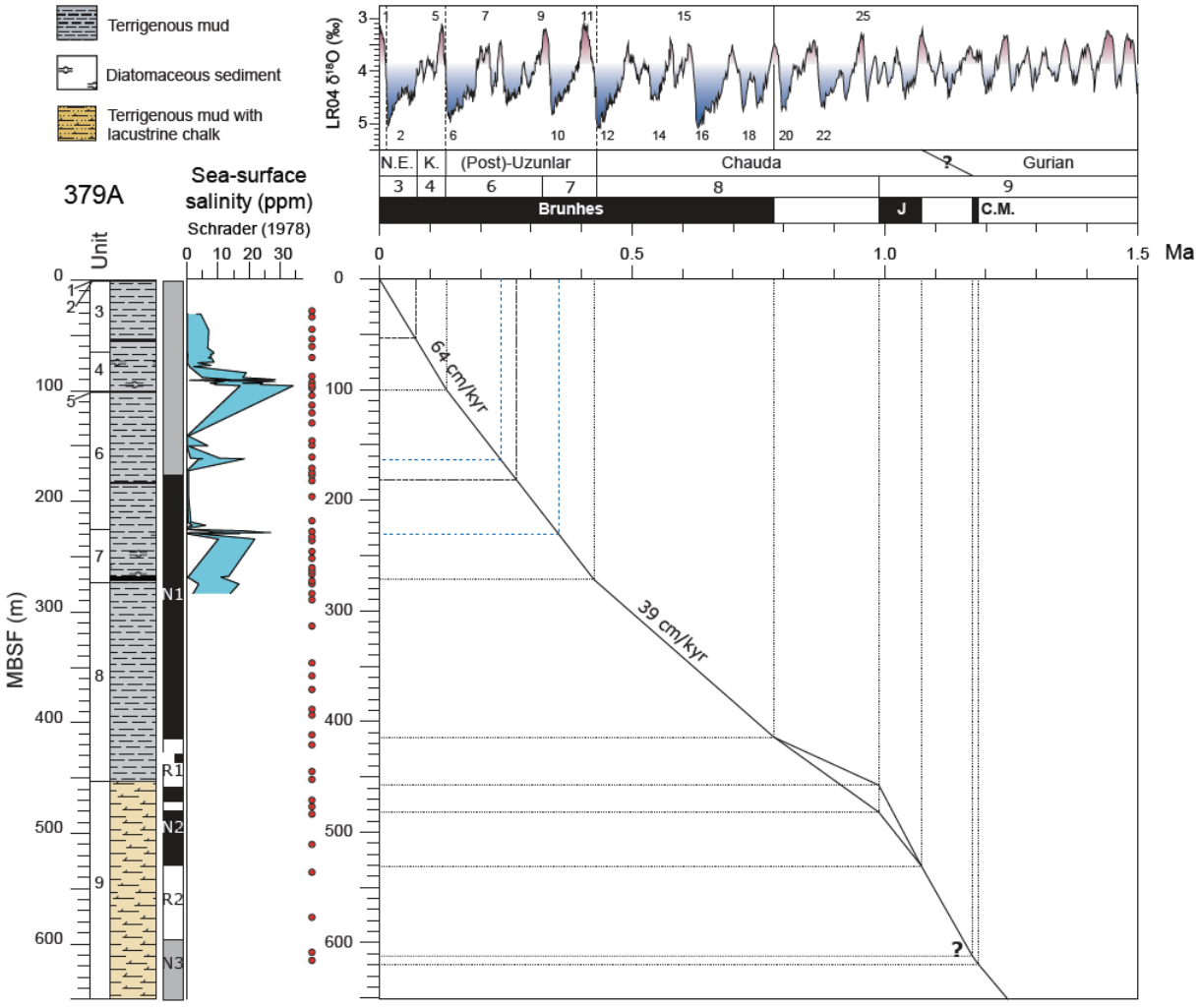

FIGURE 2.3: Age-depth correlation for DSDP core 379A with lithological units (Ross et al., 1978a), diatom-based sea-surface salinity (Schrader, 1978). Stacked δ^{18}O record of benthic foraminifera from Lisiecki and Raymo (2005). Red dots indicate the sediment sampling depth. Figure modified after van Baak et al., 2016a.

DSDP site 380/380A was recovered from near the Bosporus (Figure 2.1) at a water depth of 2107 m and maximum drilling penetration depth of 1073.5 mbsf (Figure 2.4). DSDP site 380/380A is the composite of two holes at the same location. Hole 380, drilled to 370.5 mbsf, was abandoned

because of an injury onboard (Ross et al., 1978b) and Hole 380A was drilled 100 ft south and 100 ft east of the hole 380. Hole 380A recovered sediments from 332.5 m down to 1073.5 m (Ross et al., 1978b). Five main lithological units are distinguished for the core 380/380A (Figure 2.4). Unit 1 (0 - 332.5 m) consists of terrigeneous mud correlated to Hole 379A (Ross et al., 1978b). Unit 2 (332.5 - 446.5 m) consists of intercalations of lacustrine chalk and aragonitic muds indicating isolated basin conditions and intervals of marine connection, respectively (Hsu et al., 1978). Unit 3 (446.5 - 644.5 m) represents freshwater environment indicated by lacustrine chalk and mud (Ross et al., 1978b). Unit 4 (644.6 - 969 m) represents sediments older than those found in the Hole 379A (Ross et al., 1978b) and consist of a wide variety of sediment types composed of sideritic and diatomaceous sediments, terrigeneous mud, calcite and diatoms. Coarse clastics and stromatolitic dolomite found at the bottom of the Unit 4 was originally taken as proof of the Black Sea dessication during the Messinian Salinity Crisis (MSC, Hsu and Giovanoli, 1979). However, based on dinoflagellate cysts Grothe et al. (2014) recently suggested older than the MSC age for this deposit. Unit 5 (969 - 1073.5 m) is mostly black shale with tuffaceous and zeolitic siltstones and sandstones (Ross et al., 1978b). Seismic studies in the southwestern part of the Black Sea indicate two large mass transport deposits (Tari et al., 2015), which can be correlated to 114 - 260 mbsf and 500 - 640 mbsf (or 560 - 860 mbsf) in Hole 380A (Tari et al., 2015; van Baak et al., 2016a).

The palaeomagnetic age for core 380/380A was generated by van Baak et al. (2016a) showed that the core spans the last 8 Ma of Black Sea sediment history. However, because of the mass transport complex in this core (Figure 2.4), the correlation to the Geomagnetic Polarity Time Scale (GPTS) is difficult and multiple age interpretations are possible. ^{40}Ar/ ^{39}Ar dating on an interbedded volcanic ash-layer at 706 m, however provides an absolute tie-point at 4.36 ± 0.19 Ma (van Baak et al., 2016a).

These DSDP cores are stored in the Bremen Core Repository. Total of 93 samples (40cc each) from DSDP core 379A and 17 samples from the 380A were requested from the Bremen Core Repository. Sample selection was based on fine-grained lithology, presence of ostracods, and high calcite content. Core 379A was prioritised in this study because of its continuous succession of the Pleistocene sediment and a more robust age model. Of the requested samples, 72 samples from core 379 and 3 samples from 380/380A were selected for Sr isotopic analysis. The age of individual samples are calculated assuming a constant sedimentation rate between chron boundaries.

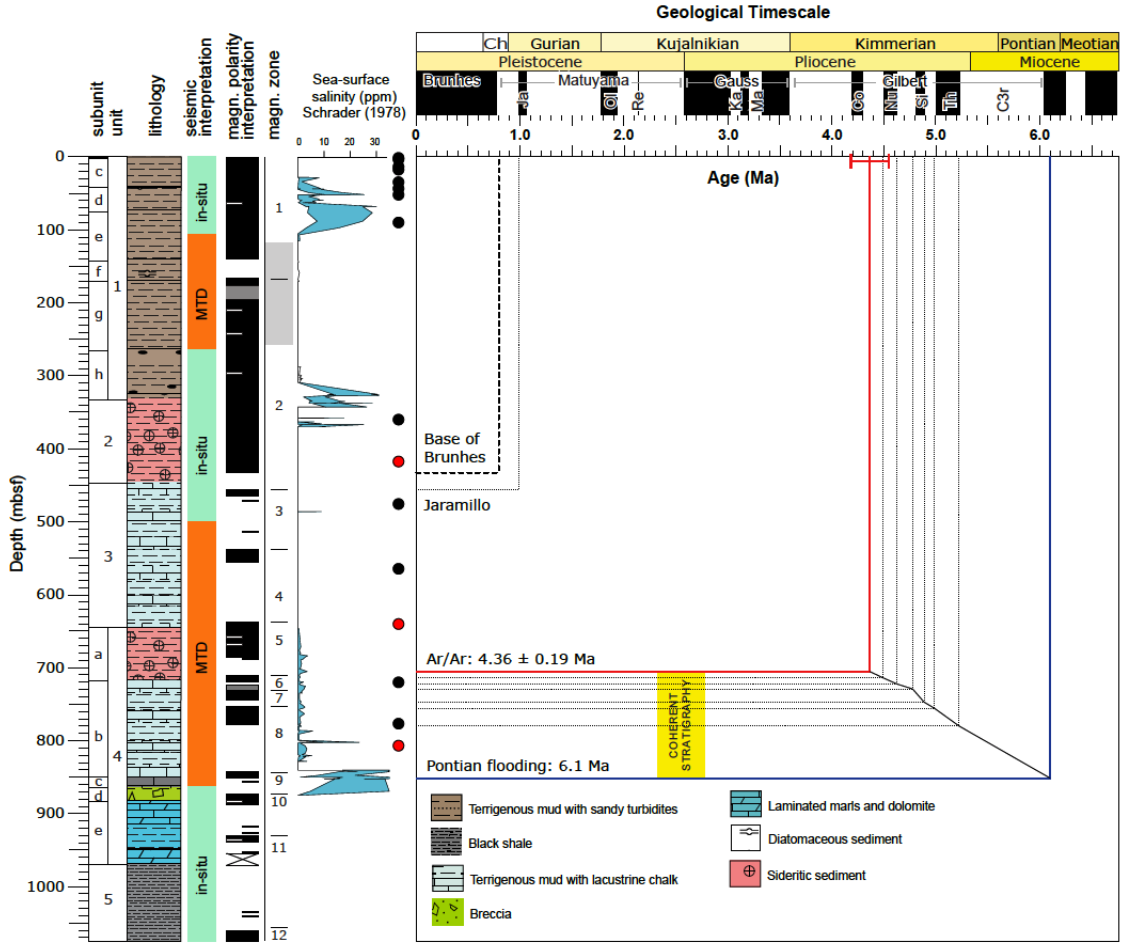

FIGURE 2.4: Age-depth correlation for DSDP core 380/380A with lithological units (Ross et al., 1978b) and diatom based sea surface salinities (Schrader, 1978). Two mass transport deposits (MTDs) within the drilled intervals (Tari et al., 2015) are indicated by orange bars. Black dots indicate sampling depth and red dots indicate samples that were analysed for Sr isotopic ratio. Figure modified after de Leeuw et al. (2018) and van Baak et al. (2016a).

2.1.2.3 Zheleznyi Rog section, Black Sea

The Zheleznyi Rog section, located in the Taman Peninsula, Russia, exposes about 500 m Neogene sedimentary succession (Figure 2.1). The section shows a clear cyclicity of dark grey clays alternating with light-gray marls with thin intercalations of diatomitic levels (Figure 2.5, Vasiliev et al., 2011). Magnetostratigraphic age constraints for the entire section was provided by Vasiliev et al., 2011 and show Late Miocene age. The section has been previously studied for Sr isotopic ratio by Grothe (2016). Even though this section is older than main temporal focus of this study, samples from this section were readily available for early laboratory training on Sr isotopic analysis. Samples used in this study were collected by Elisabeth L. Jorissen, Utrecht University for sedimentological study of the Late Miocene Black Sea as part of the PRIDE project. Twelve

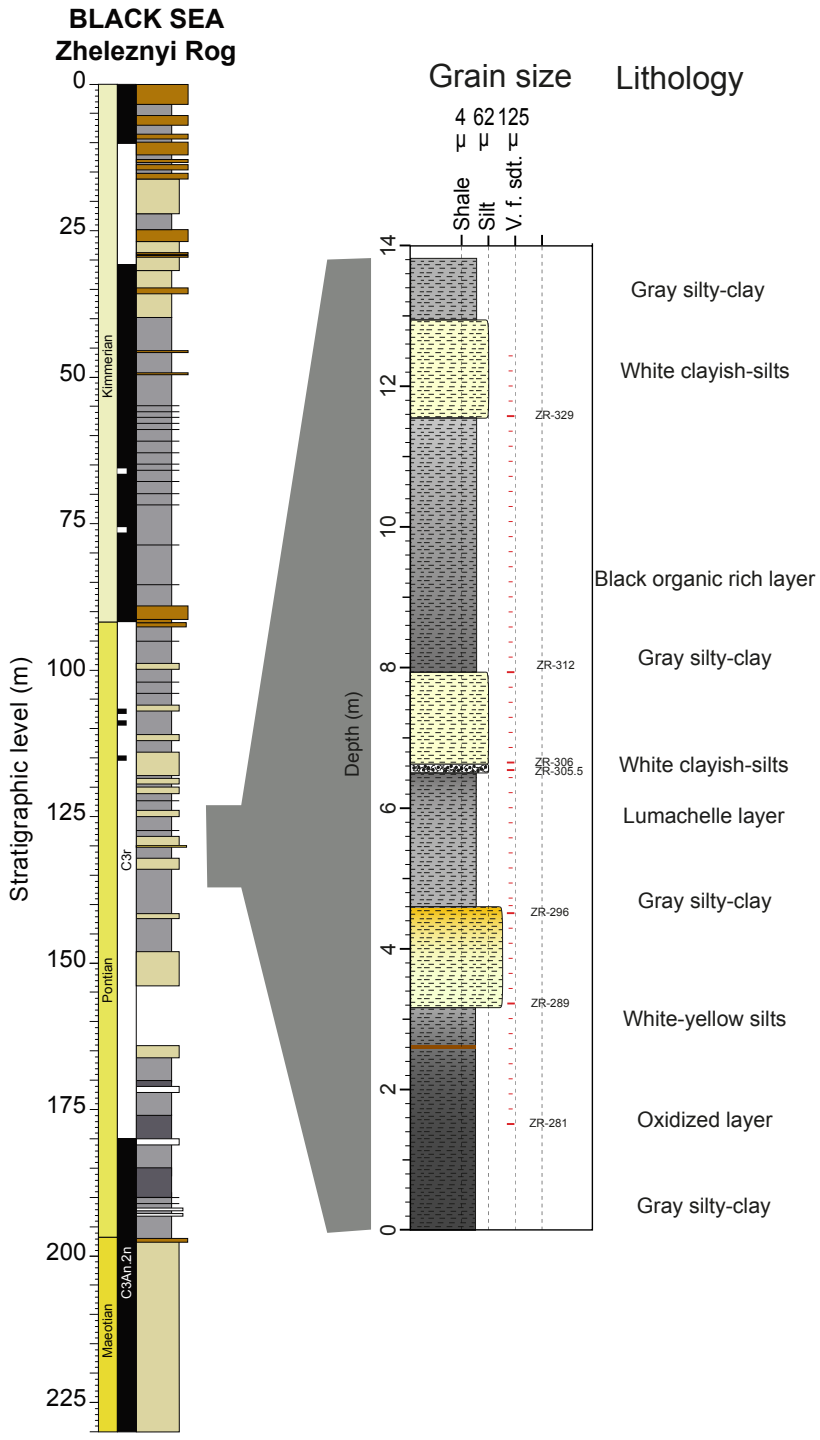

FIGURE 2.5: Detailed sedimentary log for the Zheleznyi Rog section between stratigraphic level 124 and 137 m and its correlation with longer sedimentary log by Vasiliev et al. (2011). Sampled stratigraphic levels are indicated by dots dashes.

samples between stratigraphic level 124 and 137 m were selected for Sr isotopic analysis (Figure 2.5).

2.1.2.4 Goychay section, Caspian Sea

The Goychay section is located to the west of Baku, Azerbaijan within Goychay village (Figure 2.1, Table 2.2). The 2200 m section is exposed along the Göy River. The section is characterized by three lithological units (Figure 2.6, Forte et al., 2013; Lazarev et al., 2019). Unit 1 (0 m – 675 m) consists of grey clay alternating with rare centimetre-scale layers of brownish silts and coarse sands (Forte et al., 2013; Lazarev et al., 2019). Unit 2 (675 m - 1050 m) is composed of brownish-grey muds recurrently alternating with yellowish-brown silts and conglomeratic sands with coarser and thicker sand beds towards the top (Forte et al., 2013; Lazarev et al., 2019). Unit 3 (1050 m - 2200 m) is dominated by coarse conglomerates but with occasional interbeds of both sand and finer grained intervals (Forte et al., 2013; Lazarev et al., 2019). The palaeomagnetic age model of the section constrained by micro (ostracods and foraminifera) and macro (mollusc) fauna has been produced by S. Lazarev, Utrecht University as part of his PRIDE PhD research project (Lazarev et al., 2019). The section spans 2.58 Ma to ~1.2 Ma (Figure 2.6).

Sampling fieldwork was conducted in May 2016. Few additional sediment samples was collected by S. Lazarev and E. L. Jorissen during second fieldwork in April 2017, in which I did not participate. Samples for ostracods were selected based on the fine-grained lithology and presence of macrofauna and were collected at the same stratigraphic level as palaeomagnetic drill cores. In total, 107 sediment samples were collected from the section, among which, 78 samples were analysed Sr isotopic ratio (Figure 2.6).

2.1.2.5 Hajigabul section, Caspian Sea

The Hajigabul section is located in the north-eastern part of the Kura Basin in the Hajigabul district, Azerbaijan, and is ~113 km southeast of the Goychay section (Figure 2.1, Table 2.2). The section crops out along the Hajigabul anticline, also known as the Hajigabul Mountain. The section comprises of 2035 m of stratigraphic succession and is divided into four main sedimentary units (Figure 2.7, Lazarev et al., 2019). Unit 1 (0 m - 205 m) is mostly composed of brownish fine to coarse sands with alternating yellowish-brown and reddish clays and silts (Lazarev et al.,

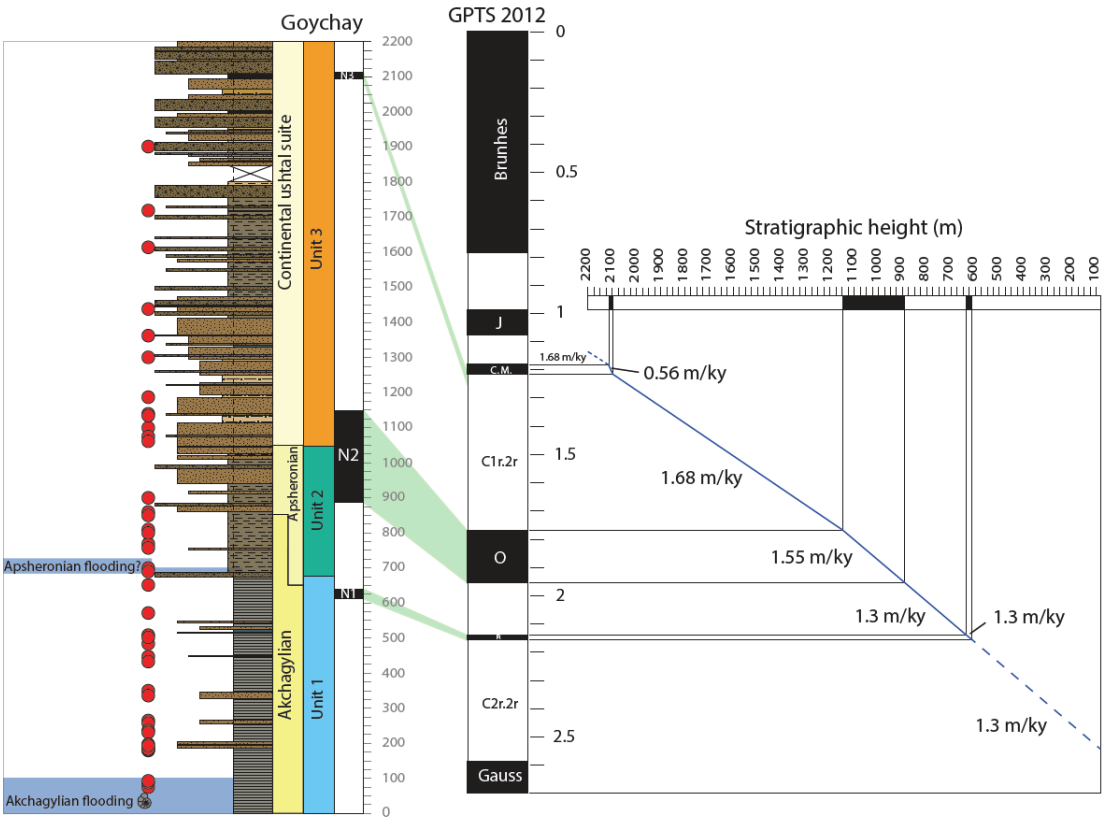

FIGURE 2.6: Age-depth correlation for the Goychay section with sampled stratigraphic levels indicated by red dots. Modified after Lazarev et al. (2019).

2019). Unit 2 (205 m – 457 m) is composed of dark grey mud with millimetre-scale horizontal laminations, made of brownish-grey mud and silts (Lazarev et al., 2019). Unit 3 (457 m - 1614 m) is composed of alternating dark-grey mud and fine to coarse-grained brownish sands. Top part of the unit 3 contains abundant molluscs (Lazarev et al., 2019). Unit 4 (1614 m- 2050 m) consists of yellowish-grey clay and silt. The palaeomagnetic age model of the section, constrained by biostratigraphy has been produced by Lazarev et al. (2019) and show that the section contains sediments deposited between 2.58 Ma and ~300 ka (Figure 2.7).

Sediment samples for ostracods from the Hajigabul section were collected by S. Lazarev and E. L. Jorissen as part of the sedimentological study, which is now in progress as part of the PRIDE. Samples selection prioritised fine grained lithology and samples were collected at the same stratigraphic level as palaeomagnetic drill cores (Lazarev et al., 2019). In total, 200 samples were collected from the Hajigabul section, among which 23 samples were analysed for Sr isotopic ratio.

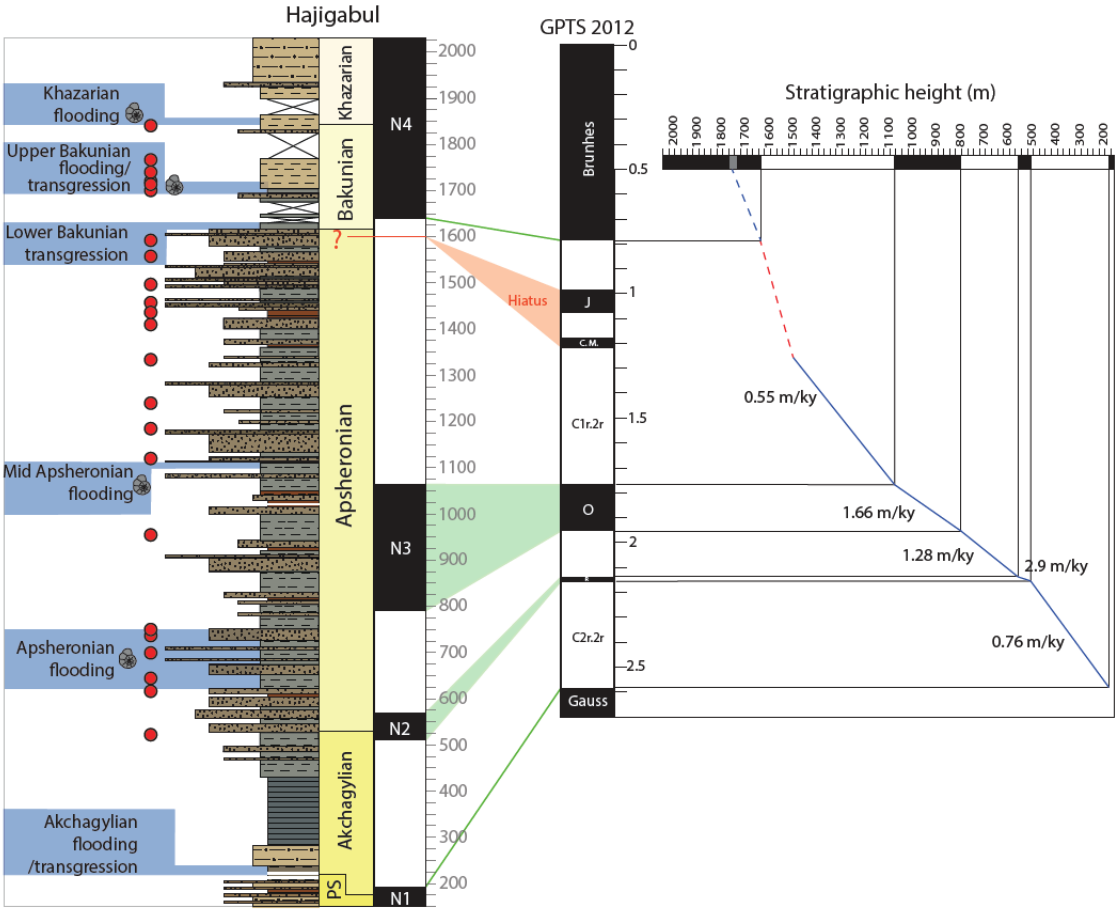

FIGURE 2.7: Age-depth correlation for the Hajigabul section with sampled stratigraphic levels indicated by red dots. Modified after Lazarev et al. (2019).

2.2 Sample preparation and analyses

All reagents used in the following procedures, except methanol, were either ultraclean quality (RomiL SpS) or produced in-house by sub-boiling distillation in a Savillex PFA jar from analytical grade. Methanol was analytical grade. MilliQ deionized water was used throughout (>18.2 2 MΩ). Hotplates used for drying samples were situated within separate chambers and supplied with filtered air to minimize contamination; no other materials or samples were allowed in the chamber during drying periods.

2.2.1 Water samples

An aliquot of 3 ml from each water sample was transferred into an acid cleaned Teflon beaker and dried down at 120°C. Once dried, a few drops of concentrated nitric acid was added to the

sample to remove any organics and dried again on the hotplate. About 500 μl of 3M HNO_3 was added to the samples and refluxed overnight prior to introducing them to chromatographic columns composed of Eichrom Technologies Sr Resin.

2.2.2 Ostracod samples (modern and fossil)

Sediment samples collected from the sections or DSDP cores were dried at 50°C for about 24 – 48 hours to remove interstitial water. This ensured easier washing and sieving. Modern surface sediments were washed without drying. All sediment samples were washed through a 63 μm sieve and the > 63 μm fraction were dried at 50°C. Prior to picking, samples were dry sieved again to retain the >150 μm fraction and ostracods were hand-picked under a light microscope using a fine paintbrush.

Whenever possible, at least 5 ostracod valves were collected in acid cleaned 2 ml pre-labelled centrifuge tubes. To minimize contamination and the effectiveness of the rigorous cleaning procedure, valves without ornamentation were preferentially selected for the analysis. Ostracod valve were rinsed three times using deionized water and subjected to 3 - 5 seconds in an ultrasonic bath after every rinse to remove any loose clay particles. Samples were then cleaned twice with methanol. If the valves were still intact, samples were subjected to ultrasonic bath again for 5 seconds between the two methanol rinses. The samples were then rinsed three times with deionized water to remove any traces of methanol. At this stage, samples were checked under the light microscope to see if there was any visible contamination. In presence of contamination, samples were washed again with deionized water until clean.

After cleaning, 250 μl of deionized water was added the centrifuge tube and topped up with 50 μl of 0.5M of HNO_3. The samples were ultrasonicated for 3 minutes. At this stage, if the valves were not dissolved completely, 50 μl of 0.5M of HNO_3 was added and ultrasonicated for another 3 minutes. Once dissolved samples were centrifuged at 12,000 RPM for 2 minutes. The solution was then carefully pipetted out into an acid cleaned pre-labelled Savillex PFA beaker and dried at 120°C on a hot plate. Once dried, a few drops of concentrated HNO_3 was added to the sample and dried again at 120°C. Samples were refluxed overnight with 520 μl of 3M HNO_3. A 20 μl aliquot was separated for elemental analysis whereas, remaining 500 μl was introduced to chromatographic

columns composed of Eichrom Sr Resin for Sr separation. A flowchart illustrating the cleaning procedure and chemistry prior to Sr separation is shown in Figure 2.8.

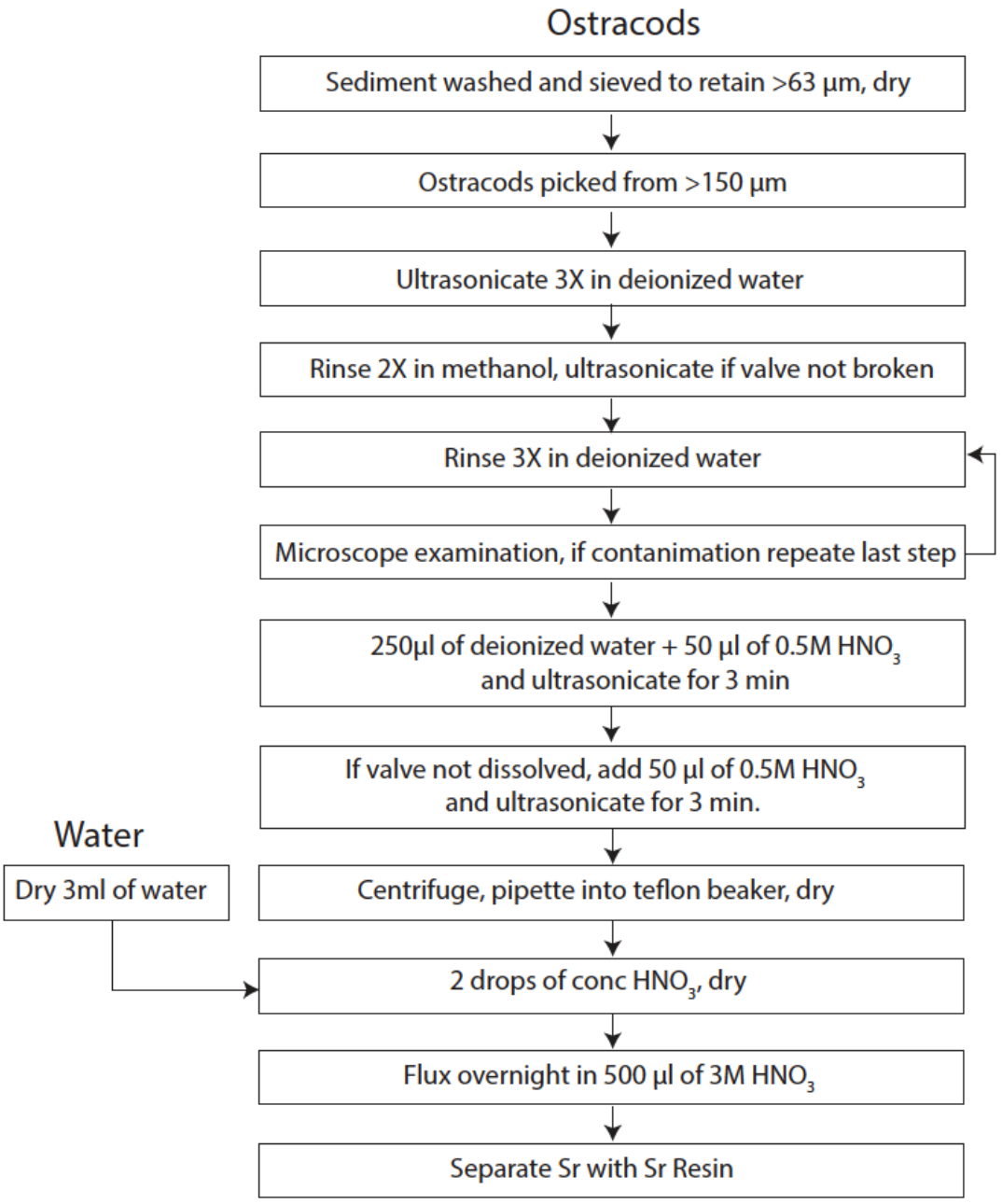

FIGURE 2.8: Flowchart of chemical procedure prior to Sr chromatographic extraction for water and ostracod samples.

2.2.3 Column chemistry and Sr isotopic measurements

After washing and pre-conditioning 100 μl of the Sr resin in heat-shrinkable FEP columns, samples were added to the resin bed. Resin was then washed four times with 500 μl of 3M HNO_3. Finally

the Sr fraction was extracted using 1.5 ml of deionized water and collected in a Savillex PFA beaker and dried at 120°C. Once dried, samples were refluxed with 2 drops of concentrated HNO_3 until ready for measurement.

Prior to the measurement, 30 μl of 0.33% H_3PO_4 was added to the samples and dried. Samples were re-dissolved in 1 μl of 10% HNO_3 and loaded onto a single rhenium filament with tantalum chloride as an activator (Birck, 1986). The measurement was carried out using a Thermo-Finnegan Triton thermal ionization mass spectrometer (TIMS). Sr isotopic measurements for the Zheleznyi Rog samples were carried out in the isotope laboratory of Vrije University, Amsterdam. All other sample measurements were carried out in the Bristol Isotope Group facilities at the University of Bristol.

The mass spectrometer was operated in multi-dynamic mode and an ^{88}Sr beam intensity is maintained between 5 and 8 V. $^{87}Sr/^{86}Sr$ ratio was corrected for mass fractionation to $^{86}Sr/^{88}Sr = 0.1194$ using the exponential law (Nier, 1938). The $^{87}Sr/^{86}Sr$ value for each run was collected in 20 blocks of 10 ratios. The internal precision within a run calculated using 2 standard error of the 200 measurements is ~4 - 12 ppm (Figure 2.9). External precision was calculated by repeated measurement of NIST SRM 987 (strontium carbonate) and produces $^{87}Sr/^{86}Sr$ of 0.710247 ± 0.0000092 (2SD, n = 67) during the course of the analysis. This is within error of the recommended value of 0.710248 (Thirlwall, 1991). Chemistry blank is negligible based on replicate measurement of standard NBS 987 with each batch of column chromatography (0.710247 ± 0.0000078, n = 36; Figure 2.10). Sample reproducibility was examined by running duplicates on a few randomly selected samples and showed $^{87}Sr/^{86}Sr$ values within error of each other for each sample (for details see data Tables in Appendix B, C, and D).

2.2.4 Trace elements

Of 20 μl dissolved sample separated for trace element analysis (Sr, Ca, Mg and Mn), 5 μl aliquot was taken from each sample and diluted to 2ml using 2% HNO_3. The trace elemental analysis was carried out on a Thermo Finnigan Element 2 high resolution sector-field inductively-coupled plasma mass spectrometer (SF-ICP-MS).

Prior to analysis, the instrument was tuned across the elemental mass range in order to get the best sensitivity using a 1 ppb multi-element tuning solution made in-house from single element standard

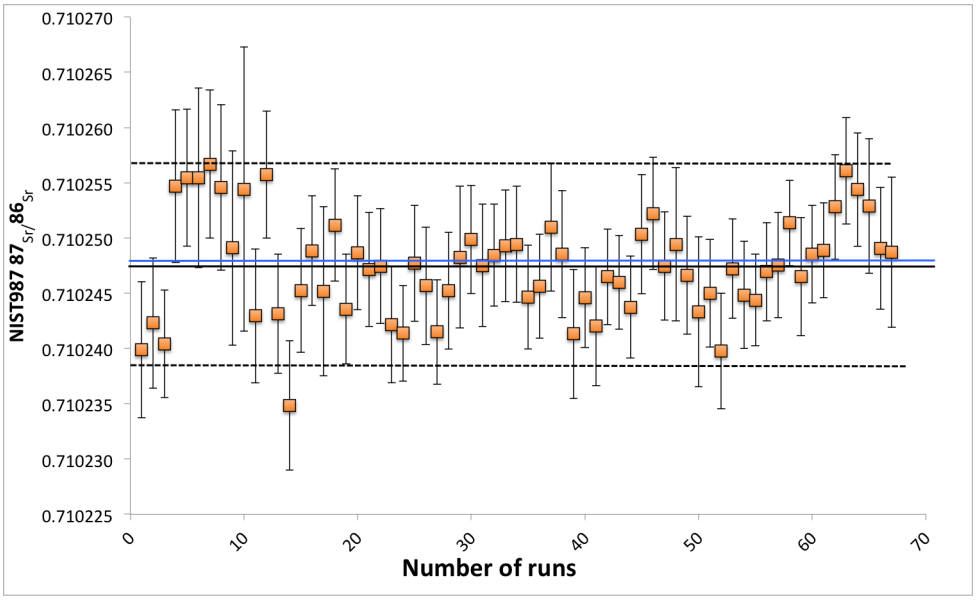

FIGURE 2.9: $^{87}Sr/^{86}Sr$ for all NIST SRM 987 standard runs during the course of this study (Feb 2016 - Mar 2018). The error bars show 2 standard errors. Blue solid line corresponds to the literature value of 0.71248 (Thirlwall, 1991). Black solid line shows average (0.710247) and dashed line shows the 2 standard deviation of 9.17×10^{-6} over 67 runs.

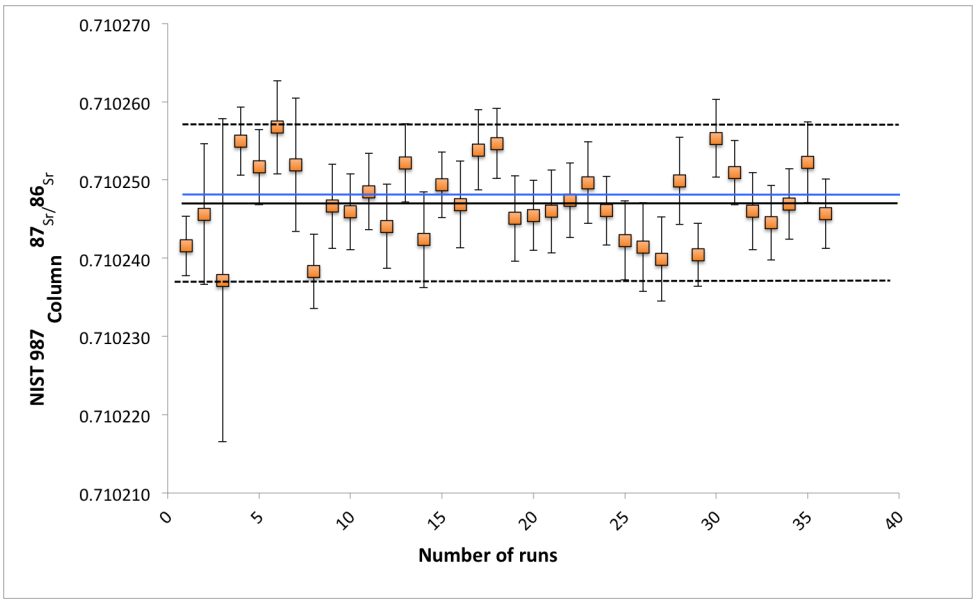

FIGURE 2.10: $^{87}Sr/^{86}Sr$ for all NIST SRM 987 standards that have gone through the column chromatography during the course of this study (Feb 2016 - Mar 2018). The error bars show 2 standard errors. Blue solid line corresponds to the literature value of 0.71248 (Thirlwall, 1991). Black solid line shows average (0.710247) and dashed line shows the 2 standard deviation of 7.83×10^{-6} over 36 runs.

solutions. The machine is tuned on ^{7}Li, ^{115}In, ^{238}U in low-resolution mode and ^{23}Na, ^{39}K, ^{56}Fe in medium resolution mode. Oxide formation was minimized by monitoring the $^{238}U^{16}O^{+}/^{238}U^{+}$ to be less than 15%.

The intensity of the sample signal was blank corrected and converted into a concentration using a

calibration curve obtained from a standard solution at five known concentration (0.5 ppb, 1 ppb, 50 ppb, 100 ppb and 500 ppb). ^{43}Ca and ^{88}Sr were measured in low-resolution mode, whereas ^{24}Mg and ^{55}Mn were measured in medium resolution mode. Each sample was measured for 20 runs with 1 (12s) pass using standard sample bracketing technique.

2.3 Micropalaeontology

Semi-quantitative micropalaeontology analysis on fossil ostracods and foraminifera was carried out for the Goychay, Hajigabul and Guria sections by Prof. Marius Stoica and Lea Rausch, University of Bucharest using standard micropalaeontological methods outlined in Stoica et al. (2013). 46 samples covering the 77.5 m - 1216.5 m stratigraphic intervals from the Goychay section, and 57 samples covering the 110 m - 1980 m stratigraphic interval from the Hajigabul section were analysed. Similarly, 10 micropalaeontological samples covering the 0.25 m - 7.15 m stratigraphic interval from the Tsikhisperdi section, and 37 samples from the Khvarbati section covering the 0.23 m - 163.5 m stratigraphic interval were analysed.

About 300 – 400 g from each sediment sample was dried to remove interstitial water. Once dried samples were washed and sieved through 150 μm to retain the larger fraction. The dried residue was handpicked using a ZEISS - GSZ light microscope. The material is housed in the Faculty of Geology and Geophysics, Department of Geology at Bucharest University (Romania).

The ostracod taxonomic concept is mainly based on previous work by Hartmann (1966), Moore (1961), and Morkoven (1962). Further information on ostracod taxonomy was provided by Agalarova (1967), Agalarova et al. (1961), Jiříček (1985), Krstić (1973, 1985, 1990), Livental (1929), Olteanu (1999a), and Yassini (1986) and the suprageneric classification was followed using Horne et al. (2002) and Meisch (2000). Based on the taxonomic outcome from the geological sections, ostracod species were correlated to specific ecological requirements with the goal of providing information on the palaeoenvironmental setting. The ecological preference of individual species was obtained by comparing fossil ostracod communities with environmental requirements of living species that closely resemble them. When no living analogues are present, the environmental preference of the species can be inferred in several ways. The most traditional concept, “taxonomic uniformitarianism” assumes that a fossil has had a similar ecological strategy to its closest living relatives (Birks, 2008). Comparable morphological features of extant species

imply similar functions and associated behaviours (Boucot, 2013). In this thesis, specific ecological preference (in particular, salinity) of individual species was obtained following Neale (1988) and Carbonel et al. (1988), who documents the environmental requirements of living non-marine ostracod species. However, it should be noted that these salinity estimates rely on the untestable assumption that the extinct fossil fauna and their nearest living relatives share the same environmental preferences. In addition, these salinity preferences are 1) approximate at best, given the transitional nature of the fauna, which survive between different salinity zones, 2) holistic because of the salinity variation in diurnal, seasonal, and annual scale within the water column and 3) may not have linear relationship with ostracod biodiversity as the abundance of species also depend on other environmental factors like oxygen content and availability of nutrients in the water. In order to classify the water salinity, salinity ranges according to the Venezian salinity classification (1958) rather than specific values for ostracod assemblages are used in this thesis.

2.4 Dinoflagellate cysts

Dinoflagellate cyst (Dinocyst) assemblages were used to constrain the palaeoenvironment and salinity conditions of the DSDP core 379A. Analysis was carried out by Tom Hoyle, Utrecht University. In total, 32 samples between 45.54 and 614.14 mbsf were processed using cold HCl (30%) to remove carbonates and cold HF (40%) to dissolve silicates. Samples were subjected to an ultrasonic bath for five minutes and sieved through 125 μm and then through 10 μm mesh to retain the fraction between 10 - 125 μm. Residues were mounted on slides using glycerine jelly and sealed with lacquer. Counting was carried out at magnifications of x400 and x1000 using a binocular transmitted-light microscope.

Dinocyst identifications were made using reference texts (Marret et al., 2004; Mudie et al., 2001, 2004, 2017; Rochon et al., 1999, 2002; Shumilovskikh et al., 2013; Soliman and Riding, 2017; Sütő-Szentai, 2010; Wall and Dale, 1973; Wall et al., 1973; Zonneveld et al., 2013). Taxa that fell along morphological gradients were grouped according to the dinocyst variability matrix of Hoyle et al. (2019). A known number of *Lycopodium clavatum* spores were added to each sample prior to processing in order to monitor concentrations.

Palynological data were processed using Psimpoll 4.27 (Bennett, 2008). Dinocyst data are represented as a percentage of the dinocyst sum, which includes all identified dinocysts (possessing an

archeopyle and cingulum) but excludes acritarchs, foraminiferal test linings, unidentified cysts and any other algal or aquatic taxa.

2.5 Diagenesis of biogenic carbonate

The use of biogenic carbonates for palaeoenvironmental and palaeoclimatic interpretation based on the geochemistry of their shell is only possible if the primary signal sought has not been modified by diagenesis. The problems that arise from diagenetic alteration of foraminiferal calcite have been elegantly demonstrated by Pearson et al. (2001) in his exploration of the "cool tropic paradox" where the sea floor recrystallization of planktonic foraminifera modified the measured δ^{18}O and led to the interpretation of much reduced sea surface temperature during the Late Cretaceous and Eocene. Diagenetic alteration of calcite shells can occur due to dissolution, overgrowth, infilling or recrystallization and can happen both, as the shell settles through the water column from its life position to the sea floor or at the burial site (Hemleben et al., 1977, 2012). Where these alterations take place in a different environment, usually with a different geochemical signal from where the organism originally calcified its shell, a secondary geochemical signal is incorporated. The secondary signal can alter or override the primary geochemical signal of the water that had been originally incorporated into the biogenic carbonate (e.g. Bennett et al., 2011; Elorza and Garcıa-Garmilla, 1996; Keatings et al., 2002; Killingley, 1983). Stable oxygen isotopes (δ^{18}O) are particularly vulnerable to this form of diagenesis and its ramification for incorrect palaeoenvironmental reconstruction is well known (e.g. Banner and Kaufman, 1994; Pearson et al., 2001; Schrag et al., 1995). Comparatively, the impact of diagenesis on the Sr isotopic ratio of ostracod valves is less problematic for a number of reasons outlined below.

The non equilibrium fractionation of these isotopes during foraminifera test formation means that any inorganic precipitation will have a different δ^{18}O even if the diagenesis occurs in the same environment . Similarly, preferential release of lighter isotopes during shell dissolution will alter the primary oxygen isotopic signature preserved in calcite shells. By contrast, there is no preferential isotopic selection during incorporation or release during dissolution for Sr isotopes (Reinhardt et al., 1999). Ostracods are bottom dwellers and calcify their valve within few hours. As such, there is no immediate change of environment associated with death, and therefore, no change in valve chemistry even if the biogenic carbonate is modified (Turpen and Angell, 1971). However, once

the moulted ostracod valves are buried in the sediment, the biogenic calcite may undergo partial dissolution and recrystallization or crystallization of inorganic carbonate may adhere on the valve (Bennett et al., 2011). These processes may affect the chemical composition of the valve as this carbonate will contain a Sr isotopic ratio of the interstitial water, which may differ from the water in which the ostracod dwelt. If the process of (re)crystallization occurs at shallow burial depths, then the diagenetic Sr isotopic ratio is likely to be similar to the bottom water signal incorporated into the original biogenic ratio because pore water at shallow sediment depth is likely to have similar chemical composition as the bottom water where ostracods dwell (Elderfield and Gieskes, 1982). Bennett et al. (2011) showed that the presence of neomophic calcite, an indicator of shallow burial depth recrystallisation, appears not to significantly alter even the primary oxygen isotopic signal of carboniferous ostracods.

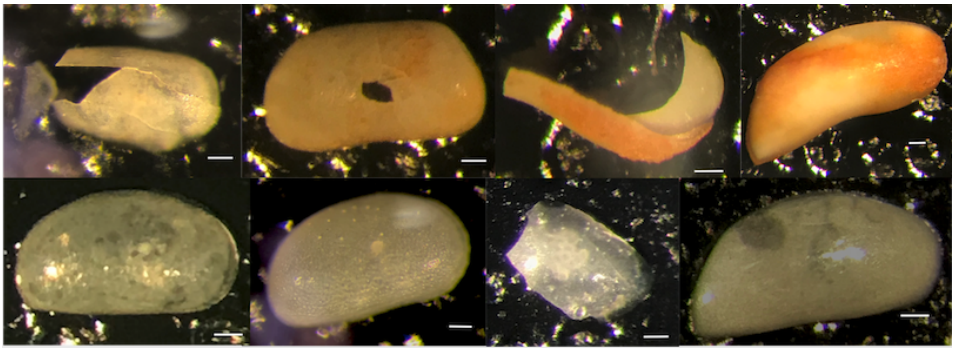

FIGURE 2.11: Images of ostracods taken under the light microscope. Top panel shows the images of ostracods that showed signs of secondary precipitation. Bottom panel shows images of ostracods that were selected for Sr analysis. The scale bar represents 100 μm.

Potentially more problematic is the adsorption of non carbonate minerals on the valve surface, which can also change the strontium isotopic signal of the ostracod valve analysed. Clay minerals, in particular, are problematic as they are more adhesive than sand and are typical for the environments that ostracods inhabit. Clay minerals tend to have high radiogenic strontium (Dasch, 1969), typically substantially higher than the ocean water values (McArthur et al., 2012). Therefore, to obtain a reliable strontium isotopic signal from ostracod valves, diagenetically unaltered ostracods should be selected and careful pre-treatment should be carried out to remove any contaminant material from the surface while leaving the composition of the ostracod valve calcite unaltered (see Section 2.2.2).

Evaluation of the suitability of ostracod valves for isotopic analysis can be done by physically assessing the ostracod valve under light microscope. This allows altered specimens to be identified

and the degree of diagenesis can then be evaluated using scanning electron microscope (Bennett et al., 2011; Keatings et al., 2002; Mischke et al., 2008).

In this study preliminary assessment of the valve for any secondary precipitation or adherent minerals was carried out under a light microscope. Only clean, transparent or translucent valves (Figure 2.11 bottom panel) were picked for isotopic analysis. Valves that appear opaque and or coloured under a light microscope are likely to indicate secondary precipitation (Figure 2.11 top panel), since living ostracods have translucent valves. SEM images provide a more detailed assessment of both, the preservation state of the valve and the effectiveness of the cleaning procedure (Section 2.2.2).

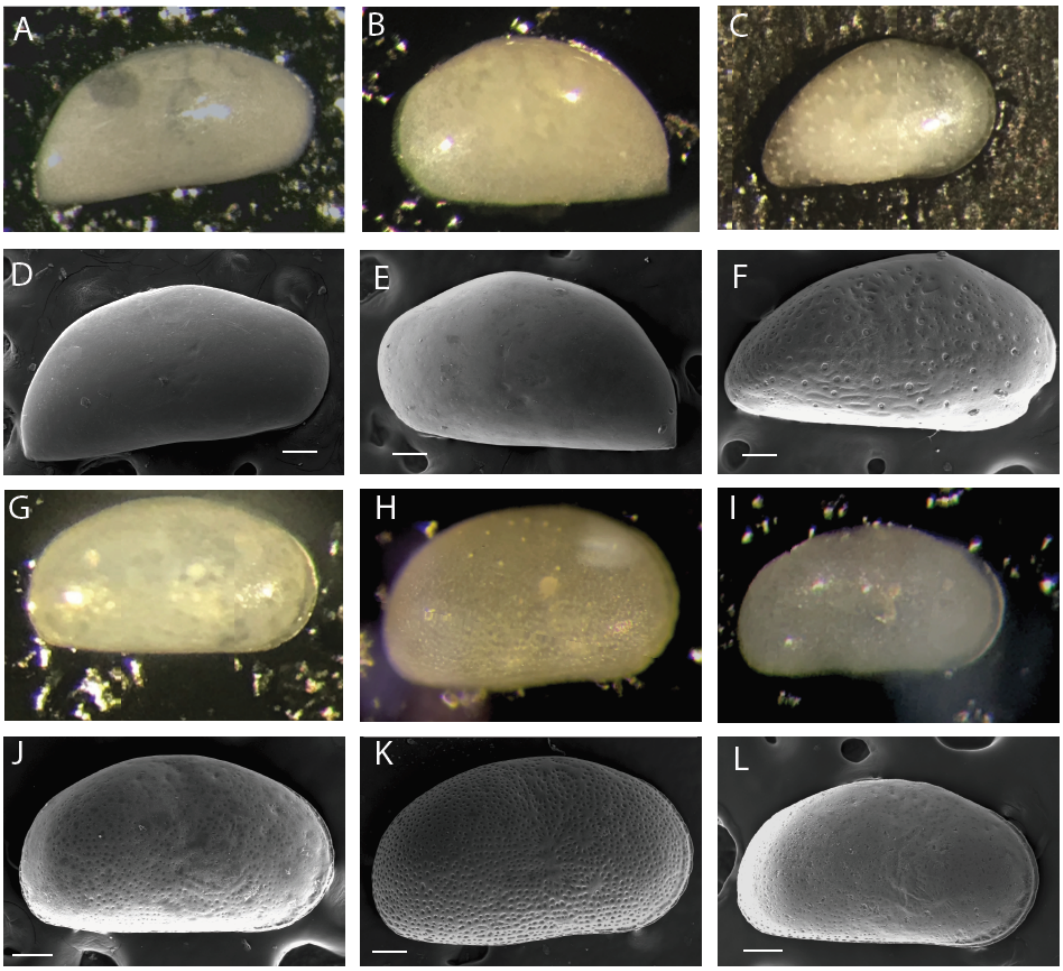

FIGURE 2.12: A – F) Images of the modern ostracod valves under light microscope (A-C) and using SEM imaging (D-F). G-H) Images of the fossil ostracod under light microscope (G-I) and using SEM imaging (J-L). The scale bar represents 100 μm.

In some cases, complete ostracod carapaces (joined left and right valves) were found in the samples.

All complete carapaces were split before picking, to ensure that they did not contain secondary mineral precipitates. Light pressure between the glass slides was exerted to break the two valves. Although this generally resulted in valve fragmentation, this also permitted the inside of the valve to be cleaned for any sediment and organic remnants. Samples where light pressure did not dislocate or fragment were discarded as these joined valves are likely to contain substantial recrystallised minerals.

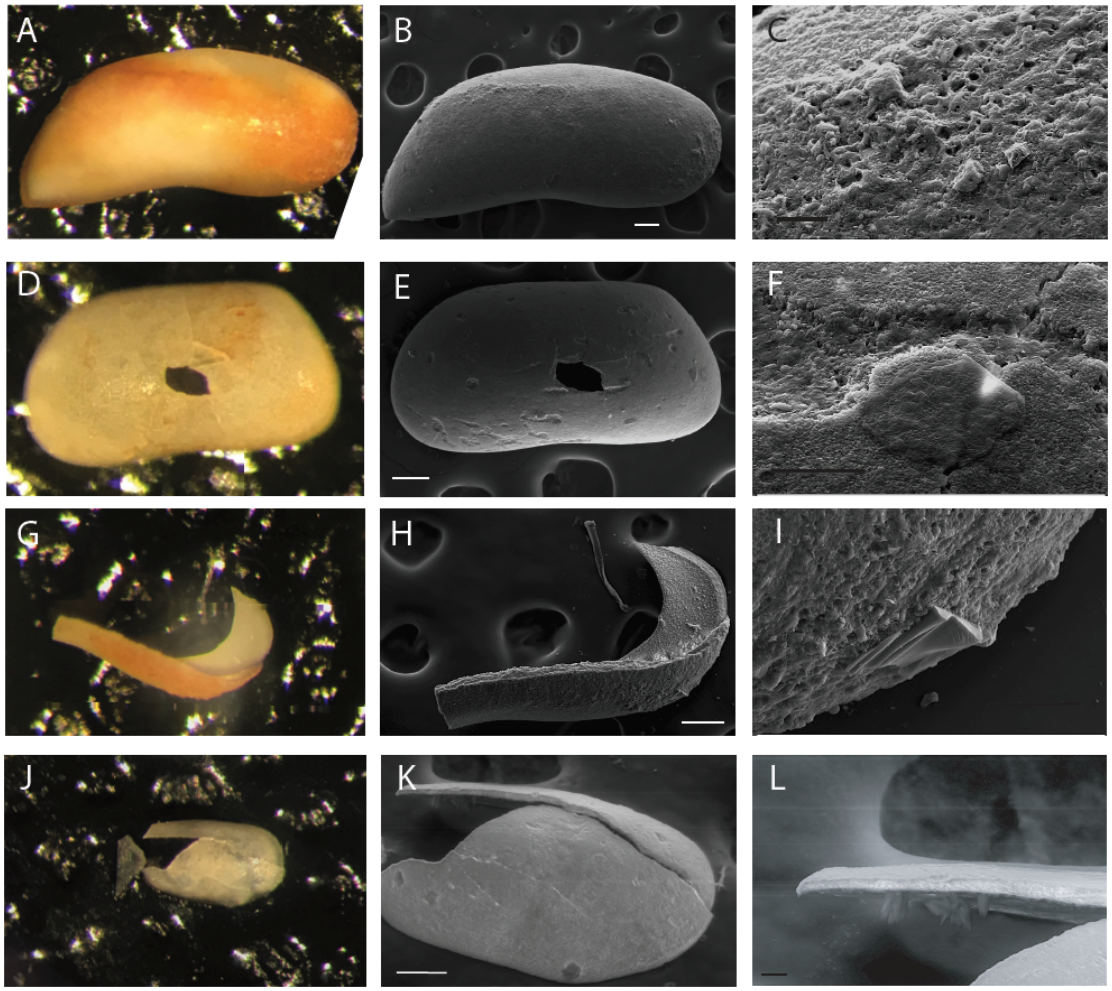

FIGURE 2.13: Light microscopy and SEM images of poorly preserved ostracods valves.

A more detailed visual assessment of the valves and evaluation of the employed cleaning procedure (Figure 2.8), was carried out using Scanning Election Microscope (SEM) imaging of ostracod valves. All SEM images were taken at the Interface Analysis Centre, HH Wills Physics Laboratory, University of Bristol. Figure 2.12 shows images of modern and fossil ostracods from the Black and Caspian Sea. Keatings et al. (2002) suggested that SEM images of ostracod valves that are diagenetically altered show pits and surface etching, removal of surface layers, cracks and extreme dissolved or re-crystallized surfaces. SEM images of the valves used in this study that appeared

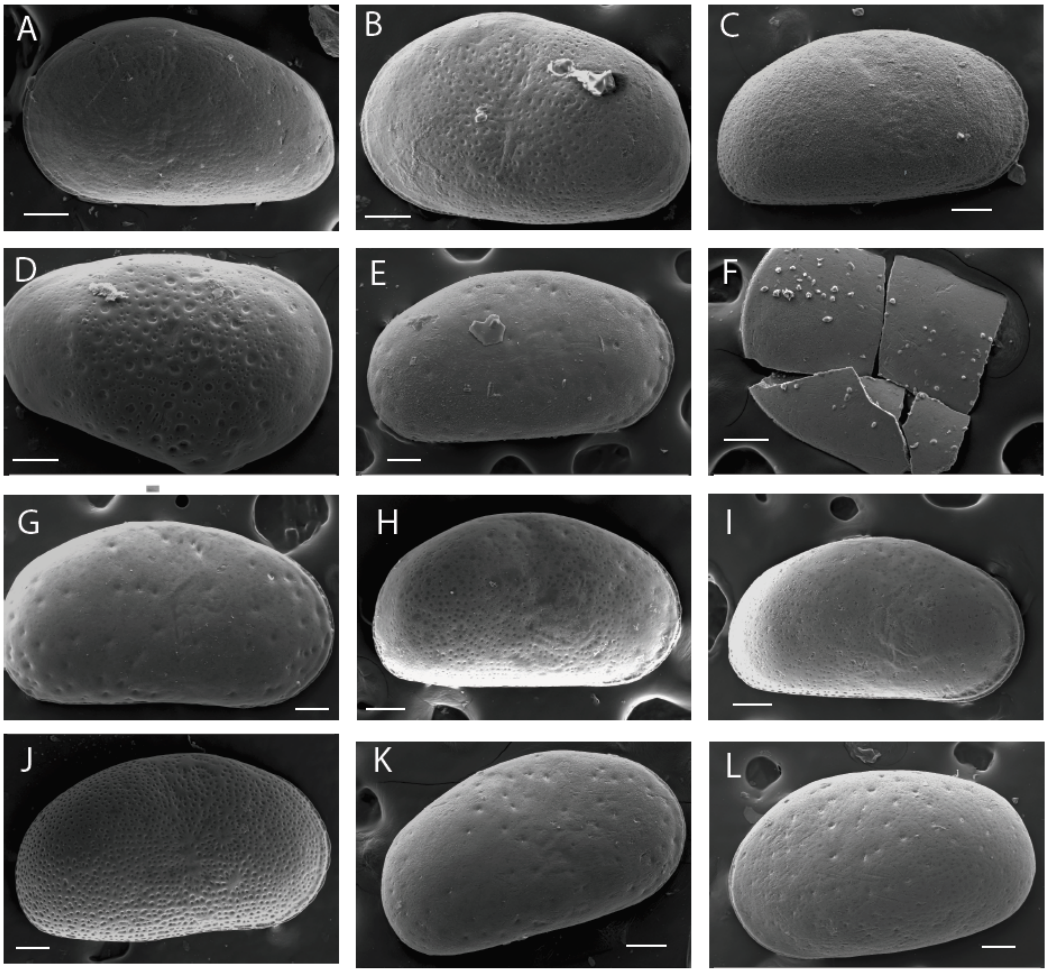

FIGURE 2.14: A- F) SEM images of the uncleaned ostracod valves. G - L) Images of the valves that have undergone cleaning procedure. All valves appeared clear or translucent under the light microscope. The scale bar represents 100 μm.

pristine under the light microscope also show well-preserved surface ornamentation with no or very little surface etchings (Figure 2.12). Valves that appeared poorly preserved under the light microscope showed heavily abraded and pitted surfaces in SEM images (Figure 2.13). SEM images also show that valves which appear to be clean, clear and transparent under a light microscope may have adherent particles that could impact the Sr isotopic ratio (Figure 2.14A - F). SEM images of these samples before and after undergoing the cleaning procedure described in Section 2.2.2 suggests that the cleaning procedure employed during this study was effective at removing adherent particles from valve surfaces (Figure 2.14 G - L).

Assessment of the ultrastructure of the calcite crystals in fossil ostracods from the Carboniferous by Bennett et al. (2011) showed six stages of calcite diagenesis; 1) replacement of the original calcite by neomorphic calcite, 2) growth of framboidal and euhedral pyrite replacing the dissolved

carapace, 3) replacement by ferroan calcite, 4) replacement by ferroan dolomite, 5) siderite growth, and 6) sphalerite and barite mineralization. However, the ultrastructure of most of the ostracod valves used in this study shows well-preserved valves with unaltered laminated crystal structure and no mineral replacement (Figure 2.15D, E, G, and H). Figure 2.15F and I, show features indicating that these valves may have undergone a small degree of partial dissolution on the surface or very early stages of neomorphic calcite formation (Bennett et al., 2011; Pearson and Burgess, 2008; Pearson et al., 2001; Sexton et al., 2006), but without any substantial recrystallization.

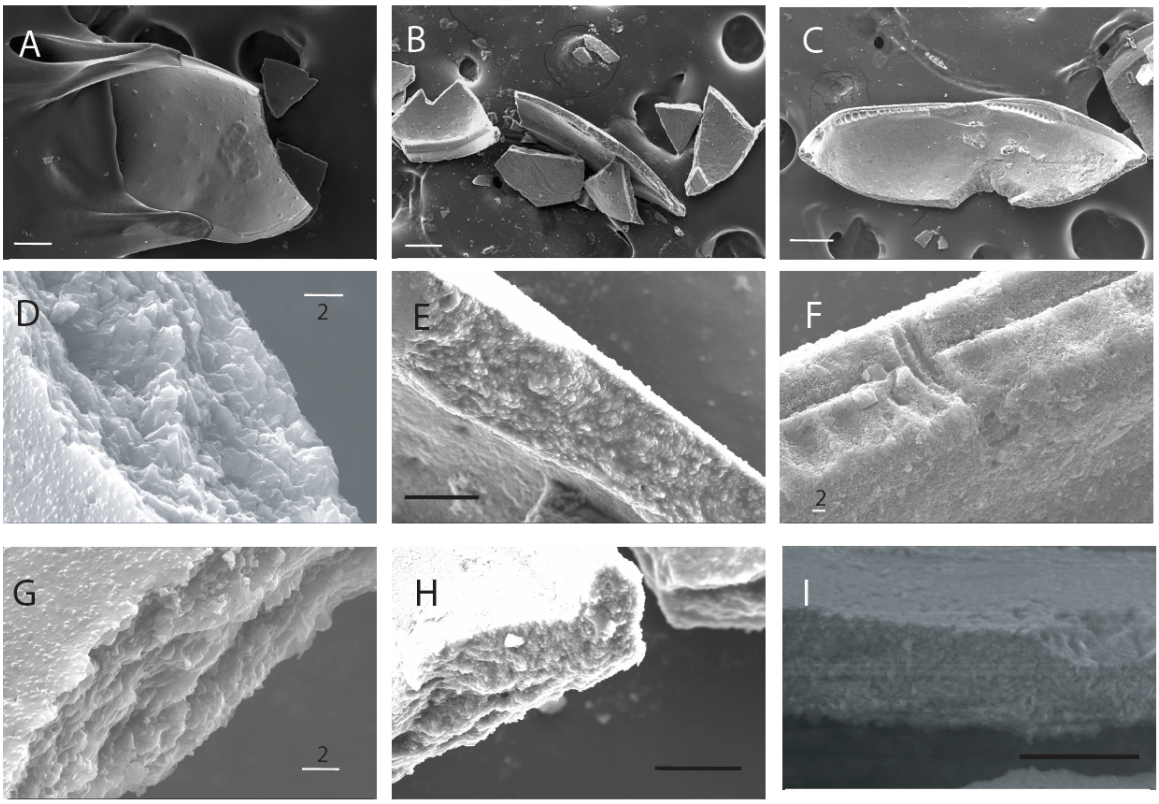

FIGURE 2.15: SEM images of ostracod valves showing ultrastructures. The white scale bar represents 100 μm and black bar represents 20 μm, unless otherwise mentioned.

In summary, the physical assessment of fossil ostracod suggests there has been minimal diagenetic alteration of the samples used in this study. Diagenetically modified specimens can be identified under a light microscope and were avoided. Consequently, careful visual inspection and use of washing protocol described in Section 2.2.2, which removes any adherent particles is sufficient to ensure that the samples analysed in this study for Sr isotopic ratios reflect the primary signal of the water.

2.6 Additional data sources

In order to investigate the connectivity history of the Black Sea and the Caspian Sea, additional datasets were required to complement the Sr isotopic record. These datasets consist of both published and unpublished data. The unpublished datasets are provided by other ESRs within the PRIDE project with their agreement. The list of complementary data used in this thesis is given in Table 2.3.

TABLE 2.3: Various datasets used in this thesis to complement the Sr isotopic record.

Dataset	**Section/Location**	**Age (Ka)**	**Chapter used**	**Reference:**
$^{87}Sr/^{86}Sr$ record	open ocean	0 - 7000	all	McArthur et al. (2012)
Age model	Guria Section		Chapter 5	Kirscher et al. (2017)
Age model	Goychay Section		Chapter 5	Lazarev et al. (2019)
$^{87}Sr/^{86}Sr$ record	Jeirankechmez Section	2000 - 2700	Chapter 5	van Baak et al. (2019)
Salinity estimates	Jeirankechmez Section	2000 - 2700	Chapter 5	Richards et al. (2018)
$^{87}Sr/^{86}Sr$ record	Karagoush Mountain Section	1000 - 2000	Chapter 5	Page (2004)
Micropalaeontology and salinity estimates	Goychay Section	1300 - 2600	Chapter 5	M. Stoica and L. Rausch, University of Bucharest and Lazarev et al. (2019)
Age model	DSDP 379/380		Chapter 6	van Baak et al. (2016a)
$^{87}Sr/^{86}Sr$ record	Composite Black Sea cores	0 – 30	Chapter 6	Major et al. (2006)

Table 4.1 Continued:

Salinity	DSDP 379	32 - 450	Chapter 6	Schrader (1978)
Salinity estimates	DSDP 379	50 - 1200	Chapter 6	Hoyle (2019) and T. Hoyle, Utrecht University
$^{87}Sr/^{86}Sr$ record	Core 22GC-8	127 - 133	Chapter 6	Wegwerth et al. (2014)
Age model	Hajigabul Section		Chapter 7	Lazarev et al. (2019)
Micropalaeontology and salinity	Hajigabul Section	700 - 2140	Chapter 7	M. Stoica and L. Rausch, University of Bucharest and Lazarev et al. (2019)
Micropalaeontology	Guria Section		Chapter 8	M. Stoica and L. Rausch, University of Bucharest
$^{87}Sr/^{86}Sr$ record	Mediterranean Sea	5000 - 7000	Chapter 8	Flecker et al. (2015)
$^{87}Sr/^{86}Sr$ record	Zheleznyi Rog section	5000 - 6800	Chapter 8	Grothe (2016)
$^{87}Sr/^{86}Sr$ record	Adzheveli section	5300 - 6100	Chapter 8	Grothe (2016)

Chapter 3

Sr isotopic variation across the present-day Black and Caspian seas

The open ocean is homogeneous with respect to strontium because its residence time water column is much longer than the ocean mixing time. Similar homogeneity assumptions are made for the Black Sea and the Caspian Sea, despite the fact that they are highly stratified, semi-isolated or endorheic basins. However, there are no empirical data to demonstrate that the Black Sea and the Caspian Sea are homogeneous with respect to strontium isotopes. This chapter, therefore, explores the homogeneity assumption in the Black Sea and the Caspian Sea by examining the Sr isotopic measurements of water samples from the Black and Caspian seas and river water samples from across the region. This chapter also explores the robustness of ostracods as palaeo archives of $^{87}Sr/^{86}Sr$ *by comparing* $^{87}Sr/^{86}Sr$ *measured in ostracods collected from modern sediment with the* $^{87}Sr/^{86}Sr$ *of the bottom water at the same sites in both Black Sea and the Caspian Sea. More explicitly, this chapter will answer* ***research questions 1, 2 and 3*** *outlined in Section 1.6.1;*

1. *Is the strontium isotopic signal in the Black and Caspian seas spatially homogeneous?*
2. *Does the strontium isotopic signal in the Black and Caspian seas vary with water depth? What influence does the density stratification have on Sr isotopic variability in the water column?*
3. *Are fossil ostracods a robust archive for preserving the primary* $^{87}Sr/^{86}Sr$ *of ambient water in the Black and Caspian seas?*

Parts of this chapter are included in the manuscript intended for *Earth and Planetary Science Letters*. This includes results and discussions regarding $^{87}Sr/^{86}Sr$ of the modern Black Sea water, its fluvial sources and the Aral Sea water.

3.1 Introduction

The Sr concentration of ocean water is ~40 times higher than average global river water (Palmer and Edmond, 1989) and, as a result, marginal basins that are connected with the open ocean generally have an oceanic Sr isotopic signal (e.g., Mediterranean Sea, Baltic Sea). However, the $^{87}Sr/^{86}Sr$ of a marginal basin can be seen to respond as a function of the balance between different input sources such as fluvial discharge and exchange with the open ocean (Topper et al., 2011), both of which control the Sr flux into the basin. Increased fluvial discharge combined with limited oceanic exchange can deviate the $^{87}Sr/^{86}Sr$ of the marginal basin from the ocean water value toward fluvial signal (Topper et al., 2011). In the Mediterranean Sea today, at least 25% increase in the fluvial discharge can deviate $^{87}Sr/^{86}Sr$ away from the ocean water curve toward its fluvial signal (Topper et al., 2011). However, the sensitivity of the $^{87}Sr/^{86}Sr$ in the marginal basin to the fluvial signal depends on the magnitude of the exchange with the open ocean. An unrestricted exchange (large oceanic input) results in an oceanic signal in the marginal basin. But, as the exchange with the open ocean becomes more restricted, the $^{87}Sr/^{86}Sr$ of the marginal basin becomes increasingly more sensitive to fluvial discharge.

Exchange of water between open ocean and marginal basins is controlled by the topography of the gateway, the hydrological budget of the marginal basin, and the density difference between the two water bodies. For the case of the Mediterranean Sea today, although the negative hydrological budget plays a role, the exchange between the Atlantic Ocean and the Mediterranean Sea is mainly controlled by outflow of the denser Mediterranean water at greater depths and surface inflow of the less dense Atlantic water. However, there is no exchange of the water mass even when the two basins are fully connected, if the two water masses lack density contrast. A recent study by Modestou et al. (2017) showed that the $^{87}Sr/^{86}Sr$ of the Mediterranean Sea deviated away from the oceanic value during Miocene when it was fully connected to the open ocean but there was no density difference between the two water masses.

It is generally assumed that the Sr isotopic ratio of the Black Sea and the Caspian Sea are homogeneous even though the former is a marginal basin semi-isolated from the Mediterranean Sea and the latter is an endorheic basin. Several studies have relied on this assumption to assess changes in water geochemistry, its input sources and changes in palaeoenvironment of the basin by measuring $^{87}Sr/^{86}Sr$ on fossil carbonates collected from one location (e.g. Grothe, 2016; van Baak et al., 2019; Vasiliev et al., 2010; Wegwerth et al., 2014). However, there are no studies that validate the Sr isotopic homogeneity assumption in the Black and Caspian seas and existing data for modern water in these basins are severely limited. Only one $^{87}Sr/^{86}Sr$ measurement with large uncertainty, from the Black Sea water has been published (Cox and Faure, 1974) and three from spatially limited set of locations with poor details are available for the Caspian Sea (Clauer et al., 2000). Consequently, it is difficult to assess whether these results represents a well-mixed basin or a local signal influenced by fluvial discharge. In addition, no studies exist that demonstrate the reliability of the biogenic archive in recording and preserving the primary Sr isotope ratio of the ambient water in hydrological settings like the Black and Caspian seas.

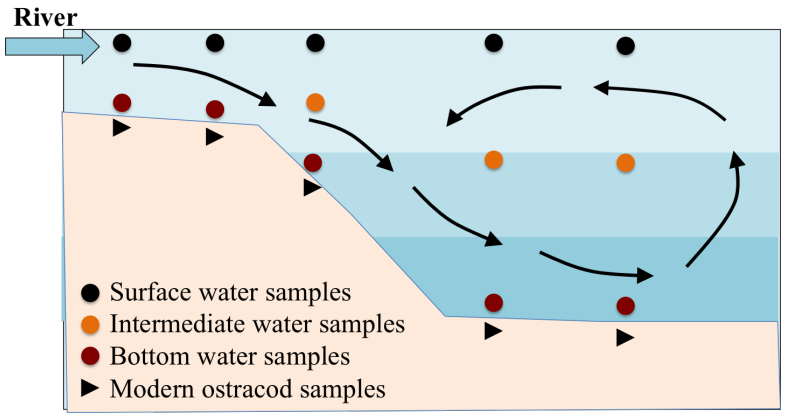

FIGURE 3.1: Schematic figure showing sampling strategy to explore the spatial homogeneity assumption and the validity of ostracods as palaeo archives.

This chapter tests the application of the Sr isotopes homogeneity assumption to the Black and Caspian seas. It also evaluates the robustness of bottom-dwelling ostracods as archives for Sr signal in the water column. Water samples were collected at a range of depths at different locations across the Black Sea and the Caspian Sea to provide a clearer indication of the present–day spatial variation in $^{87}Sr/^{86}Sr$. The Sr isotopic ratios of river water samples were also collected to appraise the fluvial sources (Figure 3.1), which have poorly constrained $^{87}Sr/^{86}Sr$ values. In addition, $^{87}Sr/^{86}Sr$ measured on ostracods collected from the modern sediment was compared to that of the water at the same location to investigate the robustness of the ostracods for preserving the Sr

isotopic signal of the water. This chapter provides a more comprehensive understanding of the three-dimensional spatial distribution of the Sr isotopic systems in the Black Sea and the Caspian Sea region. This insight is essential for validating the hydrological model presented in Chapter 4 and interpretion of fossil Sr isotopic data generated in this study (Chapter 5, 6, and 7).

3.2 Sampling sites and analytical methods

Water samples from the Caspian and Black seas were collected to cover a wide spatial and vertical range within each basin (Figure 2.1 and Table 2.1). Of the 66 water samples collected from the Black Sea, a representative sample of 30 were selected for analysis. In addition, ostracods collected from the modern sediment at 6 locations were analysed. Of 43 water samples collected from the Caspian Sea, 12 water samples from 6 locations and ostracods from modern sediment were analysed in this study. Sr isotopic analysis was carried out following procedures outlined in Section 2.2 and Figure 2.8.

3.3 Results

3.3.1 Sr isotopic ratio of rivers

The $^{87}Sr/^{86}Sr$ of the rivers feeding the Black Sea and Caspian Sea are shown in Figure 3.2 and are listed in Table B.1. The $^{87}Sr/^{86}Sr$ of these rivers vary considerably, but are consistently lower than the global average river water $^{87}Sr/^{86}Sr$ (Figure 3.2, Palmer and Edmond, 1989). The eastern Black Sea rivers exhibit the lowest values, while the northern Black Sea rivers show the highest $^{87}Sr/^{86}Sr$ (Figure 3.2A and B). The $^{87}Sr/^{86}Sr$ of the northern rivers (Don and Dnieper) are significantly higher than previous estimations provided by Palmer and Edmond (1989). Where multiple samples were taken upstream of the river mouth, the Sr isotopic ratios show substantially variation.

Compared to the Black Sea rivers, the Caspian Sea rivers show lower $^{87}Sr/^{86}Sr$ values. Three water samples along the Volga river are similar but show a slight increase upstream of the river and agree with previously published value by Clauer et al. (2000) (Figure 3.2C). Also, the $^{87}Sr/^{86}Sr$ for a water sample collected from the upstream Kura is consistent with the value provided by Clauer

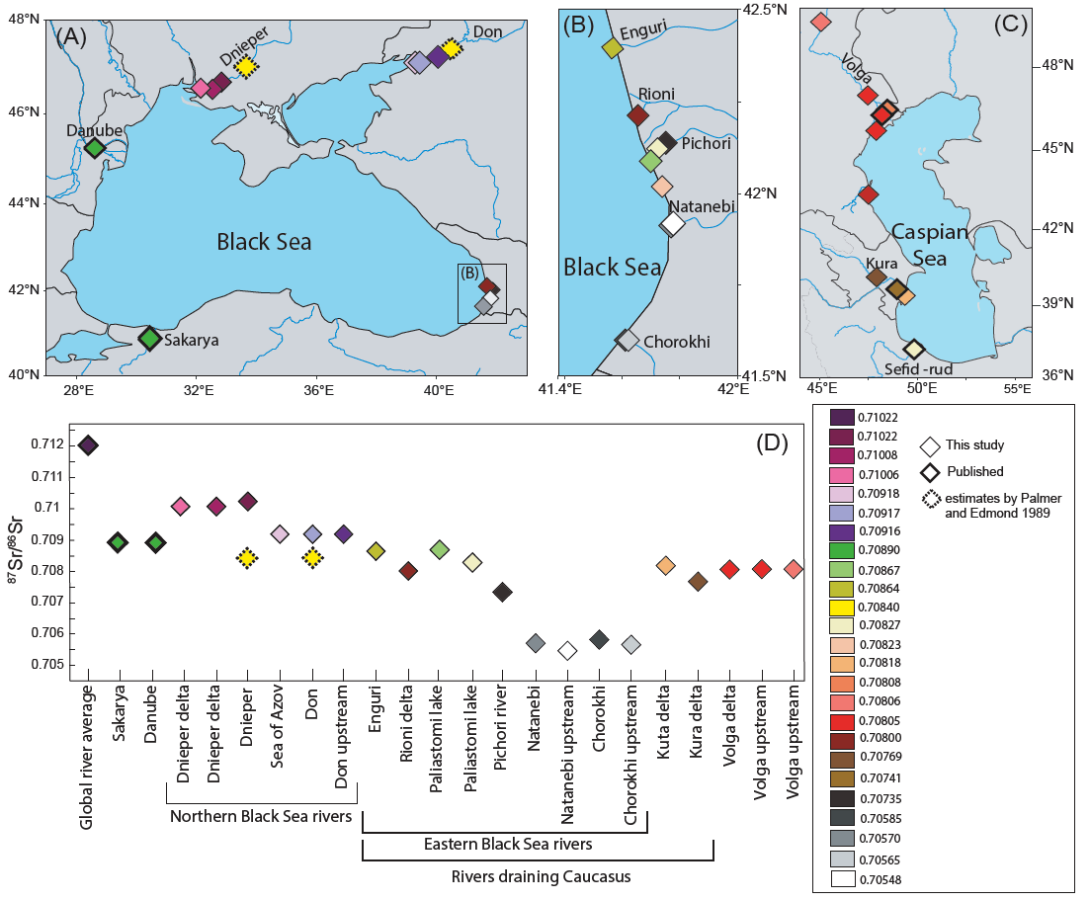

FIGURE 3.2: The $^{87}Sr/^{86}Sr$ of the Black Sea (A and B) and the Caspian Sea (C) rivers. Previously published values are shown in diamonds with thick line (Clauer et al., 2000; Major et al., 2006; Palmer and Edmond, 1989). Estimated $^{87}Sr/^{86}Sr$ based on the catchment geology for the Don and Dnieper are shown with dotted line (Palmer and Edmond, 1989). Because of the wide range in the fluvial $^{87}Sr/^{86}Sr$ in the region, the colour scale is neither linear nor continuous.

et al. (2000) for the same river. The water sample at Kura river mouth shows substantially higher value than the upstream sample and is closer to the Caspian water sample (Clauer et al., 2000).

3.3.2 Sr isotopic ratio of basin water samples

The Sr isotope measurements for modern Black Sea water samples are shown in Figure 3.3 and are listed in Table B.2. The $^{87}Sr/^{86}Sr$ values of the Black Sea surface water are lower than the modern ocean $^{87}Sr/^{86}Sr$ but are consistent spatially as almost all data lie within error of each other (Figure 3.3D). A few slightly lower measurements are from off the coast of Georgia (Figure 3.3C and D). The $^{87}Sr/^{86}Sr$ measured on intermediate and deeper water samples shows similar values to that of surface water samples (Figure 3.3D and E)). The $^{87}Sr/^{86}Sr$ measured on ostracod valves collected from grab samples are mostly consistent with the present-day water values (Figure 3.3E).

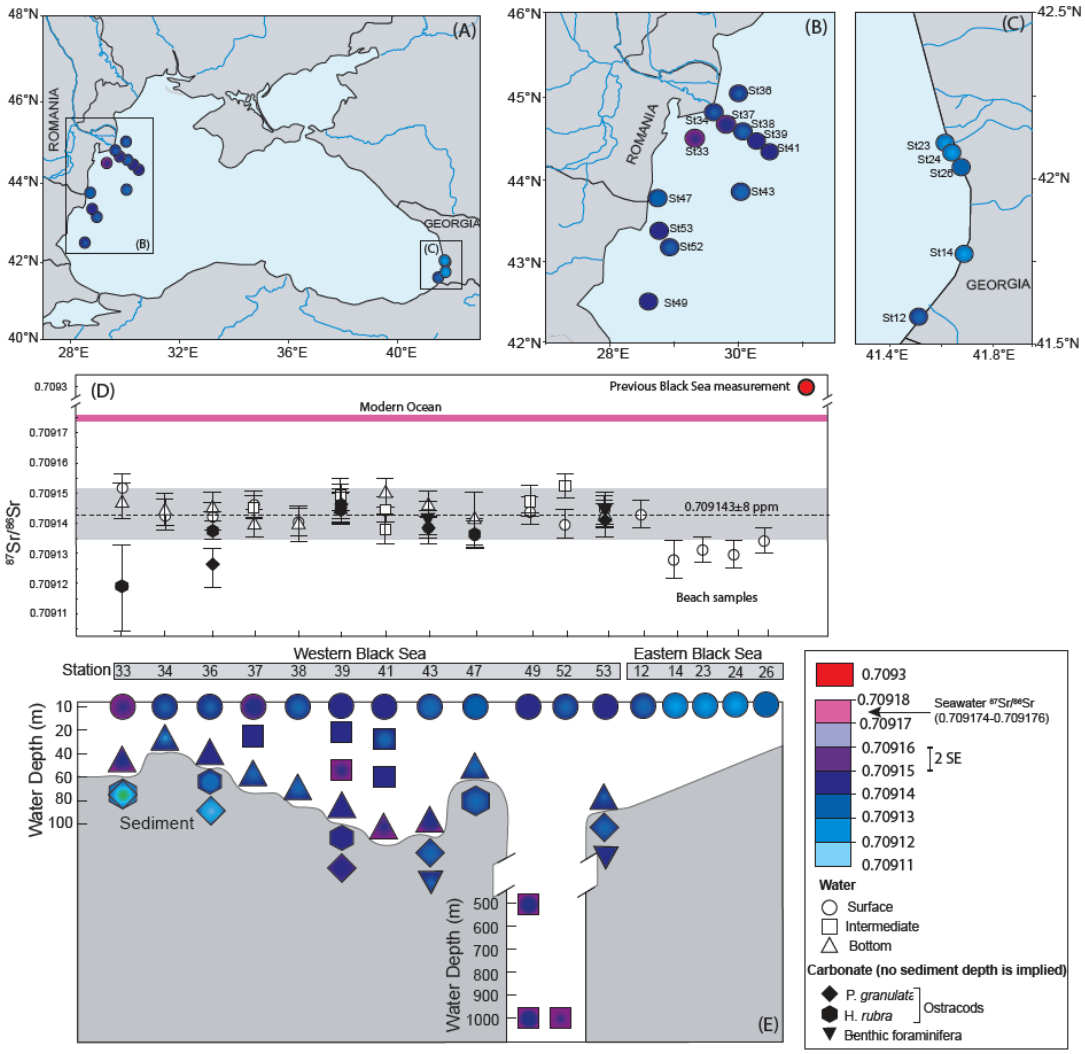

FIGURE 3.3: A) The Sr isotopic ratio of the surface water across the Black Sea, with details along the coast of Romania shown in (B) and along the coast of Georgia shown in (C). D) The $^{87}Sr/^{86}Sr$ of the water at at different stations (surface: circles, intermediate depth: boxes, and bottom: triangles) and modern carbonate shells (*P. granulate*: diamonds, *H. rubra*: hexagon, and benthic foraminifera: inverted triangles). The dashed line represents the average $^{87}Sr/^{86}Sr$ of the Black Sea with uncertainty (±2sd) highlighted by the grey bar. The pink bar indicates the $^{87}Sr/^{86}Sr$ of the modern ocean (McArthur et al., 2012) and the unusually high previous Black Sea measurement is shown in red dot (Cox and Faure, 1974). E) The $^{87}Sr/^{86}Sr$ of the water at different depths with carbonate samples taken from the surface sediment (no sediment depth is implied).

The Sr isotope measurements for the Caspian Sea and Aral Sea water samples are shown in Figure 3.4 and are listed in Table B.3. The $^{87}Sr/^{86}Sr$ of the Caspian Sea surface waters measured off the Kazakhstan coast in the Middle Caspian basin are within error of each other (Figure 3.4B and D). Similar values are also observed in the two water samples collected off the coast of Azerbaijan (Figure 3.4A and D). While no samples at greater depths were taken, those at 20 m show values within error of the surface water at the same location. The $^{87}Sr/^{86}Sr$ values of water samples collected from the Aral Sea are significantly higher than those of the Black Sea and Caspian Sea

and also modern ocean water (Figure 3.4C).

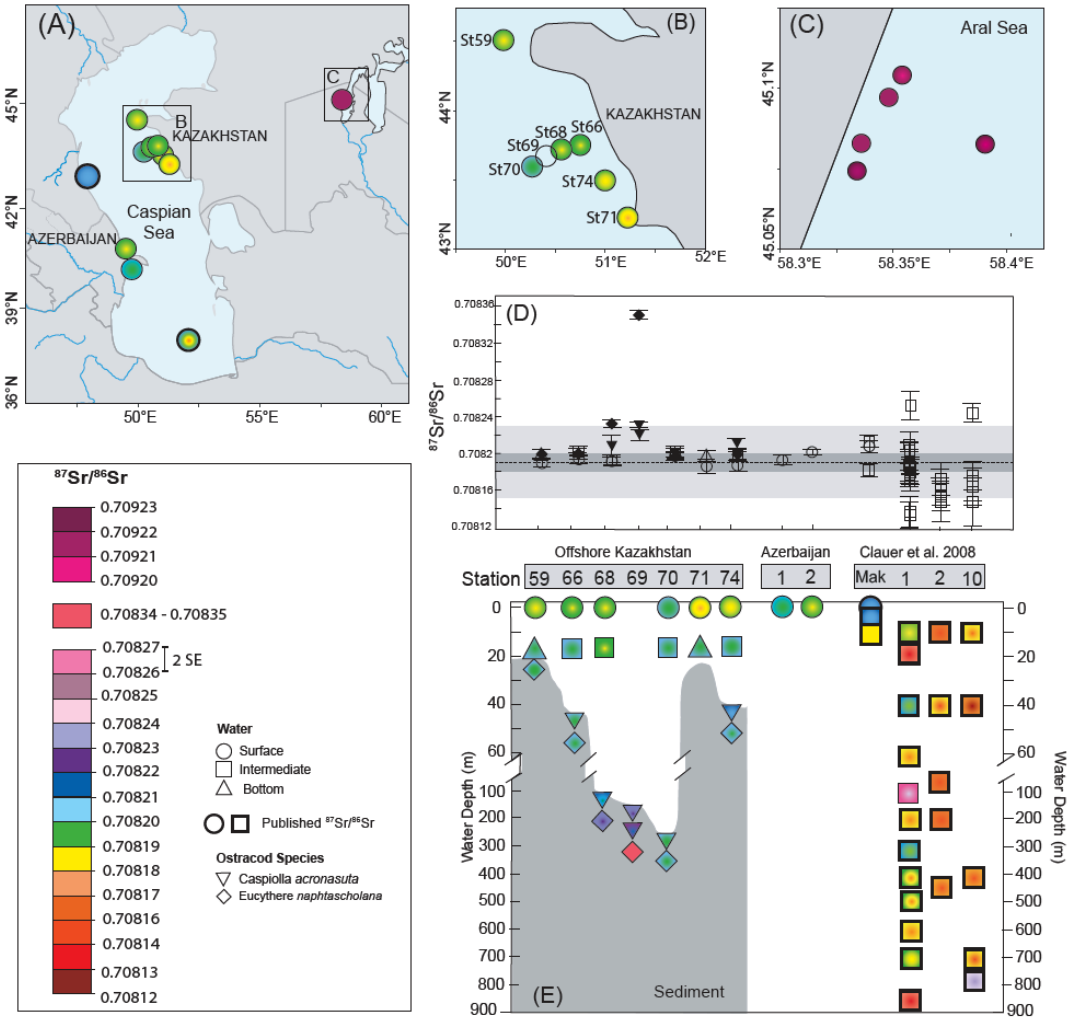

FIGURE 3.4: The Sr isotopic ratio of the surface water across the Caspian Sea (A and B) and the Aral Sea (C). D) The $^{87}Sr/^{86}Sr$ of the water at various stations (surface: circles, intermediate: boxes, and bottom: triangles) and modern carbonate shells (*C. acronasuta*: diamonds, *E. naphtascholana*: inverted triangles). The average $^{87}Sr/^{86}Sr$ of the Caspian Sea from this study is shown by dashed horizontal line with two standard deviations highlighted by darker grey bar. The uncertainty (±2sd) of previous measurements by Clauer et al. (2008) is shown by the lighter grey bar (E). The $^{87}Sr/^{86}Sr$ of the water at various depths with carbonate samples taken from the surface sediment (no sediment depth is implied). Values with thick outline represent previously published ratios.

3.4 Discussion

3.4.1 Fluvial Sr isotopic ratio

Most global river waters have high $^{87}Sr/^{86}Sr$ (Palmer and Edmond, 1989) because these rivers erode continental crust, which has a dominance of granitic rocks and contain minerals like micas

and K-feldspar with high $^{87}Sr/^{86}Sr$ (Brass, 1976). In contrast, the fluvial sources of the Black Sea and Caspian Sea have lower $^{87}Sr/^{86}Sr$ values (Figure 3.2) because the geology of the catchment area (Figure 3.5) includes Mesozoic and Paleogene carbonate deposits that have high Sr concentration with low $^{87}Sr/^{86}Sr$ (Figure 1.10).

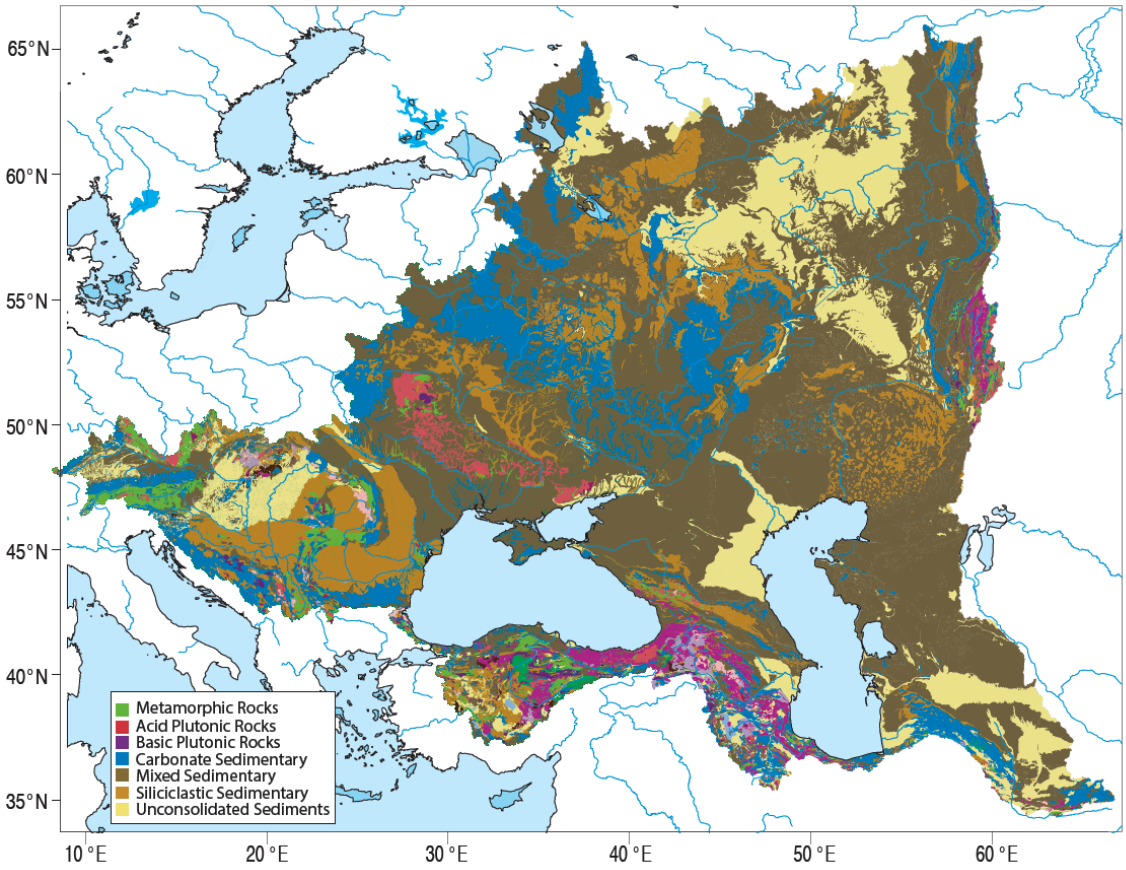

FIGURE 3.5: Lithological map of the Black and the Caspian seas' drainage basin. Modified from Hartmann and Moosdorf (2012).

3.4.1.1 Northern Black Sea rivers

Unlike the other rivers in the region, the Don and Dnieper rivers have unusually high $^{87}Sr/^{86}Sr$ values (Figure 3.2A), which are significantly higher than previously published value of 0.7084 estimated by Palmer and Edmond (1989) based on each river's catchment geology (Figure 3.6). The major part of the catchment area of the Don and Dnieper includes substantial exposure of Late Cretaceous carbonate and Palaeocene - Eocene limestones deposits (Figure 3.6, 1.10). Near its mouth, the Don also cuts through the Late Carboniferous limestone and dolomite deposits. Less than 10% of the area exposes plutonic rocks (Figure 3.6). Granitic rocks usually have high $^{87}Sr/^{86}Sr$ values and low concentrations (Brass, 1976). Given that ~25% of the total catchment

area of each river contains carbonate sedimentary deposits, the Sr signal of these rivers is expected to be dominated by low $^{87}Sr/^{86}Sr$ of the carbonates, in accordance with values estimated by Palmer and Edmond (1989).

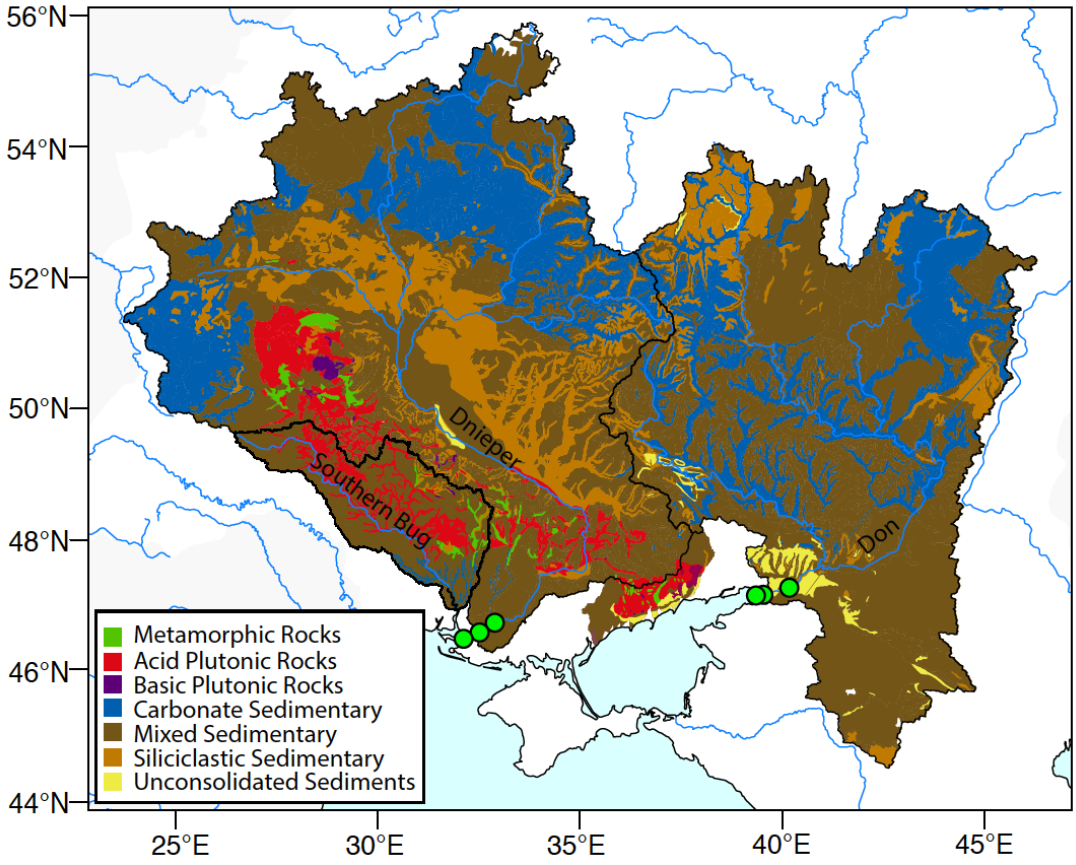

FIGURE 3.6: Lithological map of the Don and Dnieper rivers' catchment area. Green dots show the water sampling locations. Modified from Hartmann and Moosdorf (2012).

One possible explanation of the higher than expected $^{87}Sr/^{86}Sr$ in the northern river water samples collected in this study is that they may be representing local fluvial signal rather than the signal of the entire catchment. Smaller rivers along the northern coast of the Sea of Azov erode plutonic rocks (Figure 3.6). Therefore, these rivers should have radiogenic Sr isotopic ratio and may be generating a radiogenic Sr signal within the Sea of Azov. The high $^{87}Sr/^{86}Sr$ measured at the Don delta may be reflecting the Azov value rather than the Don river signal. The trend towards lower $^{87}Sr/^{86}Sr$ values upstream in the Don river (Figure 3.2A) may indicate decreasing influence of the radiogenic Azov signal away from the delta mouth towards predicted low value of the Don river (Palmer and Edmond, 1989). Compared to the Don, the Sr signal of the Dnieper does not show a consistent pattern. The southern region of the Dnieper catchment and the catchment of Southern Bug river, which drains into the same region, have large area of plutonic surfacial geology (Figure

3.6). High $^{87}Sr/^{86}Sr$ values could be a mixture between the three source end members; Dnieper river, Southern Bug and Black Sea. Therefore, further investigation is required to constrain the fluvial signal of the Don and Dnieper river.

The high values measured in the Don and Dnieper rivers may also reflect the influence of anthropogenic sources, such as fertilisers and sewage (e.g. Hosono et al., 2007; Nakano et al., 2005; Pearce et al., 2015; Vitòria et al., 2004; Widory et al., 2004). The $^{87}Sr/^{86}Sr$ of sewage effluent is likely to be high given the high Rb/Sr in biological matrices such as faeces and urine (Nirel and Revaclier, 1999). A wide range of Sr isotopic ratios (0.7033 - 0.835) have been observed for fertilisers because of wide variety of source materials used during manufacturing (Vitòria et al., 2004). Strontium in fertilisers is associated with sulphates, phosphates or carbonates and the $^{87}Sr/^{86}Sr$ value will vary depending on their origin (e.g., Antich et al., 2000; Böhlke and Horan, 2000; Négrel and Roy, 1998; Vitòria et al., 2004). Without identifying the anthropogenic sources and their correct $^{87}Sr/^{86}Sr$ composition, distinguishing between natural and human induced source for the unusually high values in these northern rivers is currently not possible.

In summary, the new $^{87}Sr/^{86}Sr$ data for both, the Don and Dnieper rivers contradict the estimates based on the catchment geology of each river. Possible reasons are presented for each case, but it is currently not possible to confirm the Sr isotopic ratio of these rivers. Consequently, the estimated values for these rivers provided by Palmer and Edmond (1989) are used in this thesis, because it is the only value most likely to be representative of the catchment geology of the Don and Dnieper. Detailed, greater spatial coverage isoscape studies of the catchment area for these rivers are required.

3.4.1.2 Rivers draining the Caucasus

Eastern Black Sea rivers along the coast of Georgia show the some of the lowest $^{87}Sr/^{86}Sr$ observed in the area (Figure 3.2A and B). A similar low values were also observed in the water samples from the Kura river draining western side of the Caspian Sea (Figure 3.2C). Given that carbonates and volcanic deposits, both of which have low Sr isotopic ratio, these low values are expected given that these rivers drain the parts of the Caucasus Mountains, which mostly consist of metamorphic Cretaceous and Jurassic carbonate (Figure 1.10) and Cenozoic volcanic rocks (Mitchell and Westaway, 1999).

3.4.1.3 Volga river

The catchment area of the Volga river lies within the East European Platforms and consists of Carboniferous and Cretaceous limestones (Figure 3.5). The $^{87}Sr/^{86}Sr$ of the Volga river shows low values (Figure 3.2), which are consistent with the geology of its drainage area (Figure 1.10).

3.4.1.4 Aral Sea measurements constraining Amu Darya river

The $^{87}Sr/^{86}Sr$ values measured on water samples collected from the Aral Sea are high (0.709214 ± 0.0000065), suggesting a radiogenic source feeding the Aral Sea. Today, Amu Darya and Syr Darya are the two main fluvial sources for the Aral Sea (Figure 3.8). Amu Darya originates in the Pamir Mountains and drains into the South (or Large) Aral Sea, and Syr Darya, which flows from the Tien Shan mountains, to the north of the Pamirs, drains into the North (or Small) Aral Sea (Figure 3.8, Asarin et al., 2010). South and North Aral Sea have been two distinct water bodies since 1986 – 1987 as a result of water level fall induced by reduced fluvial discharge due to unsustainable irrigation in the area (Micklin, 2010). After this separation, a channel formed that connected the two basins, with water flow from the higher-level North Aral Sea to the lower-level South Aral Sea. In 2005, the two basins were separated by construction of the Kok-Aral dam with an outflow control structure (Micklin, 2010). Consequently, the Aral Sea water samples collected in 2009 from the western basin of the South Aral Sea are likely to be heavily dominated by Amu Darya river water. Even if they do represent a mixture of water from both rivers, Amu Darya and Syr Darya have similar catchment geology, which includes metamorphosed Precambrian and Paleozoic rocks at their mountainous headwaters and Neogene sedimentary deposits in the lower reaches (Figure 3.8). The Sr isotopic ratios of both rivers are likely to be similar and high, reflecting the geology of their catchment area with high $^{87}Sr/^{86}Sr$. Consequently, the $^{87}Sr/^{86}Sr$ measured on the Aral Sea water samples is likely to reflect the Sr isotopic ratio of the Amu Darya river and as such, provides the first constraint on the Amu Darya river signal, for which previously only a largely speculative estimation existed (Page, 2004; Wegwerth et al., 2014).

3.4.2 Homogeneity assumption within the Black Sea

The $^{87}Sr/^{86}Sr$ measured on Black Sea surface water samples ranges between 0.709128 and 0.709152 (Figure 3.3). All of the samples collected offshore are within error of each other. The samples

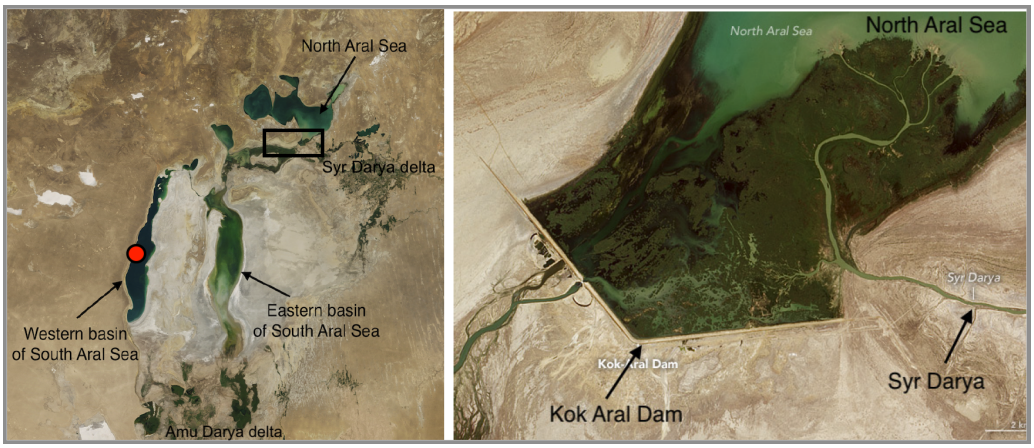

FIGURE 3.7: Satellite image of the Aral Sea taken on August 2017 showing North and South Aral Basin separated by Kok Aral Dam. Image adapted from *NASA Earth Observatory Images*.

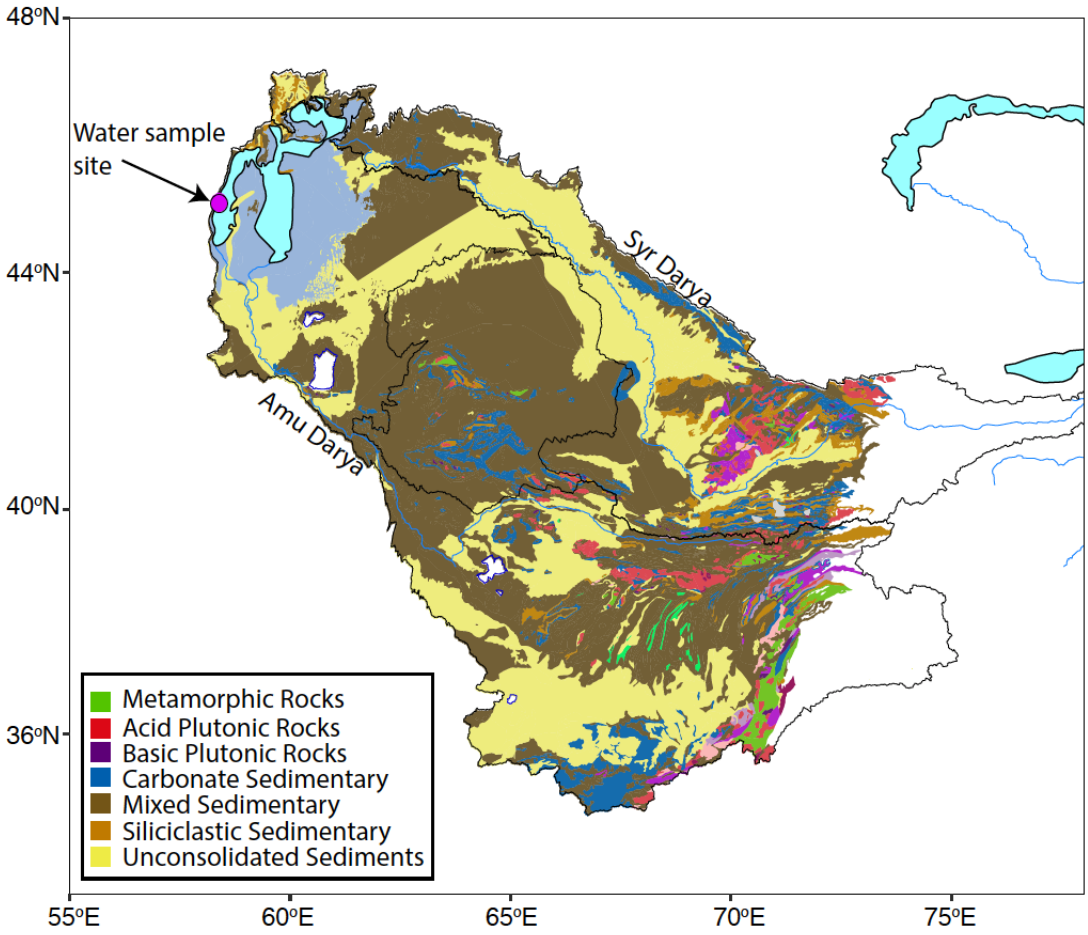

FIGURE 3.8: Lithological map of the Amu Darya and Syr Darya catchments. Pink dot represents the Aral Sea water sample location. Modified from Hartmann and Moosdorf, 2012.

taken from the beach in Georgia show lower values (Fig. 3). The average of all the offshore measurements is 0.709143 ± 8 ppm (2SD, n= 13). This value is lower than, but within error of, the previous single measurement of 0.7093 ± 0.0007, which has a large analytical error (Cox and Faure,

1974). The measurement by Cox and Faure (1974) is also significantly higher than the present-day ocean water value. Given that the major rivers draining the Black Sea have $^{87}Sr/^{86}Sr$ lower than the ocean water, the high $^{87}Sr/^{86}Sr$ measured by Cox and Faure (1974) could be anomalous and influenced by local geology. Although, specific sample location is not available, the cruise track for R/V *Atlantis II* in April and May 1969, during which this water sample was collected, shows a likely south eastern sampling location in the Black Sea (Ross et al., 1974).

The average Black Sea $^{87}Sr/^{86}Sr$ generated in this study is lower than the modern ocean ratio (McArthur et al., 2012). Today, the Black Sea receives about 2 x 10^{11} m^3/yr inflow from the Mediterranean Sea and about 3.38 x 10^{11} m^3/yr from fluvial discharge (Jaoshvili, 2003). Although the fluvial input is almost twice as much as the marine inflow, the measured $^{87}Sr/^{86}Sr$ of the Black Sea is much closer to this oceanic value compared to the weighted riverine $^{87}Sr/^{86}Sr$ of 0.708699 because of the comparatively higher concentration of Sr in oceanic water than the fluvial Sr concentration. The sensitivity of the $^{87}Sr/^{86}Sr$ of the Black Sea with changing oceanic input and fluvial discharge is explored in Chapter 4.

The Sr isotopic ratios measured on the water samples collected at depth in the Black Sea show values that are within error of the surface water samples at the same location (Figure 3.3E). Today, the Black Sea is anoxic at depths below 100 - 200 m because of strong density stratification (Kosarev and Kostianoy, 2008). Although there is strong water column stratification in the Black Sea today, the consistency between deeper water (>500 m) and surface water $^{87}Sr/^{86}Sr$ values suggests that Sr is relatively well mixed within the basin.

3.4.3 Homogeneity assumption within the Caspian Sea

The $^{87}Sr/^{86}Sr$ of the Caspian Sea surface water measured off the coast of Kazakhstan (Figure 3.4B) and Azerbaijan (Figure 3.4B) show similar values that are consistent with previously published Caspian Sea $^{87}Sr/^{86}Sr$ by Clauer et al. (2000, Figure 3.4D). The average $^{87}Sr/^{86}Sr$ of the Caspian Sea measured in this study is 0.708191 ± 0.000009 (2SD, n= 6). This value reflects the dominant influence of the Volga river, which provides ~82% of the fluvial input into the Caspian Sea (Shiklomanov et al., 1995). While there is additional input from the western (Sulak, Kura and Terek; 11.5%) and Iranian (3.5%) rivers (Shiklomanov et al., 1995), they have low $^{87}Sr/^{86}Sr$ (Clauer et al., 2000). Groundwater discharge, which has a similar Sr isotopic ratio to thermal spring water

in the Caspian Sea (0.7085), has a Sr concentration several orders of magnitude higher than riverine water (Table 4.1, Clauer et al., 2000, 2008) and therefore, elevates the $^{87}Sr/^{86}Sr$ of the Caspian above that of the Volga signal.

The measured $^{87}Sr/^{86}Sr$ of the water samples at 20 m depth shows values similar to that of the surface water (Figure 3.4D). Samples below 20 m water depth were not collected in this study, however, previously published deeper samples in the Caspian Sea (exact location unknown but likely to have been taken from the South Caspian basin, Clauer et al., 2008) have $^{87}Sr/^{86}Sr$ values that are both, higher and lower than the average $^{87}Sr/^{86}Sr$ measured in this study (Figure 3.4D). Although, Clauer et al.'s data have a larger range, the average $^{87}Sr/^{86}Sr$ of the Caspian Sea (0.708187) is similar to this study (Figure 3.4D).

Given the scatter in the $^{87}Sr/^{86}Sr$ of the Caspian data, more spatial data is required to confirm a homogeneous Caspian Sea with respect to Sr isotopes. However, on the basin of the measurements from this study and Clauer et al. (2008), the Caspian Sea is relatively well mixed, particularly considering the influence of the Volga river in the north, from where most of the samples in this study were obtained.

A basin is considered to be homogeneous with respect to an element if the residence time of that element is larger than the water turnover time. For the Black Sea, the residence time of Sr is ~16,600 yrs, much longer than the deep water turnover time of ~2000 yrs (Ostlund and Dyrssen, 1986), while in the Caspian Sea, the residence time of the Sr is calculated to be ~15,000 years compared to the mixing time of ~238 yrs. In both cases, these residence time suggests a well mixed basin with respect to $^{87}Sr/^{86}Sr$, consistent with the empirical study. However, the residence time of an element depends on the inflow and outflow from the basin, as it changes the concentration and the rate of input into the basin. Accordingly, the residence times of Sr in the Black and Caspian seas in the past is likely to have been different than the present-day values, as the inflow to and outflow from these basin have fluctuated considerably throughout their existence.

3.4.4 Validity of the ostracod archive

Of the 10 biogenic carbonate samples collected from the modern Black Sea sediment, 8 have Sr isotope values that are within error of the measured bottom water value (Figure 3.3E). Two samples show significantly lower values for ostracods compared to the bottom water; Station 33 and 36.

Where more than one type or species of biogenic carbonate (e.g. benthic foraminifera and ostracod valve, or valves from different ostracod species) from the same sample was analysed, Sr isotopic ratios are within error of each other in all but 1 sample at Station 36.

Despite the lack of bottom water measurements, ostracods from three stations show values within error of the average Caspian $^{87}Sr/^{86}Sr$ (Figure 3.4E). Modern ostracods from two locations (Station 68 and 69) show high values significantly higher than the average Caspian Sea water values. The $^{87}Sr/^{86}Sr$ measured on two different species of ostracods (*Caspiolla acronasuta* and *Eucythere naphtascholana*) collected from the modern Caspian sediment shows similar values between each other at three locations.

One possible explanation for these divergences of the ostracod $^{87}Sr/^{86}Sr$ from the water column signal in both, the Black and Caspian seas, is that they may not be representing modern archives. The sediment samples were taken from the surface grab, however these samples may include older material mixed in or exposed at the surface by erosion, downslope transport or bioturbation. This interpretation is supported by the presence of heavily reworked mollusc assemblage in the Caspian Sea at these sites (Figure B.1). In the Black Sea, measured Sr isotope values, which differ from overlying water, are consistent $^{87}Sr/^{86}Sr$ with the fossil Sr isotope data from ~5 ka (Major et al., 2006).

In summary, the $^{87}Sr/^{86}Sr$ measured on the different species of ostracods collected from the surface sediment of the Black Sea and the Caspian Sea generally show similar $^{87}Sr/^{86}Sr$ values to the surface water without any species-specific variation indicating that they can preserve primary Sr signal of the water. Where there is a small difference between bottom water and biogenic carbonate $^{87}Sr/^{86}Sr$, it is likely due to sediment reworking. Therefore, ostracods can be used as a good archive to examine the past changes in the water chemistry of a basin in the past, assuming that ostracods do not show any diagenetic alteration (Section 2.5) and a robust age model is available.

3.5 Conclusions

The additional new measurements of the $^{87}Sr/^{86}Sr$ generated in this study constrain the Sr isotopic signal of the Black and Caspian sea rivers. The present-day fluvial sources showed values consistent with their catchment geology, except the northern Black Sea rivers, Don and Dnieper. For these rivers higher $^{87}Sr/^{86}Sr$ may either reflect anthropogenic sources like fertilisers and sewage or a

local geological signal. The limited range of $^{87}Sr/^{86}Sr$ water collected within the Black Sea and the Caspian Sea show that these basins are relatively well mixed with respect to Sr isotopic ratio. While the basin $^{87}Sr/^{86}Sr$ is affected by fluvial discharge closer to river mouth and beaches, the signal further offshore is consistent along the surface and at depth. The $^{87}Sr/^{86}Sr$ measured on modern ostracods commonly shows similar values as to that of the bottom water at the same location except where there is evidence of bioturbation or sedimentary reworking.

Chapter 4

Numerical Box Model: A method to constrain the hydrological budget

This chapter describes the numerical box model used to explore the hydrological budget in subsequent results chapters (Chapter 5, 6 and 7). Model parameters are constrained by published and new $^{87}Sr/^{86}Sr$ isotopic data from Chapter 3. This chapter also tests the validity of the model by comparing the observed $^{87}Sr/^{86}Sr$ and salinity of the present-day Black Sea with outputs generated by a model that is configured for the present-day Black Sea.

4.1 Model description

The numerical box model used in this study is modified from Topper et al. (2011) and Modestou et al. (2017). These authors used coupled mass balance equations for water, salinity and the Sr isotopic ratio to provide quantitative constraints on the hydrologic budget and inter-basin exchange required to reproduce the observed $^{87}Sr/^{86}Sr$ and salinity during the Messinian Salinity Crisis. Here, a similar approach was used for the Caspian Sea (Chapter 5 and 7) and the Black Sea (Chapter 6) to constrain the inter-basin exchange required to produce observed $^{87}Sr/^{86}Sr$ and salinity estimates in these basins.

All model calculations are performed assuming steady-state solutions, where the volume of the water within the basin remains constant, i.e. total inflow into the basin is equal to the total outflow (Figure 4.1). The Black Sea or the Caspian Sea is considered as a single box with changing input sources and connection to the adjacent basins (for basin specific details see Chapters 5, 6 and 7). The inflow, outflow, river run-off, evaporation, and precipitation contribute to the hydrological

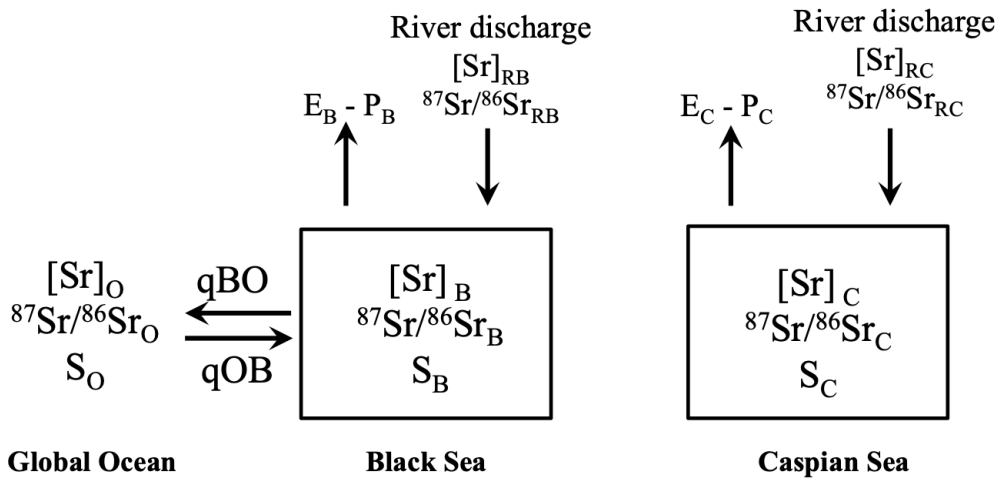

FIGURE 4.1: Diagram of the box model for the Black Sea and the Caspian Sea with arrows representing all input and output fluxes; qBO: outflux from Black Sea to the open ocean, qOB: influx from the ocean to the Black Sea, E_B - P_B: evaporation minus precipitation for the Black Sea and E_C - P_C: evaporation minus precipitation for the Caspian Sea.

budget of the basin. However, only inflow, outflow, and river run-off affect the $^{87}Sr/^{86}Sr$ of the basin because although evaporation and precipitation impacts salinity they have negligible affect on Sr isotopes (Capo et al., 1998). The different sources of Sr and their present-day fluxes into the Black and Caspian seas are discussed below.

4.1.1 Ocean water

Modern ocean Sr concentration is about 40 times higher than the average global river (Palmer and Edmond, 1989). Although it varies slightly with depth, the accepted oceanic concentration is ~ 7.85 ± 0.03 ppm (Veizer, 1989 and references therein). During the last 3 million years, the Sr isotopic ratio of the ocean water has increases slightly and ranges between 0.709060 to 0.709175. For the modern ocean $^{87}Sr/^{86}Sr$ value is 0.709175 ± 0.000001 (McArthur et al., 2012).

At present, the Black Sea receives marine water from Mediterranean Sea. According to different authors, the marine influx into the Black Sea ranges between 1.23 to 3.12 x 10^{11} m^3/yr (Jaoshvili, 2003, and references therein). For modelling purposes here, an average value of ~2 x 10^{11} m^3/yr was used.

4.1.2 Fluvial run-off

The main present-day fluvial sources in the Pontocaspian region are the Danube, Don, Dnieper and Volga. Palmer and Edmond (1989) provide the $^{87}Sr/^{86}Sr$ and Sr concentration for the three major rivers of the Black Sea (Danube, Don and Dnieper), which together provides ~75% of total fluvial discharge into the Black Sea (Jaoshvili, 2003). The $^{87}Sr/^{86}Sr$ and Sr concentration for the minor rivers along the eastern coast of the Black Sea, which provides ~20% of the run-off into the Black Sea, was measured in this study (Chapter 3). The remaining 5% comes from the other minor river draining the southern coast of the Black Sea (Jaoshvili, 2003), for which there are no Sr isotopic measurements. The $^{87}Sr/^{86}Sr$ of Volga river is from this study (Table 4.1) and for the other Caspian rivers was provided by Clauer et al. (2000).

Jaoshvili (2003) compiled different estimations for the Black Sea fluvial discharge that ranged from 2.94 x 10^{11} to 4.74 x 10^{11} m^3/yr . The mean value is 3.38 x 10^{11} m^3/yr (Table 4.1). The Caspian Sea is an isolated basin with total discharge of about 3.4 x 10^{11} m^3/yr (Shiklomanov et al., 1995). About 80% of this discharge is from the Volga, with mean annual run-off of 2.4 x 10^{11} m^3/yr (Table 4.1). The western rivers (Kura, Sulak, Samur, Terek) and the rivers along Iranian coast make up about 11 and 3.5%, respectively, of the total fluvial input into the Caspian Sea (Table 4.1, Shiklomanov et al., 1995).

4.1.3 Groundwater discharge

There are large discrepancies in estimates of groundwater discharge in the Caspian Sea, which ranges from 0.3 to 49 km^3/yr (Zektzer et al., 1973). With no direct measurements, the discharge estimates are usually obtained as a residual term of the equation for the average long-term water balance, and are therefore sensitive to uncertainties in all other parameters (Kostianoy and Kosarev, 2005).

Clauer et al. (2000) proposed that the Sr isotopic composition of the groundwater is likely to be similar to that of thermal springs located at many sites along the west coast of the Caspian Sea. Accordingly, a $^{87}Sr/^{86}Sr$ value of 0.7085 and a Sr concentration of 145 ppm are used for the groundwater discharge into the Caspian Sea (Table 4.1). Clauer et al. (2000) also estimated a groundwater discharge of ~8 x 10^8 m^3/yr into the Caspian Sea to balance the Sr isotopic ratio of the current Caspian water. Even though there are large uncertainties associated with this approach

(e.g. variability in the cumulative fluvial flux and the Sr signal), these estimates best explain the present-day ratio of the Caspian Sea given the availability of the data. Therefore, a Caspian groundwater discharge of 8 x 10^8 m^3/yr is used in the model.

For the Black Sea, Jaoshvili (2003) suggested a groundwater discharge of ~5% of surface inflow (~1.7 x 10^{10} m^3/yr) based on the estimates of groundwater contribution to the open ocean, the Mediterranean Sea and the Atlantic Ocean. However, there are no direct measurements or estimates for the Sr signal of this discharge in the Black Sea. Although it is acknowledged that groundwater discharge impacts the chemical composition of the Black Sea water, constraining this parameter is outside the scope of this study and not included in the calculation for the Black Sea. The potential contribution of groundwater discharge on the Sr isotopic signal of the Black Sea water is discussed in Section 4.3.

4.1.4 Dust

Airborne dust particles settling in the basin may also contribute to the Sr isotopic ratio of the basin (Jacobson, 2004). The isotopic composition of the dust will have significant variability and depends on the geology of the source region (Scheuvens et al., 2013). The average Sr isotopic ratio for global dust is ~0.725 (Grousset and Biscaye, 2005), which is significantly higher than the global ocean water value (0.709175, McArthur et al., 2012). However, dust is not considered a significant source of Sr to marine budgets (Frank, 2002; Goldstein and Hemming, 2003), as only a small amount of Sr is transferred to seawater relative to the already high seawater Sr concentration.

Dust deposited in the Black Sea and the Caspian Sea is most likely to be a mixture of Saharan, southwest Asian and local central Asian (Karakum desert and Aral Sea) dust sources (Hamidi et al., 2013; Lee et al., 2006; Singer et al., 2003). All of these dust sources have higher than oceanic $^{87}Sr/^{86}Sr$ (Dewan et al., 2015; Grousset and Biscaye, 2005). However, there are no measurements of the Sr contribution by dust deposition to these basins. The Sr concentration, although lower than the oceanic value, is still higher in the Black Sea and the Caspian. Therefore, any impact it has on the basin $^{87}Sr/^{86}Sr$ is likely to be small. Additionally, given the more significant Sr fluxes in the Black and Caspian Sea (e.g., run-off and marine water), dust is likely to have a small impact on the Sr budget of the basin and therefore is not included in this study.

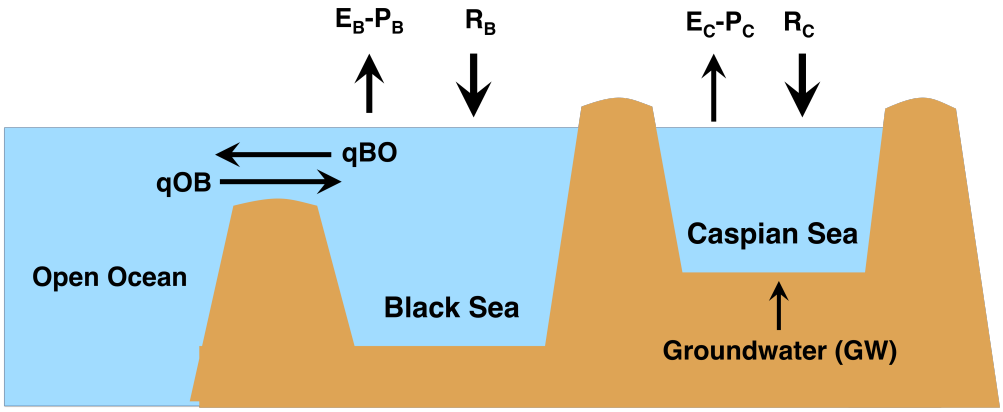

FIGURE 4.2: Schematic showing the present-day configuration of the Black Sea and the Caspian Sea with inflows and outflows. The Black Sea receives input from the Mediterranean Sea (qOB), run-off (R_B) and precipitation (P_B) and loses water from evaporation (E_B) and outflow to the Mediterranean Sea (qBO). Unlike the Black Sea, the Caspian Sea today, is an isolated basin and receives water only from fluvial run-off (R_C), groundwater (GW) and precipitation (P_C) and loses water through evaporation (E_C).

4.2 Main equations

An overview of the main equations for the present-day configuration of the Black Sea and the Caspian Sea is presented here. These equations will be modified in subsequent chapters for various connectivity scenarios. The equations are based on the principle of conservation of mass and therefore describe inflow into and outflow from the basins (Modestou et al., 2017; Topper et al., 2011).

4.2.1 Black Sea

For the present-day configuration, the Black Sea is represented by a box with inflow from the open ocean and freshwater input from its fluvial sources and precipitation. The Black Sea also loses water through evaporation and outflow to the Mediterranean Sea (Figure 4.2). In the steady state situation, the Black Sea water budget is given by,

$$qBO = qOB + R_B + P_B - E_B \tag{4.1}$$

where, qOB refers to the flux from the open ocean to the Black Sea and qBO refers to the flux from the Black Sea to the open ocean. Total river discharge, evaporation and precipitation fluxes of the Black Sea are given by R_B, E_B and P_B, respectively. Because evaporation and precipitation have a negligible effect on the fractionation of Sr isotopes (Capo et al., 1998), and the Sr signal of the

basin is controlled by its input sources, the Sr concentration, Sr isotopic ratio of the Black Sea can be determined as follows, with subscripts *O, RB* and *B* referring to oceanic, Black Sea rivers and Black Sea, respectively.

Sr concentration:

$$[Sr]_B = \frac{[Sr]_O * qOB + [Sr]_{RB} * R_B}{qOB + R_B} \tag{4.2}$$

where,

$$[Sr]_{RB} = \frac{[Sr]_{Rb1} * Rb1 + [Sr]_{Rb2} * Rb2 + ... + [Sr]_{Rbn} * Rbn}{R_B}$$

and $[Sr]_{Rbn}$ and Rbn refers to Sr concentration and discharge flux, respectively, of individual Black Sea rivers.

Sr isotopic ratio:

$$\left(\frac{^{87}Sr}{^{86}Sr}\right)_B = \frac{\left(\frac{^{87}Sr}{^{86}Sr}\right)_O * [Sr]_O * qOB + \left(\frac{^{87}Sr}{^{86}Sr}\right)_{RB} * [Sr]_{RB} * R_B}{[Sr]_O * qOB + [Sr]_{RB} * R_B} \tag{4.3}$$

and

$$\left(\frac{^{87}Sr}{^{86}Sr}\right)_{RB} = \frac{\left(\frac{^{87}Sr}{^{86}Sr}\right)_{Rb1} * [Sr]_{Rb1} * Rb1 + \left(\frac{^{87}Sr}{^{86}Sr}\right)_{Rb2} * [Sr]_{Rb2} * Rb2 + \ldots + \left(\frac{^{87}Sr}{^{86}Sr}\right)_{Rbn} * [Sr]_{Rbn} * Rbn}{[Sr]_{RB} * R_B}$$

where, the ratio of individual rivers is represented by $\left(\frac{^{87}Sr}{^{86}Sr}\right)_{Rbn}$.

The salinity of the Black Sea ($[S]_B$) is driven by the inflow from and outflow to the Mediterranean Sea which has a salinity of $[S]_O$.

$$[S]_B = \frac{[S]_O * qOB}{qBO} \tag{4.4}$$

4.2.2 Caspian Sea

Unlike the Black Sea, the Caspian Sea is currently an isolated basin, therefore its water budget is controlled by riverine input, groundwater discharge, evaporation and precipitation and the Sr signal is controlled by its fluvial and groundwater inputs. Therefore, in a steady state situation,

$$E_C = R_C + GW_C + P_C \tag{4.5}$$

where, Caspian river, groundwater discharge, evaporation and precipitation fluxes are represented by R_C, GW_C, E_C and P_C, respectively.

Sr concentration:

$$[Sr]_C = \frac{[Sr]_{RC1} * Rc1 + [Sr]_{Rc2} * Rc2 + ... + [Sr]_{Rcn} * Rcn + [Sr]_{GW} * GW_C}{R_C + GW_C} \tag{4.6}$$

where and $[Sr]_{Rcn}$ and Rcn refers to Sr concentration and discharge flux, respectively, of individual Caspian Sea rivers and $[Sr]_{GW}$ refers to the Sr concentration of the groundwater discharge.

Sr isotopic ratio:

$$\left(\frac{^{87}Sr}{^{86}Sr}\right)_C = \frac{\begin{array}{c}\left(\frac{^{87}Sr}{^{86}Sr}\right)_{Rc1} * [Sr]_{Rc1} * Rc1 + \left(\frac{^{87}Sr}{^{86}Sr}\right)_{Rc2} * [Sr]_{Rc2} * Rc2 + ... \\ ... + \left(\frac{^{87}Sr}{^{86}Sr}\right)_{Rcn} * [Sr]_{Rcn} * Rcn + \left(\frac{^{87}Sr}{^{86}Sr}\right)_{GW} * [Sr]_{GW} * GW_C\end{array}}{[Sr]_{RC} * R_C + [Sr]_{GW} * GW_C} \tag{4.7}$$

where, $\left(\frac{^{87}Sr}{^{86}Sr}\right)_{Rcn}$ and $\left(\frac{^{87}Sr}{^{86}Sr}\right)_{GW}$ represents the Sr isotopic ratio of individual rivers and groundwater discharge, respectively.

The Caspian Sea, despite being an isolated basin with only freshwater inputs, still has brackish salinity today. The salinity of the Caspian Sea is negligible near the mouth of the Volga and gradually increases towards the south, reaching ~13 g/kg in the southern basin (Figure 1.6B, Kostianoy and Kosarev, 2005). This high salinity is attributed to residual salt from the last oceanic connection (Zenkevitch, 1963) and/or input from high solute content groundwater (Clauer et al., 2008). However, there are no salinity constraints available for either of these components that can be used for the modelling.

TABLE 4.1: Overview of model parameters used in this study.

Parameters	**Present-day values**	**Reference:**
	Global Ocean	
Salinity	35 g/kg	
Sr concentration	7.85 ppm	Veizer (1989)
Sr ratio	0.709175	McArthur et al. (2012)
	Black Sea	
Outflow to the Ocean	4 x10^{11} m^3/yr	Jaoshvili (2003)
Inflow from the Ocean	2 x10^{11} m^3/yr	Jaoshvili (2003)
Evaporation	3.3 x 10^{11} m^3/yr	Jaoshvili (2003)

Table 4.1 Continued:

Precipitation	2.1x10^{11} m^3/yr	Jaoshvili (2003)
Salinity	17 g/kg	Özsoy and Ünlüata (1997)
Sr concentration	1.77 ppm	This study
Sr ratio	0.709143	This study
Caspian Sea		
Salinity	12 g/kg	Kostianoy and Kosarev (2005)
Evaporation	4.3 x 10^{11} m^3/yr	Clauer et al. (2000)
Precipitation	1.3 x 10^{11} m^3/yr	Clauer et al. (2000)
Sr concentration	4.13 ppm	This study
Sr ratio	0.708191	This study
Danube		
Water flux	2.06 x 10^{11} m^3/yr	Jaoshvili (2003)
Sr concentration	0.24 ppm	Palmer and Edmond (1989)
Sr ratio	0.7089	Palmer and Edmond (1989)
Don		
Water flux	2.94 x 10^{10} m^3/yr	Palmer and Edmond (1989)
Sr concentration	0.22 ppm	Palmer and Edmond (1989)
Sr ratio	0.70840 (estimated)	Palmer and Edmond (1989)
Dnieper		
Water flux	4.3 x 10^{10} m^3/yr	Jaoshvili (2003)
Sr concentration	0.22 ppm	Palmer and Edmond (1989)
Sr ratio	0.70840 (estimated)	Palmer and Edmond (1989)
Rioni		
Water flux	9.6 x 10^{9} m^3/yr	Jaoshvili (2003)
Sr concentration	0.18 ppm	This study
Sr ratio	0.70800	This study
Chorokhi		
Water flux	8.7 x 10^{9} m^3/yr	Jaoshvili (2003)
Sr concentration	0.11 ppm	This study
Sr ratio	0.70585	This study
Enguri		
Water flux	2.1 x 10^{9} m^3/yr	Jaoshvili (2003)
Sr concentration	0.09 ppm	This study
Sr ratio	0.70864	This study
Natanebi		
Water flux	7.7 x 10^{8} m^3/yr	Jaoshvili (2003)
Sr concentration	0.06 ppm	This study

Table 4.1 Continued:

Sr ratio	0.70570	This study
	Volga	
Water flux	2.4 x 10^{11} m^3/yr	Clauer et al. (2000)
Sr concentration	0.48 ppm	Clauer et al. (2000)
Sr ratio	0.708053	This study
	Western Rivers	
Flux	3.91 x 10^{10} m^3/yr	Clauer et al. (2000)
Sr concentration	1.65 ppm	Clauer et al. (2000)
Sr ratio	0.707795	Clauer et al. (2000)
	Southern Rivers	
Water flux	1.19 x 10^{10} m^3/yr	Clauer et al. (2000)
Sr concentration	0.85 ppm	Clauer et al. (2000)
Sr ratio	0.708293	Clauer et al. (2000)
	Groundwater	
Flux	8 x 10^8 m^3/yr	Clauer et al. (2000)
Sr concentration	145 ppm	Clauer et al. (2000)
Sr ratio	0.7085	Clauer et al. (2000)
	Amu Darya	
Flux	4 x 10^{10} m^3/yr	Asarin et al. (2010)
Sr concentration	1.42 ppm	Clauer et al. (2000)
Sr ratio	0.709214 (for Aral Sea)	This study

4.3 Model validation

Model validation was conducted using a present-day Black Sea configuration (Figure 4.2). Equations 4.1 to 4.4 were constrained by the present-day values (Table 4.1) and the model was run with a stepwise increase in the Mediterranean influx and fluvial discharge to evaluate the resulting changes in the $^{87}Sr/^{86}Sr$ and salinity of the Black Sea.

The model result (Figure 4.3) shows that Mediterranean input drives both the salinity and Sr isotopic ratio in the present-day Black Sea. With present-day Mediterranean influx and total fluvial flux, the model produces a salinity of 16.8 g/kg and $^{87}Sr/^{86}Sr$ of 0.709153. The modelled salinity is in good agreement with the observed average Black Sea salinity of 17 g/kg (Özsoy and Ünlüata, 1997). If external uncertainty of ±9 ppm is assigned to the model result, the $^{87}Sr/^{86}Sr$ produced by model is within error of the observed $^{87}Sr/^{86}Sr$ of 0.709143 ± 8ppm in the Black Sea. However,

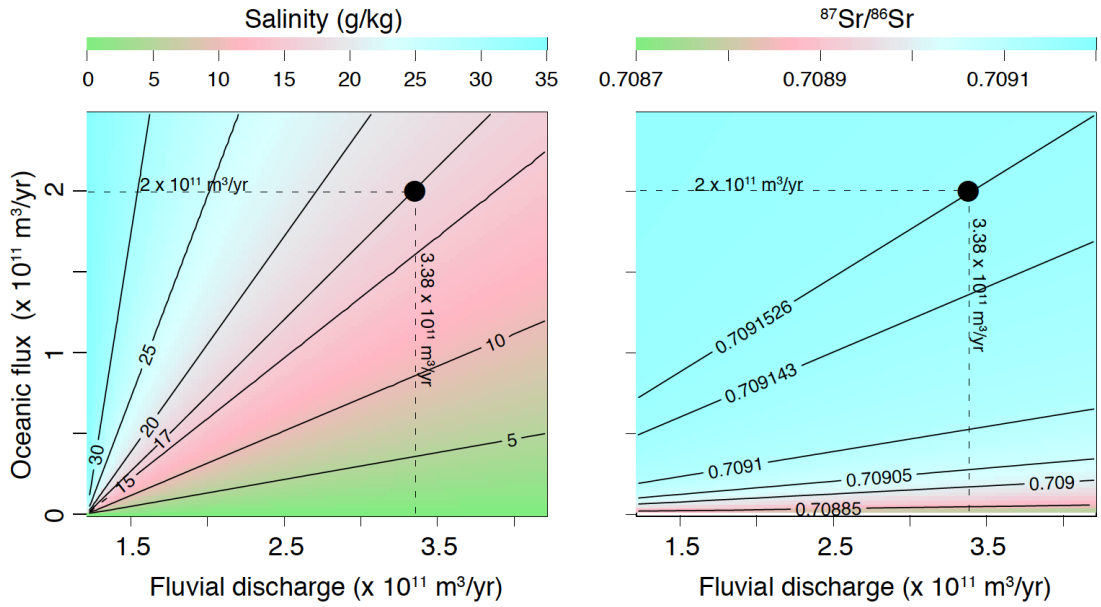

FIGURE 4.3: Model output for salinity and $^{87}Sr/^{86}Sr$ in the Black Sea with varying input from the open ocean and its fluvial sources. The black dots represents the model generated salinity and $^{87}Sr/^{86}Sr$ with present-day influxes for these sources. Present-day Mediterranean influx into the Black Sea is 2 x 10^{11} m^3/yr and fluvial discharge is 3.38 x 10 ^{11} m^3/yr (Jaoshvili, 2003).

it should be noted that only three major rivers (Danube, Don, and Dnieper) and the rivers along the eastern Black Sea are considered in this study because measurements for only these rivers are available. Given that the model output for salinity and $^{87}Sr/^{86}Sr$ in the Black Sea are similar to the observed value, despite the incomplete parameters incorporated in the model, the model used in this study can be assumed to capture the main features of the hydrologic budget in the Black Sea.

4.4 Sr signature of the Pleistocene rivers

The model is adapted for different connectivity configurations in Chapters 5 and 6 to interpret the $^{87}Sr/^{86}Sr$ measured on fossil ostracods. This requires constraints on the Sr concentration and $^{87}Sr/^{86}Sr$ of the rivers in the region during the Pleistocene. Sr concentration and $^{87}Sr/^{86}Sr$ of a river depends on its catchment geology. Given the short geological time-scale of only a three million years in this study, significant changes in the catchment geology of the major rivers draining into the Black Sea and Caspian Sea are unlikely to have occurred, although it is acknowledged that there are tectonically-active areas within the catchment. The Don, Dnieper and Volga drain the stable Russian Platform and the drainage system for these rivers has been in place since the middle Miocene (Matoshko et al., 2004). The drainage area of the Danube, however, includes

the tectonically-active Carpathian Mountains. Most of uplift of the Carpathians took place during the Middle Miocene during the last stage of continental collision (Sanders et al., 1999). Even though locally, there is 4 - 5 km of exhumations along the Carpathians in the Quaternary, the geology of the area mainly consists of high grade metamorphic granite (Matenco et al., 2016). Therefore, any local exhumation is unlikely to have changed the catchment geology of the Danube, and consequently the $^{87}Sr/^{86}Sr$ of the river water. As is the case for the Danube, some of the minor rivers in the region drain parts of active regions including the Caucasus Mountains, which have the highest uplift rate in the world (Mitchell and Westaway, 1999). However, the catchment area of these rivers is comparatively small and, any changes in the characteristics of these rivers on the overall Sr signal of the basin is likely to be insignificant. Given the study time-frame, it is assumed that there are no extreme changes in the catchment geology of the rivers draining into the Black Sea and the Caspian Sea. For purpose of modelling, the present-day $^{87}Sr/^{86}Sr$ and Sr concentration of the rivers (Table 4.1) were therefore, used to constrain the Pleistocene fluvial Sr isotopic signatures.

4.5 Additional fluvial input from the palaeo Amu Darya

In addition to current fluvial sources, geological evidence shows the presence of deltaic deposits on the eastern margin of the South Caspian basin (Abreu and Nummedal, 2007; Brunet et al., 2017) that indicates that the Caspian Sea was fed by another large river in the past. Amu Darya currently flows into the Aral Sea but river incision in the Kara Kum area suggests that the Amu Darya periodically flowed into the Caspian Sea until about 10 ka (Boomer et al., 2000; Micklin, 2010). Therefore, inclusion of the Amu Darya in the numerical model is essential for better understanding of the hydrological budget in the region. However, constraining the Amu Darya signal provides one of the dominant sources of uncertainty for the model runs.

Amu Darya currently discharges about 7.6 km^3/yr water into the Aral Sea (Asarin et al., 2010), but this run-off is significantly affected by the divergence of river water for irrigation in the surrounding area, which started in the 1960s. Prior to human interference, the discharge of Amu Darya into the Aral Sea was about 40 km^3/yr. Therefore, this latter value is used as a first order approximation for Amu Darya discharge into the Caspian Sea in this study.

The Sr concentration of the Amu Darya water was measured by Schettler et al., 2013. Although there are no direct $^{87}Sr/^{86}Sr$ measurement for the Amu Darya, $^{87}Sr/^{86}Sr$ measured in the Aral Sea water is used in this study to represent the Amu Darya signal (Section 3.4.1.4).

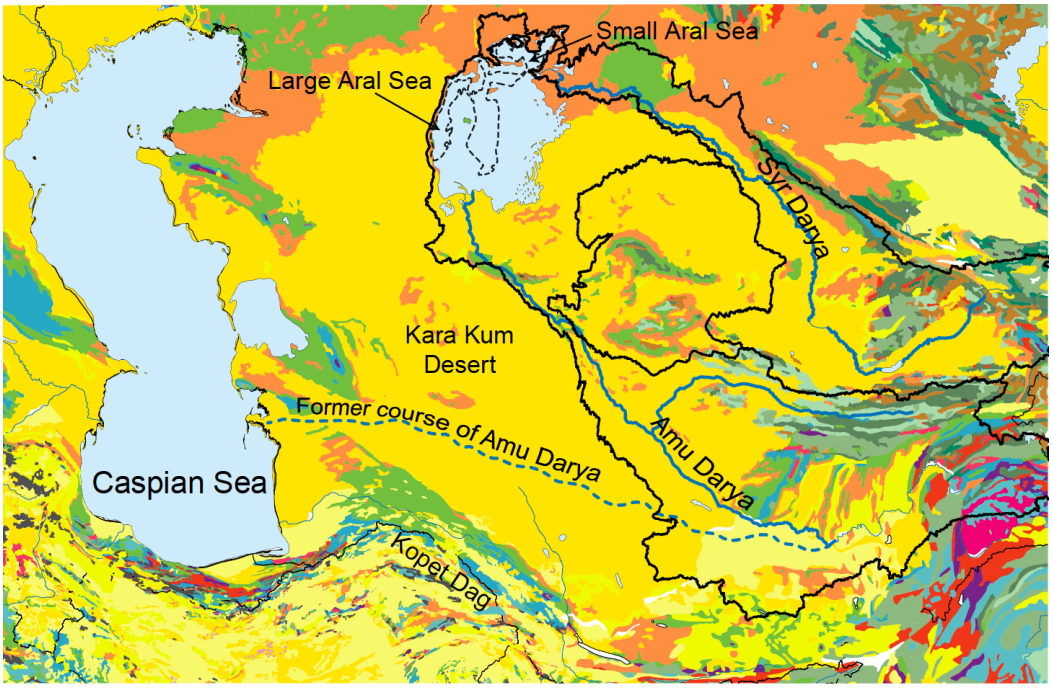

FIGURE 4.4: Geological map of the Amu Darya and Syr Darya catchment area represented in solid black lines. The former course of Amu Darya is shown by blue dashed lines. Dashed black lines show the present-day boundary of the Aral Sea. Colours represent the geological age of the deposits; Jurassic (Blue); Cretaceous (green), Paleogene (orange), Neogene - Quaternary (yellow), magmatic, volcanic rocks (red and reddish-blue). Map based on the International Geological Map of Europe *IGME5000*.

In contrast, to its current northern course into the Aral Sea, during the Late Pliocene and Pleistocene, Amu Darya flowed on a more westerly path across the lower Kara Kum Desert and reached the Caspian Sea north of the Kopet Dag escarpment (Figure 4.4). This former course of Amu Darya provided an additional catchment area, which currently is filled with Neogene - Quaternary sedimentary deposits. Brunet et al. (2017) reviewed the evolution of the Amu Darya Basin and showed that the palaeo Amu Darya river during its former course incised the Paleogene and Cretaceous deposits. These are predominantly clastics with some carbonates and anhydrites. The erosion of carbonates and anhydrite sediments by the Amu Darya during its former course may have resulted in the river water with a lower $^{87}Sr/^{86}Sr$. However, constraining this value for palaeo Amu Darya, with it's headwaters draining radiogenic western Himalayas and river channels draining carbonate deposits, is not within the scope of this study. Present-day values for the Amu Darya deduced from the Aral Sea samples (Chapter 3) were used in the model.

In the following result chapters, equations 4.1 - 4.7 are adapted and modified for different connectivity configurations to help explain the observed $^{87}Sr/^{86}Sr$ and salinity in the Black Sea and the Caspian Sea during the last 3 Ma. These chapters provide further discussions on the box model, and the implications of the modelling results.

Chapter 5

Strontium isotope constraints on early Pleistocene Caspian connectivity

Constraining the timing of connections between drainage basins is critical for understanding the rates of biological adaptation. This chapter focuses on the land-locked Caspian Sea, which contains endemic fauna and species that have close living relatives in the coastal and estuarine waters of the Arctic Ocean. Although the Caspian Sea experienced a complex connectivity history with the adjacent Black Sea and Mediterranean Sea as well as the Arctic Ocean, the timings of these connections is highly debated. This chapter explores the Early Pleistocene connectivity history between the Caspian, the Black Sea and the Arctic Ocean by evaluating the Sr isotope ratio of fossil ostracods from the Goychay (Caspian Sea) and Guria (Black Sea) sections. In particular, this chapter will answer research question 4 and will also address ***research questions 5 and 6*** *outlined in Section 1.6.2;*

4. *Does the geochemical system suggest a Caspian connection to the Arctic Ocean and if so, when did this connection occur?*
5. *How did the Sr isotopic ratio evolve in the Black and Caspian seas over the last 3 million years and what is its implication for the Quaternary connectivity history of the two basins to each other and the open ocean?*
6. *What was the nature of connection (one way flow or two way exchange) between the Black Sea, Caspian Sea and the open ocean during the Pleistocene?*

This chapter was written with intention to submit to *Geology*. However, just prior to submission, micropalaeontological analysis performed on the Gurian sections by **L. Rausch** and **M. Stoica** (University of Bucharest) revealed ostracod assemblages of late Miocene age. This contradicts the published age model (Kirscher et al., 2017) for the section, which suggested sediments were of Pleistocene age. Together with the co-authors, it was decided that the submission of the paper should be postponed until there is more certainty about the correct age model for the Gurian section. This chapter presents the Sr isotopic data from the Gurian section in accordance with the published age model representing Pleistocene Black Sea by Kirscher et al. (2017). However, implications of a possible late Miocene age for the Gurian data on the connectivity history between the Black Sea and the Caspian Sea will be further discussed in Chapter 6.

The age model for the Goychay section was provided by **S. Lazarev**, Utrecht University and the micropalaeontological analysis, and interpretation of salinity constraints for the Caspian Sea was provided by **Prof. M. Stoica** and **L. Rausch**, University of Bucharest. The age model and the ostracod assemblage and distribution chart presented in this chapter are also included in Lazarev et al. (2019):

S. Lazarev, E. L. Jorissen, S. van de Velde, L. Rausch, M. Stoica, F. P. Wesselingh, C. G. C. van Baak, T. A. Yanina, E. Aliyeva, W. Krijgsman (2019) **Magneto- biostratigraphic age constraints on the palaeoenvironmental evolution of the South Caspian Basin during the Early - middle Pleistocene (Kura Basin, Azerbaijan)**, *Quaternary Science Reviews*, 222, p. 105895.

5.1 Introduction

Today, the Caspian Sea harbours species whose sister taxa occur in coastal and estuarine waters of the Arctic Ocean (e.g. Audzijonyte, 2005; Bowman and Long, 1968; Väinölä, 1995; Väinölä et al., 2001) suggesting a Caspian connection to the Arctic Ocean in the past resulting in the transfer of these polar elements in the Caspian. The only geochemical study that implies a Caspian-Arctic connection is a published Pliocene - Early Pleistocene $^{87}Sr/^{86}Sr$ record from the Caspian Sea by van Baak et al. (2019). These authors measured the $^{87}Sr/^{86}Sr$ of Caspian Plio-Pleistocene

ostracod samples from the Jeirankechmez section (Figure 5.1) and attributed the rapid increase in $^{87}Sr/^{86}Sr$ and presence of cold-water foraminifera between 2.7 and 2.4 Ma to an increased connection between the Caspian and Black seas with additional marine influx from the Arctic Ocean (Figure 1.7D). However, there is also an alternative potential fluvial source of elevated radiogenic $^{87}Sr/^{86}Sr$; the Amu Darya river. Amu Darya currently drains the western Himalayas and enters the Aral Sea but previously deposited deltaic sediment on the eastern margin of the South Caspian Basin throughout the Plio–Pleistocene (Abreu and Nummedal, 2007). Although there are no direct Sr isotopic measurements for the Amu Darya River, the radiogenic signal of the Aral Sea water, which Amu Darya currently drains into, reflects the Sr isotopic ratio of the Amu Darya river (Chapter 3). This river could therefore also account for the high Sr isotope ratios in the Caspian Basin.

This chapter combines new $^{87}Sr/^{86}Sr$ data of modern water samples with those from the sedimentary archive of the Black Sea and the Caspian Sea. Together with salinity constraints from Caspian fossil assemblages, the$^{87}Sr/^{86}Sr$ is incorporated in a numerical box model to constrain the relative contributions of the three possible water sources, Black Sea, Amu Darya and Arctic Ocean, to the Caspian basin and their connectivity between 2.6 and 1 Ma.

5.2 Methods

Water samples were collected from the Black Sea, Caspian Sea, upstream Kura river, and Aral Sea (Figure. 5.1, Table 2.1). Early Pleistocene Caspian sediment samples were collected from the Goychay section (Section 2.1.2.4) and the Black Sea samples were collected from Guria, Georgia (Section 2.1.2.1) and DSDP core 380A (Figure 5.1, Table 2.2). Comparison is made with two existing Caspian records from Jeirankechmez (van Baak et al., 2019) and Karagoush Mountain section (Page, 2004).

Samples ages were calculated assuming constant sedimentation rates between tie-points identified in the following age models: Goychay (Lazarev et al., 2019); Guria, (Kirscher et al., 2017); DSDP 380A (van Baak et al., 2016a). Page (2004) used chemostratigraphic correlation to identify the boundary between Akchagylian and Apsheronian (1.8 Ma) at 100 m stratigraphic heights in the Karagoush Mountain section. Page (2004) obtained a $^{40}Ar/^{39}Ar$ volcanic ash date of 1.93 Ma from the sample taken at 36 m above the base of the section. Using these two tie-points, a sedimentation

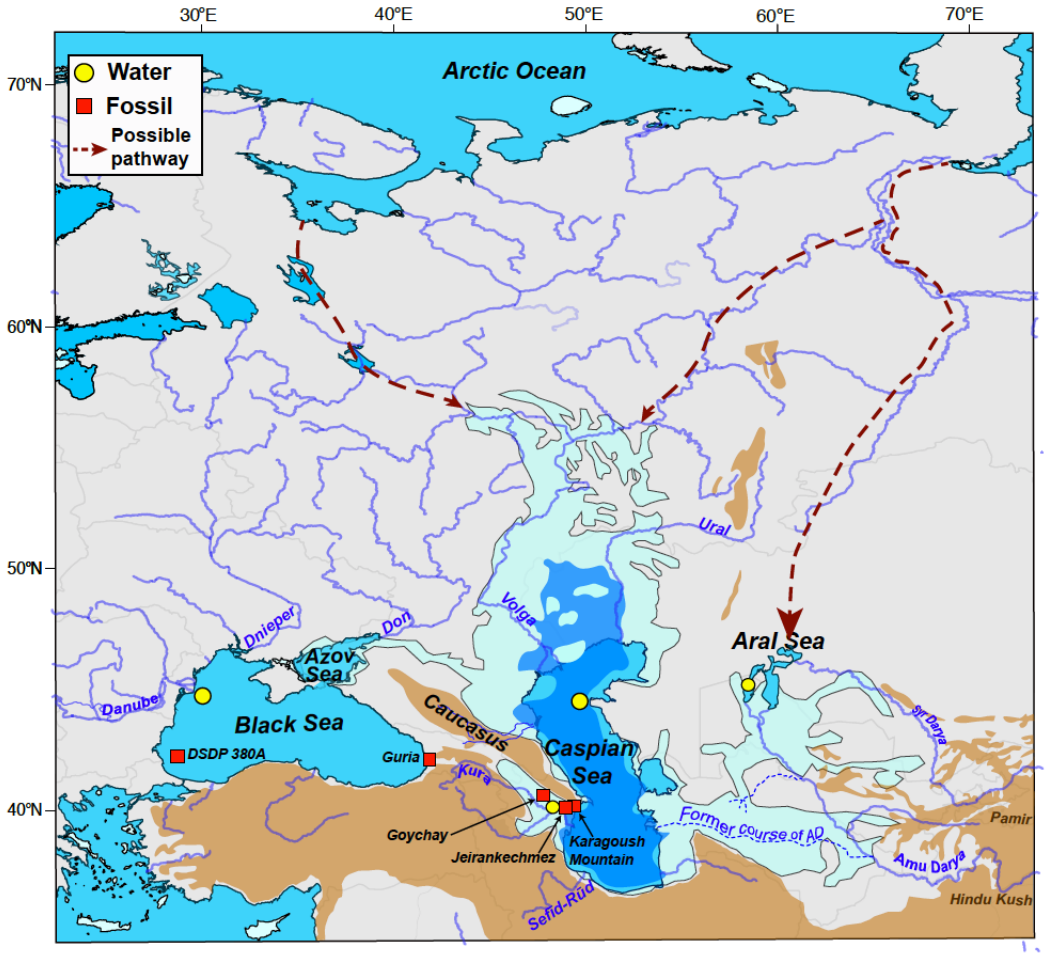

FIGURE 5.1: Location map of the study sites; Goychay, Jeirankechmez, Karagoush, Guria and DSDP 380A. Water samples were collected from the Black Sea, Caspian Sea, Kura River, and the Aral Sea. Pale blue area shows the palaeogeographic extent of the Caspian Sea during the Akchagylian period, with deep water shown in darker blue (modified from Vinogradov, 1967). Pale brown area indicates topographic highs in the region. Dotted blue lines indicate former course of the Amu Darya (AD). Red dotted arrows indicate possible pathway for the Caspian-Arctic connection.

rate of about 46 cm/ka was calculated. Page (2004) also indicates that the top of the section lies at 0.99 Ma, but the basis for this is not clear. Therefore, I use the same sedimentation rate for the samples younger than 1.8 Ma and calculate the age of each sample throughout the section.

Semi-quantitative micropalaeontological analysis of 46 sediment samples was conducted on the fossil ostracods (Section 2.3). Sr isotopic ratios were determined for 78 samples from the Goychay section and 24 samples from the Guria section following procedure outlined in Section 2.2.3. For details regarding the sampling method and analysis, refer to Chapter 2.

The $^{87}Sr/^{86}Sr$ of water in a lacustrine or marginal marine basin is a function of the discharge, Sr isotopic ratio and concentration of the contributing waters. The Early Pleistocene Caspian's input fluxes were investigated by integrating this Sr relationship using a box-model modified from Topper

et al. (2011) and Modestou et al. (2017). Present-day hydrologic fluxes, fluvial Sr concentration and $^{87}Sr/^{86}Sr$ were used (Table 4.1) because Early Pleistocene values are not available.

5.3 Results

5.3.1 Sr isotopic ratios

The Sr isotopic measurements from the Goychay and Guria sections are shown in Figure 5.2 and are listed in Table C.1 and C.3. Sr isotope data from Early Pleistocene Black Sea samples (0.70831 – 0.70868) have substantially lower $^{87}Sr/^{86}Sr$ than present-day Black Sea water samples (0.709143 ± 0.000008; Figure 5.2). Variation between samples is relatively small, indicating that the Black Sea had a stable $^{87}Sr/^{86}Sr$ throughout this period. Most of the Caspian $^{87}Sr/^{86}Sr$ data from the Karagoush (Page, 2004) and Jeirankechmez sections (van Baak et al., 2019) lies within a smaller interval of the Black Sea range (Figure 5.2) which is higher than present-day Caspian Sea values (0.708191 ± 0.000009; Figure 5.2). In contrast, the $^{87}Sr/^{86}Sr$ record of the more marginal Caspian section at Goychay has a much greater range and fluctuates substantially above and below the Early Pleistocene Caspian and Black Sea ranges (Figure 5.2). The lowest values are substantially lower than the modern Caspian Sea ratio, but are similar to those measured for the Kura river (0.707688 ± 0.000004; Figure 5.2). At its highest, the Goychay $^{87}Sr/^{86}Sr$ record approaches coeval open ocean values and/or the values measured on Aral Sea water samples (0.709214 ± 0.000006; Figure 5.2), paralleling coeval deviations to higher ratios in the Jeirankechmez Section (Figure 5.2).

5.3.2 Micropalaeontology

The outcome of micropalaeontology is shown in Figure 5.3. The lowermost part of Unit 1 (between 77.5 m and 99.4 m) contains the foraminifera *Ammonia sp.* and is dominated by an ostracod assemblage that comprises *Cyprideis torosa*, *Loxoconcha eichwaldi*, *L. petasa*, *L. babzananica*, *Eucythere naphtatscholana*, *Tyrrhenocythere bailovi*, *Amnicythere* ex. gr. *andrussovi, A. cymbula, A. monotuberculata, A. alveotuberculata*, and *Cytherissa bogatschovi*. This assemblage suggests elevated salinities and indicates mesohaline conditions (5 - 10 g/kg). The rest of the Goychay section contains a smaller number of taxa and combined with the disappearance of *Ammonia sp.* suggests oligohaline environments (1 - 5 g/kg), which are interbedded with intervals dominated

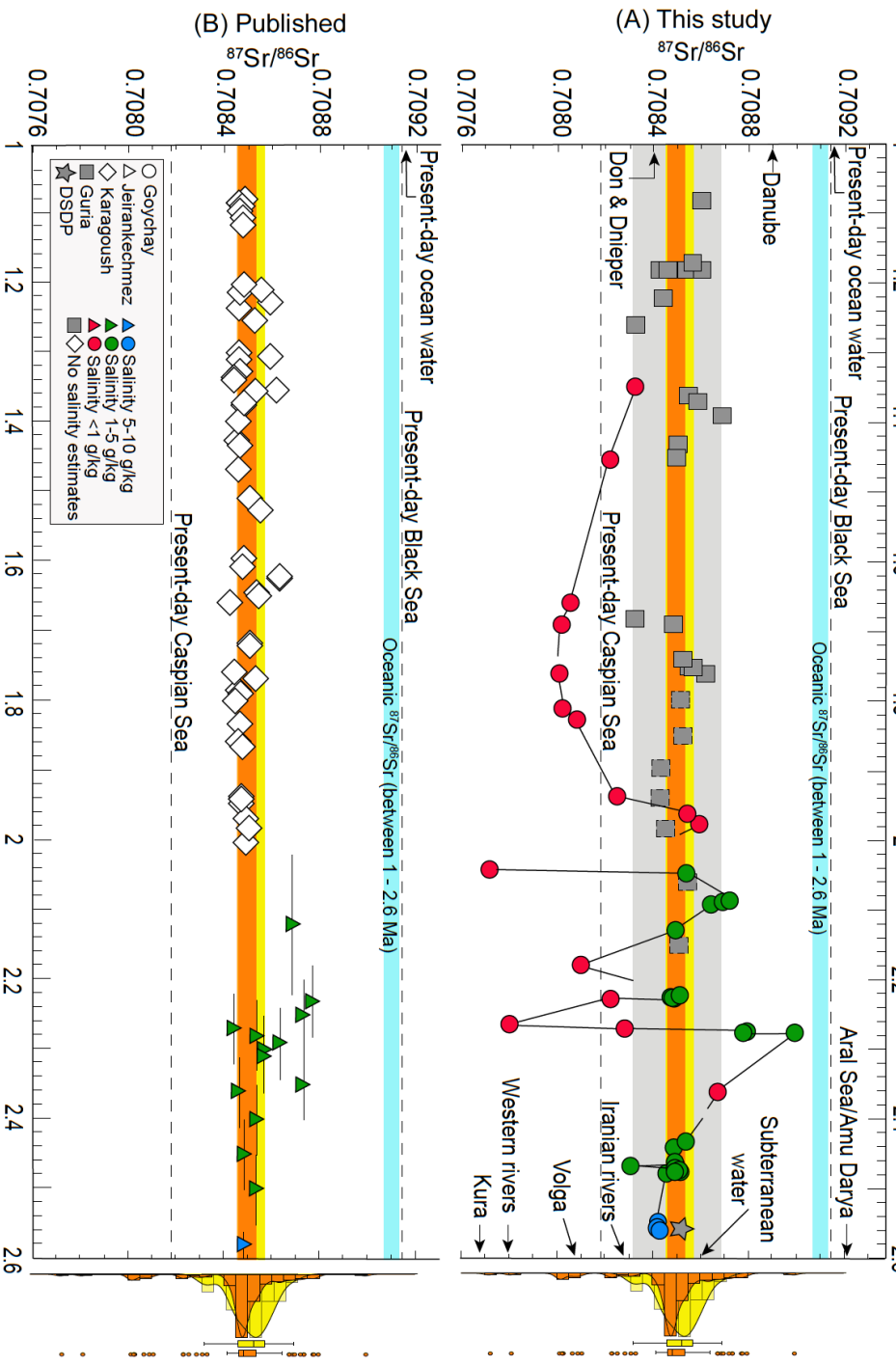

FIGURE 5.2: A) The Early Pleistocene Sr-isotope record for Goychay (circles), DSDP (star) and Guria (boxes) plotted with coeval oceanic $^{87}Sr/^{86}Sr$ (blue horizontal bar; McArthur et al., 2012) and present-day $^{87}Sr/^{86}Sr$ values of the Black and Caspian seas and their major water sources. Break in the line connecting two Goychay data points corresponds with ostracod-barren intervals. Age error for the Goychay section is between 2 – 11 ka. Data points with dashed boundary in Guria have uncertain ages as the older tie point is not known (Kirscher et al., 2017). Age of the DSDP samples (640 mbsf) is 1.8 or 2.58 or 4.2 Ma due to mass transport complex (van Baak et al., 2016a). Internal uncertainty for each individual $^{87}Sr/^{86}Sr$ measurement is between 4 and 24 ppm and external uncertainty on 36 repeat measurement on NIST 981 is ~8 ppm. Pale grey area represents the range of the Black Sea $^{87}Sr/^{86}Sr$. B) Existing Caspian Sea $^{87}Sr/^{86}Sr$ records from Jeirankechmez (triangles; van Baak et al., 2019) and Karagoush sections (diamonds; Page, 2004). Density distribution of the $^{87}Sr/^{86}Sr$ data from the Black Sea (yellow) and Caspian Sea (orange) are shown at the right side of the plot. The interquartile range containing 50% of the data for the Black Sea is shown in yellow (0.70845 – 0.70857) and for the Caspian Sea is shown in orange (0.70847 – 0.70854).

mainly by *Ilyocypris bradyi*, fragments and juveniles of *Candona sp*., and charophytic gyrogonites indicating freshwater conditions. The section also contains intervals where no ostracods were present within the sediment.

Microfossil data from Goychay can therefore be categorised into four distinct groups: (1) ostracods and foraminifera that indicate a salinity range of 5 – 10 g/kg (mesohaline conditions); (2) ostracod assemblages of 1 – 5 g/kg salinity (oligohaline conditions) (3) ostracod assemblages of salinities <1 g/kg (freswater conditions); and (4) barren intervals (Figure 5.3). Low $^{87}Sr/^{86}Sr$ data in the Goychay Section are always associated with microfossils that indicate freshwater conditions and only mid-high $^{87}Sr/^{86}Sr$ are associated with oligo and mesohaline assemblages (Figure 5.2).

5.4 Discussion

The consistency of the Sr isotope records measured on the Jeirankechmez and Karagoush sections suggests that they both reflect the Caspian's Sr isotope evolution throughout the Early Pleistocene. By contrast, the Goychay Section, which lies further from the present-day Caspian coast in the Kura catchment (Figure 5.1), is much more variable with consistently lower values after 1.9 Ma. The lowest values resemble those measured on modern Kura river water. The low $^{87}Sr/^{86}Sr$ samples contain freshwater ostracod assemblages indicating lower salinities than coeval Jeirankechmez samples at around 2.04 - 2.28 Ma (Figure 5.2). These low $^{87}Sr/^{86}Sr$ values and freshwater conditions are therefore, most likely to be the result of local river runoff as a result of progressive isolation of this western margin from the main Caspian Basin. This isolation, which is also reflected in the increasingly continental facies (Lazarev et al., 2019), is probably driven by on-going formation of the Kura fold and thrust belt (Forte et al., 2013).

Although the low $^{87}Sr/^{86}Sr$ ratios in Goychay indicate that this marginal area became permanently isolated from the main Caspian Basin around 1.9 Ma, earlier parts of its record has substantially higher $^{87}Sr/^{86}Sr$ and salinities that broadly parallel the values observed in the Jeirankechmez Section. These $^{87}Sr/^{86}Sr$ values are higher than the present-day Caspian Sea (Figure 5.2). Today, the Caspian is dominated by freshwater input from the Volga and this is reflected both in the $^{87}Sr/^{86}Sr$ and the strong salinity gradient from north (~1 g/kg) to south (~12 g/kg). Minor freshwater contributions from western (Sulak, Kura and Terek) rivers have substantially lower ratios, while Iranian rivers are slightly higher than the Volga (Figure 5.2). The input of subterranean water,

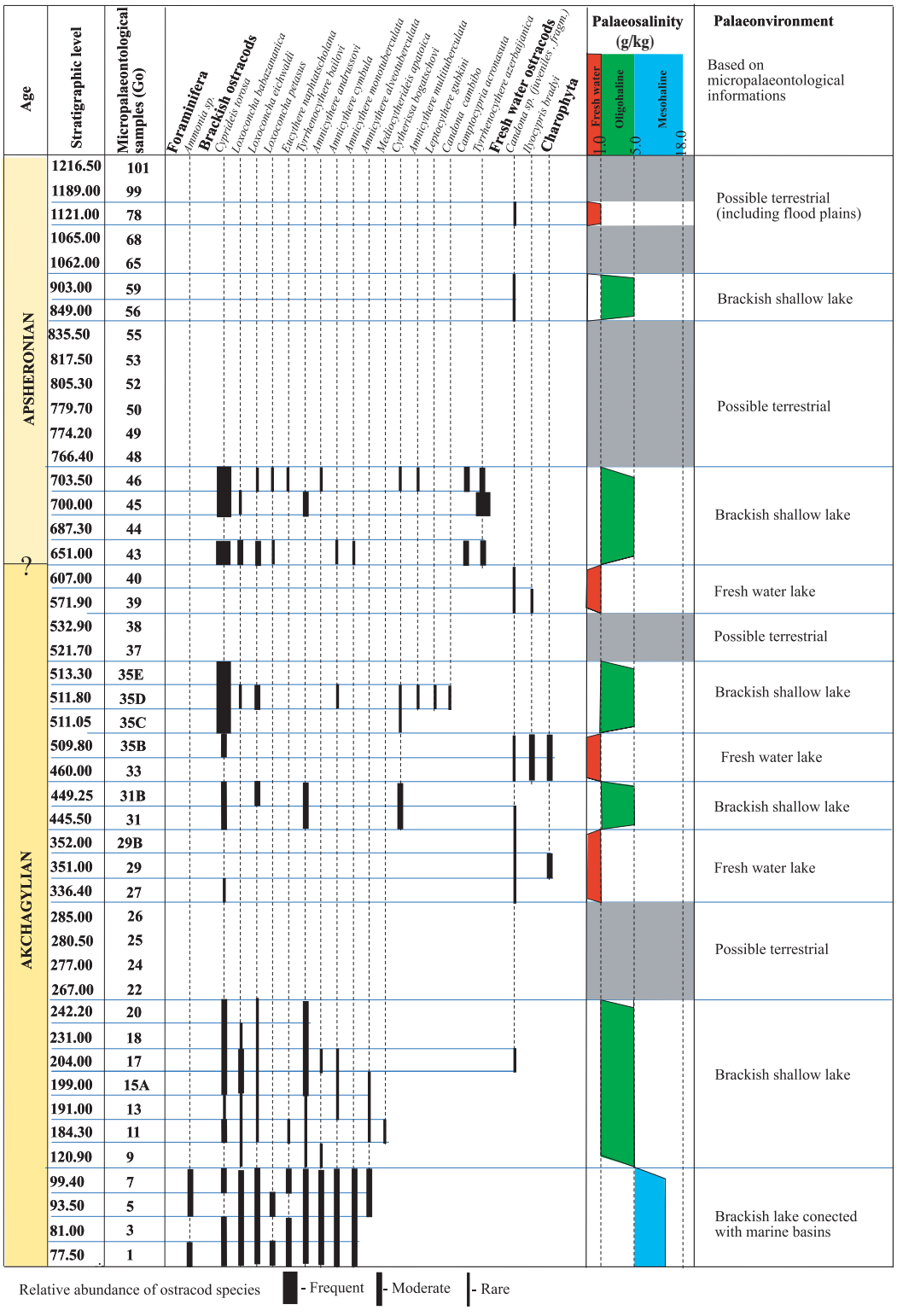

FIGURE 5.3: Ostracod distribution pattern from the Goychay section, Azerbaijan along with estimated palaeosalinity and palaeoenvironment represented by the ostracod assemblages.

which today has a much higher Sr isotope ratio and a Sr concentration several orders of magnitude higher than present-day Caspian river water (Clauer et al., 2000), raises the Caspian's Sr isotope

ratio above the dominant Volga value. However, although complete dominance of subterranean waters could theoretically account for the median Early Pleistocene Caspian $^{87}Sr/^{86}Sr$ (0.70848) observed, it could not have generated the values above 0.7086 measured on both Goychay and Jeirankechmez samples (Figure 5.2). The Caspian must therefore have had an additional, more radiogenic, water source during the Early Pleistocene at least between 2.4 - 2.1 Ma.

One possibility is that this radiogenic signal is derived from the Amu Darya river influencing the Caspian in the past (Section 3.4.1.4) and therefore could have elevated the Sr isotope ratio of the Early Pleistocene Caspian Sea above its present-day ratio and that of the groundwater input.

An alternative source of radiogenic Sr is ocean water, which could have reached the Caspian either via an Arctic connection or from the Mediterranean via the Black Sea. The Black Sea Sr isotope record tests this latter hypothesis. Modern Black Sea water has a high $^{87}Sr/^{86}Sr$, which is similar to oceanic value (Figure 5.2) reflecting the influence of Black Sea-Mediterranean exchange. Influx through the Bosporus today is ~2 x 10^{11} m^3/yr. Modelling the hydrologic budget of the Black Sea illustrates that even with a Mediterranean flux of one order of magnitude lower, the oceanic Sr ratio would still dominate the Black Sea signal because of its high Sr concentration (Appendix C.1). By contrast, the $^{87}Sr/^{86}Sr$ of Early Pleistocene Black Sea samples are substantially lower than coeval ocean water, suggesting that there was little or no Mediterranean-Black Sea exchange at the time. Consequently, an ocean water Sr isotope signal cannot have reached the Caspian via the Black Sea during the Early Pleistocene.

A Caspian connection to the Arctic Ocean has been advocated on the basis of genetic analysis of some Caspian Sea taxa (e.g., the Caspian seal and crustacean genera) whose closest relatives occur today in the coastal and estuarine waters of the Arctic Ocean (e.g. Davies, 1958; Väinölä et al., 2001). However, the timing and number of these biologically-determined connections are keenly debated and include the Late Miocene (Mclaren, 1960), Pliocene (Árnason et al., 2006), late Pliocene - Early Pleistocene (2 – 3 Ma; Palo and Väinölä, 2006; Richards et al., 2018) to as recent as 1 Ma (Fulton and Strobeck, 2010). The Sr isotopic ratio from the earliest part of the Jeirankechmez Section demonstrates the onset of an episode of Caspian-Arctic connection at 2.7 Ma (van Baak et al., 2019), shortly before the higher Sr isotope ratios observed between 1.96 - 2.4 Ma (Figure 5.2).

Based on micropalaeontological evidence for falling salinity (Richards et al., 2018), van Baak et al.

(2019) suggested that Arctic input ceased at ~2.4 - 2.5 Ma, which was too early to account for these high Sr data. However, declining salinity, even with continued input from the Arctic, can also be achieved through salt export via outflow from the Caspian. The consistency between the $^{87}Sr/^{86}Sr$ of the Black Sea and the main Caspian Basin sections (Figure 5.2) suggests a connection between the two during the Early Pleistocene. Both, two-way flow between these two basins and one way flow from the Caspian Sea into the Black Sea can explain the observed $^{87}Sr/^{86}Sr$ ratio (Figure 5.2). Given the narrower range of Caspian data relative to the Black Sea (Figure 5.2), one-way flow from the Caspian to the Black Sea is a more likely scenario to explain the Sr isotope datasets. This channel could have provided both a conduit for salt export from the Caspian to Black Sea and a corridor for the observed faunal exchange between the two basins at this time (e.g. Krijgsman et al., 2019 and references therein).

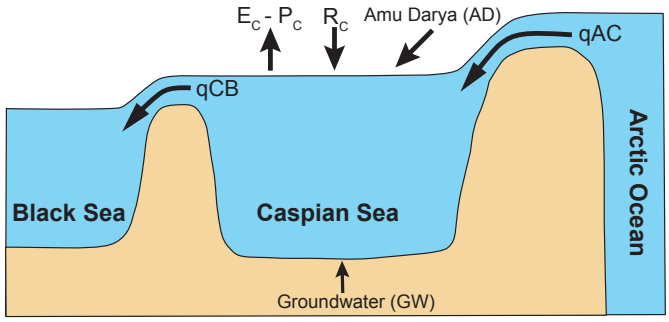

FIGURE 5.4: Spatial illustration of model configuration in a steady state situation with inflows into and outflow from the Caspian Sea.

To evaluate whether Arctic input and/or Amu Darya discharge influenced the Caspian Sea during the Early Pleistocene, the Caspian's hydrologic budget was constrained using a box model. The Caspian basin is treated as one box with its water budget regulated by various inflows into and outflows from the basin. There are two possible pathways connecting the Early Pleistocene Caspian basin to the Arctic Ocean in the north; via palaeo Volga channels or via former Turgay Seaway (Richards et al., 2018). Given the current topography of these areas relative to the global sea level, it is more likely that there was one-way flow from the Arctic Ocean into the Caspian basin. Although a two way flow between the Caspian Sea and the Arctic Ocean is also possible, but in this scenario, the outflow from the Caspian Sea to the Arctic Ocean has no impact on the $^{87}Sr/^{86}Sr$ and the salinity of the Caspian Sea. The additional water influx from the Arctic Ocean and the Amu Darya is compensated by the large increase in Caspian surface area and hence resulting in the

outflow into the Black Sea, which at the time was not connected to the Mediterranean Sea. If we consider the Caspian basin to be at constant sea level, then the water volume conservation equation results in

$$qCB = qAC + R_C + GW + AD + P_C - E_C \tag{5.1}$$

where, *qCB* refers to one way flux from the Caspian into the Black Sea and *qAC* refers to the one way flux from the Arctic Ocean into the Caspian Sea. R_C, *AD, GW,* E_C and P_C refer to the total present-day fluvial discharge (Volga, western and southern rivers), Amu Darya discharge, groundwater discharge, evaporation and precipitation of the Caspian Sea, respectively. While all seven fluxes have an effect on the water budget, only the first five changes the Sr isotopic ratio of the Caspian basin. Therefore, Sr concentration, and Sr isotopic ratio of the Caspian basin can be determined as follows, with subscript referring to Arctic (*A*), Caspian Sea rivers (*RC*), Amu Darya (*AD*), Groundwater (*GW*) and Caspian Sea (*C*).

Sr concentration:

$$[Sr]_C = \frac{[Sr]_A * qAC + [Sr]_{RC} * R_C + [Sr]_{AD} * AD + [Sr]_{GW} * GW}{qAC + R_C + AD + GW} \tag{5.2}$$

and Sr isotopic ratio:

$$[^{87}Sr/^{86}Sr\ ]_C = \frac{\left(\begin{array}{l}[^{87}Sr/^{86}Sr\ ]_A * [Sr]_A * qAC + [^{87}Sr/^{86}Sr\ ]_{RC} * [Sr]_{RC} * R_C \\ \quad + [^{87}Sr/^{86}Sr\ ]_{AD} * [Sr]_{AD} * AD + [^{87}Sr/^{86}Sr\ ]_{GW} * [Sr]_{GW} * GW\end{array}\right)}{[Sr]_A * qAC + [Sr]_{RC} * R_C + [Sr]_{AD} * AD + [Sr]_{GW} * GW} \tag{5.3}$$

If the Arctic input is the only source of salt in the Early Pleistocene Caspian basin, salinity of the basin is determined by

$$[S]_C = \frac{[S]_A * qAC}{qCB} \tag{5.4}$$

The box model was run with stepwise increases in the input from the Arctic Ocean and Amu Darya into the Caspian Sea and constrained using the $^{87}Sr/^{86}Sr$ and the salinity estimates provided by ostracod assemblages from Goychay and Jeirankechmez. Modelling output shows that both Arctic and Amu Darya input increase the $^{87}Sr/^{86}Sr$ of the Caspian, but only an Arctic influx increases the salinity (Figure 5.5). The lack of salinity variation associated with increased $^{87}Sr/^{86}Sr$ values between 2.5 and 2.27 Ma suggests that oceanic input cannot be the sole driver of higher $^{87}Sr/^{86}Sr$.

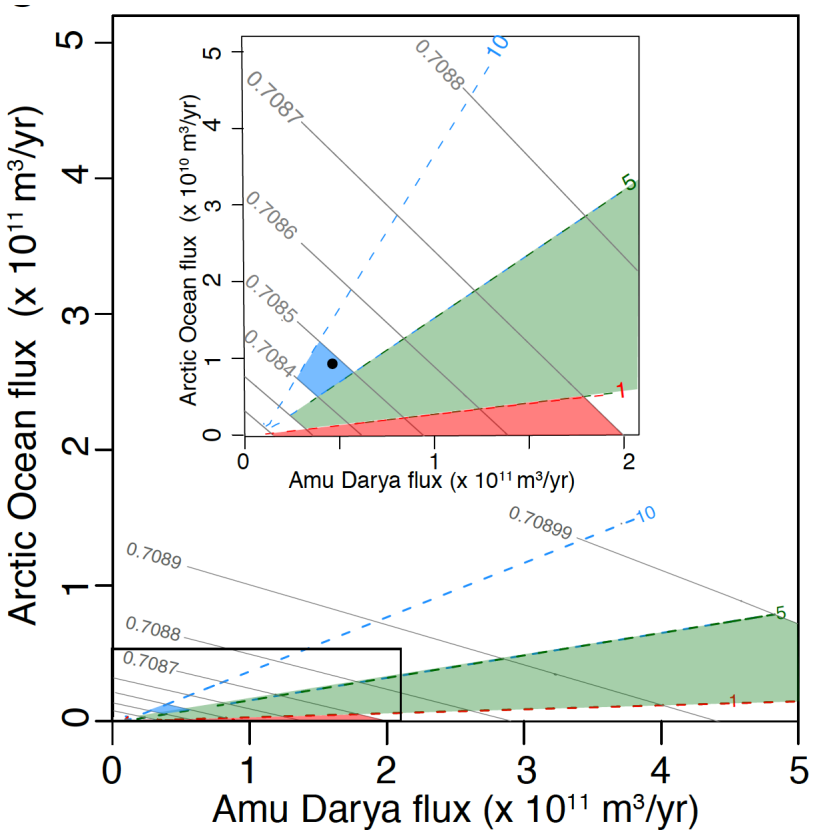

FIGURE 5.5: Model generated contour lines for salinity (coloured dashed lines) and $^{87}Sr/^{86}Sr$ (grey solid lines) in the Caspian Sea with varying input from the Arctic Ocean and Amu Darya. Rectangular box represents the zoomed in area. Salinity and $^{87}Sr/^{86}Sr$ data from the Goychay and Jeirankechmez falls within the colour shaded area representing different salinity ranges: 5 - 10 (blue), 1 - 5 (green), <1 (red) g/kg. The black dot indicates the $^{87}Sr/^{86}Sr$ of 0.70848 (the Early Pleistocene Caspian Sea median value) and salinity of 7 g/kg which results from an Amu Darya flux of 4.6 x 10^{10} m^3/yr and an oceanic influx of ~9.2 x 10^9 m^3/yr .

Consequently, the paired salinity-Sr isotope data between 2.6 and 1.96 Ma probably reflects inflow from both Arctic and Amu Darya (green and blue; Figure 5.5). With an Amu Darya flux of 4.6 x 10^{10} m^3/yr , which is similar to its pre-irrigation discharge (Asarin et al., 2010), an oceanic influx of only ~9.2 x 10^9 m^3/yr is required to increase $^{87}Sr/^{86}Sr$ from the present-day Caspian value to the Early Pleistocene median value of 0.70848 (Figure 5.2 and 5.5) and salinities >5 g/kg. The episodic higher Sr isotope values observed in Goychay and Jeirankechmez sections between 2.4 and 1.96 Ma (Figure 5.2) require an order of magnitude greater influx from both these sources (Figure 5.5). Given the observed $^{87}Sr/^{86}Sr$ -salinity relationship in the Caspian record, it is clear that the Amu Darya flowed into the Caspian throughout the Early Pleistocene. In addition, an oceanic connection to the Arctic contributed a small influx at the beginning of the Early Pleistocene (Richards et al., 2018; van Baak et al., 2019), which may have continued until 1.96 Ma. Additional salinity constraints on younger samples from the main Caspian Basin are required to determine the

duration of the Arctic-Caspian connection.

In summary, $^{87}Sr/^{86}Sr$ measurements from the modern Black Sea, Caspian Sea, and Aral Sea, together with the Early Pleistocene Sr isotopic record from the Black and Caspian seas was presented in this study. The Caspian received water from both the Arctic Ocean and Amu Darya during the Early Pleistocene and is likely to have over-spilled into the Black Sea. This connectivity record provides a framework against which faunal distributions can be used to evaluate the timing and drivers of rapid evolutionary change.

Chapter 6

The connectivity history of the Black Sea over the last 1.2 million years

The hydrological budget of the Black Sea is sensitive to global climate variation and tectonics as they control its fluvial input and its connection to the Mediterranean Sea. Changes in these drivers have resulted in the Black Sea experiencing multiple connection events with the Mediterranean and Caspian seas throughout the Quaternary. However, the interpretation of existing, largely faunal evidence for these connectivity events is contradictory, lacks precise timing and the records are rarely continuous. This chapter provides a continuous record of the Black Sea's connectivity history over the last 1.2 Ma by examining the Sr isotopic ratios measured on fossil ostracods and salinity estimates based on dinoflagellate cysts from the DSDP Site 379A. More explicitly, the results from this chapter will address the ***research questions 5, 6 and 7*** *outlined in Section 1.6.2;*

5. *How did the Sr isotopic ratio evolve in the Black and Caspian seas over the last 3 million years and what is its implication for the Quaternary connectivity history of the two basins to each other and the open ocean?*

6. *What was the nature of connection (one way flow or two way exchange) between the Black Sea, Caspian Sea and the open ocean during the Pleistocene?*

7. *Does the geochemical evidence of the connectivity and isolation between the Black Sea, Caspian Sea and the open ocean match the faunal evidence?*

This chapter is written with intention to submit to *Earth and Planetary Science Letters*. The version presented here differs from the manuscript as parts of introduction are included in Chapter 1 and results and discussions regarding $^{87}Sr/^{86}Sr$ of the modern Black Sea water and the fluvial sources are included in Chapter 3. The discussion regarding the $^{87}Sr/^{86}Sr$ of the Aral Sea water used for constraining Amu Darya signal is included in Chapter 3. Analysis and interpretation of dinocyst assemblages are provided by **T. M. Hoyle**, Utrecht University. The Sr isotopic data for the last 400 ka presented in this chapter is also included in PhD thesis of T. M. Hoyle.

T. M. Hoyle, 2019, **Biotic change and landlocked seas: ecosystem responses to climate and sea level variability in the Plio-Pleistocene of the Pontocaspian basins**, PhD thesis, Utrecht University.

6.1 Introduction

Today, the Black Sea is a brackish water basin with a restricted connection to the Mediterranean Sea and the recipient of substantial continental runoff (Jaoshvili, 2003; Özsoy and Ünlüata, 1997). Its connection with the Mediterranean Sea is governed by the interplay between changes in sill geometry at the Bosporus, which is controlled by local tectonics associated with the North Anatolian Fault (NAF), and eustatic sea level. Because its catchment is ~five times the area of the basin itself (Figure 6.1), the Black Sea also responds quickly to changes in climate that modify its fluvial discharge. Consequently, subtle changes in both climate and tectonics produce a discernible impact on the hydrology of the Black Sea, resulting a history characterised by episodic isolation from, and reconnection with, the adjacent Mediterranean and Caspian Sea basins (e.g., Badertscher et al., 2011; Jones and Simmons, 1997; Schrader, 1979; Svitoch et al., 2000; Zubakov, 1988). Records of these connection and isolation events in the Black Sea therefore provide a rich archive of information from which regional palaeoclimate and tectonics can be reconstructed.

Previously, connectivity and isolation events in the Black Sea have mainly been studied using paleontological methods (e.g., Buyukmeric and Wesselingh, 2016; Yanina, 2012, 2014; Zenkevitch, 1963). Faunal-based connectivity studies rely on the assumption that similar or identical assemblages in the different basins occur at the same time, when connected. Although physical

connections between basins facilitate faunal exchange, the evolution of their biodiversity responds to ecological conditions, which is primary controled by basin hydrography (evaporation – precipitation, river discharge, circulation etc.), not the connectivity alone. Additionally, fauna do not have an immediate evolutionary response to the changes in their environmental condition. As a result, faunal biodiversity as a primary indicator of the nature and timing of connectivity episodes in the Black Sea lacks precision and commonly results in conflicting interpretations (e.g., Krijgsman et al., 2019; Stoica et al., 2016).

Several authors have used a variety of geochemical approaches, including Sr and oxygen isotopes, to study Black Sea connectivity, particularly during the Late Pleistocene (e.g., Bahr et al., 2006, 2008; Constantinescu et al., 2015; Major et al., 2002, 2006; Piper and Calvert, 2011; Ryan, 1997) and during previous glacial termination at ~128 kyr (Wegwerth et al., 2014). The longest Pleistocene archive of geochemical data for the Black Sea is the 700 ka oxygen isotopic record (δ^{18}O) of well-dated speleothems collected from Sofular Cave, located 10 km from the southern coast of the Black Sea (Figure 6.1, Badertscher et al., 2011). Here, high δ^{18}O values indicate Mediterranean incursions, while low values reflect influx from the Caspian Sea. Although this study identifies incursion events from extreme δ^{18}O data, most of the record comprises intermediate values that are difficult to interpret (Figure 1.7). Additionally, speleothems primarily record the isotopic composition of local precipitation rather than being a direct measurement of Black Sea water (Section 1.5.3.2.1).

The chapter provides the ^{87}Sr/^{86}Sr of the Black Sea over the last 1.2 Ma, in order to reconstruct the Black Sea's hydrologic history over a much longer period than these previous studies (~1 Ma). This chapter also uses Sr isotopes to monitor the Black Sea response not just to Mediterranean connection and isolation, but to all its major water sources, which, on this timescale, includes the Caspian Sea. In a multi-endmember system where more than one combination of source waters can result in the same Black Sea Sr isotope ratio, we use new dinocyst- and published diatom-derived palaeosalinity (Schrader, 1978) as an additional independent variable to discriminate between different modelled source water solutions. Our Sr isotope record is constructed by analysing ostracod valves from the core sediments of the Deep Sea Drilling project (DSDP) Hole 379A (hereafter referred as core 379A) in the centre of the Black Sea (Figure 6.1).

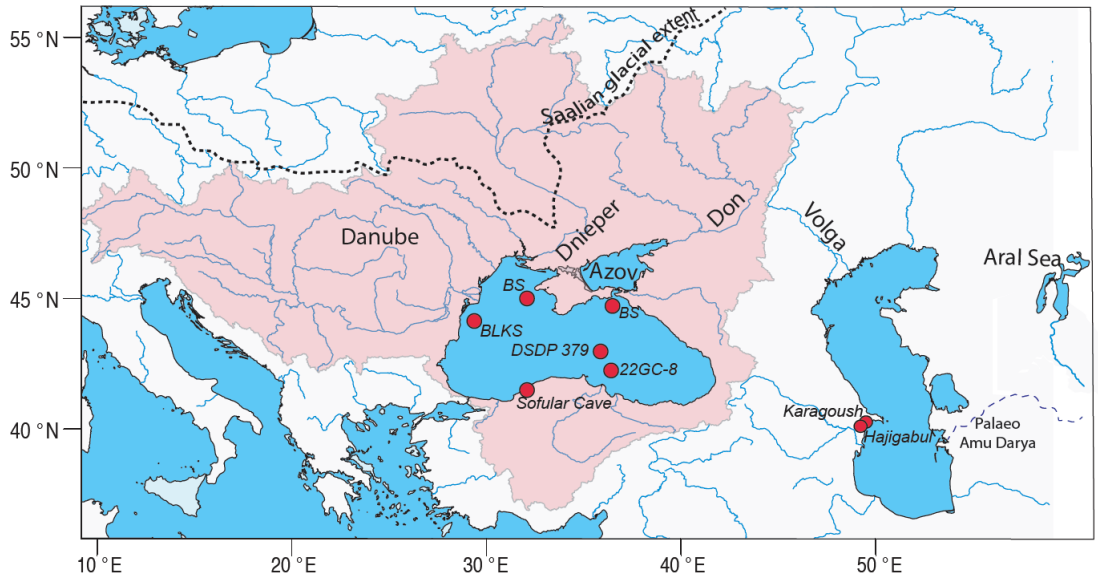

FIGURE 6.1: Map of the Black Sea and the Caspian Sea with section and core locations for this chapter. The pale red area shows the catchment area of the Black Sea basin. Dashed blue line show the course of palaeo Amu Darya river and dotted black line indicate the extent of ice sheet during the Late Saalian (~160 – 140 ka; Svendsen et al., 2004).

6.2 Material and methods

A total of 72 sediment samples (40cc each) were taken from the core 379A. Among them, 21 samples were barren of ostracods and 19 samples contained too few ostracod valves (Table D.1) and as such the Sr isotope analysis (Section 2.2) were carried out on 32 samples ranging in age between 28.7 ka and 1178 ka.

Among the sediment samples collected from core 379A for dinoflagellate cyst (dinocysts) analysis, 6 samples were completely barren. In total, 32 samples, which also included samples analysed for Sr isotopes, were processed for dinocyst assemblages following the procedure outlined in Section 2.4. Seven samples that contained dinocysts had no ostracods and therefore could not be analysed for Sr isotopes. Salinity estimates based on dinocyst assemblages are provided by T. Hoyle (Appendix D).

The sensitivity of $^{87}Sr/^{86}Sr$ and salinity of the Black Sea to different input sources is tested with a numerical box model outlined in Chapter 4. Comparing the observed $^{87}Sr/^{86}Sr$ and palaeosalinity to the model results allows to quantify the past conditions of the freshwater budget and the inter basin connections. In the timescale of 1.2 Ma, the input sources to the Black Sea included continental run-off, Mediterranean Sea and input from the Caspian Sea. All possible combinations of these

three input sources in the Black Sea can be represented in four different connectivity configuration and are shown in Figure 6.2 and are listed below;

A. Black Sea connected to Mediterranean Sea; Input from Mediterranean Sea and fluvial sources

B. Isolated Black Sea; Input only from fluvial sources

C. Black Sea connected to Caspian Sea; Input from fluvial sources and Caspian Sea (with and without Amu Darya river)

D. Black Sea connected to Caspian and Mediterranean seas; Input from fluvial sources, Mediterranean Sea and Caspian Sea (with and without Amu Darya river)

The equations for each scenario used in the model are provided in Appendix D.

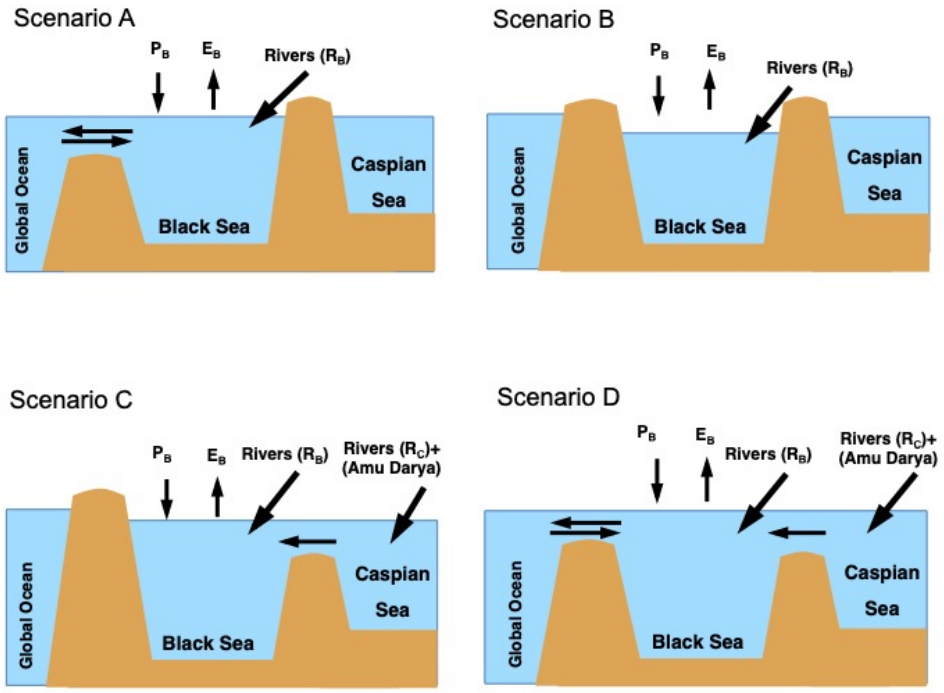

FIGURE 6.2: Schematic diagrams showing four connectivity scenarios between the Black Sea, Caspian Sea and the global ocean that are used in the modelling.

Today, the Mediterranean connection results in inflow of saline water at depth over the Bosporus Strait, while lower density fresher water caps the Black Sea and flows out as a surface current. This results in a salinity structure that increases with depth, with surface waters of 17 - 18 g/kg and deeper water salinities of 22 - 24 g/kg (Kostianoy and Kosarev, 2008). However, even when totally isolated, the Black Sea retains salt from its last oceanic connection as this can neither be precipitated nor flushed out of the system. Consequently, when the Black Sea is fed only by rivers,

its salinity is low, but not entirely fresh (Yanchilina et al., 2017). On the basis of diatoms, Schrader (1978) estimated salinities between 0 and ~8 g/kg during the last glacial lake phase when the Black Sea was isolated from the Mediterranean because of low eustatic sea level (Yanchilina et al., 2017). A salinity of 8 g/kg is therefore, assumed in the model for the Black Sea when not connected to the Mediterranean Sea. Similarly, Caspian Sea salinity of 12 g/kg is assumed for the model, given its current salinity.

6.3 Results

6.3.1 $^{87}Sr/^{86}Sr$ of the DSDP 379A

The Sr isotope ratios measured on the DSDP core 379A are presented in Figure 6.3 and Table D.1. All $^{87}Sr/^{86}Sr$ values are lower than the range of coeval oceanic values (Figure 6.3, McArthur et al., 2012, 0.709125 – 0.709175). The record shows an overall trend towards higher values with time, but does not reach the present-day Black Sea value (Figure 6.3). The Sr isotope record is characterised by periods of relatively stable Sr isotope ratios punctuated by short-lived excursions in $^{87}Sr/^{86}Sr$ towards higher values (Figure 6.3).

6.3.2 Dinocyst assemblages

The dinocyst assemblages are divided into six species groups (Figure 6.3) that are key indicators of changes in conditions within the upper water column; 1) *Pyxidinopsis psilata* (all variants of Hoyle (2019), 2) Low salinity dinocysts with Paratethyan lineage (= Komewuia? sp. of Soliman and Riding (2017), *Caspidinium rugosum*, *Pterocysta cruciformis*, cysts of *Gonyaulax apiculata*, *Impagidinium inaequalis* and *Impagidinium spongianum*), 3) *Pyxidinopsis* "TW" (described by Hoyle (2019), 4) *Spiniferites cruciformis* (all variants), 5) *Spiniferites* sp, and 6) Marine indicators (= *Lingulodinium machaerophorum* (processes >10 μm), *Operculodinium centrocarpum sensu* Wall and Dale (1966), *Tectatodinium pellitum*, *Pentapharsodinium dalei*, *Nemotophaeropsis labrynthus* and *Polysphaeridium zoharyii*). Ecological niches of these six species groups are discussed below.

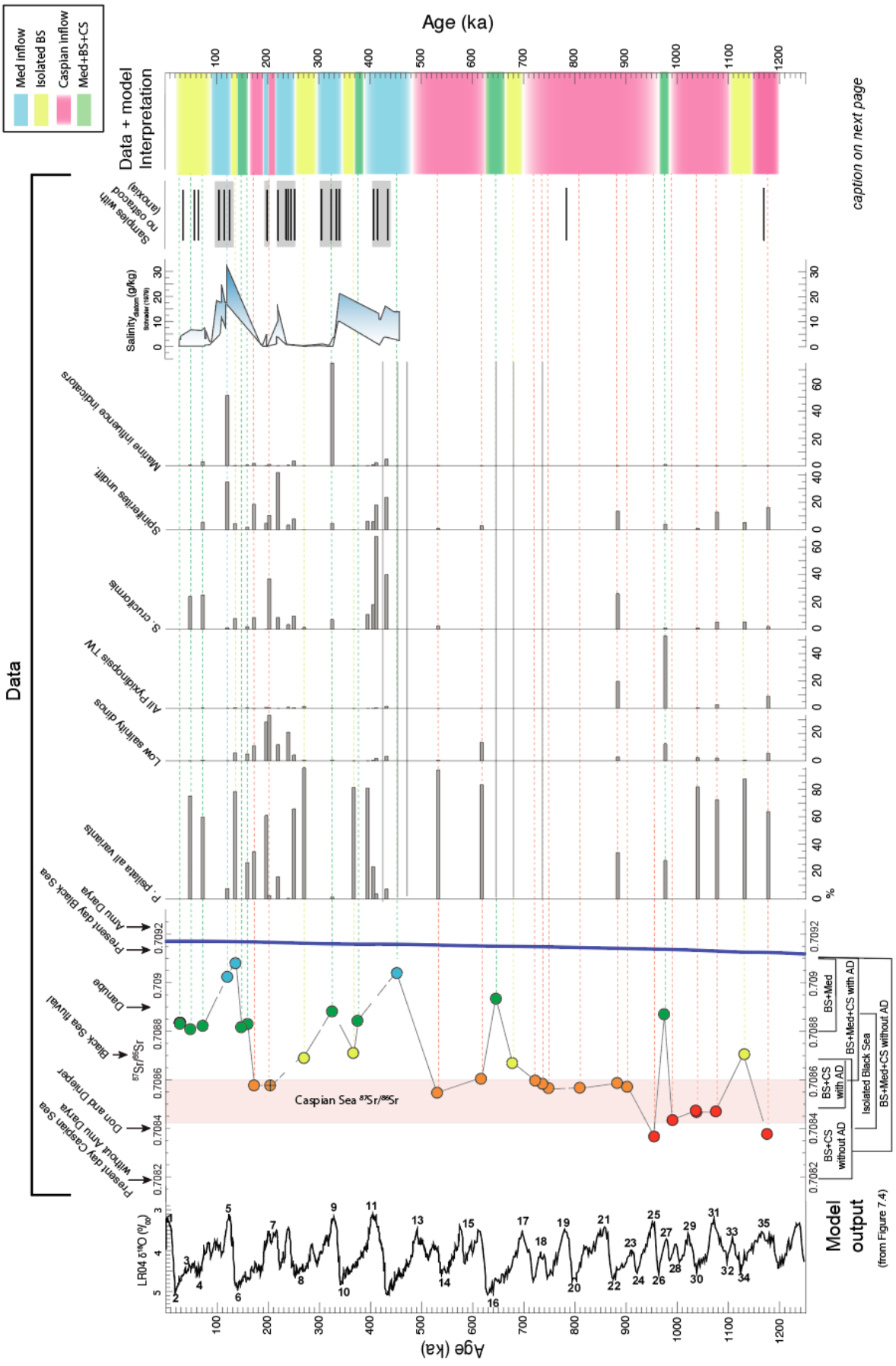
Med inflow
Isolated BS
Caspian inflow
Med+BS+CS
Age (ka)
Data + model Interpretation
caption on next page
Data
Samples with no ostracod (anoxia)
Salinity (g/kg)
Marine influence indicators
Spiniferites undiff.
S. cruciformis
All Pyxidinopsis TW
Low salinity dinos
P. psilata all variants
Present day Black Sea
Azov Daryа
Danube
Black Sea fluvial
Don and Dneper
Present day Caspian Sea without Azov Daryа
LR04 δ18O (‰)
87Sr/86Sr
Caspian Sea 87Sr/86Sr
Model output
(from Figure 7.4)
BS+Med
BS+Med+CS with AD
Isolated Black Sea
BS+Med+CS without AD
BS+CS with AD
BS+CS without AD

6.3.2.1 *Pyxidinopsis psilata*

Pyxidinopsis psilata is encountered in abundances up to 4% in surface sediments of the Black Sea and Marmara Sea, in waters with surface salinity of ~13 g/kg in the Caspian Sea and ~18 g/kg in the Black Sea (Mudie et al., 2017). However, it does not form a major part of these assemblages. *P. psilata* (documented as *Tectatodinium psilatum*) shows abundances over 75% in recent sediments from the Baltic Sea, with salinities around 7 g/kg, but does not generally occur in waters with salinity below 3 g/kg (Dale, 1996; Kouli et al., 2001).

In the Black Sea geological record, relative abundances of *P. psilata* decrease from about 37% at 8.25 ka to <4% in the mid-late Holocene, across a period when an isolated Black Sea became connected with the Mediterranean (Verleye et al., 2009). This supports the interpretation of *P. psilata* as a cyst that, although formed under a range of salinities, only becomes dominant in systems where salt content is low. It has also been suggested that *P. psilata* is a species that forms "extraordinary blooms" only in certain years, perhaps in reaction to enhanced nutrient supply (Brenner, 2005). In summary, assemblages dominated by *P. psilata* are considered to represent surface salinities somewhere below 10 g/kg, although the exact manner in which this organism responds to environmental drivers is actually not well understood.

6.3.2.2 "Low salinity dinocysts"

Of the low salinity dinocysts listed here, only *Caspidinium rugosum*, cysts of *Gonyaulax apiculata* and *Impagidinium inaequalis* have been recovered from surface sediments (Mudie et al., 2017). *C. rugosum* is most common (6%) in Caspian surface sediments at salinities of ~13 g/kg but also appears (>2%) in the Black Sea surface sediments at ~17–18 g/kg and rarely in the Volga and Danube deltas at <2 g/kg (Mudie et al., 2017). Appearance of *C. rugosum* at higher abundances

FIGURE 6.3: The $^{87}Sr/^{86}Sr$ record (coloured circles) and dinocysts assemblages (grey bars) from the DSDP cores 379A along with the coeval oceanic value (dark blue line, McArthur et al., 2012) over the last 1.2 Ma. The coloured dots represent the five data groups, i.e. $^{87}Sr/^{86}Sr$ values higher than 0.7089 (blue), values between 0.7088 and 0.7089 (green), values about 0.7087 (yellow), values about 0.7086 (orange), and $^{87}Sr/^{86}Sr$ values lower than 0.7085 (red). Internal uncertainty for each individual $^{87}Sr/^{86}Sr$ measurement is between 4 and 38 ppm and external uncertainty on 36 repeat measurement on NIST 981 standard is ~8 ppm. Pale red bar represent the coeval $^{87}Sr/^{86}Sr$ of the Caspian Sea from the Hajigabul (Chapter 7) and Karagoush Mountain section (Page, 2004). Model output range of $^{87}Sr/^{86}Sr$ for different connectivity scenarios are indicated at the bottom of the figure. The right hand side shows the connectivity interpretation based on the $^{87}Sr/^{86}Sr$, salinity estimates (dinocysts - this study and diatoms - Schrader, 1979), and model outputs.

with *P. psilata* in sediments deposited in the deeper past could suggest a preference for salinities below 10 g/kg, but this is purely speculative. *I. inaequalis* is found only rarely in the Volga delta and cysts of *Gonyaulax apiculata* occur rarely in surface sediments in coastal lakes in "fresh" waters (although quantification is not made).

Ecological tolerances for other "low salinity" taxa are inferred from their association with "low salinity" fossil assemblages in the geological record, in particular the late Miocene Pannonian Basin and the late Quaternary Black Sea (Cziczer et al., 2009; Magyar and Geary, 2012; Rochon et al., 2002; Soliman and Riding, 2017). *Impagidinium spongianum* and *Komewuia*? sp. of Soliman and Riding (2017) both occur in the Miocene Pannonian basin with inferred "low salinities", although the exact salt content is poorly constrained (Soliman and Riding, 2017). Given the "Caspian like" faunas associated with this setting we can potentially infer that salinities were somewhere below ~12–15 g/kg (Magyar and Geary, 2012; Rochon et al., 2002). However, this value remains speculative and interpretations should remain open to alteration in the light of developing biological research on the ecological tolerances of the Pontocaspian fauna.

6.3.2.3 *Pyxidinopsis* "TW"

Pyxidinopsis "TW" (thick walled; Hoyle et al., 2019) is a robust form of the genus *Pyxidinopsis* and show similarity to *Pyxidinopsis psilata* of Soliman and Riding (2017) (their plate V, 9–12). However, some of the specimen also closely resemble *Komewuia? sp.*A and *Komewuia? sp.*B from the same authors. These species are observed in sediments from the late Miocene Pannonian Basin (Soliman and Riding, 2017) and indicate low salinity conditions.

6.3.2.4 *Spiniferites cruciformis*

In the present-day, *Spiniferites cruciformis* is most abundant in salinities of 13 – 18 g/kg (Mudie et al., 2017). However, this range is likely artificially limited by the availability of modern sampling locations. The combination of surface occurrences and geological records suggest that this species can survive in salinities of 0 – 38 g/kg (Kouli et al., 2001; Mudie et al., 2017), although its abundance appears to be severely curtailed in elevated salinities such as those of the Mediterranean, where it is only encountered in locations that are freshened by river input (Mudie et al., 2017).

S. cruciformis is apparently capable of proliferating at the lower end of its salinity range, representing <95% of assemblages in Lake Kastoria at inferred salinity of 0 g/kg (Kouli et al., 2001).

However, this is at odds with the <5% occurrence in fresh water from (Leroy and Albay, 2010), and suggests that either the relationship between abundance of *S. cruciformis* and salinity is not linear, or that the motile form responds readily to water parameters other than salinity (such as temperature or nutrient availability).

6.3.2.5 *Spiniferites sp.*

The *Spiniferites sp.* include specimens from the genus *Spiniferites* that could not be identified to species level. The *Spiniferites sp.* contains both high and low salinity tolerant species (e.g., Richards et al., 2018; Soliman and Riding, 2017; Sütő-Szentai, 2010) and therefore, cannot be used to determine palaeoenvironmental conditions by itself. Its occurrence along with *Spiniferites cruciformis* and with marine influence indicators, is traditionally associated with "brackish" conditions, occurring today in the Mediterranean, Black Sea, Caspian Sea and Aral Sea (Mudie et al., 2017).

6.3.2.6 Indicators of marine influence

In its marine influenced state (such as the present-day), Black Sea dinocyst assemblages tend to be characterised by species such as *Lingulodinium machaerophorum* (long processed forms), *Operculodinium centrocarpum* and halophytic species of *Spiniferites* (e.g. *S. mirabilis, S. ramosus/hyperacanthus, S. belerius*; Marret et al. (2009) and Mudie et al. (2004, 2010, 2017)). *L. machaerophorum* has a wide tolerance of salinity from ~8 to >35 g/kg but tends to show reduced processes in lower salinities (Mertens et al., 2009, 2012). While short processed forms can reach maximum abundance (75%) at ~13 g/kg, forms with longer processes reach maximum abundances (>80%) in Black Sea only at ~17-18 g/kg (Mudie et al., 2017). It is therefore likely that high representation of long processed forms of *L. machaerophorum*, along with species such as *Operculodinium cetrocarpum* and *Tectatodinium pellitum*, probably indicate salinities somewhere above 15 g/kg.

In order to constrain the marine and freshwater source end-member for modelling, the above groups are interpreted for salinity estimates. Salinity estimates used in this study are based on a combination of culture studies (Ellegaard et al., 2002; Lewis et al., 2018), and studies relating sea bed sediment cyst assemblages with modern sea surface conditions (Mudie et al., 2017; Zonneveld et al., 2013). In cases where no living analogue is known, or where maximum abundances are observed in ancient sediments, estimates of contemporary sea surface conditions are inferred from

the geological setting and associated fossils (Baltes, 1971; Cziczer et al., 2009; Kouli et al., 2001; Leroy and Albay, 2010; Soliman and Riding, 2017). However, these salinity estimates are tentative, at best, given that there is no clear understanding of the ecological tolerance of the assemblages or that they do not exhibit linear relationship with surface salinity. As such, *Pyxidinopsis psilata* is assumed to indicate surface salinities somewhere below 10 g/kg, low salinity dinocysts are considered to indicate salinities somewhere between 12 - 15 g/kg. *Spiniferites cruciformis* indicates wide surface salinity range but traditionally are associated with brackish conditions with salinities that can be between ~13 – 18 g/kg, *Spiniferites* sp., and marine influence indicators imply higher salinity conditions likely similar to the present-day Black Sea (~16 – 18 g/kg).

The dinocyst assemblage shows that the Black Sea was mostly dominated by *Pyxidinopsis psilata* over the last 1.2 Ma with frequent periods dominated by *Spiniferites* sp.. Dinocyst indicators of marine influence occur during the last 500 ka and where the abundance is 60 – 70 % at 121 and 326 ka and coincides with the high $^{87}Sr/^{86}Sr$.

6.4 Discussion

6.4.1 Evidence of episodic Black Sea anoxia

Ostracods are bottom dwelling, environmentally and geographically diverse species (Section 1.5.3.1) and their absence in the deep sea sedimentary succession could be the result of bottom water anoxia. Although anoxic bottom water conditions prevent benthic colonisation of the Black Sea at water depths greater than 100 m, surface dwelling organisms like dinoflagellates continue to thrive. The DSDP record shows at least 5 intervals in which samples contain dinocysts but no ostracods (104 – 125 ka, 197 ka, 220 – 251 ka, 305 – 339 ka, 406 – 432 ka; Figure 6.3) indicative of similar oxygen stratification to that experienced by the Black Sea today. These intervals are characterised by the presence of *Spiniferites sp.*, (Figure 6.3) and may indicate sufficient marine input to create anoxia in the Black Sea (Hoyle, 2019), not dissimilar to today's configuration. These intervals began at around 420 ka and coincide approximately with interglacial MIS 5, 7, 9, and 11 (Figure 6.3). The DSDP record also shows 6 samples, which contained ostracods, but no dinocysts.

6.4.2 Possible water sources feeding the Black Sea

The recurrence of particular Sr isotope values at different depths in the core (Figure 6.3) allows us to categorise the entire $^{87}Sr/^{86}Sr$ record into five data groups, i.e. 1) $^{87}Sr/^{86}Sr$ values higher than 0.7089 (blue), 2) values between 0.7088 and 0.7089 (green), 3) values around 0.7087 (yellow), 4) values ~ 0.7086 (orange) and finally, 5) $^{87}Sr/^{86}Sr$ values lower than 0.7085 (red).

$^{87}Sr/^{86}Sr$ values higher than 0.7089 (blue data)

Today, the $^{87}Sr/^{86}Sr$ of the Black Sea is lower than, but close to, the open ocean's Sr ratio reflecting substantial input from the Mediterranean Sea. The Sr isotopic record from the DSDP core shows that the Black Sea did not reach the present-day value over the last 1.2 Ma (Figure 6.3). However, given that the Mediterranean is the only direct water source that has $^{87}Sr/^{86}Sr$ higher than 0.7089, values above this Sr isotope ratio in the DSDP record can be attributed to the Black Sea receiving some marine input, but less than today's influx. Modelling variable input from the Mediterranean Sea and changes in the Black Sea's fluvial flux (scenario A) produces $^{87}Sr/^{86}Sr$ ranging between 0.7088 and 0.709148 (Figure 6.4A) encompassing the value represented by the blue points ($^{87}Sr/^{86}Sr$ >0.7089). However, changing the flux of the Mediterranean water also impacts Black Sea salinity. A peak in Sr isotope data at 121 ka is associated with dinocyst assemblages indicative of marine input (Figure 6.3). Although sample at 454 ka contains no dinocysts, diatom based salinity estimates from this part of the core suggest salinities up to 14 g/kg, less than today and consistent with a smaller Mediterranean flux.

Although the sample at 136 ka has the closest $^{87}Sr/^{86}Sr$ to coeval ocean water, dinocyst assemblage in this sample indicates fresh water conditions. Wegwerth et al. (2014) observed unusually high $^{87}Sr/^{86}Sr$ (up to 0.70945) at ~131 and 133 ka in core samples collected from the southeast Black Sea (22GC-8, Figure 6.1). The authors suggested that these values were caused by high discharge from

the Amu Darya into the Caspian Sea, which then overflowed into the Black Sea raising its Sr isotope ratio to values higher than coeval seawater, without raising the salinity. However, our new measurements of Aral Sea water suggest that Amu Darya has a Sr isotopic ratio of 0.709214; too low to account for the Black Sea measurements Wegwerth et al. seek to explain. This mismatch is enhanced by the recognition that Amu Darya is only one of several large rivers that feed the Caspian, the largest of which, the Volga, has a very low Sr isotope ratio (Clauer, 1998; Clauer

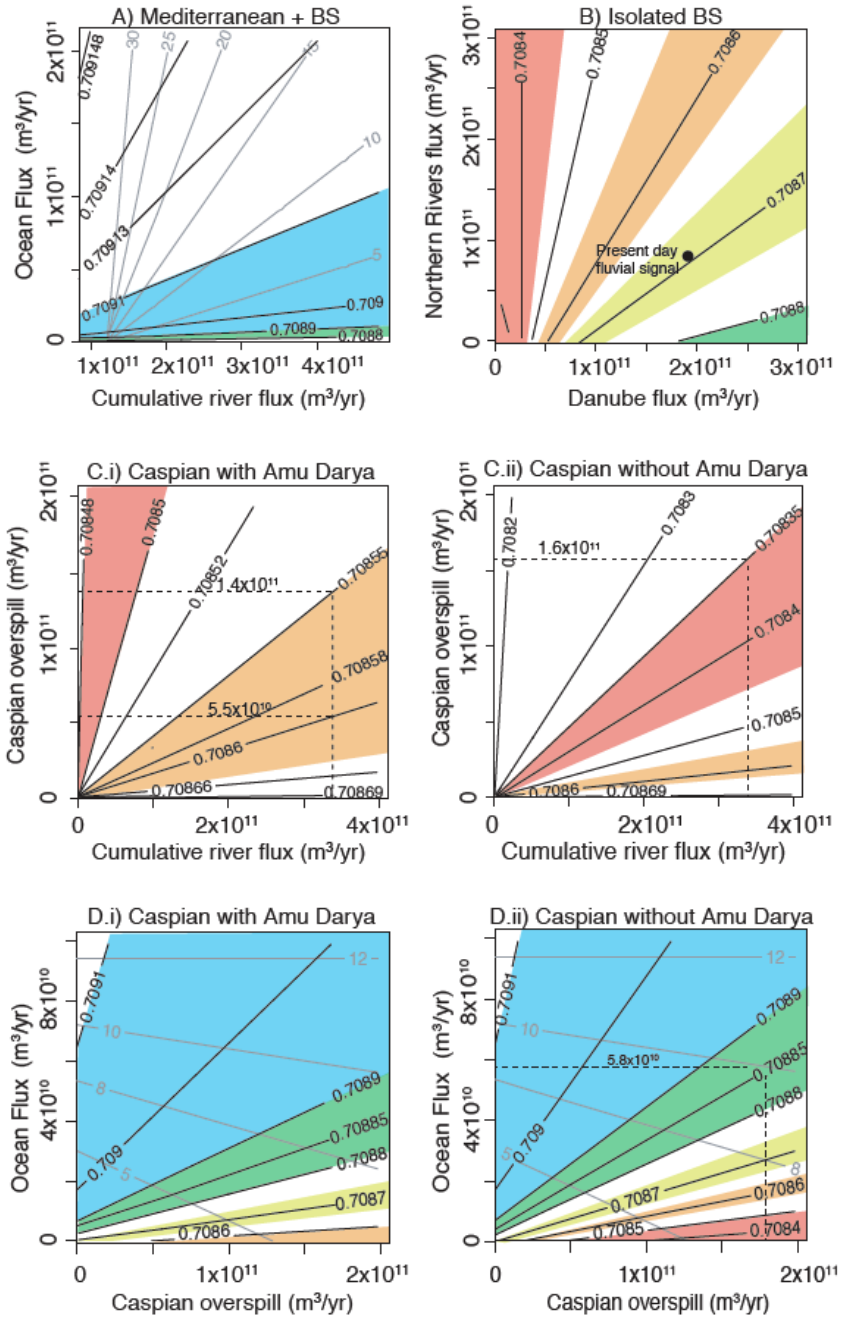

FIGURE 6.4: Model generated salinity (grey lines) and $^{87}Sr/^{86}Sr$ (black lines) in the Black Sea with variation in input fluxes for different connectivity scenarios used in this study. Colour shaded area represents the range of values of the five $^{87}Sr/^{86}Sr$ data groups. Note that scenario B and C do not have salinity contours. This is because the model is run at steady state and in these scenarios, volume and consequently salinity remain constant.

et al., 2000). Any Caspian overflow would have had a Sr isotope ratio that reflected all these inputs resulting in input to the Black Sea that was lower than Amu Darya alone.

An alternative explanation is based on the observation that this short-lived interval of high Black Sea Sr isotope ratios and fresh water dinocysts coincides with the abrupt transition from the Saalian

glacial of MIS 6 to the MIS 5 interglacial (Figure 6.3). Much of the Dnieper catchment was covered by huge ice lobe formed during the Saalian (Figure 6.1, Svendsen et al., 2004). This appears to have covered almost all the carbonate rocks exposed in the Dnieper catchment (Figure 6.5) while not impacting the Don's drainage basin. As a result, it is likely that the Dnieper's Sr isotope ratio was substantially higher than it is today during this interval, reflecting the predominantly granitic basement of the exposed pro-glacial area. The age model is insufficiently precise to be sure exactly how the two high Sr isotope ratios from this interval relate to this extremely abrupt glacial - deglacial transition and there are two possible alternatives. One is that the rising Sr isotope values observed between 160 and 130 ka reflect glacial encroachment leading up to MIS 6 (Figure 6.3). The other is that the highest Sr isotope ratio in our DSDP record and the even higher values measured by Wegwerth et al. (2014) are the product of greater erosion associated with rapid deglaciation (Hinderer, 2001) or preferential release of ^{87}Sr during early stage deglacial erosion (Blum and Erelt, 1995). A similar glacially-driven shift towards higher Sr isotope ratios in the Black Sea by northern rivers has also been proposed by Major et al. (2006) to explain two high ^{87}Sr/^{86}Sr values observed at ~18 and ~16 ka (Figure 6.6).

Values around 0.7087 (yellow data)

The four data represented in yellow in the DSDP record (Figure 6.3) have ^{87}Sr/^{86}Sr close to the ratio that an isolated Black Sea would have, if the Black Sea fluvial fluxes were the same as the present-day (Figure 6.4B, Major et al., 2006). The dinocyst assemblages in these samples consistently, contain an *Pyxidinopsis psilata*, indicative of low salinity conditions. However, it cannot be assumed that the present-day fluvial fluxes have remained constant, particularly during periods when substantial climatic change has influenced both precipitation patterns across the catchments (Bahr et al., 2006; Kwiecien et al., 2009; von Grafenstein et al., 1999) and the episodic glaciation of the northern parts of the drainage basin (Astakhov, 2004; Svendsen et al., 2004).
Model output for an isolated Black Sea (scenario B) shows that extreme fluctuations in the fluvial input can produce ^{87}Sr/^{86}Sr ranging between 0.7084 and 0.70885 (Figure 6.4B), potentially also explaining the data with ^{87}Sr/^{86}Sr about 0.70885 (green data; Figure 6.3) and those with ratios of 0.7086 or lower (orange and red data; Figure 6.3). However, while both the green and orange data points contain high concentrations of *P. psilata* (Figure 6.3), some of these samples, particularly orange data points, also contain low salinity dinocysts with Paratethyan lineage. Therefore, the data represented by green, orange and red could be the result of either, extreme changes in fluvial

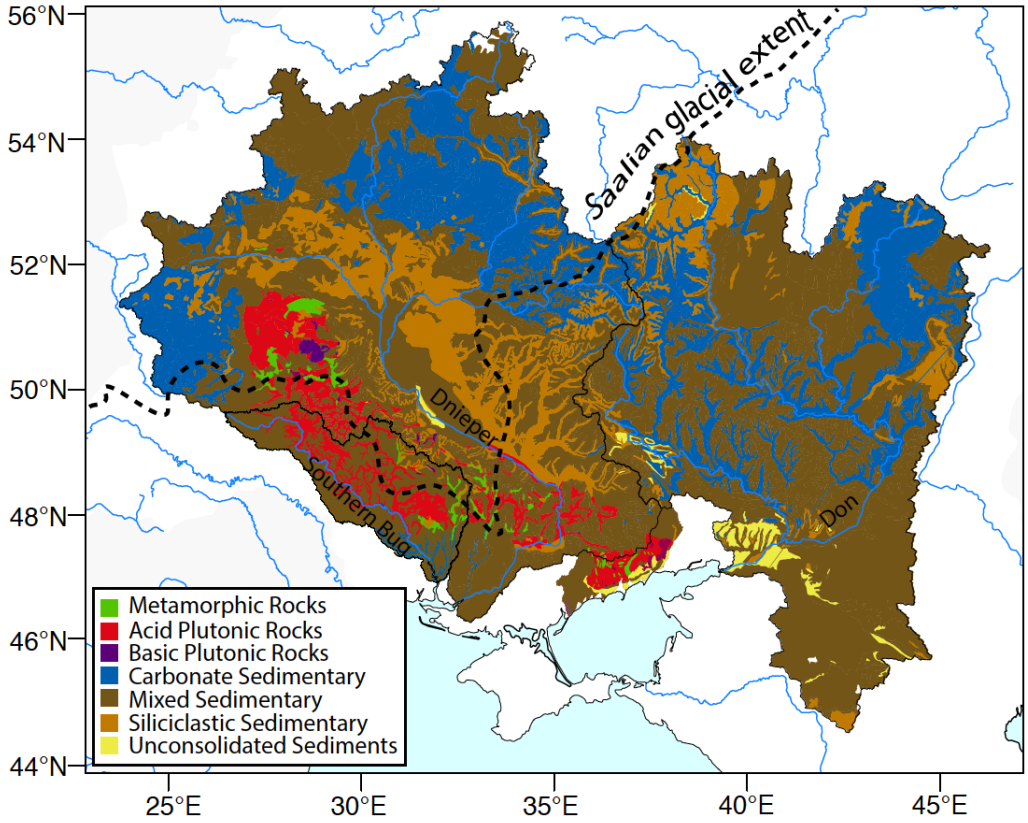

FIGURE 6.5: Lithological map of the Don and Dnieper river's catchment area. The thick dashed line shows the extent of ice sheet and Dnieper lobe during Late Saalian (~160 – 140 ka; Svendsen et al., 2004).

discharge or a possible connection with the Caspian Sea.

Values lower than 0.7086 (orange and red data)

The numerical model is used to evaluate the influence of Caspian input on the Sr isotope ratio of the Black Sea. The $^{87}Sr/^{86}Sr$ data from the older Karagoush Mountain section (Page, 2004), that spans ~1.9 Ma to ~1 Ma, are consistent within the range between 0.70842 and 0.7086 (Figure 6.3). This range of values is substantially higher than the current Caspian Sea $^{87}Sr/^{86}Sr$ of 0.708191 (Chapter 3), indicating an additional radiogenic input from the Amu Darya river (Chapter 5). A median $^{87}Sr/^{86}Sr$ of 0.70848 is assumed as the likely Sr isotope ratio of any Caspian input to the Black Sea. An additional Amu Darya flux of ~8.5 km^3/yr can generate $^{87}Sr/^{86}Sr$ of 0.70848 in the Caspian Sea (Figure C.2).

Assuming present-day Black Sea fluvial fluxes totalling about 3.38 x 10^{11} m^3/yr, only a small (~5.5 x 10^{11} m^3/yr) influx of Amu Darya-influenced Caspian water is required to produce a Black Sea Sr isotope ratio compatible with the orange data (Figure 6.3 and 6.4C.i). The alternative

hypothesis is that the lower ratios are driven by increased input from the Don and Dnieper relative to the Danube. However, this would require a four-fold increase in the discharge from the northern Black Sea rivers relative to the present-day flux (Figure 6.4B). While such increase in river flow is possible during the deglaciation, these high discharge periods are likely to have been brief and temporally associated with the glacial-interglacial transition. By contrast, the DSDP record shows prolonged periods during which the Black Sea had the $^{87}Sr/^{86}Sr$ of ~0.7086 (orange) particularly between 900 – 700 ka and appears to be unrelated to glacial advances and retreats (Figure 6.3). It is therefore more likely that the lower Sr isotope elements of the DSDP record (red and orange) are a consequence of a Black Sea isolated from the Mediterranean Sea but receiving an additional water source from the Caspian Sea.

A larger Caspian overspill of about 1.4 x 10^{11} m^3/yr can explain the three higher red Sr isotope values (~0.70855). However, Caspian water that has the $^{87}Sr/^{86}Sr$ of 0.70848, cannot account for the lowest red values, which are closer to 0.70835 (Figure 6.3). These lowest DSDP Sr isotope data require the additional fresh water source to have had an even lower Sr isotope ratio. In this instance, the Caspian overspill with the present-day fluvial sources (i.e without Amu Darya input) and Sr isotope ratio that is dominated by the Volga would be a better fit (Figure 6.4C.ii). There are two possible mechanisms by which this could be achieved. Either input from Amu Darya to the Caspian varied even before the rivers discharge was modified by irrigation (Asarin et al., 2010; Micklin, 2010), or the Volga River drained directly into the Black Sea instead of the Caspian during these intervals. The redirection of Volga, which is the dominant water source of the Caspian Sea, to the Black Sea would result in extreme change in the $^{87}Sr/^{86}Sr$ of the Caspian Sea. The current data do not constrain which of these two is more likely.

Values between 0.7088 and 0. 7089 (green data)

It is possible that the Black Sea was an isolated basin when its Sr isotope ratios were between 0.7088 and 0.7089 (e.g. green data). Although the dinocyst assemblage indicates isolated conditions between 28 – 72 ka (Figure 6.3), to achieve these Sr isotope values, which are very close to the Danube $^{87}Sr/^{86}Sr$ (Figure 6.3), there would need to be extreme reduction in discharge from the northern Black Sea rivers (Figure 6.3, Figure 6.4B). Three of the four green samples between 400 - 150 ka indicate diatoms based salinities between 10 – 15 g/kg (Schrader, 1978) whereas, the forth (326 ka) contains marine assemblages (Figure 6.3). This requires some marine input. Model output demonstrates that Mediterranean inflow is almost close to zero to produce a Black

Sea $^{87}Sr/^{86}Sr$ between 0.7088 and 0.7089 (green data, Figure 6.4A). An alternative solution is that the Black Sea received influxes from both the Mediterranean and the Caspian seas (connectivity scenario D). In this scenario, a Mediterranean flux >5.8 x 10^{10} m^3/yr is required to raise the Sr isotope ratio to ~0.70885 and to produce salinities greater than 10 g/kg in the Black Sea when it is also in receipt of Caspian Sea water with a lower Sr isotope ratio (Figure 6.4D.ii). Similar arguments may also be applicable to the green data points at 977 and 650 ka although the salinity constraints are less substantial.

6.4.3 Evolution of the Black Sea over the last 1.2 Ma

The combination of the Sr isotopic record and the available diatom and new dinocyst based salinity estimates of the DSDP core show clear evidence of a complex connectivity history involving both the Mediterranean and Caspian Sea throughout the last 1.2 Ma (Figure 6.6). Despite this complexity there is an overall transition in the relative dominance of these sources at around 500 ka, when a strong signal of Caspian Sea input is replaced by more frequent Mediterranean incursions (Figure 6.6). However, the detail of the Black Sea's connectivity history needs to be interpreted with care because even relatively small marine incursions can dominate both the Sr and the salinity record, overprinting an enduring Caspian signal. The combined interpretation of the dinocysts and isotope datasets suggests that from 1.2 Ma – 380 ka, the Black Sea was dominated by Caspian Sea input with two short episodes of isolation and two minor marine incursions from the Mediterranean (Figure 6.6). From 380 ka to present, the Black Sea oscillated between an isolated basin to one connected to the Mediterranean with only two intervals of Caspian input around 200 and 170 ka (Figure 6.6).

This interpretation of the timing of marine-influenced intervals in the Black Sea suggests that over the last ~500 ka all the major interglacial peaks can be associated with a eustatic sea-level driven inundation over the Bosporus (Figure 6.6). The variability in the Sr isotope and dinocyst response to each of these incursions results largely from the degree of connectivity of the Black with the Mediterranean and Caspian. This means that when there was a Mediterranean incursion into an isolated Black Sea such as during MIS 5 and 9, it resulted in a clear marine signal in the Sr and dinocyst data (Figure 6.3). The more complex Sr and biotic response during MIS 7 and 11 may be the product of smaller marine influxes into a basin already receiving additional fresh water from either the Caspian Sea and/or the Black Sea rivers (Figure 6.6). A similar relationship can be seen during glacial periods MIS 2 to MIS 10 when these low eustatic sea level episodes coincide

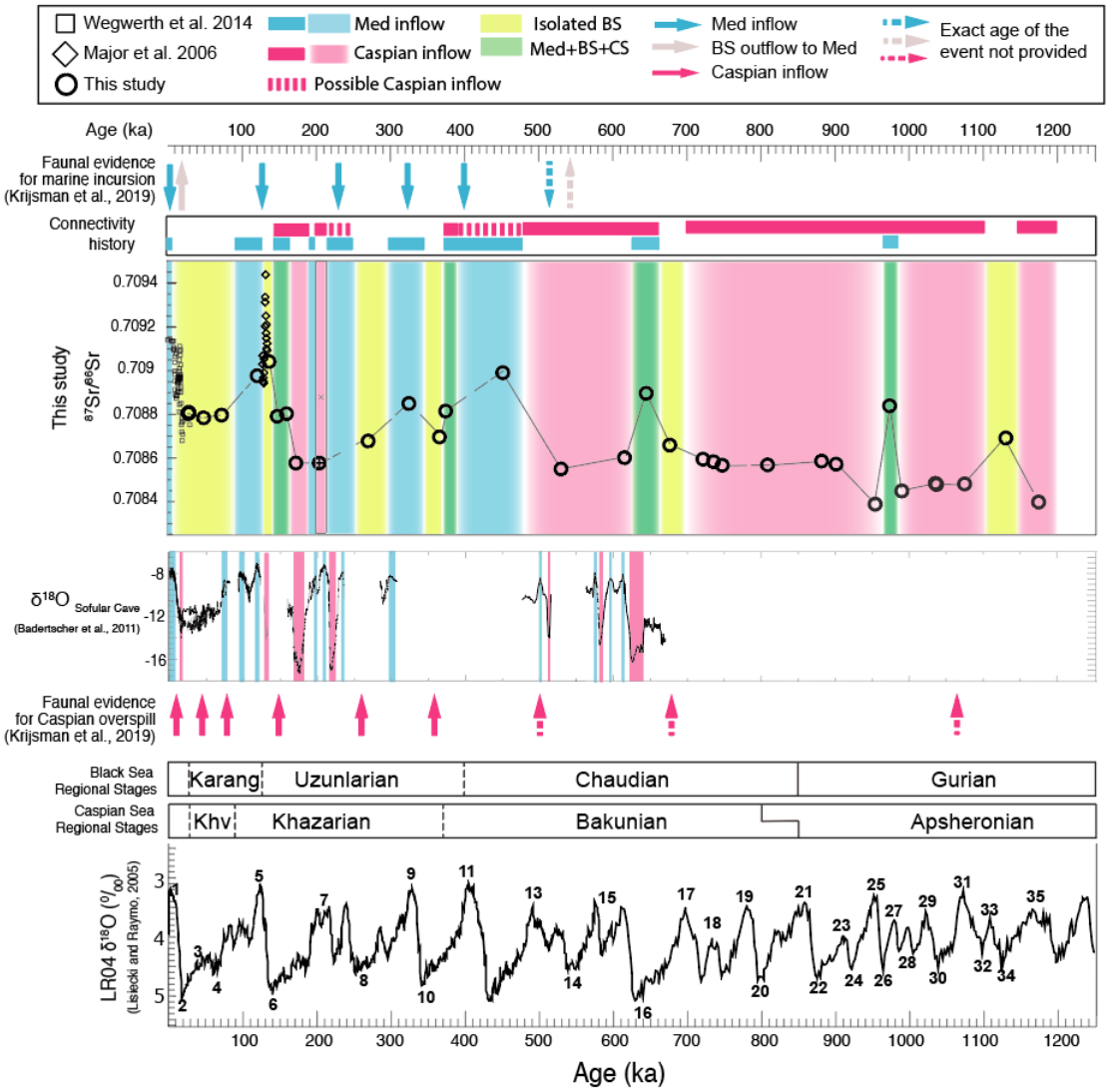

FIGURE 6.6: Reconstruction of the Black Sea connectivity history over the last 1.2 Ma based on the $^{87}Sr/^{86}Sr$ of the DSDP core 379A together with the oxygen isotope based reconstruction by Badertscher et al. (2011) and faunal based reconstruction provided in Krijgsman et al. (2019).

with times when the Sr isotope and dinocyst data indicate no marine waters entered the Black Sea. These intervals are typically characterised by Sr and dinocyst assemblages that are compatible with an entirely isolated (yellow) Black Sea (Figure 6.6).

Prior to 500 ka, the record of marine incursions into the Black Sea were much less frequent and appears to be unrelated to glacial-interglacial cyclicity (Figure 6.6). The tectonic signal controls the connectivity when the amplitude of eustatic change is insufficient to breach the gateway threshold. Given than the Bosporus lies within the active North Anatolian Fault Zone (NAFZ), which currently has a displacement velocity of ~20mm/yr (Hubert-Ferrari et al., 2002), it is likely that both the location and the evolution of the Black Sea - Mediterranean gateway is intrinsically controlled by the tectonics of NAF on geological timescales. Although eustatic sea level rise during interglacial

may have driven the Black Sea - Mediterranean connection during MIS 5, 7, 9 and 11, the marine incursion prior to MIS 11 was likely to have been driven by a combination of climatic fluctuation and active tectonics of the area. The periodicity of Caspian-Black Sea connectivity also seems to be unrelated to glacial-interglacial cycles and is therefore likely to be controlled by the tectonics associated with the uplift of the Caucasus and the formation and migration of the Manych foredeep (Mikhailov et al., 1999).

This broader interpretation fits well with the fragmentary connectivity history deduced from extreme fluctuations in the existing oxygen isotopic record from the Sofular Cave (Badertscher et al., 2011). Given the uncertainty in the age model for the DSDP core, the relative scarcity of the Sr isotope and dinocyst data constraints, and the growth discontinuities in the stalagmite record, the coincidence of the high δ^{18}O values (> -8.5 ±1‰) interpreted as marine incursions (Badertscher et al., 2011) with Sr and dinocyst indicators of Mediterranean input is very good, particularly from ~300 ka onwards (Figure 6.6). Both interpretations also identify Caspian overspill events at around 170 and 600 ka (Figure 6.6). However, a much higher resolution Sr-dinocyst record is required to test the hypothesis that these connectivity events are brief incursions as represented by the speleothem data (Figure 6.6).

The Sr isotope and dinocyst reconstruction also fits well with published palaeontological evidence for Mediterranean incursions over the last 400 ka (Figure 6.6). However, the timing of Caspian-Black Sea connections and separation events deduced from these data is much less consistent with the new geochemical connectivity interpretation (Figure 6.6). For example, the distinctly different faunal assemblages prior to 800 ka between the Black Sea (Gurian Stage) and the Caspian Sea (Apsheronian Stage) suggest isolation with only ephemeral connections between the two basins (Krijgsman et al., 2019, and references therein) at a time when much of the Sr and dinocyst data indicate an enduring contribution of Caspian Sea water to the Black Sea (Figure 6.6). Even taking into account the challenges of dating some of the faunal evidence, there is an apparent contradiction here. One possible explanation is that the Caspian-Black Sea connection during this period did not result in homogenised environmental conditions across the two basins for full faunal exchange.

6.5 Conclusion

The newly obtained fluvial measurements (Chapter 3) were incorporated in a numerical box model (Chapter 4) to constrain the source end-members for Black Sea water in order to explain the Sr

isotopes and dinocysts based salinity variation observed in the DSDP record over the last 1.2 Ma. The combination of empirical measurements and modelled Sr and salinity proves to be a powerful tool for disentangling complex connectivity histories with multiple water sources. The data show that the Black Sea was connected to the Caspian Sea for most of the period prior to 500 ka, whereas more frequent Black Sea - Mediterranean connection took place after 500 ka. Although, the Black Sea may have sustained a connection with the Caspian during the last 500 ka, the DSDP data cannot differentiate this as the Caspian input may be masked by a marine dominated signal with high salinity and radiogenic Sr isotopic ratio in the Black Sea. Relating the connectivity events to the climatic and tectonic drivers shows that while eustatic sea level variation may have controlled the connection between the Black Sea and the Mediterranean Sea in MIS 5, 7, 9 and 11, and combination of tectonics and climate may have driven the Black Sea- Mediterranean connection prior to MIS 11. However, to disentangle the role of climate and tectonics during each glacial-interglacial cycle, a much higher resolution study is required.

Chapter 7

Sr isotopic record of the Hajigabul section, Azerbaijan: Implications for the Pleistocene connectivity between the Black Sea and Caspian Sea

A connectivity history framework focusing on the Early Pleistocene Caspian Sea and the Pleistocene Black Sea was established in Chapter 5 and Chapter 6, respectively. This chapter provides additional new Sr isotopic data from the Caspian Sea (Hajiqabul section) and helps expand the connectivity history developed in the previous chapters. The age model indicates that the section spans most of the Pleistocene including an interval that is younger than previously studied Caspian Sea sections (Goychay section- Chapter 5 and Karagoush section, Page, 2004). This interval overlaps with the Black Sea data described in Chapter 6. This chapter therefore describes this Caspian Sr record and explores the evolution of the Caspian-Black Sea connectivity during the Middle to Late Pleistocene and mainly addresses ***research questions 5 and 6*** *outlined in Section 1.6.2;*

5. *How did the Sr isotopic ratio evolve in the Black and Caspian seas over the last 3 million years and what is its implication for the Quaternary connectivity history of the two basins to each other and the open ocean?*
6. *What was the nature of connection (one way flow or two way exchange) between the Black Sea, Caspian Sea and the open ocean during the Pleistocene?*

The age model for the Hajigabul section was constructed and provided by **S. Lazarev**, PRIDE ESR at Utrecht University. The micropalaeontological analysis, the ostracod assemblages and associated salinity constraints were provided by **L. Rausch** (PRIDE ESR) and **Prof. M. Stoica**, the University of Bucharest. Both, the age model and the ostracod assemblage chart included in this chapter are from Lazarev et al. (2019):

S. Lazarev, E. L. Jorissen, S. van de Velde, L. Rausch, M. Stoica, F. P. Wesselingh, C. G. C. van Baak, T. A. Yanina, E. Aliyeva, W. Krijgsman (2019) **Magneto- biostratigraphic age constraints on the palaeoenvironmental evolution of the South Caspian Basin during the Early - middle Pleistocene (Kura Basin, Azerbaijan)**, *Quaternary Science Reviews*, 222, p. 105895.

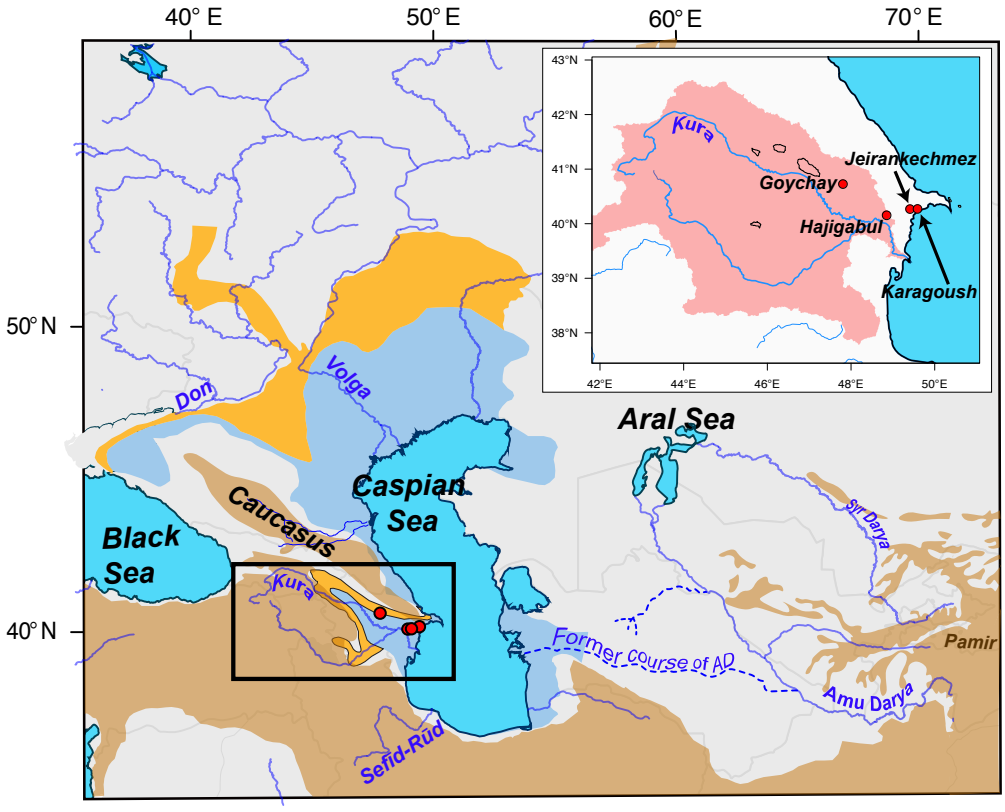

FIGURE 7.1: Location map of the study sites; Hajigabul, Goychay, Jeirankechmez, and Karagoush sections. Pale blue area shows the palaeogeographic extent of the Caspian Sea during the Apsheronian period, with fluvial plains shown in yellow (modified from Krijgsman et al., 2019). Pale brown area indicates topographic highs in the region. Dotted blue lines indicate former course of the Amu Darya (AD). Pale red area indicates catchment area of the Kura river.

7.1 Materials and methods

Sediment samples were collected from the Hajigabul section, which lies ~55 km from the present-day Caspian coastline within the Kura catchment (Figure 7.1). The section is substantially closer to the Caspian Sea than the Goychay section (~155 km) but further away than the Karagoush section (~5 km, Figure 7.1). 23 sediment samples from the Hajigabul section (Chapter 2, Section 2.1.2.5) were picked for ostracods and analysed for their Sr isotopic ratio (Section 2.2.3).

The magnetostratigraphy of the Hajigabul section (Lazarev et al., 2019) allowed age estimates of individual samples to be calculated assuming constant sedimentation rates between chron boundaries. However, the top of the section did not reach the upper boundary of the Bruhnes chron (Figure 2.7). Therefore, to calculate the age of the samples that fall within this chron, a chronological constraint is required for the top of the section. Sedimentology and palaeontology studies indicate two flooding events in the section are at ~1714 m and ~1842 m (Lazarev et al., 2019). These events are considered to be the upper Bakunian and lower Khazarian flooding events, respectively, based on the presence of euryhaline foraminifera and bivalve assemblages that are specific to each event in other parts of the Caspian Sea (Yanina, 2014). According to U-Th, thermoluminescent and electron spin resonance data, lower Khazarian deposits are dated at approximately MIS 10 - 6 (364 - 190 ka, Shkatova, 2010; Zastrozhnov et al., 2018). Therefore samples that lie within the Bruhnes chron but below the identified Khazarian flooding event, i.e. samples between 1641 - 1842 (Figure 2.7), are considered to have age between 781 and 364 ka. The youngest Hajigabul sample at 1842.5 m falls within the Khazarian flooding event and as such is considered have an age between 364 to 190 ka. Consequently, the age of the upper six samples of the Hajigabul section are substantially less certain than those constrained by the palaeomagnetic results. This age uncertainty are illustrated by the use of horizontal bars on the data plot (e.g. Figure 7.2).

Semi-quantitative micropalaeontological analysis of 57 sediment samples was conducted on the fossil ostracods and foraminifera. Samples were processed following the method outlined in Section 2.3.

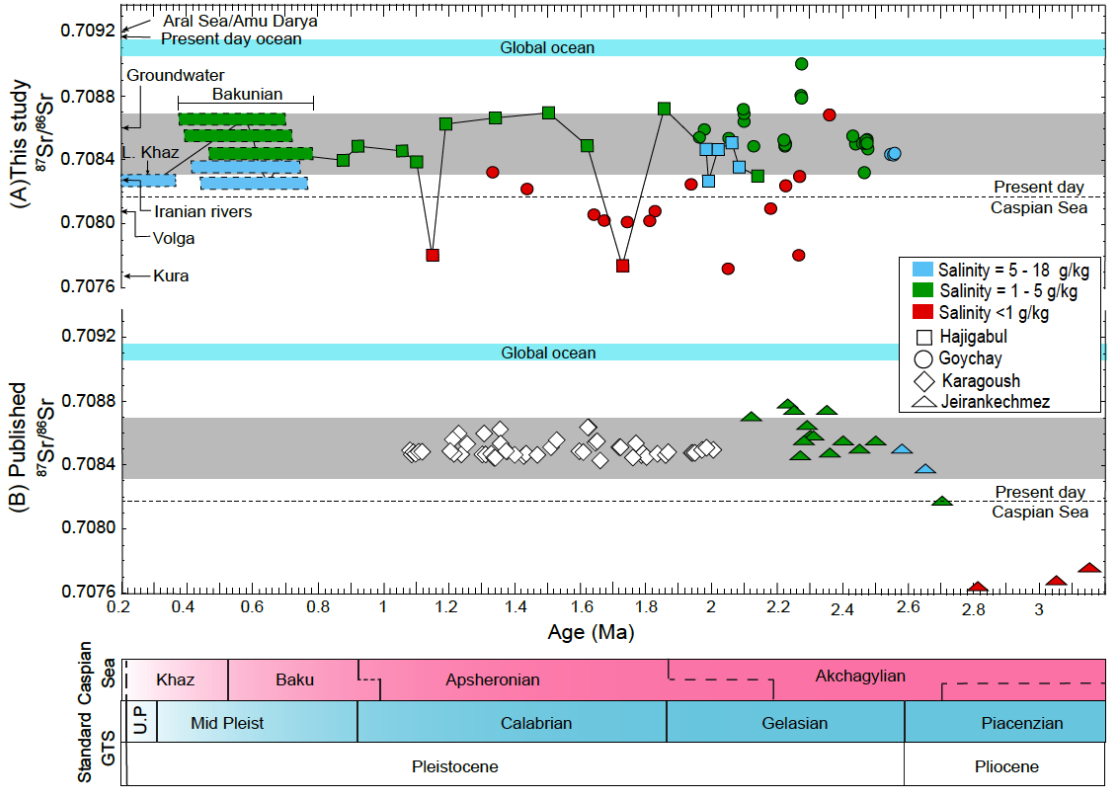

FIGURE 7.2: A) The Sr-isotope record for the Hajigabul (coloured boxes) and Goychay (coloured circles) sections plotted with coeval oceanic $^{87}Sr/^{86}Sr$ (blue horizontal bar; McArthur et al., 2012), the $^{87}Sr/^{86}Sr$ values of the present-day Caspian Sea (dashed horizontal line) and its major water sources. Internal uncertainty for each individual $^{87}Sr/^{86}Sr$ measurement on Hajigabul samples is between 4 and 14 ppm and external uncertainty on 36 repeat measurement on NIST 981 standard is ~8 ppm.The grey shaded area indicates the range of $^{87}Sr/^{86}Sr$ of the Black Sea from the Guria section. Six youngest data from the Hajigabul section have uncertain ages and therefore are indicated by coloured bars. B) Previously published Sr-isotope record for the Jeirankechmez (coloured triangles; van Baak et al., 2019) and Karagoush Mountain sections (white diamonds; Page, 2004).

7.2 Results

7.2.1 Sr isotopic ratios

The Sr isotopic measurements of fossil ostracods collected from the Hajigabul section are shown in Figure 7.2 and listed in Table E.1. The range of $^{87}Sr/^{86}Sr$ data from the Hajigabul section are consistent with the Goychay section (Chapter 5) and with the previously published Sr isotopic record from the coeval Karagoush Mountain section (Page, 2004) and Jeirankechmez section (van Baak et al., 2019). These values are significantly lower than the coeval oceanic $^{87}Sr/^{86}Sr$ ratio and but are mostly higher than the present-day Caspian Sea value (Figure 7.2). The record also shows two episodes with the $^{87}Sr/^{86}Sr$ values lower than the present-day Caspian Sea ratio at 1.15 and 1.73 Ma. These low values are close to Sr isotopic ratio of the nearby Kura river water (Chapter

3) and resemble the similar low $^{87}Sr/^{86}Sr$ observed in Goychay section at ~2.04 and ~2.28 Ma (Chapter 5) and the late Pliocene Jeirankechmez data (Figure 7.2, van Baak et al., 2019).

7.2.2 Micropalaeontology

The micropalaeontology of the Hajigabul section shows frequent variations in ostracod and foraminifera assemblages (Figure 7.3). The bottom part of the section (211 m – 453 m) shows moderately dense, but taxonomically diverse species indicative of oligohaline (1 - 5 g/kg) to mesohaline (5 - 18 g/kg) assemblages (Figure 7.3). The interval between 453 m - 755 m contains the high abundant euryhaline *Cyprideis torosa* and also contains foraminifera, mainly species of *Ammonia, Cibicides* and *Cassidulina*; these are indicative of marine salinity conditions. Between 755 m – 1701 m, the section contains ostracod assemblages suggesting oligohaline environments (1 - 5 g/kg) indicated by the presence of *Cyprideis torosa*, *Tyrrhenocythere azerbaidjanica*, and *Xestoleberis chanakovi* alternating with numerous freshwater intervals containing *Ilyocypris bradyi, Eucypris sp., Candona sp.* and *Darwinula stevensoni*. The top part of the section (1714 - 1980 m) shows increased ostracod diversity and the assemblages indicate rapid and frequent environmental changes, altering between mesohaline and oligohaline conditions.

Microfossil data from Hajigabul section can therefore be categorised into three salinity conditions; 1) mesohaline conditions (between 5 – 18 g/kg) indicated by the presence of foraminifera, 2) oligohaline (between 1 – 5 g/kg), and 3) freshwater salinity (Figure 7.2, Lazarev et al., 2019). These are similar to the salinity ranges interpreted from ostracod assemblages at the Goychay section (Chapter 5). The samples with anomalously low Sr values observed at 1120 m and 1439 m (1.73 and 1.15 Ma) contain freshwater assemblages, while the higher $^{87}Sr/^{86}Sr$ are associated with both salinities between 1 - 5 g/kg (green) and 5 - 18 g/kg (blue, Figure 7.2). Unlike the Goychay section, the Hajigabul only contains one brief barren interval between 498 and 520 m, close to the base of the section (Figure E).

7.3 Discussion

7.3.1 Hajigabul data constraining Caspian between 2.2 Ma - 300 ka

The similarity in the range of Sr isotopic values in the Hajigabul and Goychay sections suggests that these two sections experienced broadly similar condition. Although the highest $^{87}Sr/^{86}Sr$ from the Hajigabul does not reach the highest $^{87}Sr/^{86}Sr$ observed in the Goychay section (Figure 7.2),

FIGURE 7.3: Ostracod distribution pattern from the Hajigabul section, Azerbaijan along with estimated palaeosalinity and palaeoenvironment represented by the ostracod assemblages.

the two lowest Sr isotopic ratios from the Hajigabul section at 1.15 and 1.73 Ma are consistent with the low values observed at Goychay. Both sections lie within the Kura catchment (Figure 7.1), it is therefore likely that the freshwater conditions associated with the low $^{87}Sr/^{86}Sr$ values (Figure 7.2), and the similarity with these low $^{87}Sr/^{86}Sr$ and the Kura river ratio (Chapter 3) indicates episodic enhanced local river influence during these intervals. By comparison, the coeval $^{87}Sr/^{86}Sr$ from the section closer to the present-day Caspian coastline, the Karagoush Mountain section, is consistently higher than these low $^{87}Sr/^{86}Sr$ intervals from the Hajigabul and Goychay suggesting that the low values may be the results of isolation of these lower reaches of the Kura river catchment from the main Caspian basin. The difference in the duration of these isolated intervals in each section may be due to the relative proximity of the palaeo Caspian Sea. As such the more westerly Goychay section experienced a more enduring period of isolation between 1.9 - 1.4 Ma, while Hajigabul was isolated for a shorter interval around 1.73 Ma. It is not possible to infer Caspian Sea lake level change from this transact of sites because of the likely influence of tectonics of the Caucasus in the region. However, the higher than the present-day $^{87}Sr/^{86}Sr$ and salinities >1 g/kg in the Hajigabul section indicates that this section was part of the main Caspian basin for most of the Middle - Late Pleistocene (Figure 7.2) .

The base of the Hajigabul section (samples between 2.1 to 1.98 Ma), show intermediate $^{87}Sr/^{86}Sr$ values of ~0.7084 but a high salinity conditions (5 - 18 g/kg). Although the coeval $^{87}Sr/^{86}Sr$ from the Goychay section shows similar values, the micropalaeontology suggest a lower salinity conditions (1 - 5 g/kg) during this period (Figure 7.2). The discrepancy could be due to the sampling resolution and that the samples with high salinity condition were not captured from the Goychay section. However it is more likely that the discrepancy in salinities between the two sections may be the result of asynchronous evolution of the fauna in these proximal location of the Goychay section (Lazarev et al., 2019). This is supported by the later turnover of mollusc species on Goychay relative to the Hajigabul section (Lazarev et al., 2019). The Sr - salinity combination observed during this interval in the Hajigabul section, however, is consistent with the more enduring Caspian - Arctic connection interpreted in Chapter 5. However, there are no samples between 1.98 and 1.86 Ma from the Hajigabul section to confirm the timing of termination for this connection.

Both, the Karagoush mountain and the Hajigabul sections show that the Pleistocene $^{87}Sr/^{86}Sr$ remained higher than present-day Caspian values after 1.9 Ma and micropalaeontology from Hajigabul section shows salinity condition between 1 - 5 g/kg in the Caspian Sea. There are multiple scenarios that could result in this combination of Sr - salinity conditions in the Caspian

Sea. Each of these scenarios is discussed below and its potential feasibility is evaluated.

1) There is a possibility that the Arctic connection to the Caspian Sea may have continued even after 1.96 Ma. If this was the case, analogous to the condition between 2.7 - 1.96 Ma, the Sr - salinity conditions could be achieved with inflow from Arctic Ocean and Amu Draya but outflow to the Black Sea. However, there is no palaeontological or phylogenetic evidence that supports a continued Arctic connection.

2) If the Arctic connection was severed at ~1.96 Ma, the observed Sr-salinity combination observed in the Hajigabul section could be achieved by continued input of radiogenic water from the Amu Darya but no outflow to the Black Sea, trapping the salt in the basin, assuming there is no change in evaporation minus precipitation. This scenario, however would require no change in the Caspian volume to maintain consistent salinity in the basin. Sedimentological evidence from the Hajigabul section however, indicates repetitive shallowing trends, from distal offshore settings to coastal and continental environments (Figure 2.7), implying a reduction in Caspian lake level at least locally.

3) The most likely scenario to explain the observed Caspian Sr- salinity combination is a continued inflow from Amu Draya to maintain higher than present-day $^{87}Sr/^{86}Sr$ combined with a two way exchange with the Black Sea, which contains salt that was exported prior to 2 Ma (Chapter 5). The Black Sea $^{87}Sr/^{86}Sr$ from the Guria section (if it is of the Pleistocene age) shows similar overlapping values with the Hajigabul and Karagoush sections' $^{87}Sr/^{86}Sr$ (Figure 7.2), which would support a two way exchange between the two basins. However only, the interval of 1.2 Ma to ~200 ka has an equivalent Black Sea record (DSDP 379A- Chapter 6) with less speculative age constraints. This interval from the Hajugabul section and DSDP 379A (Chapter 6) and such as, coeval record from Hajigabul and DSDP core 379A is discussed in the detail below.

7.3.2 Evolution of the Black Sea and Caspian Sea between 1.2 Ma to 200 ka

The first isolation of the Black Sea from the Caspian Sea observed in the Sr isotopic record is at ~1.13 Ma (Chapter 6). This coincides with the isolation of Hajigabul section from the main Caspian basin at ~1.15 Ma (Figure 7.4). It may be the case that at this time, change in the hydrological budget of the region or tectonic uplift resulted in either an absolute or relative Caspian water level drop, isolating the Hajigabul area from the main Caspian basin and severing the connection between the Black Sea and the Caspian Sea. The DSDP record shows that the Black Sea received inflow from the Caspian Sea almost continuously between 1.2 Ma to ~700 ka (Chapter 6). The overlapping Caspian values from the Karagoush and Hajigabul sections with the

DSDP record, particularly between 1 Ma and 1.1 Ma (Figure 7.4), further supports this idea that the two way exchange between the Black Sea and the Caspian Sea existed during this period. The first Mediterranean input into the Black Sea is observed at 977 ka (Chapter 6). Although the Black Sea $^{87}Sr/^{86}Sr$ suggests Caspian inflow into the basin, there are no $^{87}Sr/^{86}Sr$ data from this brief marine influenced interval from the Caspian Sea to document it's impact in the Caspian Sea.

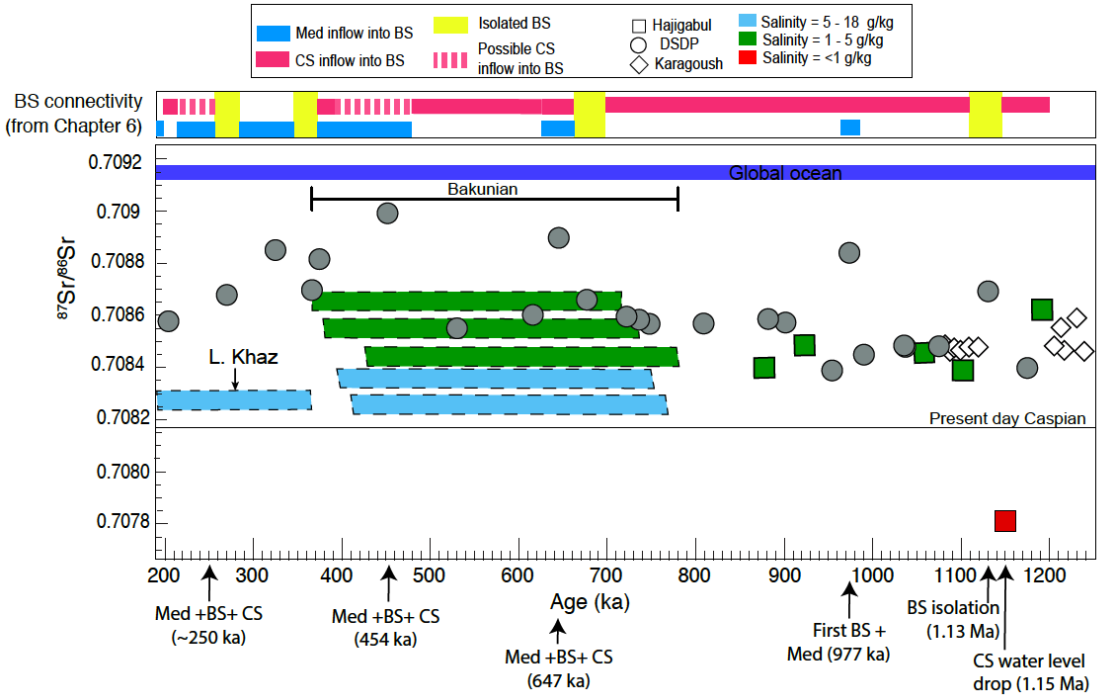

FIGURE 7.4: The Caspian Sr-isotope record from the Hajigabul (coloured boxes), Karagoush sections (white diamonds; Page, 2004) and the coeval Black Sea $^{87}Sr/^{86}Sr$ record from the DSDP 379A (grey circles) plotted with coeval oceanic $^{87}Sr/^{86}Sr$ (dark blue horizontal bar; McArthur et al., 2012) and present-day $^{87}Sr/^{86}Sr$ values of the present-day Caspian seas (dashed horizontal line) and their major water sources. Data points with dashed boundary have uncertain ages.

Three of the six youngest samples after 800 ka from the Hajigabul section contain foraminifera implying increased salinity (between 5 - 18 g/kg) in the Caspian Sea at some point between 781 and 200 ka . These samples are taken from an interval which shows facies that are clearly indicative of a water level rise event in the Caspian Sea (Lazarev et al., 2019). Additionally, the presence of molluscs assemblages similar to the Black Sea (Lazarev et al., 2019) indicates that the input of the saline water into the Caspian Sea is likely to have been derived from the Black Sea, which may have been connected to the Mediterranean Sea at this time. The DSDP record shows Mediterranean-Black Sea-Caspian connection was not continuous, but rather occurred in at least, three separate events around 647 ka, 454 ka and ~250 ka. Given the age uncertainty of the Hajigabul samples younger than 800 ka, it is possible that the samples with salinity between 5 - 18 g/kg may represent

inflow of the marine influenced Black Sea water to the Caspian Sea during these same episodes (Figure 7.4).

Although the saline inflow from the Mediterranean could explain the high salinities (between 5 - 18 g/kg) in the Caspian Sea, the $^{87}Sr/^{86}Sr$ of these samples are lower than previously observed values in the Hajigabul section and are much closer to the present-day Caspian $^{87}Sr/^{86}Sr$. A numerical model (Chapter 4) is therefore, used to investigate if the Mediterranean-Black-Caspian Sea connection could produce the $^{87}Sr/^{86}Sr$ and salinity observed in the Caspian Sea during these intervals. This model set up differs from that used in Chapter 5 and 6 because it includes two way exchange both, between the Black Sea and Mediterranean, and between the Black Sea and the Caspian Sea. Therefore, when the Caspian Sea and Black Sea are connected with each other and the open ocean, the water volume conservation equation results in ,

$$\text{Black Sea}: \; qBO = qOB + qCB + R_B + P_B - E_B - qBC$$

$$\text{Caspian Sea}: \; qCB = qBC + R_C + P_C - E_C$$

where, qOB and qBO refers to inflow and outflow between Black Sea and the open ocean, respectively and qCB and qBC refers to flux from the Caspian Sea into the Black Sea and flux from the Black Sea to the Caspian Sea, respectively. Total river discharge, evaporation and precipitation fluxes of the Black Sea are given by R_B, E_B and P_B, respectively and for the Caspian Sea are given by R_C, E_C and P_C, respectively. The Sr concentration and Sr isotopic ratio of the Black Sea and Caspian Sea can be therefore be determined as follows, with subscripts O, RB, B, C and RC referring to oceanic, Black Sea rivers, Black Sea, Caspian Sea and Caspian Sea rivers, respectively.

Sr concentration in the Black Sea :

$$[Sr]_B = \frac{[Sr]_O * qOB + [Sr]_C * qCB + [Sr]_{RB} * R_B}{qOB + qBC}$$

Sr concentration in the Caspian Sea :

$$[Sr]_C = \frac{[Sr]_B * qBC + [Sr]_{RC} * R_C}{qCB}$$

Sr isotopic ratio in:

$$\text{Black Sea}: \left(\frac{^{87}Sr}{^{86}Sr}\right)_B = \frac{\left(\frac{^{87}Sr}{^{86}Sr}\right)_O * [Sr]_O * qOB + \left(\frac{^{87}Sr}{^{86}Sr}\right)_C * [Sr]_C * qCB + \left(\frac{^{87}Sr}{^{86}Sr}\right)_{RB} * [Sr]_{RB} * R_B}{[Sr]_O * qOB + [Sr]_C * qCB + [Sr]_{RB} * R_B}$$

Caspian Sea :

$$\left(\frac{^{87}Sr}{^{86}Sr}\right)_C = \frac{\left(\frac{^{87}Sr}{^{86}Sr}\right)_B * [Sr]_B * qBC + \left(\frac{^{87}Sr}{^{86}Sr}\right)_{RC} * [Sr]_{RC} * R_C}{[Sr]_B * qBC + [Sr]_{RC} * R_C}$$

Salinity of the Black Sea results from mixing of oceanic water and saline Caspian water, whereas the salinity of the Caspian Sea is resultant of the Black Sea input. Therefore,

$$\text{Black Sea}: [S]_B = \frac{[S]_O * qOB + [S]_C * qCB}{qBO}$$

$$\text{Caspian Sea}: [S]_C = \frac{[S]_B * qBC}{qCB}$$

The model result shows that both, $^{87}Sr/^{86}Sr$ and salinity in the Caspian Sea is governed by the input from the Black Sea and can produce the low $^{87}Sr/^{86}Sr$ and the salinity between 5 - 18 g/kg observed in the Hajigabul section (Figure 7.5B). This is because the Black Sea water is influenced by the oceanic $^{87}Sr/^{86}Sr$ and salinity resulting from its connection to the Mediterranean Sea. However, in a scenario where all three basins (Mediterranean, Black and Caspian seas) are connected, the Caspian Sea can only produce an $^{87}Sr/^{86}Sr$ close to the present-day value if Amu Darya did not drain into the Caspian Sea or its discharge was very low (<10 km^3/yr). A small oceanic input of ~8 x 10^{10} m^3/yr into the Black Sea, which also receives water from the Caspian Sea, produces the $^{87}Sr/^{86}Sr$ between 0.7089 and 0.7090 observed in the DSDP record (Figure 6.4) at 647 ka, 454 ka. Consequently, Black Sea input between 2 x 10^{10} m^3/yr and 3 x 10^{10} m^3/yr is required to produce the $^{87}Sr/^{86}Sr$ between 0.70825 and 0.70835 and salinity of ~15 - 18 g/kg observed in the Hajigabul section of the Caspian Sea.

In summary, the evolution of the Caspian Sea during the Pleistocene was influenced by several additional input sources that do not feed it today. These include Arctic Ocean, Amu Darya river and the Black Sea and the Mediterranean water that reached the Caspian Sea via the Black Sea. The first clear evidence of separation of the Caspian from the Black Sea is ~1.15 Ma. However, a longer Black Sea record is required to test this. The first marine input in the Black Sea is observed

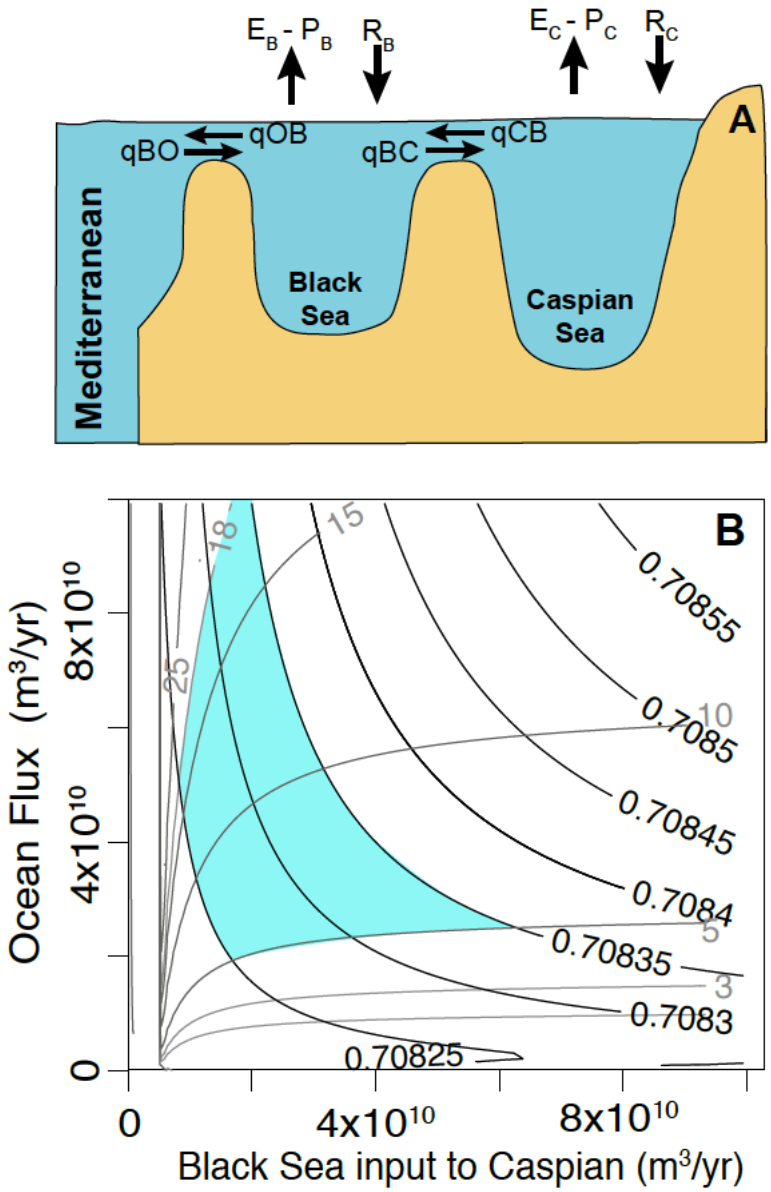

FIGURE 7.5: A) Schematic showing the connectivity configuration between the Mediterranean, Black and Caspian seas. B) Model generated contour lines for salinity (grey solid lines) and $^{87}Sr/^{86}Sr$ (black solid lines) in the Caspian Sea with varying Mediterranean input into the Black Sea and the Black Sea influx into the Caspian Sea. Amu Darya discharge is kept at 5 km^3/yr. Blue shaded area indicate the salinity and $^{87}Sr/^{86}Sr$ combination observed from Hajigabul section in three samples younger than 781 ka.

at 977 ka but this signal is not visible in the Caspian Sea because of low sampling resolution. There is clear evidence of Mediterranean influenced water reaching the Caspian Sea via the Black Sea between 650 to 250 ka, but the timing for these events are not well constrained. There is also evidence that, although Amu Darya continuously flowed into the Caspian Sea, its discharge was ~10% of the pre-irrigation flux between 250 to 650 ka.

Chapter 8

Synthesis and conclusions

This chapter brings together the key findings of this study in order to assess the two main goals outlined in Section 1.6.1 and 1.6.2. Here I summarize the results from Chapter 3, which evaluates the three-dimensional spatial distribution of Sr isotopic systems in the Black Sea and the Caspian Sea. The results discussed in Chapter 5, 6, and 7 together with existing $^{87}Sr/^{86}Sr$ based connectivity evidence from the Black Sea and the Caspian Sea (Section 1.5) are then synthesised to provide an overview of the Miocene to present-day connectivity history reconstruction between them and the open ocean. Finally this chapter outlines several remaining questions, which impact our understanding of the connectivity of the Pontocaspian region.

This chapter includes palaeontological analysis of ostracods collected from the Guria section, Georgia. This analysis, ostracod distribution chart and tentative age for the Gurian samples have been provided by **L. Rausch** (PRIDE ESR) and Prof. **M. Stoica**, University of Bucharest.

8.1 Modern Sr isotopic data across the Black and Caspian seas

By generating a much more substantial modern Sr isotopic data across the Black Sea and the Caspian Sea than previously had been available, it has been possible to evaluate existing assumptions about Sr isotopic behaviour and distribution in the marginal marine and endorheic systems. The $^{87}Sr/^{86}Sr$ of the water collected from offshore Black and Caspian seas shows values that are consistent spatially and with depth indicating that both basins are well mixed with respect to Sr isotopes. The $^{87}Sr/^{86}Sr$ isotopes closer to river mouths may be impacted by the fluvial discharge and can show values that deviate from the average basin ratio. This is because these marginal, semi-isolated systems are more sensitive to their water sources compared to the open ocean setting where the

oceanic $^{87}Sr/^{86}Sr$ can penetrate up estuaries.

This study also provides the first Sr isotopic measurements for the rivers draining along the eastern Black Sea, and two major northern Black Sea rivers (Don and Dnieper), and for the Aral Sea water as well as generates additional new measurements for the Kura and Volga rivers that drains into the Caspian Sea. The $^{87}Sr/^{86}Sr$ of the Aral Sea water, for the first time, constrains the Sr isotopic signal of the Amu Darya river water, which until now, has been the subject of speculation.

Modern ostracods collected from surface sediment were also analysed for their Sr isotopic ratios and the results were compared to the bottom water $^{87}Sr/^{86}Sr$ at the same location. These data suggest that bottom dwelling ostracods preserve the $^{87}Sr/^{86}Sr$ of the overlying water in a well mixed basin and therefore, can be used as a reliable archives for the past Sr isotopic ratio of the basin. Consequently, the Sr isotopic data for the modern system provides a framework in which we can interpret the past Sr isotopic records for the Black and Caspian seas and reconstruct the connectivity history between these two basins and the open ocean.

8.2 Connectivity history between the Black Sea, Caspian Sea and the open ocean

The Miocene to Quaternary evolution of the Black and Caspian seas is dominated by major changes in basin water levels driven by both the tectonics of the region, which controls the gateways between adjacent basins (Mediterranean Sea or Arctic Ocean) and by regional and global climate, which impacts the fluvial discharge to each system. Numerous scientific studies, using a variety of methods, have been dedicated to understanding the connectivity history of these basins over time (Section 1.5). However, palaeontology based reconstructions are typically low resolution and identify no clear boundaries between connection and isolation events. Phylogenetic studies also have large uncertainties associated with the timing of connection. Although geochemical studies provide a more direct approach for connectivity reconstruction, previously published geochemical data are fragmentary (see Chapter 1) and in places contradict palaeontological evidence of connectivity. This study generates several Pleistocene Sr isotopic records from the Black and Caspian seas, using fossil ostracods collected from (well) dated sedimentary successions (Chapters 5, 6, and 7). The data are combined with existing $^{87}Sr/^{86}Sr$ based connectivity evidence from the Black Sea and the Caspian Sea (Section 1.5.3) to provide a more longer and a more complete connectivity history between these basins and the open ocean since the Miocene (Figure 8.1). Given that the

ostracod assemblages of the Guria section in Georgia indicate a much older, Late Miocene age for the section compared to the published palaeomagnetic based Pleistocene age, this chapter also considers the implications of the Guria Sr record assuming it has a Late Miocene age.

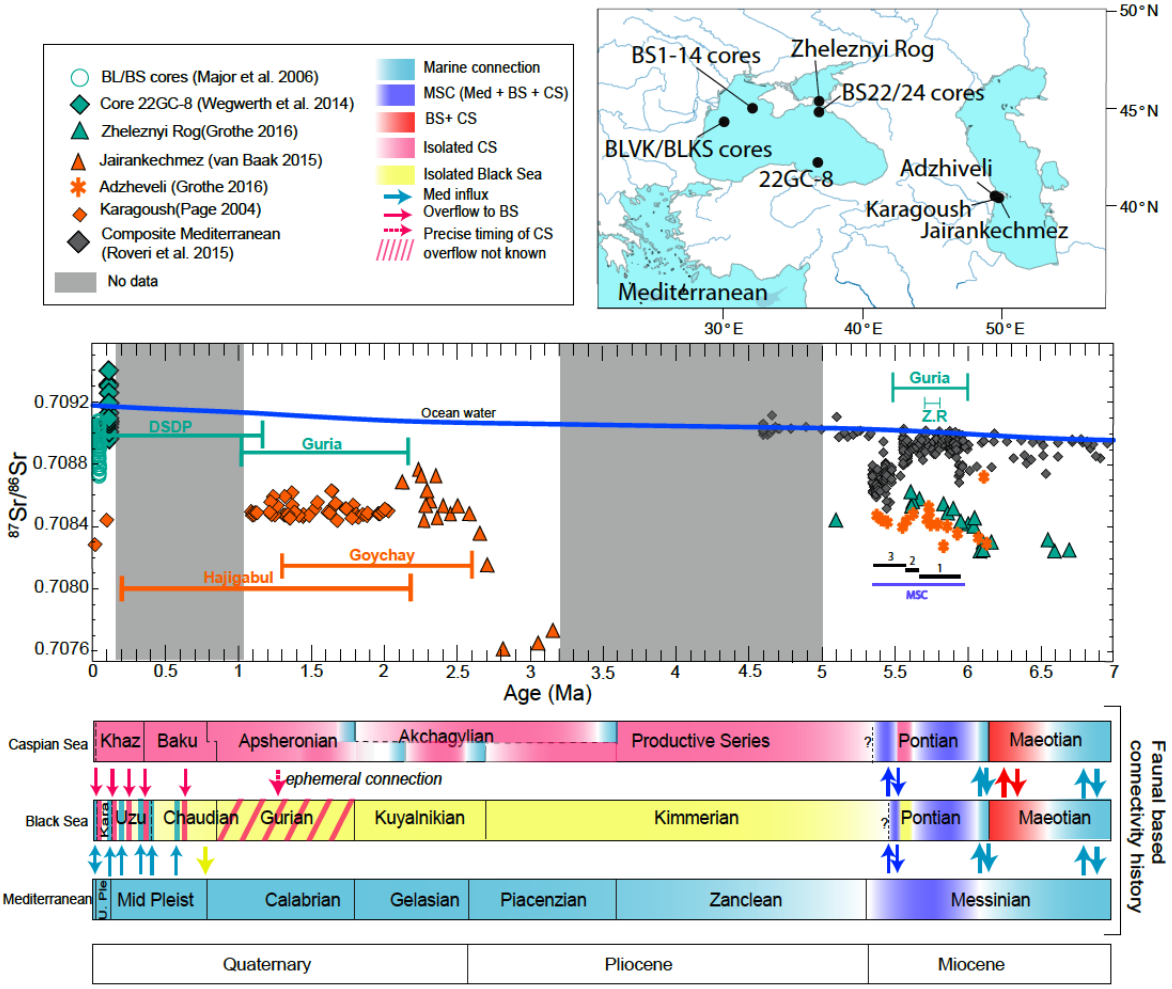

FIGURE 8.1: The previously published $^{87}Sr/^{86}Sr$ records from the Black Sea (green; Grothe, 2016), Caspian Sea (orange; Grothe, 2016; Page, 2004; van Baak et al., 2019) and Mediterranean Sea (grey; Flecker et al., 2015) over the last 7 Ma. The $^{87}Sr/^{86}Sr$ of the global ocean is shown as a blue line (McArthur et al., 2012). Grey area indicate intervals where there are no published $^{87}Sr/^{86}Sr$ data for Black and Caspian seas. Faunal based connectivity history during this period is shown with coloured arrows (Krijgsman et al., 2019; Popov et al., 2006). Colour and direction of the arrow of indicate the source water and direction of the input. Dashed arrows represent ephemeral connections between the Caspian Sea and the Black Sea without any precise timing. Labelled solid lines indicate the duration of the Pleistocene sections studied here to address Quaternary data gap. The Black Sea and the Caspian Sea regional stages are plotted against standard geological time scale (Krijgsman et al., 2019).

8.2.1 An alternative age for the Guria section and its implications for the Late Miocene connectivity history of the Pontocaspian region

The Guria section (Figure 8.4) is a composite of two sections; Khvarbeti section and Tsikhisperdi section (Section 2.2). The new ostracod assemblages from the Tsikhisperdi section show a moderately diverse oligohaline (salinity <5 g/kg) to mesohaline (5 – 15 g/kg) faunal assemblage (Figure 8.2). Within the lower part of the section (0.25 m - 3.45 m) the occurrence of *C. tocorjescui* (Figure 8.2) was first been described by Hanganu in1962 from the Pontian (Late Miocene) strata of the Dacian Basin (Central Paratethys). Since then, this species has been recognized by different authors in several places in Paratethys within the Pontian (Krstić, 1990; Olteanu, 1999a; Stoica et al., 2013) or Kimmerian (Vekua, 1975). The common ostracod species from the Tsikhisperdi are comparable to Pontian assemblages known from the Ramnicu Sarat and Badislava sections in the Dacian Basin (Floroiu et al., 2012; Stoica et al., 2013), the Zheleznyi Rog section on the Taman Peninsula of the Russian Black Sea margin and the Lago-Mare deposits from Cuevas del Almanzora section in the Vera Basin of the Spanish Mediterranean margin (Stoica et al., 2016).

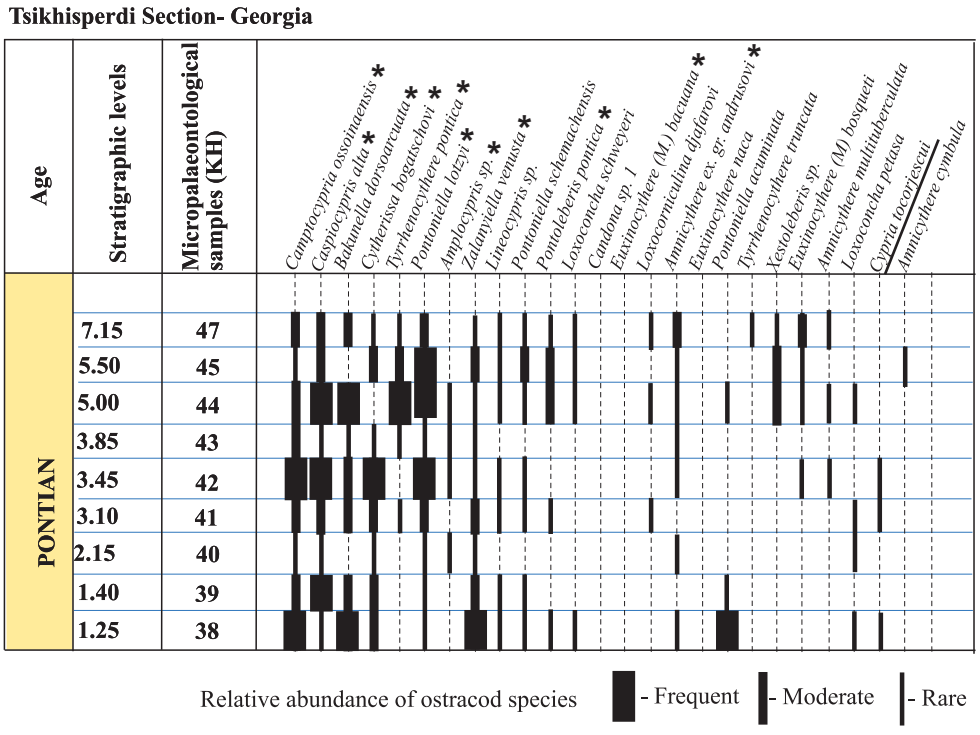

FIGURE 8.2: Ostracod distribution pattern from the Guria section (Tsikhisperdi section), Georgia. Common occurring species are indicated by asterisks.

Faunal assemblage from the Khvarbeti section resembles the fauna described in the Tsikhisperdi

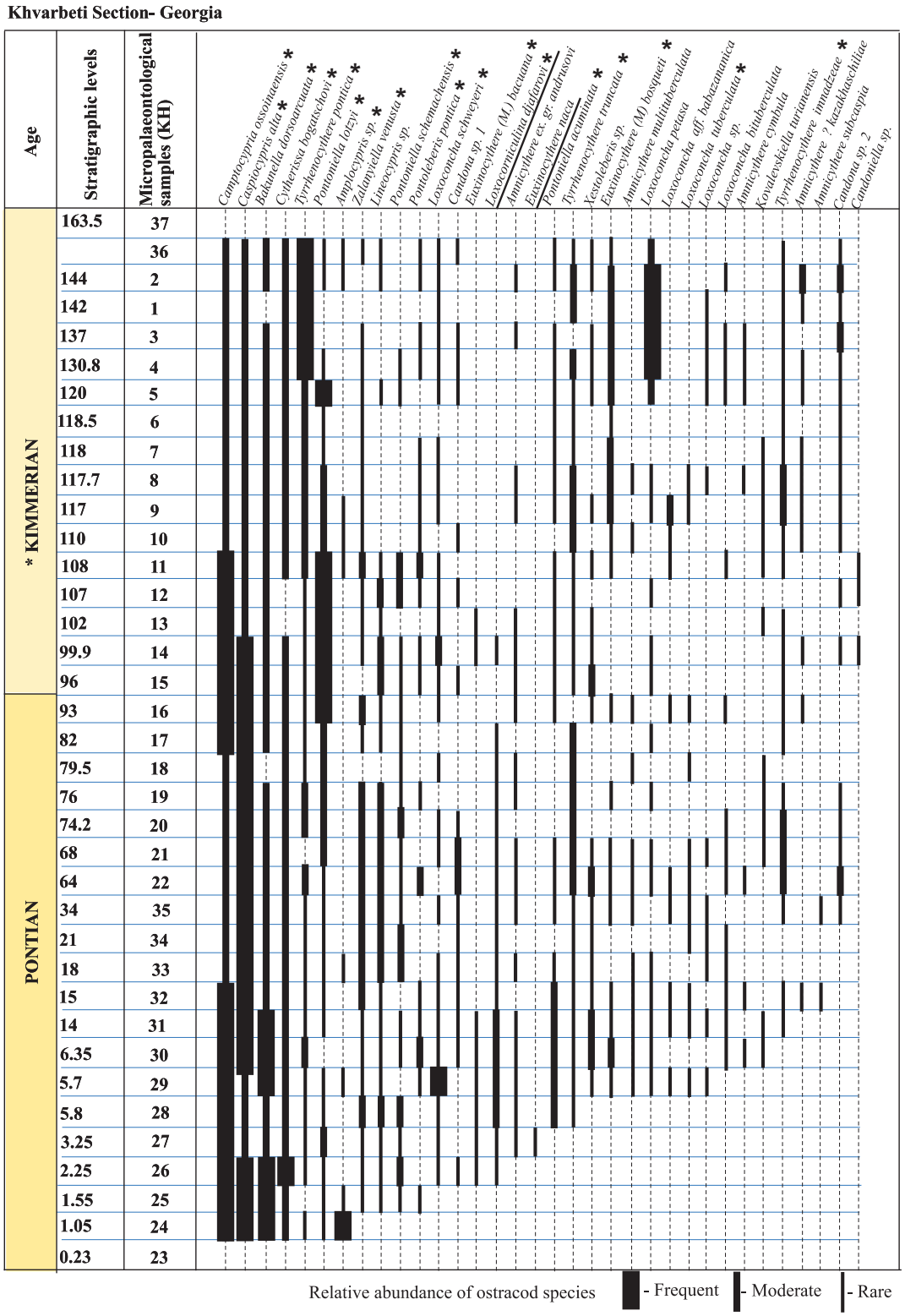

FIGURE 8.3: Ostracod distribution pattern from the Guria section (Khvarbeti section), Georgia. Common occurring species are indicated by asterisks. The base of the Kimmerian is uncertain (van Baak et al., 2017) in the Black Sea.

section but with a higher faunal diversity (Figure 8.3). These assemblages also indicate an oligo-to mesohaline environment (salinity between 5 to 15 g/kg). Within the lower part of the section *Loxocorniculina djaforovi* and *Euxinocythere naca* can be found (Figure 8.3), both of which are well-known from Upper Miocene deposits from the Pannonian Basin (Cziczer et al., 2009; Krstić, 1972; Olteanu, 1989; Sokac, 1989), the Dacian Basin, Black Sea and Caspian Sea (Agalarova, 1967; Agalarova et al., 1961; Olteanu, 1989, 1999b; Schneider, 1949; Vekua, 1975) as well as from the Lago-Mare successions around the Mediterranean (Cosentino et al., 2007; Stoica et al., 2016). As such, the species within the lower part of the section (approx. 80%) are indicative of a Pontian age, while the assemblages above 93 m are likely to be of Kimmerian age (Figure 8.3). Therefore, the ostracod assemblages from the Khvarbeti and Tsikhisperdi sections suggests a Pontian - early Kimmerian age (between 6.1 to ~5.3 Ma, Marius Stoica and Lea Rausch, *personal communication*).

In the light of the biostratigraphic constraints provided by ostracod assemblages, the palaeomagnetic polarity pattern of the Guria section was also revisited and is found to be also compatible with the GPTS for the Late Miocene (Wout Krijgsman, *personal communication*). Resolving the age contradiction between the new ostracod based age model and existing pollen based age model (Kirscher et al., 2017) is currently underway. Here, no assumptions were made regarding the likely age for the section and only the implications of the different ages on the Sr isotopic record from the Guria section were considered.

A Late Miocene age makes the Guria section coeval with the Black Sea Zheleznyi Rog section (Grothe, 2016). Consistently, the Sr isotopic records from the two sections show similar values (Figure 8.4, this study; Grothe, 2016). These values are also similar to the Caspian Sea Adzhiveli section between 5.5 and 6 Ma (Figure 8.4, Grothe, 2016) and suggests the Black Sea and the Caspian Sea were part of a single Pontocaspian basin during this time possibly with two way exchange between them.

Hiatuses in key sections from the Black Sea and the Caspian Sea results in problematic age models for these basins (e.g. Chang et al., 2014; Krijgsman et al., 2010; Popov et al., 2016; Radionova and Golovina, 2011; van Baak et al., 2016b). As such, correlation between the Black Sea data with the MSC substages (e.g. Stage 2 - acme interval, Stage 3 - PLG) is difficult. However, at the larger scale of the MSC, the $^{87}Sr/^{86}Sr$ isotopic data from the Mediterranean clearly shows a decreasing trend indicating its progressive isolation from the global ocean during the Stage 1 (Figure 8.4). The concurrent increase in the Pontocaspian $^{87}Sr/^{86}Sr$ may suggest an influence of the Mediterranean

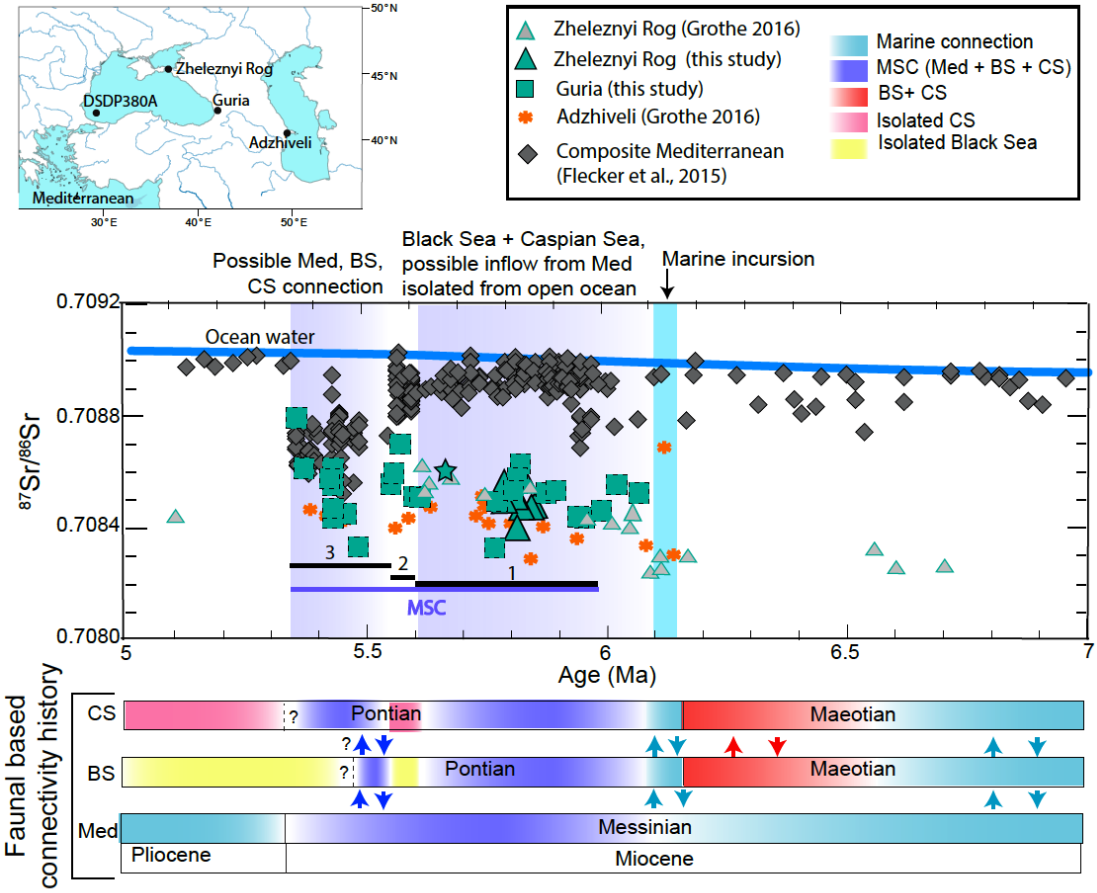

FIGURE 8.4: The Late Miocene $^{87}Sr/^{86}Sr$ record from the Black Sea (green; this study, Grothe, 2016), Caspian Sea (orange; Grothe, 2016) and Mediterranean Sea (grey; Flecker et al., 2015) along with coeval oceanic $^{87}Sr/^{86}Sr$ shown in blue line. The Black Sea and the Caspian Sea regional stages are plotted against standard geological time scale (Krijgsman et al., 2019). Note the uncertain upper boundary for the Pontian regional stage. Faunal based connectivity history during this period is shown by coloured arrows (Krijgsman et al., 2019). Colour and direction of the arrow of indicate the source water and direction of the input.

water into the Pontocaspian basin. The isolation of the Mediterranean Sea during the MSC acme interval (Stage 2) fits well with the observation of rising salinity in the basin (Roveri et al., 2014) but can be tentatively correlated to episodes of declining salinity in the Pontocaspian basin (van Baak, 2015; van Baak et al., 2016b). This suggests that there may not be a connection between the two at the time. Given that the Mediterranean has alternative fluvial sources of very low $^{87}Sr/^{86}Sr$, the decreasing $^{87}Sr/^{86}Sr$ values in the Mediterranean during the acme interval is independent of the Pontocaspian input.

Although the absolute age for the base of the Kimmerian in the Black Sea is not recognised, it has been suggested to be ~5.5 Ma (Krijgsman et al., 2010) based on regional stages correlation between the Black and the Dacian Basin (Central Paratethys). If this was the case, the top of the Khvarbeti section, which contains Kimmerian ostracod assemblages, is younger than 5.5 Ma

and may be tentatively correlated with the Lago Mare period (Stage 3) of the MSC. During this stage 3 interval, the $^{87}Sr/^{86}Sr$ from the Black Sea (Guria) and the Caspian Sea (Adzhiveli, Grothe, 2016) are similar to the Mediterranean $^{87}Sr/^{86}Sr$ values (Figure 8.4). In contrast to the stage 2, the occurrence of brackish – freshwater conditions in the Mediterranean Sea and evidence of faunal exchange between the Black Sea and the Mediterranean Sea (Cosentino et al., 2007; Londeix et al., 2007; Rouchy et al., 2001; Stoica et al., 2016) indicates that the Mediterranean, Black and Caspian seas were all connected during this period. Finally at the onset of the Pliocene, the Mediterranean Sr isotopic values adjust back to oceanic values indicating reconnection to the open ocean (Figure 8.4). One $^{87}Sr/^{86}Sr$ data from the Black Sea at ~5.1 Ma (Grothe, 2016) suggests that there was no input from the Mediterranean or the open ocean to the Black Sea (and possibly to the Caspian Sea) during this time presumably because the connection with the Mediterranean had been severed at some point at, or just after the Mio - Pliocene boundary. Faunal evidence also suggests no connection between the Black Sea and the Caspian Sea at this time (Nevesskaya et al., 2003; Popov et al., 2006).

A review of all Sr isotopic data from the Black Sea over the past 7 million years shows that $^{87}Sr/^{86}Sr$ from the Guria section has reoccurred more than once since the Late Miocene (Figure 8.5). Most of the Guria $^{87}Sr/^{86}Sr$ ranges between 0.7084 and 0.7085 and these values reappear at about ~1 Ma in the DSDP core 379A, in the DSDP 380A (age somewhere between 1.8 and 4.2 Ma) and again in the Zheleznyi Rog section between 6 and 5 Ma (Figure 8.5). Therefore, despite the age uncertainty surrounding the Guria section, these reoccurring values may suggest that the Black Sea had a persistent $^{87}Sr/^{86}Sr$ value resulting from enduring supply of river water from their sources throughout the early Pleistocene. Although this requires empirical testing, if this was the case, model results suggest that this $^{87}Sr/^{86}Sr$ value can be produced in the Black Sea if the basin was isolated from the Mediterranean but received an input from the Caspian Sea (Figure 6.4). The similarity of the Black Sea $^{87}Sr/^{86}Sr$ with the Caspian Sr isotopic values from the Miocene Adzheveli section (Grothe, 2016), Early Pleistocene Karagoush section (Page, 2004) and Hajigabul section (Chapter 7) also suggests that the Black Sea may have been connected to the Caspian Sea, but was isolated from the Mediterranean Sea during this time.

8.2.2 Pliocene connectivity history

No geochemical data are available for the Black and Caspian seas for the Pliocene (Figure 8.1). Sedimentological (Section 1.3) and palaeontological (Section 1.5.1) evidence suggests a prolonged

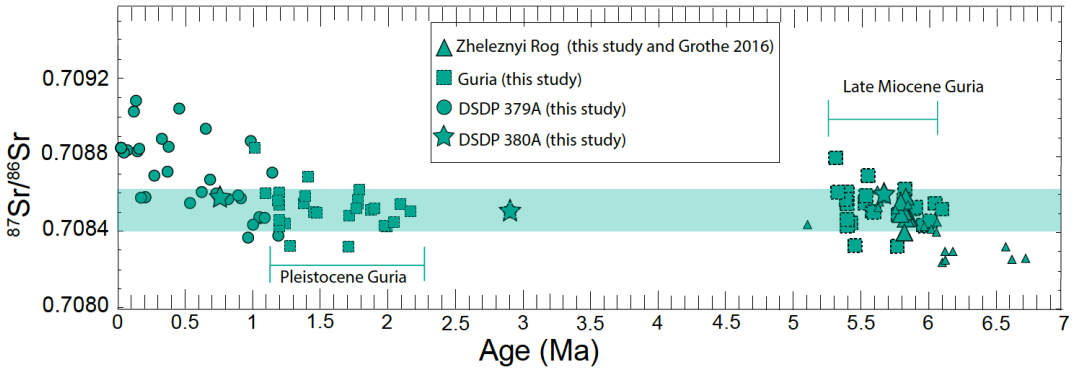

FIGURE 8.5: The Black Sea Sr isotopic record over the last 7 Ma with Guria $^{87}Sr/^{86}Sr$ plotted according to both Pleistocene and Late Miocene age model. The green shaded bar highlights the range of $^{87}Sr/^{86}Sr$ that consistency reoccurs between Late Miocene and early Pleistocene.

isolation of the Black Sea and the Caspian Sea from each other and the open ocean. This has yet to be tested with the Sr isotopic data.

8.2.3 Pleistocene connectivity history

The Caspian connection to the Arctic Ocean at the Plio - Pleistocene boundary resulted in a rapid rise in the $^{87}Sr/^{86}Sr$ of the Caspian Sea, which may have contributed to the dramatic increase in the Caspian surface area (van Baak et al., 2019). The timing of this northern connection to the Arctic Ocean is broadly consistent with the phylogenetic studies of Caspian Seals (Árnason et al., 1995, 2006; Dooh et al., 2006; Palo and Väinölä, 2006), and the crustacean *Mysis* (Väinölä, 1995; Väinölä et al., 2001) both of which, suggest an early Pleistocene connection resulting in the transfer of Arctic taxa to the Caspian Sea. New data from this study suggests that the Arctic connection lasted longer than previously thought (van Baak et al., 2019), spanning the interval from 2 .7 Ma to ~1.96 Ma (Chapter 5). Although there are no coeval data from the Black Sea during this period of Caspian-Arctic connection, the $^{87}Sr/^{86}Sr$ of the Black Sea may have had a $^{87}Sr/^{86}Sr$ within the range of 0.7084 and 0.7086 (Figure 8.5 and Section 8.2.1), which can be achieved with an additional Caspian inflow. If this was the case, both one way flow from the Caspian Sea into the Black Sea or a two way exchange between the two basins is possible and can explain the Caspian $^{87}Sr/^{86}Sr$ data. Existing (Karagoush section, Page, 2004) as well as new (Hajigabul section, Chapter 7) data from the Caspian Sea and from the Black Sea (Pleistocene Guria section, Chapter 5, older samples from DSDP 379A, Chapter 6) show overlapping $^{87}Sr/^{86}Sr$ values indicating a prolonged connection between the two basins but isolated from the open ocean through most of the early Pleistocene until ~1 Ma. Considering the higher salinity conditions (>5

g/kg) in the Caspian Sea during this time (Chapter 7), two way exchange between the two basins is a more feasible mechanism to maintain the Caspian salinity, after the severance of marine inflow from the Arctic Ocean (Chapter 7), instead of a one way flow which removes salt from the Caspian Sea resulting in a declining salinity.

An enduring connection between the Black Sea and the Caspian Sea however, contradicts the palaeontological data, which suggests that the Caspian Sea Akchagylian (early Pleistocene) molluscs extended only as far as the Sea of Azov and not into the Black Sea basin during the Kuyalnikian (Danukalova, 1996; Nevesskaya et al., 1986). Similarly, mollusc assemblages suggest only ephemeral connections between the Apsheronian Caspian Sea and Gurian Black Sea (Nevesskaya, 2007), while the geochemical data suggest a enduring connection between the two basins. A more detailed comparison between the faunal and geochemical is currently not possible as the timing of these faunal events are not provided. However, a general incompatibility between faunal and geochemical evidence of connectivity can arise due to evolutionary lag experienced by biota. Once the connection is established, faunal ecosystems require time to adapt and evolve in new environmental conditions (Fleitmann et al., 2009) and as such, the evolution of fauna is not always synchronous with the timing of the connection. Therefore, although faunal assemblages of the two basins are not accurate or direct proxy for reconstructing connectivity history, these data together with the geochemical evidence of the connection can be used to evaluate the evolutionary rate of the fauna within a basin.

The $^{87}Sr/^{86}Sr$ record of the Black Sea and the Caspian Sea show progressive divergence from each other after about 1 Ma (Figure 8.6). The first isolation of the Black Sea from the Caspian Sea is observed at ~1.1 Ma and this is followed by progressively more isolation events during the last ~500 ka. Similarly, the first Mediterranean and Black Sea connection is observed at 1 Ma (Figure 8.6) with more frequent Black Sea - Mediterranean connection after 500 ka. Although, the Black Sea was progressively more connected to the Mediterranean over the last 1 Ma, the connection with the Caspian Sea was still active until ~150 ka, which marks the last influence of the Caspian water on the $^{87}Sr/^{86}Sr$ values of the Black Sea (Figure 8.6). Consequently, the last 1 Ma of the Black Sea and the Caspian Sea record shows the most dynamic connectivity history in the region with the Black Sea connection to the Mediterranean Sea, or to the Caspian Sea or to both with intervals of isolation from both (Figure 8.6). The Black Sea - Mediterranean connection, when it exists, is likely to always permit two way exchange, unless changes in climatic conditions resulted in a negative Black Sea hydrological budget and a resulting drop in the Black Sea water level below

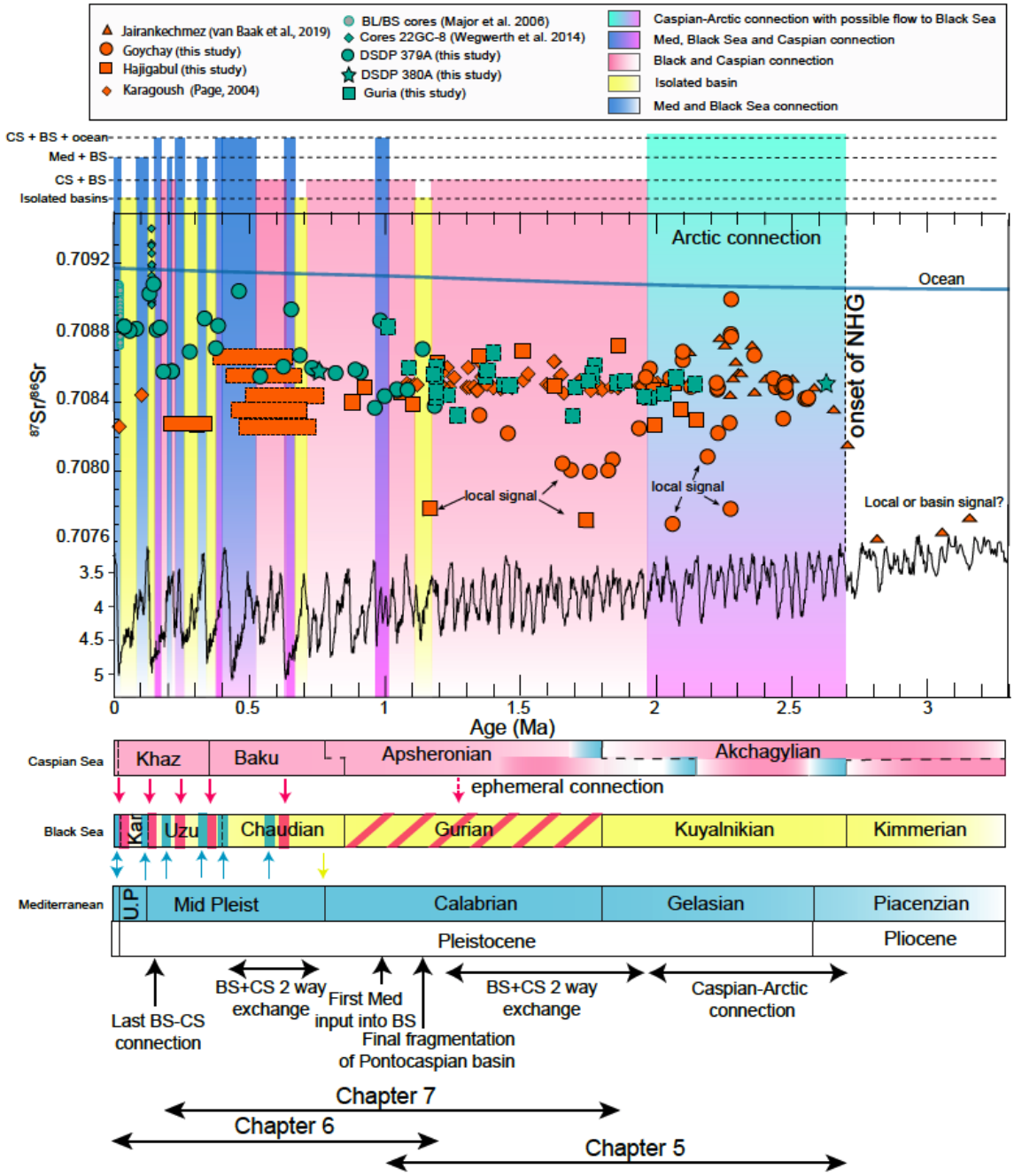

FIGURE 8.6: The Pleistocene connectivity history between the Black Sea, Caspian Sea and the open ocean based on the $^{87}Sr/^{86}Sr$ record from the Black Sea (green data; this study) and the Caspian Sea (orange data; this study, Page, 2004; van Baak et al., 2019) along with coeval oceanic $^{87}Sr/^{86}Sr$ shown in blue line. Colour shaded area reflects the timing of the connectivity and isolation events. The Black Sea and the Caspian Sea regional stages are plotted against standard geological time scale (Krijgsman et al., 2019). Faunal based connectivity history during this period is shown by coloured arrows. Colour and direction of the arrow indicate the source water and direction of the input. Key connectivity events are highlighted at the bottom of the figure.

the Bosporus sill height during these periods.

Faunal evidence of the connectivity history over the last 500 ka suggests overflow events from

the Caspian Sea into the Black Sea via Manych strait occurred during glacial periods as the Caspian water level rose due to increased fluvial discharge fed by glacial melt water (Popov, 1983; Yanina, 2014). Additionally, Mediterranean incursions to the Black Sea due to eustatic sea level rise was suggested during interglacial periods (Hoyle, 2019; Krijgsman et al., 2019). Although, faunal evidence agrees with the $^{87}Sr/^{86}Sr$ record of Mediterranean-Black Sea connection during interglacials, it does not fully agree with the Black Sea and the Caspian connection only during glacial periods (Figure 8.6). In addition to the Mediterranean, the $^{87}Sr/^{86}Sr$ record shows that the Black Sea was also connected to the Caspian Sea during interglacial MIS 7 (~200 ka) and the later part of MIS 11 (~380 ka). Given the dominant Mediterranean signal, the ecological conditions in the Black Sea were likely to have been more similar to that of the Mediterranean Sea and as such, organisms from the Mediterranean Sea survived while those from the Caspian Sea are unlikely to have been able to tolerate the higher salinity conditions during these periods. However, it should be noted that neither faunal nor geochemical data over the last 500 ka have sufficient resolution to study this disagreement in detail.

The long term connectivity history between the Black Sea, Caspian Sea and the open ocean show that both, climate and tectonics control the gateways connecting these basins, particularly prior to 500 ka. Climate variation during the glacial - interglacial cycles over the last 500 ka was the dominant driver for the Black Sea, Mediterranean connectivity, while the connection between Black Sea and the Caspian Sea is likely to have been a combination of climate as well as tectonics. The $^{87}Sr/^{86}Sr$ from the Black Sea shows large variability indicating rapid and frequent changes in the hydrological budget over the last 500 ka. As such, to disentangle the impact of high amplitude glacial - interglacial cyclicity on the connectivity history of the Pontocaspian basin over the last 500 ka, a much higher resolution study is required.

8.3 Answering the research questions

1. **Is the strontium isotopic signal in the Black and Caspian seas spatially homogeneous?**
   Although the existing Sr isotopic dataset has been greatly expanded during this study, sample coverage is still not complete. However, these data suggest that the spatial distribution of the $^{87}Sr/^{86}Sr$ across the Black Sea and the Caspian Sea is largely homogeneous with respect to Sr isotopic ratio. However, the $^{87}Sr/^{86}Sr$ values near the river mouth and along the beaches can be impacted by the local fluvial signal. This suggests that brackish marginal basin or

endorheic basins are more sensitive to fluvial input than the marine system. The $^{87}Sr/^{86}Sr$ of the fluvial sources of the Black Sea and the Caspian Sea vary substantially. As such, caution should be applied when interpreting the $^{87}Sr/^{86}Sr$ data collected from the site with potential fluvial dominance.

2. **Does the strontium isotopic signal in the Black and Caspian seas vary with water depth? What influence does the density stratification have on Sr isotopic variability in the water column?**

   The $^{87}Sr/^{86}Sr$ of the deeper water collected from the Black Sea is consistent with the surface water indicating a well mixed signal even at location with bottom water anoxia. However, only two stations with anoxic deep water were sampled during this study. Although these values indicate a homogeneous Black Sea, a more detailed study with more sampling sites within the anoxic Black Sea is required. Similarly, a lack of deep water samples from the Caspian Sea hinders in the interpretation of conservative behaviour of $^{87}Sr/^{86}Sr$ in the Caspian Sea. However, the limited measurements from this study and by Clauer et al. (2008) show that the Caspian Sea is also relatively well mixed with depth, particularly considering the influence of the Volga river in the north. However, again a more thorough study of Sr isotopic behaviours in both basins is essential.

3. **Are fossil ostracods a robust archive for preserving the primary $^{87}Sr/^{86}Sr$ of ambient water in the Black and Caspian seas?**

   The $^{87}Sr/^{86}Sr$ measured on the modern ostracods are commonly within error of the bottom water at the same location without any species-specific variation. This suggests that ostracods can preserve primary Sr signal of the ambient water and can be used as a good archive to examine the past basin environment, providing they are well preserved without any post mortem diagenetic alteration.

4. **Does the geochemical system suggest a Caspian connection to the Arctic Ocean and if so, when did this connection occur?**

   The potential gateway for the marine input into the Caspian Sea during the early Pleistocene has been a much debated topic (Ali-zadeh and Aliyeva, 2016; Krijgsman et al., 2019; Popov et al., 2006). There are two potential directions of marine connection between the Caspian Sea

and the global oceans have been proposed previously; from the west (via the Mediterranean and Black Sea) and from the north (Arctic Ocean). The Black Sea $^{87}Sr/^{86}Sr$ from the Guria section (if it is of the Pleistocene age) indicate little or no Mediterranean-Black Sea exchange at the time, thus eliminating the marine input into the Caspian Sea from the Mediterranean via the Black Sea. Consistent with the phylogenetic studies (e.g., Árnason et al., 1995, 2006; Palo and Väinölä, 2006; Väinölä, 1995) and studies by Richards et al. (2018) and van Baak et al. (2019), the $^{87}Sr/^{86}Sr$ of the Caspian Sea supports a northern marine connection between the Caspian Sea and the Arctic Ocean (Chapter 5 and Figure 8.7).

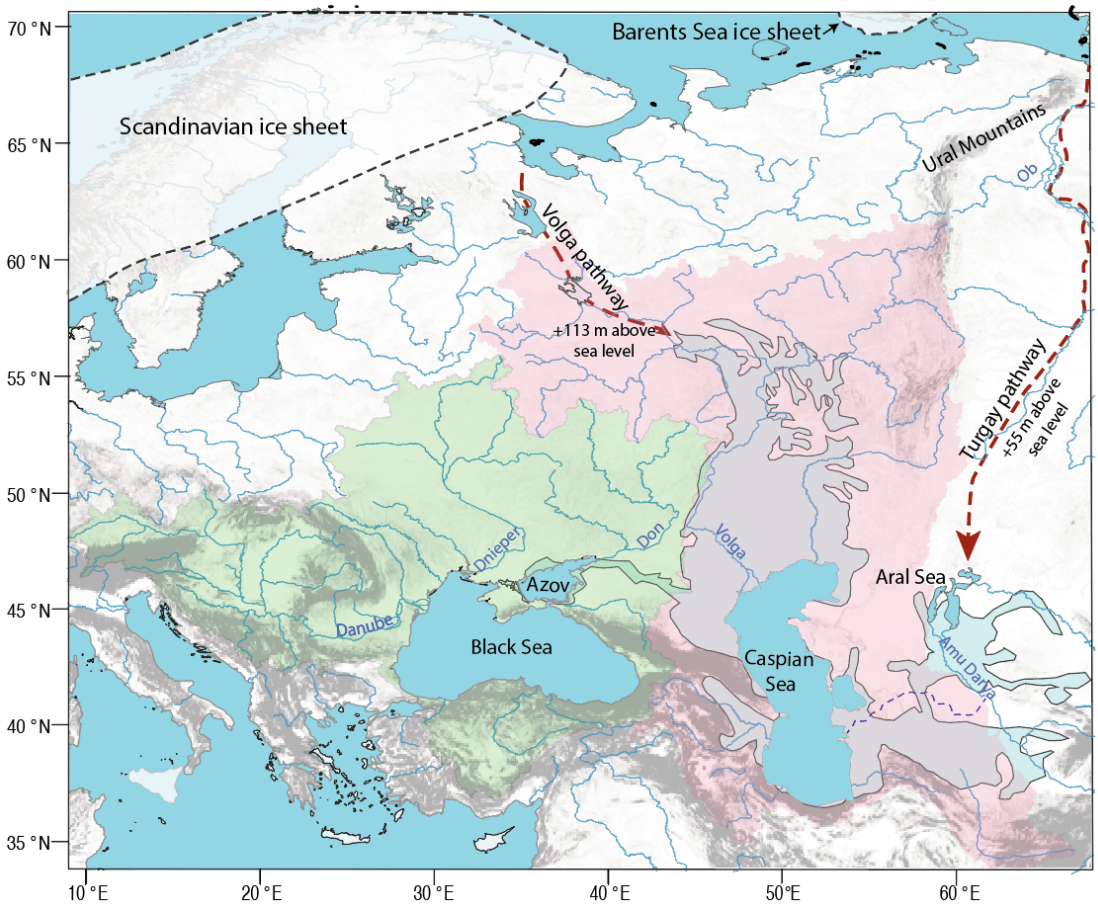

FIGURE 8.7: Paleogeographic map of the Black Sea and the Caspian Sea during the early Pleistocene. The current drainage area for the Black Sea is shown in pale green and for the Caspian Sea is shown in pale red. Pale blue area shows the extent of the Caspian Sea during the Akchagylian period (modified from Vinogradov, 1967). Dotted blue lines indicate former course of the Amu Darya. Red dashed arrows indicate possible pathway for the Caspian-Arctic connection with the minimum present-day elevation which needs to be crossed for marine water to enter the Caspian drainage. The shaded area with dashed black lines indicate the likely extent of the Scandinavian and Barents ice sheets during the early Pleistocene.

van Baak et al. (2019) suggested that this Caspian-Arctic connection was formed due to isostatic loading and started at the onset of the Northern Hemisphere Glaciation at ~2.7

Ma. The result from this study shows that the connection lasted until ~1.96 Ma, longer than previously assumed and that the Caspian Sea also sustained a connection to the Black Sea during the time (Chapter 5). The pathway for Caspian-Arctic connection, however, is still unknown. Two possible options have been previously proposed (Richards et al., 2018). The first possible pathway is via the Volga river as the ocean water reaches the Volga catchment area, which extends northwards to 60°N (Figure 8.7). Although, the current topographic height of the upper Volga region is about 113 m above global sea level, this is the shortest route for the Arctic marine water to reach the Caspian Sea. The second potential pathway for the marine water into the Caspian Sea is via the Ob river, east of the Ural Mountains and into the Aral Sea, which during the early Pleistocene was part of the Caspian Sea (Figure 8.7). This pathway provides the lowest water divide between the West Siberian Plain and the Aral Sea at only 50 m above global sea level (Astakhov, 2006) and may be more plausible as it follows the Turgay pass that traces a former gateway connecting the Arctic Ocean and the Tethyan Ocean during the Paleogene (Akhmetiev et al., 2012).

5. **How did the Sr isotopic ratio evolve in the Black and Caspian seas over the last 3 million years and what is its implication for the Quaternary connectivity history of the two basins to each other and the open ocean.**

   The $^{87}Sr/^{86}Sr$ record from the Caspian Sea over the last 3 Ma shows that the $^{87}Sr/^{86}Sr$ values in this basin was always higher than the present-day $^{87}Sr/^{86}Sr$ value suggesting additional radiogenic water fed the Caspian Sea in the past. Larger variability observed in the Caspian Sea prior to 2 Ma suggests multiple water sources from Arctic ocean, Black Sea and the Amu Darya river, while the Caspian Sea shows a much narrower range in the $^{87}Sr/^{86}Sr$ values after 2 Ma. This range is similar to the coeval Black Sea $^{87}Sr/^{86}Sr$ values implying an enduring connection between the two basins with possibly an additional fluvial discharge from the Amu Darya river into the Caspian Sea.

   The $^{87}Sr/^{86}Sr$ record from the Black Sea however, shows an opposing trend. The $^{87}Sr/^{86}Sr$ is consistent until ~1 Ma, implying that, in addition to the fluvial sources, the Black Sea only received additional water from the Caspian Sea prior to 1 Ma. However, the Black Sea $^{87}Sr/^{86}Sr$ record shows a larger variability and moves towards increasing ratios over the last 1 Ma suggesting more frequent connections with the Mediterranean Sea with intervals of isolation from both, the Mediterranean and the Caspian Sea.

6. **What was the nature of connection (one way flow or two way exchange) between the Black Sea, Caspian Sea and the open ocean during the Pleistocene?**

   The Caspian connection to the Arctic Ocean is likely to have been a one way flow from the ocean into the basin. Between 2.7 Ma to ~2 Ma, the Caspian possibly may have overspilled into the Black Sea (Figure 8.7). However between 2 Ma to ~1 Ma the Black Sea and the Caspian Sea, when connected, probably experienced a two way exchange between them (Figure 8.8). The resolution of the data in this study however is not sufficient to tease apart the nature of the Black Sea and Caspian connection over the last 1 Ma. A two way exchange existed between Mediterranean and the Black Sea over the last 500 ka. The Black Sea may have overflowed into the Marmara Sea during eustatic low stands during this period. However, determining these outflow events is outside the scope of this study and requires a Pleistocene $^{87}Sr/^{86}Sr$ record from the Marmara Sea.

7. **Does the geochemical evidence of the connectivity between the Black Sea, Caspian Sea and the open ocean match the faunal evidence?**

   Geochemical evidence of Mediterranean - Black Sea connection during interglacials over the last 500 ka is consistent with the faunal evidence. However, geochemical record provides more details regarding the connectivity history of the Black Sea, Caspian Sea and the open ocean than previous faunal based connectivity reconstruction. Although, differing in some aspects, these data compliment each other and can therefore be used to evaluate faunal evolutionary response to the basin connectivity.

8.4 Limitations and outstanding issues

The Sr isotopic record from the Black and Caspian Sea generated in this study is the first complete record from both basins for the Pleistocene. This study also provides quantitative constraints on the timing and nature of connectivity and isolation events and helps to disentangle the role of climatic and tectonic drivers on the connectivity between the Black Sea, Caspian Sea and the open ocean. However, some outstanding issues still remain and require further investigation to get a continuous long-term connectivity history of the region. A few issues and unanswered questions are listed below.

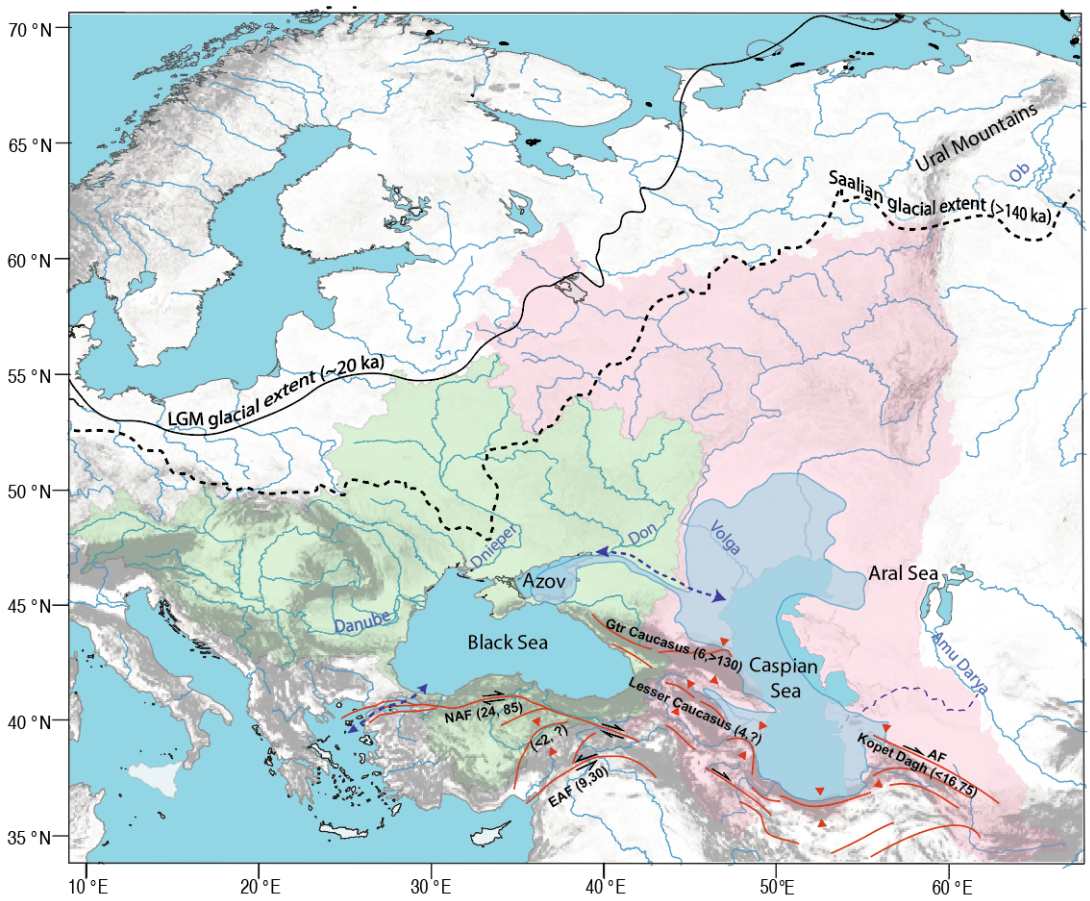

FIGURE 8.8: Map of the Black Sea and the Caspian Sea with current drainage area for the Black Sea shown in pale green and for the Caspian Sea shown in pale red. Pale blue area represent the palaeogeographic extent of the Caspian Sea during the Apsheronian period (modified from Krijgsman et al., 2019). Blue dashed arrows indicate possible pathways for the Mediterranean, Black Sea and the Caspian Sea connection during the Pleistocene. Solid black line shows the extent of ice sheet during the last glacial maximum (~20 ka) and dashed black line shows the extent of ice sheet during the Late Saalian (~160 – 140 ka; Svendsen et al., 2004). Red lines indicate active faults in the region with numbers in brackets showing the present shortening or slip rate in mm/yr, followed by finite shortening or strike-slip in kilometres (Allen et al., 2004). Abbreviation are as follows: North Anatolian Fault (NAF), East Anatolian Fault (EAF), Ashgabat Fault (AF).

1. The most pressing issue regarding the reconstruction of the connectivity history in the Black Sea and the Caspian Sea is the lack of robust age models. As already discussed earlier and shown by contradictory age estimates for the Guria section, the Black and Caspian Sea region suffers from the serious lack of independent absolute dated age models for the sections and as such, cross correlation of regional stages with each other and to the standard geological time scale remains difficult and uncertain. While significant progress has been made recently (Krijgsman et al., 2019, and references therein), stratigraphic and geochronologic data for the Caspian Sea and the Black Sea still consist of large uncertainties.
2. The $^{87}Sr/^{86}Sr$ measured on the Aral Sea water samples was used to constrain the Sr isotopic

ratio of the Amu Darya river in this study. However, the actual $^{87}Sr/^{86}Sr$ of the Amu Darya water may be higher than 0.709214 (Chapter 3). This is because, although the Aral Sea water is dominated by the input from the Amu Darya river, there is an additional source of Sr into the basin via the groundwater discharge. The average Sr concentration of groundwater discharge in the Aral Sea region is significantly higher (~18 ppm) than that of the Amu Darya river water (1.42 ppm, Schettler et al., 2013). Although no $^{87}Sr/^{86}Sr$ values are available for Aral Sea groundwater, it is likely to be lower, given that this water interact with the underlying sedimentary rocks which are mostly formed of Mesozoic carbonate. Consequently, the measured $^{87}Sr/^{86}Sr$ of the Aral Sea water is likely to provide a lower limit of the constraint on the Sr isotopic ratio of the Amu Darya river water.

3. The numerical box model used in this study captures the main features of the hydrologic budget in the Black Sea and the Caspian Sea and constrains the inter-basin exchange required to reproduce the observed $^{87}Sr/^{86}Sr$ and salinity during the Pleistocene. However, the model is performed in a steady state scenario and therefore, is only able to capture a snapshot of an event when the volume of the water within the basin remains constant. A transient model, with changing water budget and as such, changing sea level (water volume) is required to investigate the connectivity history between these basins. Additionally, because of the lack of palaeo data, the model used in this study assumes present-day values for evaporation and precipitation over the basins, and the Sr signal (Sr concentration and Sr isotopic ratios) for rivers. Given that these parameters are likely to have fluctuated in the past over glacial-interglacial timescales, using present-day values in the model only provides a first order approximation of the past hydrological budget of the Black Sea and the Caspian Sea.
4. The sedimentological evidence suggests a dramatic sea level drop in the Caspian Sea and isolation of the Black and Caspian Sea during the Pliocene. However, the entire period between 3 to 5 Ma lack any geochemical data. This is because regressive stages are prone to erosion and consequently, there are no onshore sedimentary successions representing this period in the region. Deep sea cores from the regions are also hard to come by. Although there are possibilities of using industrial wells to retrieve the Pliocene record, these also bear the problem of drilling contaminations for any geochemical analysis (Meilijson et al., 2019). Consequently, our understanding of this regressive stage in the Black and Caspian Sea remains elusive.

5. The isostatic loading by the Northern Hemisphere Glaciation at the Plio- Pleistocene boundary have been suggested by van Baak et al. (2019) as the driver for the connection between the Caspian Sea and the Arctic Ocean. Logically, the Pleistocene glaciation which shows increasingly more intense glaciations as suggested by larger amplitude benthic oxygen isotopic record (Lisiecki and Raymo, 2005) during the Pleistocene, should have reestablished the Caspian connection to the Arctic ocean in the north. However, Sr isotopic records from the Caspian sea during the Pleistocene do not suggest a direct marine connection. The question therefore remains, why was the Caspian-Arctic gateway not impacted by the Pleistocene glaciations? One explanation is that the post-glacial rebound may have increased the height of the Caspian - Arctic gateway. Alternatively, there may have been an additional drivers that controlled the connection between the Caspian Sea and the Arctic Ocean during Plio-Pliestocene boundary. However, the current available record is not sufficient to answer this assumption.

8.5 Recommendations for future work

8.5.1 Young sedimentary archive

Besides the recovery of Quaternary sediments from deep sea sediment cores, young sedimentary archives in the Caspian can be found in few places on land as a result of rapid uplift of the mountains in the area. Early to mid Pleistocene sedimentary deposits are found mainly within the Kura basin, located to the south-east of the Great Caucasus (Figure 8.9). The Kura depression facilitated sedimentary deposition while the active orogeny and uplift of the Caucasus have resulted in the exposure of these deposits, especially along the Kura Thrust Fold Belt (KTFB; Figure 8.9). Consequently, continuous exposure of the Pleistocene sedimentary record can be found in Azerbaijan dating up-to about 200 ka (Lazarev et al., 2019). Exposure of Pleistocene deposits can also be found north of the Greater Caucasus, in Dagestan (Arslanov et al., 2016; Yanina, 2013; Yanina and Svitoch, 1990). However, sampling these deposits is difficult because of the unstable political condition in the country. In the south eastern Caspian region, uplift of the Kopet Dag (Figure 8.9) has resulted in the exposure of Quaternary sedimentary deposits in Turkmenistan (Torres, 2007). Like Dagestan, political instability makes sampling in the area difficult. Mid to late Pleistocene sedimentary deposits for the Caspian Sea can be found in southern Russia along the Volga river (Arslanov et al., 2016; Yanina, 2012). By contrast with the tectonic driver

for exposure elsewhere, this is because the Volga river erodes and exposes the young sediments deposited on the north Caspian lowland during Caspian highstands. However, the exposed sections are not continuous and as such there is much debate regarding the stratigraphy of the northern Caspian region and the number of transgression and regression stages that characterise the mid - late Pleistocene period (e.g., Krijgsman et al., 2019; Yanina, 2012; Yanina, 2013; Yanko-Hombach et al., 2014; Yanko-Hombach et al., 2013).

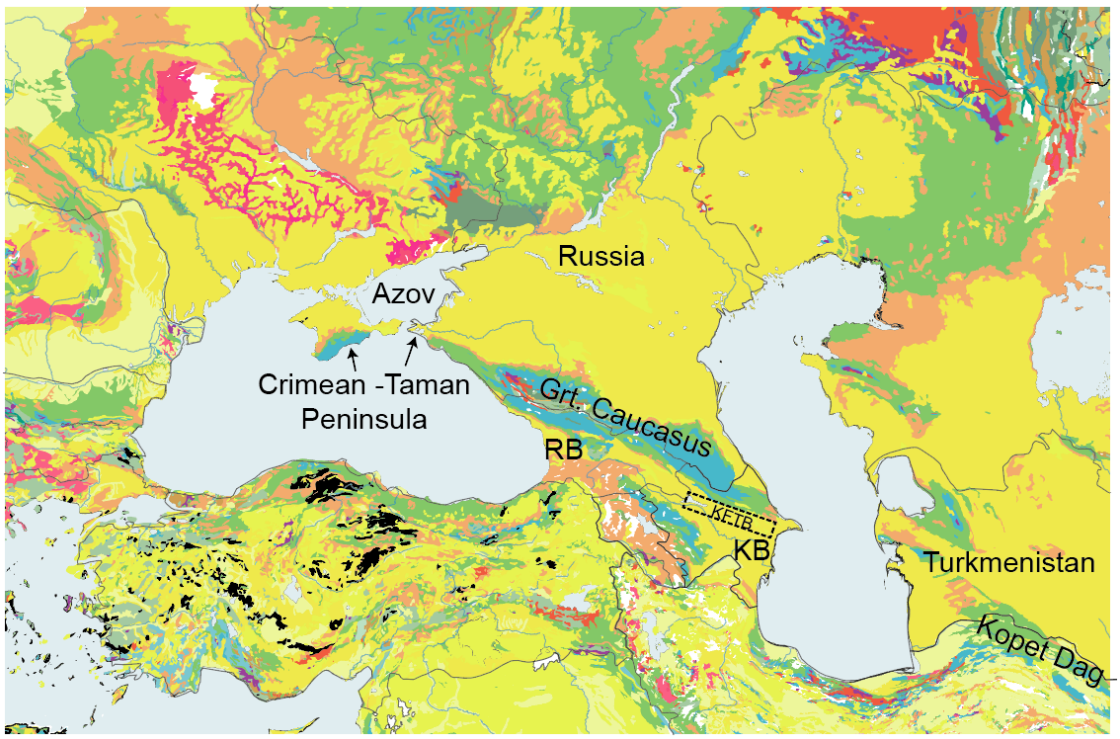

FIGURE 8.9: Geological map of the Black Sea and the Caspian Sea. Colours represent the geological age of the deposits; Purple (Triassic); Jurassic (Blue); Cretaceous (green), Paleogene (orange), Neogene - Quaternary (yellow), magmatic, volcanic rocks (red and reddish-blue). Map based on the Based on USGS world geological maps (*https://certmapper.cr.usgs.gov/data/apps/world-maps/*). Area enclosed by dotted rectangle shows the Kura Fold Thrust Belt (KFTB). Abbreviation are as follows: Rioni basin(RB), Kura basin (KB).

Terrestrial exposure of Pleistocene sediment in the Black Sea region is much harder to come by. This is because subaerial exposure of Pleistocene deposits by active orogeny is limited to the Azov-Kuban region and Rioni basin (Figure 8.9). The Taman and Crimean peninsulas, which are at the north western tip of the Greater Caucasus and connects the Black Sea with the Sea of Azov, are plausible locations for younger Black Sea sedimentary archives (Chepalyga et al., 1989; Saintot and Angelier, 2000; Tesakov et al., 2007). Similarly, uplift of the Caucasus has resulted in the exposure of Pliocene and Pleistocene sedimentary deposits of the Rioni depression in western Georgia (Adamia et al., 2010; Molostovsky, 1997). The Guria section (Chapter 5) is one of the

Black Sea Pleistocene exposures. However, recently the age of this section has been brought into question (Section 8.2.1).

8.5.2 Constraints on anthropogenic inputs

In semi-isolated and isolated basins like the Black and Caspian seas, a significant portion of the water comes from continental runoff. Measuring the correct $^{87}Sr/^{86}Sr$ of the river water is therefore, essential to understanding the hydrological system of these basins. One of the issues of generating strontium isotopic ratios of the modern river water is the potential influence of anthropogenic sources such as fertilisers and sewage on the $^{87}Sr/^{86}Sr$ values (e.g. Hosono et al., 2007; Nakano et al., 2005; Pearce et al., 2015; Vitòria et al., 2004; Widory et al., 2004). As such, river water influenced by anthropogenic sources can significantly modify the $^{87}Sr/^{86}Sr$ of the basin, resulting in potential biases when estimating modern as well as past input sources into these basins.
A wide range of $^{87}Sr/^{86}Sr$ (0.7033- 0.835) have been measured on fertilisers, reflecting variation in the type and source of the raw materials (e.g., Böhlke and Horan, 2000; Négrel and Roy, 1998; Vitòria et al., 2004). Identifying the $^{87}Sr/^{86}Sr$ composition of the fertilisers used in the area is one way to distinguishing between natural strontium signal of the rivers and impact of human induced source on the $^{87}Sr/^{86}Sr$ values. However, this requires an exhaustive study of all the anthropogenic sources in the region. Another approach to mitigate the anthropogenic impact on the $^{87}Sr/^{86}Sr$ ratio is to measure pre-industrial strontium isotopic signature of the river water. This can be achieved by analysing strontium isotopes on pre-industrial biogenic carbonates collected from well dated sediment cores from the rivers.

8.5.3 Coeval Black Sea and Caspian Sea record for the MSC

The Messinian Salinity Crisis is one of the most dramatic events in the region and the role of the Paratethys and its interaction with the Mediterranean during the MSC has been previously highlighted by Krijgsman et al. (2010), Marzocchi et al. (2016), and Stoica et al. (2016). However, high-resolution records from both basins are still missing particularly for the Stage 2 and Stage 3 of the MSC. Recently, a research project within another Marie Curie ITN project SALTGIANT has aimed to revisit the Lago-mare interval in the Mediterranean Sea in order to understand the hydrological and palaeoenvironmental variation during this stage. Concurrent studies in the Black and Caspian seas are necessary to understand the interaction between the Paratethys and Mediterranean region during the time.

8.5.4 High resolution record

The climatic variation over the last 1 Ma contain high amplitude glacial-interglacial cycles. Therefore, in addition to tectonic controls, the connectivity between the Black Sea, Caspian Sea and the open ocean can result from both, eustatic sea level rise during interglacials as well as meltwater driven lake level rise during glacial periods. In order to tease apart the impact of individual signals on the connectivity between basins, a much higher resolution study is required. However, this study demonstrates that combination of Sr isotopic ratios, faunal records and numerical box modelling provides constraints on the hydrologic budget of the region and as such is an excellent tool for reconstructing the connectivity history of the Black Sea, Caspian Sea and the open ocean.

References

Abdullayev, N.A., G.W. Riley, and A.P. Bowman (2012). "Regional Controls on Lacustrine Sandstone Reservoirs: The Pliocene of the South Caspian Basin". In: *Lacustrine sandstone reservoirs and hydrocarbon systems: AAPG Memoir 95* January 2018, pp. 71–98. ISSN: 10970045. DOI: 10.1306/13291385M953446.

Abreu, V. and D. Nummedal (2007). "Miocene to Quaternary sequence stratigraphy of the South and Central Caspian basins". In: *Oil and Gas in the Greater Caspian Area: AAPG Studies in Geology 55* January, pp. 65–86. DOI: 10.1306/1205845St553000.

Adamia, S., V. Alania, A. Chabukiani, G. Chichua, O. Enukidze, and N. Sadradze (2010). "Evolution of the Late Cenozoic basins of Georgia (SW Caucasus): a review". In: *Geological Society, London, Special Publications* 340.1, pp. 239–259.

Agalarova, D.A. (1967). "Microfauna of Ponthian deposits of Azerbaijan and adjacent areas". In: *Az Nile po Dobyce Nefti A [in Russian]* 204, p. 123.

Agalarova, D.A., Z.K. Kadyrova, and S.A. Kulieva (1961). *Ostracoda from Pliocene and Post-Pliocene deposits of Azerbaijan, Baku.*

AJgloe (2018). *Exaggerated Relief Map of the Caucasus and surrounding area [2048 x 2048].* URL: https://www.reddit.com/r/MapPorn/comments/9cknvw/exaggerated_relief_map_of_the_caucasus_and/?st=JLNKSNFI&sh=b792c72e (visited on 02/26/2019).

Akhmetiev, M. A., N. I. Zaporozhets, V. N. Benyamovskiy, G. N. Aleksandrova, A. I. Iakovleva, and T. V. Oreshkina (2012). "The Paleogene history of the Western Siberian Seaway- a connection of the Peri-Tethys to the Arctic Ocean". In: *Austrian Journal of Earth Sciences* 105.1.

Aksu, A. E., R. N. Hiscott, M. Kaminski, P. J. Mudie, H. Gillespie, T. Abrajano, and D. Yasar (2002). "Last glacial Holocene paleoceanography of the Black Sea and Marmara Sea: stable isotopic, foraminiferal and coccolith evidence". In: *Marine Geology* 190, pp. 119–149.

Albarède, F. and A. Michard (1987). "Evidence for slowly changing 87Sr/86Sr in runoff from freshwater limestones of southern France". In: *Chemical Geology* 64.1-2, pp. 55–65.

Ali-Zade, A. A., S. G. Salaev, and A. I. Aliev (1985). "Scientific Assessment of Hydrocarbon Prospects in Azerbaijan and the South Caspian and the Direction of Exploration Work". In: *Elm: Baku*.

Ali-zadeh, A. A. and E.G. Aliyeva (2016). “The evolution of the benthic fauna and bionomic conditions of the South Caspian basin in Pliocene-Pleistocene”. In: *Stratigraphy and sedimentology of oil-gas basin (Baku, Azerbaijan)*, pp. 1–22.

Allen, M., J. Jackson, and R. Walker (2004). “Late Cenozoic reorganization of the Arabia-Eurasia collision and the comparison of short-term and long-term deformation rates”. In: *Tectonics* 23. DOI: 10.1029/2003TC001530.

Allen, M. B., S. Jones, A. Ismail-Zadeh, M. Simmons, and L. Anderson (2002). “Onset of subduction as the cause of rapid Pliocene-Quaternary subsidence in the South Caspian basin”. In: *Geology* 30.9, pp. 775–778.

Andrusov, N.I. (1912). “About age and Stratigraphic situation of the Aktshagylian Stratum *(in Russian)*”. In: *Notes SPb Min. Soc.* 48.1, pp. 271–291.

Antich, N., A. Canals, A. Soler, D. P. F. Darbyshire, and B. F. Spiro (2000). “The isotope composition of dissolved strontium as tracer of pollution in the Llobregat River, northeast Spain.” In: *Tracers and Modelling in Hydrogeology*. March 2014, pp. 207–212.

Armijo, R. and A. Hubert (1999). “Westward propagation of the North Anatolian fault into the northern Aegean : Timing and kinematics”. In: 3, pp. 267–270.

Árnason, Ú., K. Bodin, A. Gullberg, C. Ledje, and M. Suzette (1995). “A molecular view of pinniped relationships with particular emphasis on the true seals”. In: *Journal of Molecular Evolution* 40.1, pp. 78–85. DOI: 10.1007/BF00166598.

Árnason, Ú., A. Gullberg, A. Janke, M. Kullberg, N. Lehman, E. A. Petrov, and R. Väinölä (2006). “Pinniped phylogeny and a new hypothesis for their origin and dispersal”. In: 41, pp. 345–354. DOI: 10.1016/j.ympev.2006.05.022.

Arslanov, K. A., T. A. Yanina, A. L. Chepalyga, A. A. Svitoch, R. R. Makshaev, F. E. Maksimov, S. B. Chernov, N. I. Tertychniy, and A. A. Starikova (2016). “On the age of the Khvalynian deposits of the Caspian Sea coasts according to 14C and 230Th/234U methods”. In: *Quaternary international* 409, pp. 81–87.

Asarin, A. E., V. I. Kravtsova, and V. N. Mikhailov (2010). “Amudarya and Syrdarya rivers and their deltas”. In: *The Aral Sea Environment*. Springer, pp. 101–121.

Astakhov, V. (2004). “Middle Pleistocene glaciations of the Russian North”. In: *Quaternary Science Reviews* 23, pp. 1285–1311. DOI: 10.1016/j.quascirev.2003.12.011.

Astakhov, V. I. (2006). “Evidence of Late Pleistocene ice-dammed lakes in West Siberia”. In: *Boreas* 35.4, pp. 607–621.

Audzijonyte, A. (2005). "Diversity and distributions of circumpolar fresh- and brackish-water Mysis (Crustacea : Mysida): Descriptions of M . relicta Loven , 1862 , M . salemaai n . sp ., M . segerstralei n . sp . and M. diluviana n. Sp. based on molecular and morphological cha". In: *Hydrobiologia* 544, pp. 89–141. DOI: 10.1007/s10750-004-8337-7.

Badertscher, S., D. Fleitmann, H. Cheng, R. L. Edwards, O. M. Göktürk, A. Zumbühl, M. Leuenberger, and O. Tüysüz (2011). "Pleistocene water intrusions from the Mediterranean and Caspian seas into the Black Sea". In: *Nature Geoscience* 4.4, pp. 236–239. DOI: 10.1038/ngeo1106.

Bahr, A., H. W. Arz, F. Lamy, and G. Wefer (2006). "Late glacial to Holocene paleoenvironmental evolution of the Black Sea, reconstructed with stable oxygen isotope records obtained on ostracod shells". In: *Earth and Planetary Science Letters* 241.3-4, pp. 863–875. DOI: 10.1016/j.epsl.2005.10.036.

Bahr, A., F. Lamy, H.W. Arz, C. Major, O. Kwiecien, and G. Wefer (2008). "Abrupt changes of temperature and water chemistry in the late Pleistocene and early Holocene Black Sea". In: *Geochemistry, Geophysics, Geosystems* 9.1. DOI: 10.1029/2007GC001683.

Baidin, S.S. and A.N. Kosarev (1986). "The Caspian Sea. Hydrology and hydrochemistry". In: *Nauka. Moscow* 261.272, p. 25.

Baltes, N. (1971). "Pliocene dinoflagellata and acritarcha in Romania". In: *Proceedings of the Second Planktonic Conference , Rome 1970*. Ed. by A Farinacci, pp. 1–16.

Banner, J. L. (2004). "Radiogenic isotopes : systematics and applications to earth surface processes and chemical stratigraphy". In: *Earth-Science Reviews 65* 65, pp. 141–194. DOI: 10.1016/S0012-8252(03)00086-2.

Banner, J. L. and J. Kaufman (1994). "The isotopic record of ocean chemistiy and diagenesis preserved in non-luminescent brachiopods from Mississippian carbonate rocks , Illinois and Missouri". In: *Geological Society of America Bulletin* 106, pp. 1074–1082.

Beni, A. N., H. Lahijani, R. M. Harami, K. Arpe, S. A G Leroy, N. Marriner, M. Berberian, V. Andrieu-Ponel, M. Djamali, A. Mahboubi, and P. J. Reimer (2013). "Caspian sea-level changes during the last millennium: Historical and geological evidence from the south Caspian Sea". In: *Climate of the Past* 9.4, pp. 1645–1665. DOI: 10.5194/cp-9-1645-2013.

Bennett, C. E., M. Williams, M. J. Leng, D. J. Siveter, S. J. Davies, H. J. Sloane, and I. P. Wilkinson (2011). "Diagenesis of fossil ostracods: Implications for stable isotope based palaeoenvironmental reconstruction". In: *Palaeogeography, Palaeoclimatology, Palaeoecology* 305.1-4, pp. 150–161. DOI: 10.1016/j.palaeo.2011.02.028.

Bennett, K. (2008). *Psimpoll and pscomb: www.chrono.qub.ac.uk/psimpoll/psimpoll.html*.

Beşiktepe, Ş. T., I. Sur, Halil, M. A. Latif, Ü. Ouz T.and Ünlüata, and E. Özsoy (1994). "The circulation and hydrography of the Marmara Sea". In: *Progress in Oceanography* 34.4, pp. 285–334. DOI: 10.1016/0079-6611(94)90018-3.

Birck, J. L. (1986). "Precision K - Rb- Sr isotopic analysis: Application to Rb–Sr chronology". In: *Chemical Geology* 56, pp. 73–83.

Birks, H. J. B. (2008). "Paleoecology". In: *Encyclopedia of Ecology*, pp. 2623–2634. DOI: 10.1016/B978-008045405-4.00525-5.

Blum, J. D. and Y. Erelt (1995). "A silicate weathering mechanism linking increases in marine 87Sr/86Sr with global glaciation". In: *Nature* 373, pp. 0–3.

Boerner, N., Q. De Baere B.and Yang, K. P. Jochum, P. Frenzel, M. O. Andreae, and A. Schwalb (2013). "Ostracod shell chemistry as proxy for paleoenvironmental change". In: *Quaternary International* 313-314, pp. 17–37. DOI: 10.1016/j.quaint.2013.09.041.

Böhlke, J. K. and M. Horan (2000). "Strontium isotope geochemistry of groundwaters and streams affected by agriculture, Locust Grove, MD". In: *Applied Geochemistry* 15.5, pp. 599–609. ISSN: 08832927. DOI: 10.1016/S0883-2927(99)00075-X.

Boomer, I., N. Aladin, I. Plotnikov, and R. Whatley (2000). "The palaeolimnology of the Aral Sea: A review". In: *Quaternary Science Reviews* 19.13, pp. 1259–1278. DOI: 10.1016/S0277-3791(00)00002-0.

Boomer, I., D. J. Horne, and I. J. Slipper (2003). "The Use of Ostracods in Palaeoenvironmental studies, or what can you do with an ostracod shell?" In: *Bridging the gap: Trends in the Ostracode Biological and Geological Sciences* January, pp. 153–179.

Boucot, A. J. (2013). *Evolutionary paleobiology of behavior and coevolution*. Elsevier. DOI: 10.1016/C2009-0-08704-2.

Bowman, T. E and A. Long (1968). "Relict Populations of Drefianofius bungei and Limnocalanus macrurus grimaldii (Copepoda: Calanoida) from Ellesmere Island, N. W.T." In: *Arctic*, pp. 172–180.

Brass, G. (1976). "The variation of the marine 87Sr/86Sr ratio during Phanerozoic time: interpretation using a flux model". In: *Geochimlca et Cosmoch!mica Acta* 40.1974, pp. 721–730.

Brenner, W. W. (2005). "Holocene environmental history of the Gotland Basin (Baltic Sea)—a micropalaeontological model". In: *Palaeogeography, Palaeoclimatology, Palaeoecology* 220.3-4, pp. 227–241.

Brückner, E. (1890). "Climatic fluctuations since 1700: together with remarks about the climatic fluctuations of the diluvial time". In: *Vienna: E. Holzel (in German)* 4.2.

Brunet, F. F., M. V. Korotaev, A. V. Ershov, and A. M. Nikishin (2003). "The South Caspian Basin: A review of its evolution from subsidence modelling". In: *Sedimentary Geology* 156.1-4, pp. 119–148. DOI: 10.1016/S0037-0738(02)00285-3.

Brunet, O., A. V Ershov, M. V. Korotaev, V. N. Melikhov, E. Barrier, D. O. Mordvintsev, I. P. Sidorova, and T. D. De Paris (2017). "Late Palaeozoic and Mesozoic evolution of the Amu Darya Basin (Turkmenistan, Ukbekistan)". In: *Geological Evolution ofCentral Asian Basins and the Western Tien Shan Range*. Vol. 427, pp. 89–144.

Buyukmeric, Y. and F. P. Wesselingh (2016). "Middle e late Pleistocene marine molluscs from Izmit Bay area (eastern Marmara Sea , Turkey) and the nature of Marmara e Black Sea corridors". In: *Quaternary International* 401, pp. 153–161. DOI: 10.1016/j.quaint.2015.07.020.

Cagatay, M. N., N. Gorur, R. Flecker, M. Sakinc, C. Tunoglu, R. Ellam, W. Krijgsman, S. Vincent, and A. Dikbas (2006). "Paratethyan-Mediterranean connectivity in the Sea of Marmara region (NW Turkey) during the Messinian". In: *Sedimentary Geology* 188-189, pp. 171–187. DOI: 10.1016/j.sedgeo.2006.03.004.

Capo, R. C., B. W. Stewart, and O. A. Chadwick (1998). "Strontium isotopes as tracers of ecosystem processes: theory and methods". In: *Geoderma* 82.1-3, pp. 197–225. DOI: 10.1016/S0016-7061(97)00102-X.

Carbonel, P., J.P. Colin, D. L. Danielopol, H. Löffler, and I. Neustrueva (1988). "Paleoecology of limnic ostracodes: a review of some major topics". In: *Palaeogeography, Palaeoclimatology, Palaeoecology* 62.1-4, pp. 413–461.

Chang, L., I. Vasiliev, C. G. C. Van Baak, W. Krigsman, M. J. Dekkers, A. P. Roberts, J. D. Fitz Gerald, and M. van Hoesel A.and Winklhofer (2014). "Identification and environmental interpretation of diagenetic and biogenic gregite in sediments: A lesson from the Messinian Black Sea". In: *Geochemistry, Geophysics, Geosystems Research* 15, pp. 3612–3627.

Chapin III, F. S., P. A. Matson, and P. Vitousek (2011). *Principles of Terrestrial Ecosystem Ecology*. 2nd. Springer Science+Business Media.

Chepalyga, A. L., K. D. Mikhaylesku, and Y. A. Izmaylov (1989). "Problems of stratigraphy and paleogeography of the Black Sea Pleistocene". In: *Quaternary Period. Stratigraphy. Nauka, Moscow*, pp. 113–121.

Chivas, A. R., J. De Deckker P.and Shelley, and Michael G. (1985). "Strontium content of ostracods indicates lacustrine palaeosalinity". In: *Nature* 316.6025, pp. 251–253. DOI: 10.1038/316251a0.

Clauer, N. (1998). "Compositions chimiques et isotopiques d ' eaux de la mer Caspienne et de tributaires de la region de Makachkala (Russie): premi & res donnees sur le fonctionnement d ' un systeme endorgique particulier " Prelimina y information on the chemical and isot". In: *Earth and Planetary Sciencez* 327, pp. 17–24.

Clauer, N., S. Chaudhuri, T. Toulkeridis, and G. Blanc (2000). "Fluctuations of Caspian Sea level: Beyond climatic variations?" In: *Geology* 28.11, pp. 1015–1018. DOI: 10.1130/0091-7613(2000)28<1015.

Clauer, N., M. C. Pierret, and S. Chaudhuri (2008). "Role of subsurface brines in Salt Balance: The case study of the Caspian Sea and Kara Bogaz Bay". In: *Aquatic Geochemistry* 15.1-2, pp. 237–261. DOI: 10.1007/s10498-008-9048-x.

Constantinescu, A. M., S. Toucanne, B. Dennielou, S. J. Jorry, T. Mulder, and G. Lericolais (2015). "Evolution of the Danube Deep-Sea Fan since the Last Glacial Maximum : new insights into Black Sea water-level fl uctuations". In: *Marine Geology* 367, pp. 50–68. DOI: 10.1016/j.margeo.2015.05.007.

Cosentino, D., E. Gliozzi, and G. Pipponzi (2007). "The late Messinian Lago-Mare episode in the Mediterranean Basin: preliminary report on the occurrence of Paratethyan ostracod fauna from central Crete (Greece)". In: *Geobios* 40.3, pp. 339–349.

Cox, J. and G. Faure (1974). "Isotope composition of strontium in carbonate phase of two cores from Black Sea". In: *AAPG Special Volumes*.

Craig, H. (1965). "The measurement of oxygen isotope paleotemperatures." In: *Stable isotopes in oceanographic studies and paleotemperatures: Consiglio Nazionale delle Richerche*, pp. 161–182.

Craig, H., L. I. Gordon, and Y. Horibe (1963). "Isotopic Exchange Effects in the Evaporation of Water 1." In: *Journal of geophysical research* 68.17, pp. 151–194.

Cziczer, I., I. Magyar, Ra. Pipík, M. Böhme, S. Ćorić, K. Bakrač, M. Sütő-Szentai, M. Lantos, E. Babinszki, and P. Müller (2009). "Life in the sublittoral zone of long-lived Lake Pannon: Paleontological analysis of the Upper Miocene Szák Formation, Hungary". In: *International Journal of Earth Sciences* 98.7, pp. 1741–1766. DOI: 10.1007/s00531-008-0322-3.

Dale, B. (1996). "Dinoflagellate cyst ecology: modeling and geological applications". In: *Palynology: principles and applications*, pp. 1249–1275.

Dansgaard, W. (1964). "Stable isotopes in precipitation". In: *Tellus* 16.4, pp. 436–468. DOI: 10.3402/tellusa.v16i4.8993.

Danukalova, G. A. (1996). "Bivalves and Aktschagylian stratigraphy". In: *Trudy Paleontologicheskogo Instituta Rossia Akademii Nauk* 265, pp. 1–132.

Dasch, E. J. (1969). "Strontium isotopes in weathering profiles, deep-sea sediments, and sedimentary rocks". In: *Geochimica et Cosmochimica Acta* 33.12, pp. 1521–1552.

Davies, A. J. L. (1958). "Pleistocene Geography and the Distribution of Northern Pinnipeds". In: *Ecology* 39.1, pp. 97–113.

Davis, A. C., M. J. Bickle, and D. A. H. Teagle (2003). "Imbalance in the oceanic strontium budget". In: *Earth and Planetary Science Letters* 211.1-2, pp. 173–187.

de Deckker, P. and R.M. Forester (1988). "The use of ostracodes to reconstruct continental paleoenvironment records". In: *Ostracoda in the earth sciences, Elsevier, Amsterdam* 175–199.

de Leeuw, A., A. Morton, C. G.C. van Baak, and S. J. Vincent (2018). "Timing of arrival of the Danube to the Black Sea: Provenance of sediments from DSDP site 380/380A". In: *Terra Nova* 30.2, pp. 114–124. DOI: 10.1111/ter.12314.

Decrouy, L., T. Walter Vennemann, and D. Ariztegui (2011a). "Controls on ostracod valve geochemistry, Part 1: Variations of environmental parameters in ostracod (micro-)habitats". In: *Geochimica et Cosmochimica Acta* 75.22, pp. 7364–7379. DOI: 10.1016/j.gca.2011.09.009.

Decrouy, L., T. W. Vennemann, and D. Ariztegui (2011b). "Controls on ostracod valve geochemistry: Part 2. Carbon and oxygen isotope compositions". In: *Geochimica et Cosmochimica Acta* 75.22, pp. 7380–7399. DOI: 10.1016/j.gca.2011.09.008.

Delorme, L. D. (1989). "Methods in Ecology Freshwater Ostracods". In: *Geoscience Canada* 16.2.

Dewan, N., B. J Majestic, M. E. Ketterer, J. P. Miller-schulze, M. M. Shafer, J. J. Schauer, P. A. Solomon, M. Artamonova, B. B. Chen, S. A. Imashev, and G. R. Carmichael (2015). "Stable isotopes of lead and strontium as tracers of sources of airborne particulate matter in Kyrgyzstan". In: *Atmospheric Environment* 120, pp. 438–446. DOI: 10.1016/j.atmosenv.2015.09.017.

Dooh, R.T., J. Adamowicz, and D.N. Hebert (2006). "Comparative phylogeography of two North American ' glacial relict ' crustaceans". In: *Molecular Ecology* 15, pp. 4459–4475. DOI: 10.1111/j.1365-294X.2006.03095.x.

Drapun, I., E. Anufriieva, and Y. Shadrin N.and Zagorodnyaya (2017). "Ostracods in the plankton of the Sivash Bay (the Sea of Azov) during its transformation from brackish to hypersaline state". In: *Ecologica Montenegrina* 14, pp. 102–108.

Dumont, H. J. (1998). "The Caspian Lake: History, biota, structure, and function". In: *Limnology and Oceanography* 43.1, pp. 44–52. DOI: 10.4319/lo.1998.43.1.0044.

Eglinton, G. and R. J. Hamilton (1967). "Leaf epicuticular waxes". In: *Science* 156.3780, pp. 1322–1335.

El Meknassi, S., Dera, T. Cardone, M. De Rafélis, C. Brahmi, and V. Chavagnac (2018). "Sr isotope ratios of modern carbonate shells: Good and bad news for chemostratigraphy". In: *Geology* 46.11, pp. 1003–1006. DOI: 10.1130/G45380.1.

Elderfield, H. (1986). "Strontium isotope stratigraphy". In: *Palaeogeography, palaeoclimatology, palaeoecology* 57.1, pp. 71–90.

Elderfield, H. and J. M. Gieskes (1982). "Sr isotopes in interstitial waters of marine sediments from Deep Sea Drilling Project cores". In: *Nature* 300.5892, p. 493.

Ellegaard, M., J. Lewis, and I. C. Harding (2002). "Cyst-theca relationship, life cycle and effects of temperature and salinity on the cyst morphology of Gonyaulax baltica sp. nov. (Dinophyceae) from the Baltic Sea area". In: *Journal of Phycology* 38, pp. 775–789.

Elorza, J. and F. Garcıa-Garmilla (1996). "Petrological and geochemical evidence for diagenesis of inoceramid bivalve shells in the Plentzia Formation (Upper Cretaceous, Basque–Cantabrian Region, northern Spain)". In: *Cretaceous Research* 17.4, pp. 479–503.

Esin, N. V., V. Yanko-Hombach, O. N. Kukleva, and N. I. Esin (2010). "Main regularities of the Late Pleistocene-Holocene transgression of the Black Sea". In: *Doklady Earth Sciences*. Vol. 430. 2. Springer, pp. 194–197.

Fairchild, I. J., C. L. Smith, L. Baker A.and Fuller, C. Spötl, D. Mattey, and F. McDermott (2006). "Modification and preservation of environmental signals in speleothems". In: *Earth-Science Reviews* 75.1-4, pp. 105–153. DOI: 10.1016/j.earscirev.2005.08.003.

Faure, G. and J. L. Powell (1972a). *Strontium isotope geology*. Springer-Verlag, New York.

– (1972b). "The Geochemistry of Rubidium and Strontium". In: *Strontium Isotope Geology*. Springer-Verlag, New York, pp. 1–8. DOI: 10.1007/978-3-642-65367-4_1.

Flecker, R., W. Krijgsman, W. Capella, C. de Castro Martins, E. Dmitrieva, J. P. Mayser, A. Marzocchi, S. Modestu, D. Ochoa, D. Simon, M. Tulbure, B. van den Berg, M. van der Schee, G. de Lange, R. Ellam, R. Govers, M. Gutjahr, F. Hilgen, T. Kouwenhoven, J. Lofi, P. Meijer, F. J. Sierro, N. Bachiri, N. Barhoun, A.C. Alami, B. Chacon, J.A. Flores, J. Gregory, J. Howard, D. Lunt, M. Ochoa, R. Pancost, S. Vincent, and M. Z. Yousfi (2015). "Evolution of the Late

Miocene Mediterranean-Atlantic gateways and their impact on regional and global environmental change". In: *Earth-Science Reviews* 150, pp. 365–392. DOI: 10.1016/j.earscirev.2015.08.007.

Fleitmann, D., H. Cheng, S. Badertscher, R. L. Edwards, M. Mudelsee, O. M. Göktürk, A. Fankhauser, R. Pickering, C. C. Raible, A. Matter, J. Kramers, and O. Tuysuz (2009). "Timing and climatic impact of Greenland interstadials recorded in stalagmites from northern Turkey". In: *Geophysical Research Letters* 36.19.

Floroiu, A., M. Stoica, W. Krijgsman, and I. Vasiliev (2012). "Maeotian/Pontian Boundary from the East Carphatian Foredeep (Dacian Basin)". In: *EGU General Assembly Conference Abstracts*. Vol. 14, p. 9409.

Forte, A. M., E. Cowgill, I. Murtuzayev, T. Kangarli, and M. Stoica (2013). "Structural geometries and magnitude of shortening in the eastern Kura fold-thrust belt , Azerbaijan : Implications for the development of the Greater Caucasus Mountains". In: *Tectonics* 32, pp. 688–717. DOI: 10.1002/tect.20032.

Frank, M. (2002). "Radiogenic isotopes: tracers of past ocean circulation and erosional input". In: *Review of Geophysics* 40.1.

Fulton, T. L. and C. Strobeck (2010). "Multiple fossil calibrations , nuclear loci and mitochondrial genomes provide new insight into biogeography and divergence timing for true seals". In: *Journal of Biogeography* 37.5, pp. 814–829. DOI: 10.1111/j.1365-2699.2010.02271.x.

Gat, J. R. and R. Gonfiantini (1981). "Stable isotope hydrology. Deuterium and oxygen-18 in the water cycle". In: *International Atomic Energy Agency (IAEA): IAEA*.

Gilfillan, E. S. (1934). "The isotopic composition of sea water". In: *Journal of the American Chemical Society* 56.2, pp. 406–408.

Goldstein, S. L. and S. R. Hemming (2003). "Long-lived isotopic tracers in oceanography, paleoceanography, and ice-sheet dynamics". In: *Treatise on geochemistry* 6, p. 625.

Green, T., N. Abdullayev, J. Hossack, G. Riley, and A. M. Roberts (2009). "Sedimentation and subsidence in the South Caspian Basin, Azerbaijan". In: *Geological Society, London, Special Publications* 312.1, pp. 241–260. DOI: 10.1144/SP312.12.

Grigorovich, I. A., H. J. Macisaac, N. V. Shadrin, and E. L. Mills (2002). "Patterns and mechanisms of aquatic invertebrate introductions in the Ponto-Caspian region". In: *Canadian Journal of Fisheries and Aquatic Sciences* 59.7, pp. 1189–1208. DOI: 10.1139/F02-088.

Grigorovich, I. A., T. W. Therriault, and H. J. Macisaac (2003). "History of aquatic invertebrate invasions in the Caspian Sea". In: *Marine bioinvasions: Patterns, processes and perspectives*. Springer, pp. 103–115.

Grothe, A. (2016). "The Messinian Salinity Crisis: a Paratethyan Perspective". PhD thesis. University Utrecht.

Grothe, A., F. Sangiorgi, Y. R. Mulders, I. Vasiliev, G.-J. Reichart, H. Brinkhuis, M. Stoica, and W. Krijgsman (2014). "Black Sea desiccation during the Messinian Salinity Crisis: Fact or fiction?" In: *Geology* 42.7, pp. 563–566. DOI: 10.1130/G35503.1.

Grothe, A., F. Sangiorgi, H. Brinkhuis, M. Stoica, and W. Krijgsman (2018). "Migration of the dinoflagellate Galeacysta etrusca and its implications for the Messinian Salinity Crisis". In: *Newsletters on Stratigraphy* 51.1, pp. 73–91.

Grousset, F. E. and P. E. Biscaye (2005). "Tracing dust sources and transport patterns using Sr, Nd and Pb isotopes". In: *Chemical Geology* 222.3-4, pp. 149–167. DOI: 10.1016/j.chemgeo.2005.05.006.

Hamidi, M., M. R. Kavianpour, and Y. Shao (2013). "Synoptic Analysis of Dust Storms in the Middle East". In: *Asia-Pacific Journal of Atmospheric Sciences* 49.3, pp. 279–286. DOI: 10.1007/s13143-013-0027-9.

Hartmann, G. (1966). *Dr. HG Bronns Klassen und Ordnungen des Tierreichs Fünfter Band: Arthropoda I. Abteilung: Crustacea 2. Buch, IV. Teil 1*. Geest and Portig, Leipzig.

Hartmann, J. and N. Moosdorf (2012). "The new global lithological map database GLiM: A representation of rock properties at the Earth surface". In: *Geochemistry, Geophysics, Geosystems* 13.12.

Harzhauser, M., W. E Piller, and F. F. Steininger (2002). "Circum-Mediterranean Oligo ˆ Miocene biogeographic evolution ˆ the gastropods ' point of view". In: *Palaeogeography, Palaeoclimatology, Palaeoecology* 183.

Hemleben, C., A. W. H. Be, O. R. Anderson, and S. Tuntivate (1977). "Test morphology, organic layers and chamber formation of the planktonic foraminifer Globorotalia menardii (d'Orbigny)". In: *The Journal of Foraminiferal Research* 7.1, pp. 1–25.

Hemleben, C., M. Spindler, and O. R. Anderson (2012). *Modern planktonic foraminifera*. Springer Science & Business Media.

Hilgen, F. J., L. J. Lourens, and J. A. van Dam (2012). "The neogene period". In: *The Geologic Time Scale 2012*, p. 923.

Hinderer, M. (2001). "Late quaternary denudation of the Alps, Valley and lake fillings and modern river loads". In: *Geodinamica Acta* 14.4, pp. 231–263. DOI: 10.1080/09853111.2001.11432446.

Hinds, D. J., E. Aliyeva, M. B. Allen, C. E. Davies, S. B. Kroonenberg, M. D. Simmons, and S. J. Vincent (2004). "Sedimentation in a discharge dominated fluvial-lacustrine system: The Neogene Productive Series of the South Caspian Basin, Azerbaijan". In: *Marine and Petroleum Geology* 21.5, pp. 613–638. DOI: 10.1016/j.marpetgeo.2004.01.009.

Holland, H. D. (1984). *The chemical evolution of the atmosphere and oceans*. Princeton University Press.

Holmes, J. A. (1996). "Trace-element and stable-isotope geochemistry of non-marine ostracod shells in Quaternary palaeoenvironmental reconstruction". In: *Journal of Paleolimnology* 15.3, pp. 223–235. DOI: 10.1007/Bf00213042.

Holmes, J. A., P. E. Hales, and F. A. Street-Perrott (1992). "Trace-element chemistry of non-marine ostracods as a means of palaeolimnological reconstruction: An example from the Quaternary of Kashmir, northern India". In: *Chemical Geology* 95.1-2, pp. 177–186. DOI: 10.1016/0009-2541(92)90054-9.

Holmquist, C. (1959). *Problems on marine-glacial relicts on account of investigations on the genus Mysis*. Berlingska boktryckeriet.

Horne, D. J., A. Cohen, and K. Martens (2002). "Taxonomy, morphology and biology of Quaternary and living Ostracoda". In: *The Ostracoda: applications in Quaternary research* 131, pp. 5–36.

Hosono, T., A. Nakano T.and Igeta, I. Tayasu, T. Tanaka, and S. Yachi (2007). "Impact of fertilizer on a small watershed of Lake Biwa: Use of sulfur and strontium isotopes in environmental diagnosis". In: *Science of the Total Environment* 384.1-3, pp. 342–354. DOI: 10.1016/j.scitotenv.2007.05.033.

Hoyle, T. M. (2019). "Biotic change and landlocked seas: Ecosystem responses to climate and sea level variability in the Plio-Pleistocene of the Pontocaspian basins". PhD thesis. University Utrecht.

Hoyle, T. M., M. Sala-Pérez, and Sangiorgi F. (2019). "Where should we draw the lines between dinocyst "species"? Morphological continua in Black Sea dinocysts". In: *Journal of Micropalaeontology* 38.1, pp. 55–65.

Hsu, K. J. and F. Giovanoli (1979). "Messinian event in the black sea". In: *Palaeogeography, Palaeoclimatology, Palaeoecology* 29.C, pp. 75–93. DOI: 10.1016/0031-0182(79)90075-0.

Hsu, K. J., K. Kelts, A. Matter, and M. E. Tucker (1978). "Late Neogene chemical sedimentation in the Black Sea". In: *Special Publication International Association of Sedimentologists* 2, pp. 129–145.

Hubert-Ferrari, A., R. Armijo, G. King, B. Meyer, and A. Barka (2002). "Morphology , displacement , and slip rates along the North Anatolian Fault , Turkey". In: *Journal of geophysical research* 107. DOI: 10.1029/2001JB000393.

Ingram, B. L. and D. Sloan (1992). "Strontium isotopic composition of estuarine sediments as paleosalinity-paleoclimate indicator." In: *Science* 255.5040, pp. 68–72. DOI: 10.1126/science.255.5040.68.

Ivanova, E., E. Schornikov, F. Marret, I. Murdmaa, M. Zenina, R. Aliev, L. Bradley, A. Chepalyga, L. Wright, V. Kremenetsky, and V. Kravtsov (2014). "Environmental changes on the inner northeastern Black Sea shelf , off the town of Gelendzhik , over the last 140 years". In: *Quaternary International* 328-329, pp. 338–348. DOI: 10.1016/j.quaint.2013.09.044.

Jacobson, A. D. (2004). "Has the atmospheric supply of dissolved calcite dust to seawater influenced the evolution of marine87Sr/86Sr ratios over the past 2.5 million years?" In: *Geochemistry, Geophysics, Geosystems* 5.12, pp. 1–9. DOI: 10.1029/2004GC000750.

Jaoshvili, S. (2003). *The rivers of the Black Sea Technical report No 71*. European Environment Agency Copenhagen.

Jiříček, R. (1985). "The ostracods of Pannonia". In: *Chronostratigraphy and Neostratotypes, Mioz "a n of the Central Paratethys, Pannonia .– 7 M* 6, pp. 378–425.

Jones, R.W. and M.D Simmons (1997). "A review of the stratigraphy of Eastern Paratethys (Oligocene-Holocene)". In: *Bulletin-Natural History Museum Geology Series*, pp. 25–50.

Karpychev, Y. A. (1998). "Dating of Regressive Stages in the Caspian Sea Using 14C". In: *Vodn. Resur* 25, pp. 274–278.

– (2001). "Variations in the Caspian Sea Level in the Historic Epoch". In: *Water Resources* 28.1, pp. 1–14. DOI: 10.1023/A:1018868511359.

Keatings, K. W., T. H. E. Heaton, and J. A. Holmes (2002). "The effects of diagenesis on the trace element and stable isotope geochemistry of non-marine ostracod valves". In: *Journal of Paleolimnology* 28.2, pp. 245–252. DOI: 10.1023/A:1021641800338.

Kideys, A. E. (2002). "Fall and Rise of the Black Sea Ecosystem". In: 509.1999, pp. 63–66.

Killingley, J. S. (1983). "Effects of diagenetic recrystallization on 18O/16O values of deep-sea sediments". In: *Nature* 301.5901, p. 594.

Kirscher, U., O. Oms, A. A. Bruch, I. Shatilova, G. Chochishvili, and V. Bachtadse (2017). "The Calabrian in the Western Transcaucasian basin (Georgia): Paleomagnetic constraints from the Gurian regional stage". In: *Quaternary Science Reviews* 160, pp. 96–107. DOI: 10.1016/j.quascirev.2017.01.017.

Kislov Ã., A. and P. Toropov (2007). "East European river runoff and Black Sea and Caspian Sea level changes as simulated within the Paleoclimate modeling intercomparison project". In: *Quaternary International* 168, pp. 40–48. DOI: 10.1016/j.quaint.2006.10.005.

Kosarev, A. N. and A. G. Kostianoy (2008). "Introduction". In: *The Black Sea Environment*. Ed. by Andrey G. Kostianoy and Alexey N. Kosarev. Berlin, Heidelberg: Springer Berlin Heidelberg, pp. 1–10. DOI: 10.1007/698_5_092.

Kosarev, A. N. and E. A. Yablonskaya (1994). *The Caspian sea*. SPB Acedemic Publishing, The Hauge.

Kostianoy, A. G. and A. Kosarev (2005). *The Caspian Sea Environment: The Handbook of Environmental Chemistry*. Ed. by Andrey G. Kostianoy and Aleksey N. Kosarev. Springer Berlin Heidelberg.

– (2008). *The Handbook of Environmental Chemistry: The Black Sea Environment*. Vol. 5.

Kouli, K., H. Brinkhuis, and B. Dale (2001). "Spiniferites cruciformis: A fresh water dinoflagellate cyst?" In: *Review of Palaeobotany and Palynology* 113.4, pp. 273–286. DOI: 10.1016/S0034-6667(00)00064-6.

Krijgsman, W., M. Stoica, I. Vasiliev, and V. V. Popov (2010). "Rise and fall of the Paratethys Sea during the Messinian Salinity Crisis". In: *Earth and Planetary Science Letters* 290.1-2, pp. 183–191. DOI: 10.1016/j.epsl.2009.12.020.

Krijgsman, W., A. Tesakov, T. Yanina, S. Lazarev, G. Danukalova, C. G. C. van Baak, J. Agustí, M. C. Alçiçek, E. Aliyeva, D. Bista, A. Bruch, Y. Büyükmeriç, M. Bukhsianidze, S. B. Kroonenberg, D. Lordkipanidze, O. Oms, L. Rausch, J. Singarayer, and M. Stoica (2019). "Quaternary time scales for the Pontocaspian domain : Interbasinal connectivity and faunal evolution". In: *Earth Science Reviews* 188.October 2018, pp. 1–40. DOI: 10.1016/j.earscirev.2018.10.013.

Krom, M. D., R. A. Cliff, L. M. Eijsink, B. Herut, and R. Chester (1999). "The characterisation of Saharan dusts and Nile particulate matter in surface sediments from the Levantine basin using Sr isotopes". In: *Marine Geology* 155.3-4, pp. 319–330.

Kroonenberg, S. B. and M. Park (2005). “Two Deltas , Two Basins , One River , One Sea : the Modern Volga Delta As an Analogue of the Neogene Productive Series , South Caspian Basin”. In: *Society of Sedimentary Geology* 83, pp. 231–256.

Kroonenberg, S. B., E. N. Badyukova, J. E. A. Storms, E. I. Ignatov, and N. S. Kasimov (2000). “A full sea-level cycle in 65 years: barrier dynamics along Caspian shores”. In: *Sedimentary Geology* 134.3-4, pp. 257–274.

Krstić, N. (1972). “Ostracodi Kongeriskih Slojeva: 10. Loxoconcha”. In: *Bulletin of the Natural History Museum, Belgrade, ser. A* 27, pp. 243–275.

– (1973). *Biostratigrafija kongerijskih slojeva okoline Beograda na osnovy ostrakoda, sa opisom vrsta roda Amplocypris*. Institut za geološko-rudarska istraživanja i ispitivanja nuklearnih i drugih mineralnih sirovina.

– (1985). “Ostracoden in Pannonia near Belgrade”. In: *Chronostratigraphy and Neostratotypes, Mioz "a n M* 6, pp. 103–143.

– (1990). “Contribution by ostracods to the definition of the boundaries of the Pontian in the Pannonian Basin”. In: *Chronostratigraphie und Neostratotypen. Neogen der Westlichen (‘Zentrale’) Paratethys VIII, Pl1, Pontien (eds Stevanovic PM, Nevesskaja LA, Marinescu F, Sokac A, Jambor A)*, pp. 45–47.

Kvach, Y. (2009). “First report of Saduria (Mesidotea) entomon (Linnaeus , 1758) (Isopoda : Chaetiliidae) in the Black Sea”. In: *Aquatic Invasions* 4.2, pp. 393–395. DOI: 10.3391/ai.2009.4.2.17.

Kwiecien, O., H. W. Arz, F. Lamy, B. Plessen, A. Bahr, and G. H. Haug (2009). “North Atlantic control on precipitation pattern in the eastern Mediterranean / Black Sea region during the last glacial”. In: *Quaternary Research* 71.3, pp. 375–384. DOI: 10.1016/j.yqres.2008.12.004.

Lazarev, S., E. L. Jorissen, S. van de Velde, L. Rausch, M. Stoica, F. P. Wesselingh, C. G. C. van Baak, T. A. Yanina, E. Aliyeva, and W. Krijgsman (2019). “Magneto- biostratigraphic age constraints on the palaeoenvironmental evolution of the South Caspian Basin during the Early - middle Pleistocene (Kura Basin, Azerbaijan)”. In: *Quaternary Science Reviews* 222.

Le Pichon, X., R. Saatc, and B. Tok (2001). “The active Main Marmara Fault”. In: *Earth and Planetary Science Letters* 192.4, pp. 595–616.

Le Pichon, X., A. C. Şengör, J. Kende, C. İmren, P. Henry, C. Grall, and H. Karabulut (2015). “Propagation of a strike-slip plate boundary within an extensional environment: the westward

propagation of the North Anatolian Fault". In: *Canadian Journal of Earth Sciences* 53.11, pp. 1416–1439.

Leaney, F. W., C. B. Osmond, G. B. Allison, and H. Ziegler (1985). "Hydrogen-isotope composition of leaf water in C 3 and C 4 plants: its relationship to the hydrogen-isotope composition of dry matter". In: *Planta* 164.2, pp. 215–220.

Lee, H. N., Y. Igarashi, M. Chiba, M. Aoyama, K. Hirose, and T. Tanaka (2006). "Global model simulations of the transport of Asian and Sahara dust: total deposition of dust mass in Japan". In: *Water, air, and soil pollution* 169.1-4, pp. 137–166.

Leroy, S. A. G. and M. Albay (2010). "Palynomorphs of brackish and marine species in cores from the freshwater Lake Sapanca, NW Turkey". In: *Review of Palaeobotany and Palynology* 160.3-4, pp. 181–188. DOI: 10.1016/j.revpalbo.2010.02.011.

Lewis, J., J. D. Taylor, K. Neale, and S. A. G. Leroy (2018). "Expanding known dinoflagellate distributions : investigations of slurry cultures from Caspian Sea sediment". In: *Botanica Marina* 61.1, pp. 21–31.

Lisiecki, L. E. and M. E. Raymo (2005). "A Pliocene-Pleistocene stack of 57 globally distributed benthic D18O records". In: *Paleoceanography* 20.May, pp. 1–17. DOI: 10.1029/2004PA001071.

Livental, V. E. (1929). "Ostracoda of Akchagilian and Apsheronian beds of the Babazan Section". In: *Izvestiya Azerbajdzahnskogo Politekhnischeskogo Instituta* 1, pp. 1–58.

Londeix, L., M. Benzakour, J. P. Suc, and J. L. Turon (2007). "Messinian palaeoenvironments and hydrology in Sicily (Italy): the dinoflagellate cyst record". In: *Geobios* 40.3, pp. 233–250.

Luo, Y. H. and L. D. S. L. Sternberg (1992). "Hydrogen and oxygen isotopic fractionation during heterotrophic cellulose synthesis". In: *Journal of Experimental Botany* 43.1, pp. 47–50. DOI: 10.1093/jxb/43.1.47.

Magyar, I. and D. H. Geary (2012). "Biostratigraphy in a Late Neogene Caspian-Type Lacustrine Basin: Lake Pannon, Hungary". In: *Lacustrine Sandstone Reservoirs and Hydrocarbon Systems: AAPG Memoir 95* 95, pp. 255–264.

Major, C. O., W. B. F. Ryan, G. Lericolais, and I. Hajdas (2002). "Constraints on Black Sea out£ ow to the Sea of Marmara during the last glacial-interglacial transition". In: *Marine Geology* 190, pp. 19–34.

Major, C. O., S. L. Goldstein, W. B. F. Ryan, G. Lericolais, A. M. Piotrowski, and I. Hajdas (2006). "The co-evolution of Black Sea level and composition through the last deglaciation and

its paleoclimatic significance". In: *Quaternary Science Reviews* 25.17-18, pp. 2031–2047. DOI: 10.1016/j.quascirev.2006.01.032.

Marret, F., S. A. G. Leroy, F. Chalié, and F. Gasse (2004). "New organic-walled dinoflagellate cysts from recent sediments of Central Asian seas". In: *Review of Palaeobotany and Palynology* 129.1-2, pp. 1–20. DOI: 10.1016/j.revpalbo.2003.10.002.

Marret, F., P. Mudie, A. Aksu, and R. N. Hiscott (2009). "A Holocene dinocyst record of a two-step transformation of the Neoeuxinian brackish water lake into the Black Sea". In: *Quaternary International* 197.1-2, pp. 72–86.

Marzocchi, A., R. Flecker, C. G. C. van Baak, D. J. Lunt, and W. Krijgsman (2016). "Mediterranean outflow pump : An alternative mechanism for the Lago-mare and the end of the Messinian Salinity Crisis". In: *Geological society of America* 44.7, pp. 1–4. DOI: 10.1130/G37646.1.

Matenco, L., I. Munteanu, M. ter Borgh, A. Stanica, M. Tilita, G. Lericolais, C. Dinu, and G. Oaie (2016). "The interplay between tectonics, sediment dynamics and gateways evolution in the Danube system from the Pannonian Basin to the western Black Sea". In: *Science of the Total Environment* 543, pp. 807–827. DOI: 10.1016/j.scitotenv.2015.10.081.

Matoshko, A. V., P. F. Gozhik, and G. Danukalova (2004). "Key Late Cenozoic fluvial archives of eastern Europe: The Dniester, Dnieper, Don and Volga". In: *Proceedings of the Geologists' Association* 115.2, pp. 141–173. DOI: 10.1016/S0016-7878(04)80024-5.

McArthur, J. M., R. J. Howarth, and G. A. Shields (2012). *Strontium Isotope Stratigraphy*. Felix M. Gradstein, James G. Ogg, Mark Schmitz and Gabi Ogg, pp. 127–144. DOI: 10.1016/B978-0-444-59425-9.00007-X.

McCulloch, M. T. and P. De Deckker (1989). "Sr isotope constraints on the Mediterranean environment at the end of the Messinian salinity crisis". In: *Nature* 342.6245, pp. 62–65.

McDermott, F. (2004). "Palaeo-climate reconstruction from stable isotope variations in speleothems: a review". In: *Quaternary Science Reviews* 23.7-8, pp. 901–918.

McHugh, C. M. G., D. Gurung, L. Giosan, W. B. F. Ryan, Y. Mart, U. Sancar, L. Burckle, and M. N. Cagatay (2008). "The last reconnection of the Marmara Sea (Turkey) to the World Ocean: A paleoceanographic and paleoclimatic perspective". In: *Marine Geology* 255.1-2, pp. 64–82. DOI: 10.1016/j.margeo.2008.07.005.

Mclaren, I. (1960). "On the origin of the Caspian and Bailan Seals and the paleoclimatological implication". In: *American Journal of Science* 258, pp. 47–65.

Meilijson, A., F. Hilgen, J. Sepúlveda, J. Steinberg, V. Fairbank, R. Flecker, N. D Waldmann, S. A Spaulding, O. M. Bialik, F. G. Boudinot, et al. (2019). "Chronology with a pinch of salt: Integrated stratigraphy of Messinian evaporites in the deep Eastern Mediterranean reveals long-lasting halite deposition during Atlantic connectivity". In: *Earth-Science Reviews*.

Meisch, C. (2000). *Crustacea: Ostracoda. Süßwasserfauna von Mitteleuropa*. Spektrum Akademischer Verlag, Heidelburg.

Mertens, K. N., S. Ribeiro, I. Bouimetarhan, H. Caner, N. Combourieu-Nebout, B. Dale, A. De Vernal, M. Ellegaard, M. V. Filipova-Marinova, A. Godhe, E. Goubert, K. Grøsfjeld, U. Holzwarth, U. Kotthoff, S. A. G. Leroy, L. Londeix, F. Marret, K. Matsuoka, P. J. Mudie, L. Naudts, J. L. Peña-Manjarrez, A. Persson, S. M. Popescu, V. Pospelova, F. Sangiorgi, M. T. J. Van der Meer, A. Vink, K. A. F. Zonneveld, D. Vercauteren, J. Vlassenbroeck, and S. Louwye (2009). "Process length variation in cysts of a dinoflagellate, Lingulodinium machaerophorum, in surface sediments: Investigating its potential as salinity proxy". In: *Marine Micropaleontology* 70.1-2, pp. 54–69. DOI: 10.1016/j.marmicro.2008.10.004.

Mertens, K. N., L. R. Bradley, Y. Takano, P. J. Mudie, F. Marret, A. E. Aksu, R. N. Hiscott, T. J. Verleye, E. A. Mousing, L. L. Smyrnova, S. Bagheri, M. Mansor, V. Pospelova, and K. Matsuoka (2012). "Quantitative estimation of Holocene surface salinity variation in the Black Sea using dinoflagellate cyst process length". In: *Quaternary Science Reviews* 39, pp. 45–59. DOI: 10.1016/j.quascirev.2012.01.026.

Micklin, P. (2010). "The past, present, and future Aral Sea". In: *Lakes & Reservoirs: Research & Management* 15.3, pp. 193–213. DOI: 10.1111/j.1440-1770.2010.00437.x.

Mikhailov, V. O., L. V. Panina, R. Polino, N. V. Koronovsky, E. A. Kiseleva, N. V. Klavdieva, and E. I. Smolyaninova (1999). "Evolution of the North Caucasus foredeep: Constraints based on the analysis of subsidence curves". In: *Tectonophysics* 307.3-4, pp. 361–379. DOI: 10.1016/S0040-1951(99)00053-0.

Mischke, S., C. Zhang, and A. Börner (2008). "Bias of ostracod stable isotope data caused by drying of sieve residues from water". In: *Journal of Paleolimnology* 40.1, pp. 567–575.

Mitchell, J. and R. Westaway (1999). "Chronology of Neogene and Quaternary uplift and magmatism in the Caucasus : constraints from K – Ar dating of volcanism in Armenia". In: *Tectonophysics* 304.3, pp. 157–186.

Modestou, S., D. Simon, M. Gutjahr, A. Marzocchi, T. J. Kouwenhoven, R. M. Ellam, and R. Flecker (2017). "Precessional variability of 87 Sr/ 86 Sr in the late Miocene Sorbas Basin: An

interdisciplinary study of drivers of interbasin exchange". In: *Paleoceanography* 32, pp. 1–22. DOI: 10.1002/2016PA003061.

Molostovsky, E. A. (1997). "Magnetostratigraphy of the Pliocene deposits in Black Sea, Caspian regions and adjacent areas". In: *Geodiversitas* 19.2, pp. 471–495.

Moore, R. C. (1961). "Glossary of morphological terms applied to Ostracoda". In: *Arthropoda* 3, pp. 47–56.

Morkoven, F. P. C. M. van (1962). *Post-Palaeozoic ostracoda; their morphology, taxonomy and economic use; general*.

Mudie, P. J., A. E. Aksu, and D. Yasar (2001). "Late Quaternary dinoflagellate cysts from the Black, Marmara and Aegean seas: Variations in assemblages, morphology and paleosalinity". In: *Marine Micropaleontology* 43.1-2, pp. 155–178. DOI: 10.1016/S0377-8398(01)00006-8.

Mudie, P. J., A. Rochon, A. E. Aksu, and H. Gillespie (2004). "Late glacial, Holocene and modern dinoflagellate cyst assemblages in the Aegean-Marmara-Black Sea corridor: Statistical analysis and re-interpretation of the early Holocene Noah's Flood hypothesis". In: *Review of Palaeobotany and Palynology* 128.1-2, pp. 143–167. DOI: 10.1016/S0034-6667(03)00117-9.

Mudie, P. J., F. Marret, A. Rochon, and A. E. Aksu (2010). "Non-pollen palynomorphs in the Black Sea corridor". In: *Vegetation History and Archaeobotany* 19.5-6, pp. 531–544.

Mudie, P. J., F. Marret, K. N. Mertens, L. Shumilovskikh, and S. A. G. Leroy (2017). "Atlas of modern dinoflagellate cyst distributions in the Black Sea Corridor: From Aegean to Aral Seas, including Marmara, Black, Azov and Caspian Seas". In: *Marine Micropaleontology*. DOI: 10.1016/j.marmicro.2017.05.004.

Müller, D. W. and P. A. Mueller (1991). "Origin and age of the Mediterranean Messinian evaporites: implications from Sr isotopes". In: *Earth and Planetary Science Letters* 107.1, pp. 1–12.

Nakano, T., I. Tayasu, E. Wada, A. Igeta, F. Hyodo, and Y. Miura (2005). "Sulfur and strontium isotope geochemistry of tributary rivers of Lake Biwa: implications for human impact on the decadal change of lake water quality". In: *Science of the total environment* 345.1-3, pp. 1–12.

Neale, J. W. (1988). "Ostracods and palaeosalinity reconstruction". In: *Ostracoda in the earth sciences*, pp. 125–155.

Négrel, P. and S. Roy (1998). "Chemistry of rainwater in the Massif Central (France): A strontium isotope and major element study". In: *Applied Geochemistry* 13.8, pp. 941–952. DOI: 10.1016/S0883-2927(98)00029-8.

Nevesskaya, L. A. (1965). "Late Quaternary Mollusks of the Black Sea, Their Systematics and Ecology". In: *Academy of Science of the USSR, Moscow*, p. 392.

– (2007). "History of the genus Didacna (Bivalvia: Cardiidae)". In: *Paleontological Journal* 41.9, pp. 861–949. DOI: 10.1134/S0031030107090018.

Nevesskaya, L. A., I. A. Goncharova, L. B. Ilyina, N. P Paramonova, S. V. Popov, E. V. Babak, K. G. Bagdasarjan, and A. A. Voronina (1986). "Istorija neogenovych mollyuskov Paratetisa (in Russian)". In: *Paleontol. Inst. In: AN SSSR. Nauka Press, Moscow.*

Nevesskaya, L. A., I. A. Goncharova, L. B. Ilyina, N. P.. Paramonova, and S. O. Khondkarian (2003). "The Neogene Stratigraphic Scale of the Eastern Paratethys". In: *Stratigraphy and Geological Correlation* 11.2, pp. 105–127.

Nier, A. O. (1938). "The isotopic constitution of strontium, barium, bismuth, thallium and mercury". In: *Physical Review* 54.4, p. 275.

Nikishin, A. M., M. V. Korotaev, and A. V. Ershov (2003). "The Black Sea basin : tectonic history and Neogene – Quaternary rapid subsidence modelling". In: *Sedimentary Geology* 156.1-4, pp. 149–168.

Nirel, P. M. and R. Revaclier (1999). "Assessment of sewage treatment plant effluents impact on river water quality using dissolved Rb/Sr ratio". In: *Environmental Science and Technology* 33.12, pp. 1996–2000. DOI: 10.1021/es981097g.

Okay, A. I., A. M. Celal Sengor, and N. Gorur (1994). "Kinematic history of the opening of the Black Sea and its effect on the surrounding regions". In: *Geology* 22.3, pp. 267–270.

Olteanu, R. (1989). "The "Cimpia Moment"(late Miocene, Romania) and the Pannonian-Pontian boundary, defined by ostracods". In: *Journal of Micropalaeontology* 8.2, pp. 239–247.

– (1999a). "Dacian ostracodes". In: *Chronostratigraphie und Neostratotypen, Neogene der Zentrale Paratethys*, 268 –386.

– (1999b). "The Loxoconcha genus (Crustacea, Ostracoda) within Paratethys area, 47-90, I-XXVI, Memoires Inst". In: *Geol. al Romaniei* 37.

Ostlund, H. G. and D. Dyrssen (1986). "Renewal rates of the Black Sea deep water". In: *Proceedings of the chemical and physical oceanography of the Black Sea, International meeting, University of Göteborg, Göteborg, Sweden*.

Özsoy, E. and Ü. Ünlüata (1997). "Oceanography of the Black Sea: A review of some recent results". In: *Earth-Science Reviews* 42.4, pp. 231–272. DOI: 10.1016/S0012-8252(97)81859-4.

Page, A. G. (2004). "Geochemistry and paleoclimate of the Plio-Pleistocene deposits of the Caspian Sea. - Royal Holloway, University of London". PhD thesis. Royal Holloway University of London.

Palmer, M. R. and J. M. Edmond (1989). "The strontium isotope budget of the modern ocean". In: *Earth and Planetary Science Letters* 92.1, pp. 11–26. DOI: 10.1016/0012-821X(89)90017-4.

Palo, J. U. and R. Väinölä (2006). "The enigma of the landlocked Baikal and Caspian seals addressed through phylogeny of phocine mitochondrial sequences". In: *Biological Journal of the Linnean Society* 88.1, pp. 61–72.

Pearce, C. R., I. J. Parkinson, J. Gaillardet, B. Chetelat, and K.W. Burton (2015). "Characterising the stable (δ88/86Sr) and radiogenic (87Sr/86Sr) isotopic composition of strontium in rainwater". In: *Chemical Geology* 409, pp. 54–60. DOI: 10.1016/j.chemgeo.2015.05.010.

Pearson, P. N. and C. E. Burgess (2008). "Foraminifer test preservation and diagenesis : comparison of high latitude Eocene sites". In: *Geological Society, London, Special Publications* 303.1, pp. 59–72.

Pearson, P. N., P. W. Ditch, J. Singano, K. G. Harcourt-brown, C. J. Nicholas, R. K. Olsson, N. J. Shackleton, and M. A. Hall (2001). "Warm tropical sea surface temperatures in the Late Cretaceous and Eocene epochs". In: *Nature* 413.6855, pp. 481–488.

Piper, D Z and S E Calvert (2011). "Holocene and late glacial palaeoceanography and palaeolimnology of the Black Sea : Changing sediment provenance and basin hydrography over the past 20 , 000 years". In: *Geochimica et Cosmochimica Acta* 75.19, pp. 5597–5624. ISSN: 0016-7037. DOI: 10.1016/j.gca.2011.07.016. URL: http://dx.doi.org/10.1016/j.gca.2011.07.016.

Popov, G. I. (1983). *The Pleistocene of the Black Sea-Caspian straits*. Nauka, Moscow.

Popov, S. V., I. G. Shcherba, L. B. Ilyina, L. A. Nevesskaya, N. P. Paramonova, S. O. Khondkarian, and I. Magyar (2006). "Late Miocene to Pliocene palaeogeography of the Paratethys and its relation to the Mediterranean". In: *Palaeogeography, Palaeoclimatology, Palaeoecology* 238.1-4, pp. 91–106. DOI: 10.1016/j.palaeo.2006.03.020.

Popov, S. V., M. P. Antipov, A. S. Zastrozhnov, E. E. Kurina, and T. N. Pinchuk (2010). "Sea level Fluctuations on the Northern Shelf of the Eastern Paratethys in the Oligocene – Neogene". In: *Stratigraphy and Geological Correlation* 18.2, pp. 200–224. DOI: 10.1134/S0869593810020073.

Popov, S. V., Y. V. Rostovtseva, N. Y. Fillippova, L. A. Golovina, E. P. Radionova, I. A. Goncharova, Y. V. Vernyhorova, N. I. Dykan, T. N. Pinchuk, L. B. Iljina, et al. (2016). "Paleontology and stratigraphy of the Middle–Upper Miocene of the Taman Peninsula: Part 1. Description of key sections and benthic fossil groups". In: *Paleontological Journal* 50.10, pp. 1039–1206.

Radionova, E. and L. Golovina (2011). “Upper Maeotian-Lower Pontian "transitional Strata" in the Taman Peninsula: Stratigraphic position and paleogeographic interpretation”. In: *Geologica Carpathica* 62.1, pp. 77–90. DOI: 10.2478/v10096-011-0007-x.

Radionova, E., L. Golovina, N. Filippova, V. Trubikhin, S. Popov, I. Goncharova, Y. Vernigorova, and T. Pinchuk (2012). “Middle-Upper Miocene stratigraphy of the Taman Peninsula, Eastern Paratethys”. In: *Open Geosciences* 4.1, pp. 188–204. DOI: 10.2478/s13533-011-0065-8.

Reid, D. F. and M. I. Orlova (2002). “Geological and evolutionary underpinnings for the success of Ponto-Caspian species invasions in the Baltic Sea and North American Great Lakes”. In: *Canadian Journal of Fisheries and Aquatic Sciences* 59.7, pp. 1144–1158. DOI: 10.1139/f02-099.

Reinhardt, E. G., D. J. Stanley, and R. T. Patterson (1998). “Strontium isotopic-paleontological method as a high-resolution paleosalinity tool for lagoonal environments”. In: *Geology* 26.11, pp. 1003–1006.

Reinhardt, E. G., J. Blenkinsop, and R. T. Patterson (1999). “Assessment of a Sr isotope vital effect (87Sr/86Sr) in marine taxa from Lee Stocking Island , Bahamas”. In: *Geo-Marine Letters* 18, pp. 241–246.

Reynolds, A. D., M. D. Simmons, M. B. J. Bowman, J. Henton, A. C. Brayshaw, A. A. Ali-Zade, I. S. Guliyev, S. F. Suleymanova, E. Z. Ateava, D. N. Mamedova, and R. O. Koshkarly (1998). “Implications of outcrop geology for reservoirs in the neogene productive series: Apsheron Peninsula, Azerbaijan”. In: *AAPG Bulletin* 82.1, pp. 25–49. DOI: 10.1306/1D9BC38B-172D-11D7-8645000102C1865D.

Richards, K., N. S. Bolikhovskaya, M. Robert, S. B. Kroonenberg, S. A. G. Leroy, and J. Athersuch (2014). “Reconstructions of deltaic environments from Holocene palynological records in the Volga delta , northern Caspian Sea”. In: *The Holocene* 24.10, pp. 1226–1252. DOI: 10.1177/0959683614540961.

Richards, K., C. G.C. van Baak, J. Athersuch, T. M. Hoyle, M. Stoica, W. E. N. Austin, A. G. Cage, A. A.H. Wonders, F. Marret, and C. A. Pinnington (2018). “Palynology and micropalaeontology of the Pliocene - Pleistocene transition in outcrop from the western Caspian Sea, Azerbaijan: Potential links with the Mediterranean, Black Sea and the Arctic Ocean?” In: *Palaeogeography, Palaeoclimatology, Palaeoecology* July, pp. 1–25. DOI: 10.1016/j.palaeo.2018.07.018.

Rochon, A., A. de Vernal, J. L. Turon, J. Matthiessen, and M. J Head (1999). “Distribution of recent dinoflagellate cysts in surface sediments from the North Atlantic Ocean and adjacent seas

in relation to sea-surface parameters". In: *American Association of Stratigraphic Palynologists* 35.35, pp. 1–146. DOI: 10.1016/0377-8398(94)00016-G.

Rochon, A., P. J. Mudie, A. E. Aksu, and H. Gillespie (2002). "Pterocysta gen. nov.: A new dinoflagellate cyst from pleistocene glacialstage sediments of the black and Marmara Seas". In: *Palynology* 26.1, pp. 95–105. DOI: 10.1080/01916122.2002.9989568.

Roden, J. S. and J. R. Ehleringer (1999). "Observations of hydrogen and oxygen isotopes in leaf water confirm the Craig-Gordon model under wide-ranging environmental conditions". In: *Plant physiology* 120.4, pp. 1165–1174.

Rodionov, S. N. (1994). *Global and Regional Climate Interaction: The Caspian Sea Experience*. Springer Netherlands, p. 256. ISBN: 9401110743.

Rögl, F. (1997). *Palaeogeographic Considerations for Mediterranean and Parathethys Seaways (Oligocene to Miocene)*. Natural History Museum, pp. 279–310. DOI: 10.2307/41702129.

– (1998). "Palaeogeographic Considerations for Mediterranean and Paratethys Seaways (Oligocene to Miocene)". In: *Annalen des Naturhistorischen Museums in Wien. Serie A für Mineralogie und Petrographie, Geologie und Paläontologie, Anthropologie und Prähistorie* 99.A, pp. 279–310.

– (1999). "Palaeogeographic considerations for Mediterranean and Paratethys seaways". In: *Ann. Naturhist. Mus. Wien* 99A.April, pp. 279–310.

Rohling, E. J. and S. De Rijk (1999). "Holocene Climate Optimum and Last Glacial Maximum in the Mediterranean: the marine oxygen isotope record". In: *Marine Geology* 153.1-4, pp. 57–75.

Rosenthal, Y. and A. Katz (1989). "The applicability of trace elements in freshwater shells for paleogeochemical studies". In: *Chemical Geology* 78.1, pp. 65–76. DOI: 10.1016/0009-2541(89)90052-1.

Rosenthal, Y., C. H. Lear, D. W. Oppo, and B. K. Linsley (2006). "Temperature and carbonate ion effects on Mg/Ca and Sr/Ca ratios in benthic foraminifera: Aragonitic species Hoeglundina elegans". In: *Paleoceanography* 21.1, pp. 1–14. DOI: 10.1029/2005PA001158.

Ross, D. A (1978). "Summary of results of Black Sea drilling". In: *Initial Reports of the Deep Sea Drilling Project* 42.Part 2.

Ross, D. A., P. Stoffers, and E. S. Trimonis (1974). "Black Sea sedimentary framework". In: *Initial reports of the Deep Sea Drilling Project* 42.2, pp. 359–372.

Ross, D. A., Y. P. Neprochnov, E. T. Degens, A. J. Erickson, K. J. Hsu, J. M. Hunt, F. T. Manheim, Jr. Percival, S. F., M. Senalp, P. Stoffers, P. Supko, A. Traverse, E. S. Trimonis, J. L. Usher,

Y. P. Neprochnov, and E. T. Degens (1978a). "Site 379". In: *Initial Reports of the Deep Sea Drilling Project* 42.Part 2, pp. 29–118.

– (1978b). "Site 380". In: *Initial reports of the Deep Sea Drilling Project* 42.Part 2, pp. 119–291.

Rouchy, J. M., F. Orszag-Sperber, M. M. Blanc-Valleron, C. Pierre, M. Rivière, N. Combourieu-Nebout, and I. Panayides (2001). "Paleoenvironmental changes at the Messinian–Pliocene boundary in the eastern Mediterranean (southern Cyprus basins): significance of the Messinian Lago-Mare". In: *Sedimentary Geology* 145.1-2, pp. 93–117.

Roveri, M., R. Flecker, W. Krijgsman, J. Lofi, S. Lugli, V. Manzi, F. J. Sierro, A. Bertini, A. Camerlenghi, G. De Lange, R. Govers, F. J. Hilgen, C. Hubscher, P. T. Meijer, and M. Stoica (2014). "The Messinian Salinity Crisis: Past and future of a great challenge for marine sciences". In: *Marine Geology* 352, pp. 25–58. DOI: 10.1016/j.margeo.2014.02.002.

Ryan, W. B. F. (1997). "An aprupt drowning of the Black Sea shelf". In: *Marine Geology* 138, pp. 119–126.

Ryan, W. B. F., C. O. Major, G. Lericolais, and S. L. Goldstein (2003). "Catastrophic flooding of the Black Sea". In: *Annual Review of Earth and Planetary Sciences* 31.1, pp. 525–554.

Sachse, D., J. Radke, and G. Gleixner (2006). "δD values of individual n-alkanes from terrestrial plants along a climatic gradient - Implications for the sedimentary biomarker record". In: *Organic Geochemistry* 37.4, pp. 469–483. DOI: 10.1016/j.orggeochem.2005.12.003.

Saintot, A. and J. Angelier (2000). "Plio-Quaternary paleostress regimes and relation to structural development in the Kertch–Taman peninsulas (Ukraine and Russia)". In: *Journal of structural geology* 22.8, pp. 1049–1064.

Sanders, C. A. E., P. A. M. Andriessen, and S. A. P. L Cloetingh (1999). "Life cycle of the East Carpathian orogen: Erosion history of a doubly vergent critical wedge assessed by fission track thermochronology". In: *Journal of Geophysical Research: Solid Earth* 104.B12, pp. 29095–29112.

Schettler, G., H. Oberhänsli, G. Stulina, A. A. Mavlonov, and R. Naumann (2013). "Hydrochemical water evolution in the Aral Sea Basin . Part I : Unconfined groundwater of the Amu Darya Delta – Interactions with surface waters". In: *Journal of Hydrology* 495, pp. 267–284. DOI: 10.1016/j.jhydrol.2013.03.044.

Scheuvens, D., L. Schütz, K. Kandler, M. Ebert, and S. Weinbruch (2013). "Bulk composition of northern African dust and its source sediments - A compilation". In: *Earth-Science Reviews* 116.1, pp. 170–194. DOI: 10.1016/j.earscirev.2012.08.005.

Schneider, G. F. (1949). “Miotsenovaya fauna ostrakod Kavkaza i Kryma [Miocene ostracod fauna of Caucasus and Crimea]”. In: *Microfauna of oil deposits of the USSR (in Russian)* 11, pp. 89–182.

Schrader, H. J. (1978). “Quaternary through Neogene history of the Black Sea, deduced from the paleoecology of diatoms, silicoflagellates, ebridians, and chrysomonads”. In: *Initial reports of the Deep Sea Drilling Project, Volume 42, Part 2*, pp. 789–901.

– (1979). “Quaternary Paleoclimatology of the Black Sea basin”. In: *Sedimentary Geology* 23.1-4, pp. 165–180. DOI: 10.1016/0037-0738(79)90013-7.

Schrag, D. P., D. J. DePaolo, and F. M. Richter (1995). “Reconstructing past sea surface temperatures: Correcting for diagenesis of bulk marine carbonate”. In: *Geochimica et Cosmochimica Acta* 59.11, pp. 2265–2278.

Scotese, C. R. (2016). “PALEOMAP PaleoAtlas for GPlates and the PaleoData Plotter Program, PALEOMAP Project”. In: *See http://www. earthbyte. org/paleomap-paleoatlas-for-gplates (accessed 17 October 2017)*.

Selifonova, J. P. (2008). “Functioning of the Sea of Azov Ecosystem”. In: *Inland Water Biology* 1.3, pp. 199–203. DOI: 10.1134/S1995082908030012.

Sexton, P. F., P. A. Wilson, and P. N. Pearson (2006). “Microstructural and geochemical perspectives on planktic foraminiferal preservation: “Glassy” versus “Frosty””. In: *Geochemistry, Geophysics, Geosystems* 7.12. DOI: 10.1029/2006GC001291.

Shackleton, N. (1967). “Oxygen isotope analyses and Pleistocene temperatures re-assessed”. In: *Nature* 215.5096, p. 15.

Shiklomanov, I. A., V. Georgievski, and Z. D. Kopaliani (1995). “Water balance of the Caspian Sea and reasons of water level rise in the Caspian Sea”. In: *Paris, UNESCO, Intergovernmental Oceanographic Commission, Workshop Report*. Vol. 28, pp. 1–27.

Shkatova, V. K. (2010). “Paleogeography of the Late Pleistocene Caspian Basins: Geochronometry, paleomagnetism, paleotemperature, paleosalinity and oxygen isotopes”. In: *Quaternary International* 225.2, pp. 221–229.

Shumilovskikh, L. S., F. Marret, D. Fleitmann, H. W. Arz, N. Nowaczyk, and H. Behling (2013). “Marine Micropaleontology Eemian and Holocene sea-surface conditions in the southern Black Sea : Organic-walled dinoflagellate cyst record from core 22-GC3”. In: *Marine Micropaleontology* 101, pp. 146–160. DOI: 10.1016/j.marmicro.2013.02.001.

Singer, T., A. Zobeck, L. Poberezsky, and E. Argaman (2003). "The PM10 and PM 2.5 dust generation potential of soils / sediments in the Southern Aral Sea Basin , Uzbekistan". In: *Journal of Arid Environment* 54, pp. 705–728. DOI: 10.1006/jare.2002.1084.

Sokac, A. (1989). "Pontian ostracod fauna in the Pannonian Basin". In: *Chronostratigraphie und Neostratotypen, Bd* 8, pp. 672–721.

Soliman, A. and J. B. Riding (2017). "Late Miocene (Tortonian) gonyaulacacean dinoflagellate cysts from the Vienna Basin , Austria". In: *Review of Palaeobotany and Palynology* 244, pp. 325–346. ISSN: 0034-6667. DOI: 10.1016/j.revpalbo.2017.02.003.

Stein, M., A. Starinsky, A. Katz, S. L. Goldstein, M. Machlus, and A. Schramm (1997). "Strontium isotopic, chemical, and sedimentological evidence for the evolution of Lake Lisan and the Dead Sea". In: *Geochimica et Cosmochimica Acta* 61.18, pp. 3975–3992. DOI: 10.1016/S0016-7037(97)00191-9.

Steininger, F. F. and F. Rögl (1984). "Paleogeography and palinspastic reconstruction of the Neogene of the Mediterranean and Paratethys". In: *Geological Society, London, Special Publications*.

Stoica, M., I. Laz, W. Krijgsman, I. Vasiliev, D. Jipa, and A. Floroiu (2013). "Paleoenvironmental evolution of the East Carpathian foredeep during the late Miocene – early Pliocene (Dacian Basin ; Romania)". In: *Global and Planetary Change journal* 103, pp. 135–148. DOI: 10.1016/j.gloplacha.2012.04.004.

Stoica, M., W. Krijgsman, A. Fortuin, and E. Gliozzi (2016). "Paratethyan ostracods in the Spanish Lago-Mare: More evidence for interbasinal exchange at high Mediterranean sea level". In: *Palaeogeography, Palaeoclimatology, Palaeoecology* 441, pp. 854–870. DOI: 10.1016/j.palaeo.2015.10.034.

Stuiver, M. (1970). "Oxygen and carbon isotope ratios of fresh-water carbonates as climatic indicators". In: *Journal of Geophysical Research* 75.27, pp. 5247–5257.

Sütő-Szentai, M. (2010). "Definition and description of new dinoflagellate genus, species and subspecies from the Pannonian Stage (Hungary)". In: *Acta Naturalia Pannonica* 1.2, pp. 223–239.

Svendsen, J. I., H. Alexanderson, V. I. Astakhov, I. Demidov, A. Dowdeswell, S. Funder, V. Gataullin, M. Henriksen, C. Hjort, M. Houmark-nielsen, H. W. Hubberten, M. Jakobsson, K. H. Kjær, E. Larsen, H. Lokrantz, J. Pekka, A. Lys, J. Mangerud, A. Matiouchkov, A. Murray, M. Per, F. Niessen, O. Nikolskaya, L. Polyak, M. Saarnisto, C. Siegert, M. J. Siegert, R. F.

Spielhagen, and R. Stein (2004). “Late Quaternary ice sheet history of northern Eurasia”. In: *Quaternary Science Reviews* 23, pp. 1229–1271. DOI: 10.1016/j.quascirev.2003.12.008.

Svitoch, A. A. (2008). “Quaternary Paleogeography of the Azov–Black Sea Basin”. In: *The Black Sea Environment*. Ed. by Andrey G. Kostianoy and Alexey N. Kosarev. Berlin, Heidelberg: Springer Berlin Heidelberg, pp. 31–46. DOI: 10.1007/698_5_079.

– (2010). “The Neoeuxinian basin of the Black Sea and the Khvalinian transgression of the Caspian Sea”. In: *Quaternary International* 225.2, pp. 230–234. ISSN: 1040-6182. DOI: 10.1016/j.quaint.2009.03.005. URL: http://dx.doi.org/10.1016/j.quaint.2009.03.005.

– (2013). “The Pleistocene Manych straits: Their structure, evolution and role in the Ponto-Caspian basin development”. In: *Quaternary International* 302, pp. 101–109. DOI: 10.1016/j.quaint.2012.03.015.

Svitoch, A. A., A. O. Selivanov, and T. A. Yanina (2000). “Paleohydrology of the Black Sea Pleistocene Basins”. In: *Water Resources* 27.6, pp. 594–603. ISSN: 00978078. DOI: 10.1023/A:1026661801941.

System, Venice (1958). “Symposium on the Classification of Brackish Waters, Venice, April 8-14”. In: *Archives Oceanography and Limnology* 11, pp. 1–248.

Tari, G., M. Fallah, W. Kosi, J. Floodpage, J. Baur, and Z. Bati (2015). “Is the impact of the Messinian Salinity Crisis in the Black Sea comparable to that of the Mediterranean ?” In: 66, pp. 135–148. DOI: 10.1016/j.marpetgeo.2015.03.021.

Tesakov, A. S., A. E. Dodonov, V. V. Titov, and V. M. Trubikhin (2007). “Plio-Pleistocene geological record and small mammal faunas, eastern shore of the Azov Sea, Southern European Russia”. In: *Quaternary International* 160.1, pp. 57–69.

Thirlwall, M. F. (1991). “Long-term reproducibility of multicollector Sr and Nd isotope ratio analysis”. In: *Chemical Geology: Isotope Geoscience section* 94.2, pp. 85–104.

Topper, R. P. M., R. Flecker, P. T. Meijer, and M. J. R. Wortel (2011). “A box model of the Late Miocene Mediterranean Sea: Implications from combined 87Sr/86Sr and salinity data”. In: *Paleoceanography* 26.September, PA3223. DOI: 10.1029/2010pa002063.

Torres, M.A (2007). “The petroleum geology of Western Turkmenistan: the Gograndag-Okarem Province”. In: *Oil and Gas of the Greater Caspian Area*, pp. 109–132. ISBN: 9780769531588. DOI: 10.1109/SUTC.2008.30.

Turpen, J. and R. W. Angell (1971). “Aspects of Molting and Calcification in the Ostracod Heterocypris”. In: *Reference : Biol. Bull* 140, pp. 331–338. DOI: 10.2307/1540077.

Väinölä, R. (1995). “Origin and Recent Endemic Divergence of a Caspian Mysis Species Flock with Affinities to the "Glacial Relict" Crustaceans in Boreal Lakes”. In: *Evolution* 46.December 1995, pp. 1215 –1223. DOI: 10.2307/2410446.

Väinölä, R., J. K. Vainio, and J. U. Palo (2001). “Phylogeography of “ glacial relict ” Gammaracanthus (Crustacea , Amphipoda) from boreal lakes and the Caspian and White seas”. In: *Canadian Journal of Fisheries and Aquatic Sciences,* 58, pp. 2247–2257. DOI: 10.1139/cjfas-58-11-2247.

van Baak, C. G. C. (2015). “Mediterranean-Paratethys connectivity during the late Miocene to Recent: Unravelling geodynamic and paleoclimatic causes of sea-level change in semi-isolated basins”. PhD thesis. Utrecht University. ISBN: 9789062663996.

van Baak, C. G. C., I. Vasiliev, M. Stoica, K. F. Kuiper, A. M. Forte, E. Aliyeva, and W. Krijgsman (2013). “A magnetostratigraphic time frame for Plio-Pleistocene transgressions in the South Caspian Basin , Azerbaijan”. In: *Global and Planetary Change* 103, pp. 119–134. DOI: 10.1016/j.gloplacha.2012.05.004.

van Baak, C. G. C., I. Vasiliev, D. V. Palcu, and M. J. Dekkers (2016a). “A Greigite-Based Magnetostratigraphic Time Frame for the Late Miocene to Recent DSDP Leg 42B Cores from the Black Sea”. In: *Frontiers in Earth Sciences* 4.May, pp. 1–18. DOI: 10.3389/feart.2016.00060.

van Baak, C. G. C., M. Stoica, A. Grothe, E. Aliyeva, and W. Krijgsman (2016b). “Mediterranean-Paratethys connectivity during the Messinian salinity crisis : The Pontian of Azerbaijan”. In: *Global and Planetary Change* 141, pp. 63–81. DOI: 10.1016/j.gloplacha.2016.04.005.

van Baak, C. G. C., W. Krijgsman, I. Magyar, O. Sztanó, L.A. Golovina, A. Grothe, T. M. Hoyle, O. Mandic, I. S. Patina, S. V. Popov, E. P. Radionova, M. Stoica, and I. Vasiliev (2017). “Paratethys response to the Messinian salinity crisis”. In: *Earth-Science Reviews* 172.February, pp. 193–223. DOI: 10.1016/j.earscirev.2017.07.015.

van Baak, C. G. C., A. Grothe, K. Richards, M. Stoica, E. Aliyeva, G. R. Davies, K. F. Kuiper, and W. Krijgsman (2019). “Flooding of the Caspian Sea at the intensification of Northern Hemisphere Glaciations”. In: *Global and Planetary Change* 174.January, pp. 153–163. DOI: 10.1016/j.gloplacha.2019.01.007.

Varushchenko, S. I., A. N. Varushchenko, R. K. Klige, and R. K. Klige. *Changes in the regime of the Caspian Sea and closed basins in time*. Vol. 240. Nauka, Moscow.

Vasiliev, I., G. J. Reichart, G. R. Davies, W. Krijgsman, and M. Stoica (2010). “Strontium isotope ratios of the Eastern Paratethys during the Mio-Pliocene transition; Implications for interbasinal

connectivity". In: *Earth and Planetary Science Letters* 292.1-2, pp. 123–131. DOI: 10.1016/j.epsl.2010.01.027.

Vasiliev, I., A. G. Iosifidi, A. N. Khramov, W. Krijgsman, K. Kuiper, C. G. Langereis, V. V. Popov, M. Stoica, V. A. Tomsha, and S. V. Yudin (2011). "Magnetostratigraphy and radio-isotope dating of upper Miocene-lower Pliocene sedimentary successions of the Black Sea Basin (Taman Peninsula, Russia)". In: *Palaeogeography, Palaeoclimatology, Palaeoecology* 310.3-4, pp. 163–175. DOI: 10.1016/j.palaeo.2011.06.022.

Vasiliev, I., G. J. Reichart, and W. Krijgsman (2013). "Impact of the Messinian Salinity Crisis on Black Sea hydrology-Insights from hydrogen isotopes analysis on biomarkers". In: *Earth and Planetary Science Letters* 362, pp. 272–282. DOI: 10.1016/j.epsl.2012.11.038.

Vasiliev, I., G. J. Reichart, A. Grothe, J. S. Sinninghe Damste, W. Krijgsman, F. Sangiorgi, J. W. H. Weijers, and L. van Roij (2015). "Recurrent phases of drought in the upper Miocene of the Black Sea region". In: *Palaeogeography, Palaeoclimatology, Palaeoecology* 423, pp. 18–31. DOI: 10.1016/j.palaeo.2015.01.020.

Vasiliev, I., C. G. C van Baak, G. J. Reichart, T. Hoyle, and W. Krijgsman (2017). "Marine influx hits Caspian Sea at the Pleistocene transition". In: *EGU General Assembly Conference Abstracts*. Vol. 19, p. 13557.

Veizer, J. (1989). "Strontium isotopes in seawater through time". In: *Annual Review of Earth and Planetary Sciences* 17.1, pp. 141–167.

Vekua, M. L. (1975). "The ostracods of the Kimmerian and Kujalinikian deposits of Abkhazia and their stratigraphic significance". In: *Metzniereba, Tibilisi*.

Verleye, T. J., K. N. Mertens, S. Louwye, and H. W. Arz (2009). "Holocene salinity changes in the southwestern Black Sea: a reconstruction based on dinoflagellate cysts". In: *Palynology* 33.1, pp. 77–100.

Viehberg, F. A. and F. Mesquita-Joanes (2012). "Ostracoda as proxies for Quaternary climate change". In: *Developments in Quaternary Science* 17, pp. 47–64.

Vitòria, L., N. Otero, A. Soler, and À. Canals (2004). "Fertilizer Characterization: Isotopic Data (N, S, O, C, and Sr)". In: *Environmental Science & Technology* 38.12, pp. 3254–3262. DOI: 10.1021/es0348187.

von Grafenstein, U., H. Erlenkeuser, and A. Brauer (1999). "A Mid-European Decadal Isotope-Climate Record from 15 , 500 to 5000 Years B . P ." In: *Science* 284.JUNE 1999, pp. 1654–1658.

Wall, D. and B. Dale (1966). ""Living Fossils"in Western Atlantic Plankton". In: *Nature* 211.5053, pp. 1025–1026.

– (1973). "Paleosalinity relationships of dinoflagellates in the late quaternary of the black sea—a summary". In: *Geoscience and Man* 7.1, pp. 95–102. DOI: 10.1080/00721395.1973.9989739.

Wall, D., B. Dale, and K. Harada (1973). "Descriptions of new fossil dinoflagellates from the Late Quaternary of the Black Sea". In: *Micropaleontology* 19.1, pp. 18–31.

Wegwerth, A., O. Dellwig, J. Kaiser, G. Ménot, E. Bard, L. Shumilovskikh, B. Schnetger, I. C Kleinhanns, M. Wille, and H. W. Arz (2014). "Meltwater events and the Mediterranean reconnection at the Saalian – Eemian transition in the Black Sea". In: *Earth and Planetary Science Letters* 404, pp. 124–135. DOI: 10.1016/j.epsl.2014.07.030.

Widory, D., W. Kloppmann, L. Chery, J. Bonnin, H. Rochdi, and J. L. Guinamant (2004). "Nitrate in groundwater: an isotopic multi-tracer approach". In: *Journal of contaminant hydrology* 72.1-4, pp. 165–188.

Yanchilina, A. G., W. B. F. Ryan, J. F. Mcmanus, P. Dimitrov, D. Dimitrov, K. Slavova, and M. Filipova-marinova (2017). "Compilation of geophysical , geochronological , and geochemical evidence indicates a rapid Mediterranean-derived submergence of the Black Sea ' s shelf and subsequent substantial salini fi cation in the early Holocene". In: *Marine Geology* 383, pp. 14–34. DOI: 10.1016/j.margeo.2016.11.001.

Yanina, T. A. (2012). "Correlation of the Late Pleistocene paleogeographical events of the Caspian Sea and Russian Plain". In: *Quaternary International* 271, pp. 120–129. DOI: 10.1016/j.quaint.2012.06.003.

Yanina, T. A (2013). "Biostratigraphy of the Middle and Upper Pleistocene of the Caspian Region". In: *Quaternary International* 284, pp. 85–97. DOI: 10.1016/j.quaint.2012.02.008.

Yanina, T. A. (2014). "The Ponto-Caspian region: Environmental consequences of climate change during the Late Pleistocene". In: *Quaternary International* 345, pp. 88–99. DOI: 10.1016/j.quaint.2014.01.045.

Yanina, T. A. and A. A. Svitoch (1990). "The malacofauna of the reference sections of the Dagestan". In: *Geology and Geomorphology of the Caspian Sea. Nauka, Moscow (in Russian)*, pp. 41–51.

Yanina, T. A., V. Sorokin, Y. Bezrodnykh, and B. Romanyuk (2017). "Late Pleistocene climatic events re fl ected in the Caspian Sea geological history (based on drilling data)". In: *Quaternary International*, pp. 1–12. DOI: 10.1016/j.quaint.2017.08.003.

Yanko-Hombach, V., P. J. Mudie, S. Kadurin, and E. Larchenkov (2014). “Holocene marine transgression in the Black Sea : New evidence from the northwestern Black Sea shelf”. In: *Quaternary International* 345, pp. 100–118. DOI: 10.1016/j.quaint.2013.07.027.

Yanko-Hombach, V. V., T. A. Yanina, and I. Motnenko (2013). “Neopleistocene stratigraphy of the ponto-caspian corridors”. In: *IGCP 610*. LTD" Sachino".

Yanko-Hombach, Valentina, Allan S Gilbert, and Pavel Dolukhanov (2007). “Controversy over the great flood hypotheses in the Black Sea in light of geological , paleontological , and archaeological evidence”. In: *Quaternary International* 168, pp. 91–113. DOI: 10.1016/j.quaint.2006.08.004.

Yassini, I. (1986). “Ecology, paleoecology and stratigraphy of ostracodes from Upper Pliocene and Quaternary deposits of the South Caspian Sea, North Iran”. In: *Lake Illawarra Management Committee*, pp. 1–78.

Zastrozhnov, A., G. Danukalova, M. Golovachev, V. Titov, E. Osipova, A. Simakova, A. Yakovlev, T. Yakovleva, G. Aleksandrova, A. Shevchenko, et al. (2018). “Biostratigraphical investigations as a tool for palaeoenvironmental reconstruction of the Neopleistocene (Middle-Upper Pleistocene) at Kosika, Lower Volga, Russia”. In: *Quaternary International*.

Zektzer, I. S., V. A. Ivanov, and A. V. Meskheteli (1973). “The problem of direct groundwater discharge to the seas”. In: *Journal of Hydrology* 20.1, pp. 1–36. DOI: 10.1016/0022-1694(73)90042-5.

Zenkevitch, L. (1963). “The Caspian Sea”. In: *Biology of the Seas of the USSR*, pp. 538–645.

Zonneveld, K. A. F., F. Marret, R. Verreussel, K. Bogus, S. Bonnet, I. Bouimetarhan, E. Crouch, A. De Vernal, R. Elshanawany, L. Edwards, O. Esper, S. Forke, K. Grøsfjeld, M. Henry, U. Holzwarth, J. F. Kielt, S.Y. Kim, S. Ladouceur, D. Ledu, L. Chen, A. Limoges, L. Londeix, S. H. Lu, M. S. Mahmoud, G. Marino, K. Matsuoka, J. Matthiessen, D. C. Mildenhal, P. J. Mudie, H. L. Neil, V. Pospelova, Y. Qi, T. Radi, T. Richerol, A. Rochon, F. Sangiorgi, S. Solignac, J. L. Turon, T. J. Verleye, Y. Wang, Z. Wang, and M. D. Young (2013). “Atlas of modern dinoflagellate cyst distribution based on 2405 data points”. In: *Review of Palaeobotany and Palynology* 191, pp. 1–197. DOI: 10.1016/j.revpalbo.2012.08.003.

Zubakov, V A (1988). “Climatostratigraphic scheme of the Black Sea pleistocene and its correlation with the oxygen-isotope scale and glacial events”. In: *Quaternary Research* 29.1, pp. 1–24. ISSN: 10960287. DOI: 10.1016/0033-5894(88)90067-1.

Şengör, A. M. C. and N. Canitez (1982). “The North Anatolian fault”. In: *Alpine-Mediterranean geodynamics*. Ed. by H. Berckhemer and K. Hsü. American Geophysical Union (AGU), pp. 205–216. ISBN: 9781118670248. DOI: 10.1029/GD007p0205.

Şengör, A. M. C., O. Tüysüz, C. İmren, M. Sakınç, H. Eyidoğan, N. Görür, X. Le Pichon, and C. Rangin (2005). “The North Anatolian fault: A new look”. In: *Annual Review of Earth and Planetary Sciences* 33.1, pp. 37–112. DOI: 10.1146/annurev.earth.32.101802.120415.

APPENDIX A

Letters of permission

To whom it may concern,

I, Elisabeth L. Jorissen, hereby give permission to Diksha Bista to use in her thesis the sedimentological log of the Zheleznyi Rog section (Taman Peninsula, Russia), generated by the palaeomagnetism research team of Utrecht University in August 2015. We are colleagues within the PRIDE ITN, who actively collaborated through this project. The integrated study was carried out in order to determine the forcing mechanisms driving the cyclic lithological changes observed along the 100 m long Pontian interval. Specifically, I logged the section by performing detailed sedimentological observations and provided the 12 sediment samples used by Diksha for Sr isotopic analyses.

Contact email: e.l.jorissen@uu.nl

Sincerely,

Elisabeth L. Jorissen

To whom it may concern,

We, Lea Rausch and Prof. Dr. Marius Stoica, hereby give permission to Diksha Bista to use data generated by me for her thesis. Specifically, we counted 46 samples of washed sediment for ostracod analysis. Both Marius Stoica and myself have been working with Neogene ostracod assemblages from the Paratethys for an extended period of time as proved by our publication record.

After analysing the material, I explained the results to Diksha and pointed out the important details that made us consider the age and the paleoenvironmental signature of the assemblage implicated by certain species. We provided Diksha with a distribution table and we together discussed the potential implications of this data, following which Diksha wrote up the results for publication and I assessed the text for accuracy. These data were generated for the purpose of indicating the age of the Tsikhisperdi-and the Khvarbati section in the Rioni subbasin in Georgia. We are colleagues who actively collaborate through the PRIDE ITN.

Contact email: leanrausch@gmail.com

Sincerely,

Lea Rausch and **Prof. Marius Stoica**

Appendix B

The content of this appendix belong to Chapter 3.

Table B.1: Site locations, temperature, salinity and Sr isotopic ratio with 2σ standard error of the fluvial sources in the region.

Field ID	**Location**	**Lat [N]**	**long [E]**	**Temp (°C)**	**Sal (g/kg)**	**$^{87}Sr/^{86}Sr$**	**Error (x 10^{-6})**
St. 003	Kura delta	39.40502	49.36538			0.708182	4.81
St. 004	Kura upstream	40.12028	48.08528			0.707688	4.39
St. 007	Dnieper river	46.68881	32.81876	18.2	0.31	0.710220	5.33
St. 008	Dnieper delta	46.53733	32.53658			0.710080	4.99
St. 009	Dnieper gulf	46.54662	32.14368	17.5	0.5	0.710060	4.80
St. 011	Chorokhi river	41.60472	41.57611	14.2	0.12	0.705854	4.37
St. 013	Chorokhi upstream	41.59000	41.60194	15.2	0.07	0.705653	4.88
St. 015	Natanebi upstream	41.91167	41.77833	16.5	0.05	0.705481	5.53
St. 016	Natanebi river	41.91222	41.76889	16.2	0.02	0.705702	6.50
St. 017	Enguri river	42.39320	41.56089	20.2	0.12	0.708640	5.11
St. 018	Palliastomi Lake	42.08119	41.70482	21.7	18.68	0.708937	4.29
St. 019	Palliastomi Lake	42.09290	41.70799	19.9	0.75	0.708265	3.53
St. 020	Palliastomi Lake	42.12253	41.73241	19.1	1.39	0.708672	4.42
St. 021	Pichori river	42.13711	41.75948	17.6	0.13	0.707346	5.26
St. 027	Rioni delta	42.19750	41.66222	20.2	0.15	0.708000	14.37
St. 081	Sea of Azov	47.08833	39.24778			0.709178	5.17
St. 082	Don delta	47.11028	39.31222			0.709170	4.84
St. 092	Don upstream	47.22964	40.03950			0.709157	4.82
St.088	Volta delta	45.74874	47.89408			0.708052	4.15
St. 091	Volga upstream	47.01889	47.44667			0.708047	4.35
St. 097	Volga upstream	49.54360	45.08047			0.708055	4.84

TABLE B.2: Site locations, water depth, temperature, salinity and Sr isotopic ratio with 2σ standard error across the Black Sea.

Station Name	**Water depth (m)**	**Lat [N]**	**long [E]**	**Temp (°C)**	**Sal (g/kg)**	**$^{87}Sr/^{86}Sr$**	**Error (x 10^{-6})**
St. 012	0	41.58222	41.56667	22.3	18.72	0.709143	4.7
St. 014	0	41.77250	41.75583	22.2	16.68	0.709128	6.2
St. 022	0	42.12556	41.64944	21.7	17.16	0.709088	3.4
St. 023	0	42.10861	41.67056	22.5	17.56	0.709131	4.1
St. 024	0	42.07250	41.70722	22	17.62	0.709130	4.6
St. 025	0	42.01722	41.75028	19.1	1.31	0.708227	5.5
St. 026	0	42.03454	41.73816	22.7	17.62	0.709134	4.3
St033 Surface	0	44.50848	29.34632	12.77	15.94	0.709152	4.6
St033 Bottom	42.5	44.50848	29.34632	6	18.5	0.709147	5.8
St034 Surface	0	44.82365	29.65432	11.5	14.39	0.709143	5.0
St034 Bottom	23.4	44.82365	29.65432	6.32	18.36	0.709145	5.2
St036 Surface	0	45.03992	30.04095	14.33	12.87	0.709142	4.7
St036 Bottom	34.7	45.03992	30.04095	5.9	18.29	0.709145	4.7
St037 Surface	0	44.67305	29.81687	13.67	16.11	0.709146	4.3
St037 25m	24.7	44.67305	29.81687	7.81	18.11	0.709145	3.8
St037 Bottom	53.5	44.67305	29.81687	6.48	18.4	0.709140	4.7
St038 Surface	0	44.59153	30.10050	14.1	14.97	0.709141	4.8
St038 Bottom	65.3	44.59153	30.10050	6.4	18.41	0.709139	5.6
St039 Surface	0	44.46740	30.31027	14.41	15.46	0.709146	4.4
St039 21m	21	44.46740	30.31027	7.59	17.63	0.709146	5.2
St039 54m	54	44.46740	30.31027	6.75	18.45	0.709149	5.4
St039 78m	78.1	44.46740	30.31027	7.73	18.79	0.709145	4.8
St041 Surface	0	44.34152	30.52328	12.94	17.75	0.709144	4.1
St041 28m	28	44.34152	30.52328	8.42	18.22	0.709138	5.0
St041 60m	60	44.34152	30.52328	7.32	18.53	0.709145	3.4
St041 Bottom	95.6	44.34152	30.52328	8.24	19.11	0.709150	5.0
St043 Surface	0	43.85260	30.05995	13.76	18.01	0.709139	3.7
St043 Bottom	89.6	43.85260	30.05995	7.7	18.65	0.709146	4.4
St047 Surface	0	43.77280	28.73985	15.27	16.5	0.709136	4.5
St047 Bottom	46.1	43.77280	28.73985	8	18.67	0.709141	8.7
St049 Surface	0	42.49305	28.66172	15.47	18.47	0.709144	4.4
St049 500m	500	42.49305	28.66172	8.88	22.03	0.709148	4.4
St049 1000m	1000	42.49305	28.66172	8.96	22.28	0.709147	5.0

Table B.2 Continued:

St052 Surface	0	43.16897	28.98323			0.709140	4.7
St052 1000m	1000	43.16897	28.98323			0.709152	4.1
St053 Surface	0	43.36750	28.81597	16.26	17.94	0.709145	5.6
St053 Bottom	74.8	43.36750	28.81597	7.8	18.58	0.709143	4.6

TABLE B.3: Site locations, water depth, temperature, salinity and Sr isotopic ratio with 2σ standard error across the Caspian Sea.

Station Name	**Water depth (m)**	**Lat [N]**	**long [E]**	**Temp (°C)**	**Sal (g/kg)**	**$^{87}Sr/^{86}Sr$**	**Error (x 10^{-6})**
St059 Surface	0	44.50904	49.99442	21.9	4.8	0.708189	3.6
St059 Bottom	19	44.50904	49.99442			0.708199	5.6
St066 Surface	0	43.75634	50.75752	21.08	10.2	0.708194	4.3
St066 20m	20	43.75634	50.75752			0.708202	5.5
St068 Surface	0	43.72398	50.57025	21.22	10.3	0.708191	4.0
St068 20m	20	43.72398	50.57025			0.708193	5.1
St070 Surface	0	43.59659	50.27940	19.75	11.4	0.708197	4.6
St070 20m	20	43.59659	50.27940			0.708202	5.7
St071 Surface	0	43.23659	51.25584	16.86	11.3	0.708186	7.5
St071 Bottom	20	43.23659	51.25584			0.708197	6.3
St074 Surface	0	43.49924	51.01059	21.53	10.4	0.708186	5.8
St074 20m	20	43.49924	51.01059			0.708197	5.0
St074 20m	20	43.49924	51.01059			0.708196	4.1
A2	0	45.08208	58.39103	25		0.709214	8.4
A49	2.5	45.08334	58.33631	27		0.709212	6.5
A43	12.5	45.07456	58.33446			0.709221	5.5
A61	5	45.10433	58.35492			0.709207	7.1
A63	5	45.09694	58.34881			0.709216	5.4

TABLE B.4: Location and Sr isotopic ratio with 2σ standard error for the Caspian Sea water samples shown in Figure 3.4 in Chapter 3.

Location	**Field ID**	**Water depth (m)**	**Lat [N]**	**long [E]**	**Ost. Species**	**$^{87}Sr/^{86}Sr$**	**Error (x 10^{-6})**
Black Sea	St033	42.5	44.50848	29.34632	Ost	0.709119	14.3
Black Sea	St036	34.7	45.03992	30.04095	*P. granulata*	0.709127	8.2
Black Sea	St036	34.7	45.03992	30.04095	*H. rubra*	0.709138	6.0
Black Sea	St039	78.1	44.46740	30.31027	*P. granulata*	0.709146	6.4
Black Sea	St039	78.1	44.46740	30.31027	*H. rubra*	0.709145	5.2
Black Sea	St043	89.6	43.85260	30.05995	*P. granulata*	0.709139	5.5
Black Sea	St043	89.6	43.85260	30.05995	Foram	0.709142	5.4
Black Sea	St047	46.1	43.77280	28.73985	*Hi. rubra*	0.709137	4.8
Black Sea	St053	74.8	43.36750	28.81597	*P. granulata*	0.709141	5.4
Black Sea	St053	74.8	43.36750	28.81597	Foram	0.709145	4.7
Caspian Sea	St059	8	44.72741	50.22056	*E. naphtascholana*	0.708199	4.6
Caspian Sea	St066	44.3	43.75634	50.75752	*E. naphtascholana*	0.708200	5.7
Caspian Sea	St066	44.3	43.75634	50.75752	*C. acronasuta*	0.708197	3.9
Caspian Sea	St068	101	43.72398	50.57025	*E. naphtascholana*	0.708232	4.6
Caspian Sea	St068	101	43.72398	50.57025	*C. acronasuta*	0.708209	10.3
Caspian Sea	St069	142	43.69947	50.46807	*E. naphtascholana*	0.708353	4.5
Caspian Sea	St069	142	43.69947	50.46807	*C. acronasuta*	0.708233	4.2
Caspian Sea	St069	142	43.69947	50.46807	*C. acronasuta*	0.708222	4.9
Caspian Sea	St070	249	43.59659	50.27940	*E. naphtascholana*	0.708197	4.0
Caspian Sea	St070	249	43.59659	50.27940	*C. acronasuta*	0.708200	4.9
Caspian Sea	St074	41.8	43.49924	51.01059	*E. naphtascholana*	0.708199	5.0
Caspian Sea	St074	41.8	43.49924	51.01059	*C. acronasuta*	0.708211	5.1

FIGURE B.1: Sediment fraction larger than 1 mm from Station 68 and 69 of the Caspian Sea. The fraction contains heavily broken mollusc and gastropods shells indicating sediment reworking.

Appendix C

The content of this appendix belong to Chapter 5.

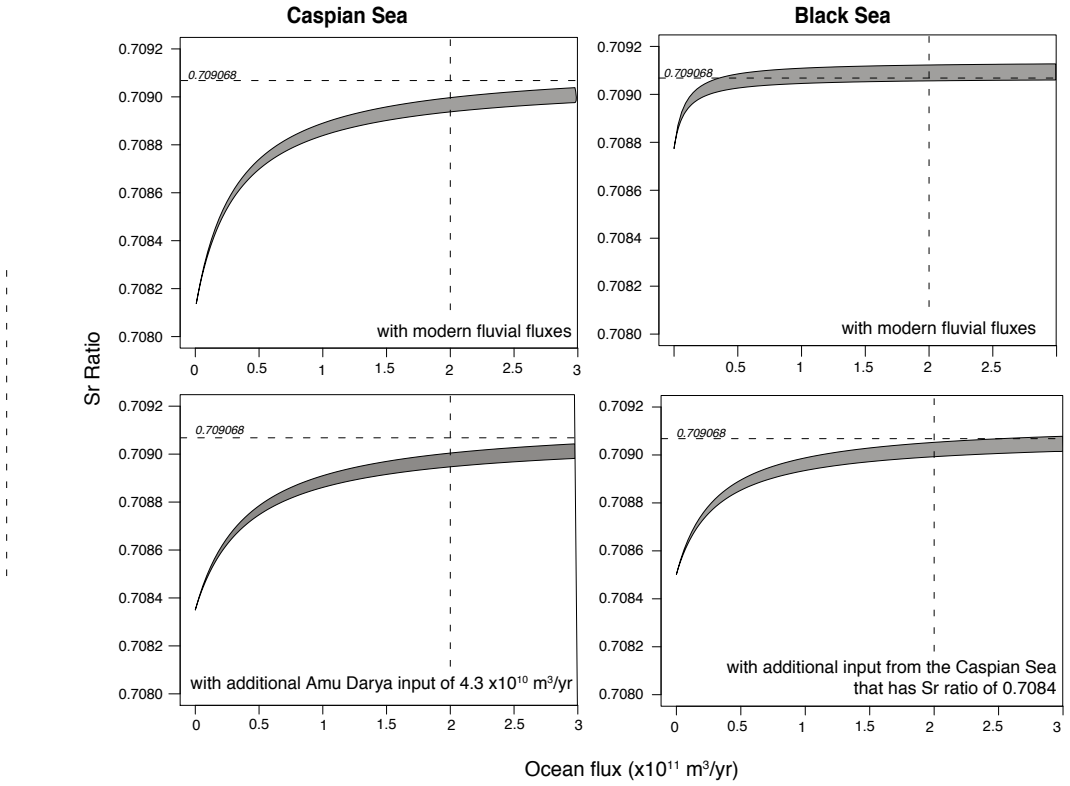

Figure C.1: Sr isotopic ratio of the Caspian Sea (left panel) and the Black Sea (right panel) with increasing oceanic influx. The shaded areas represent the change in Sr isotopic ratio with two ocean $^{87}Sr/^{86}Sr$ between 0.709068 (2.6 Ma) and 0.709137 (1 Ma). Present day value for the oceanic input into the Black Sea (2 x 10^{11} m^3/yr) is shown in dashed vertical line. Black Sea is more sensitive to the oceanic input because the Sr ratio of its fluvial fluxes is higher (0.708774) than that from the Caspian Sea.

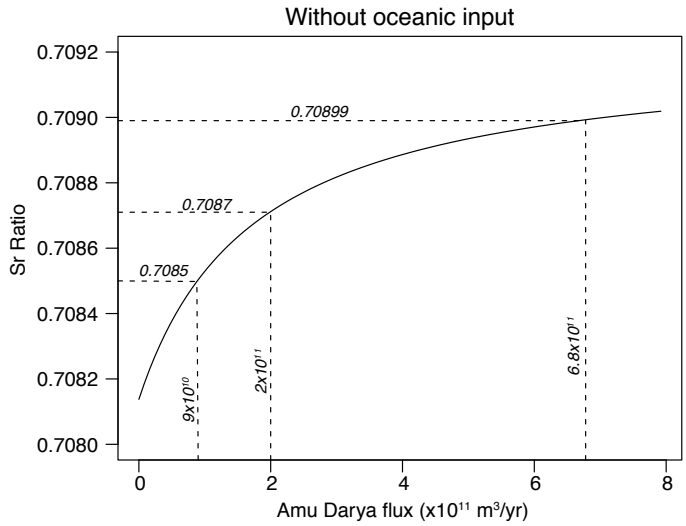

FIGURE C.2: Sr isotopic ratio of the Caspian Sea with increasing Amu Darya influx. Without any oceanic input, about 6.8 x 10^{11} m^3/yr from the Amu Darya is required to increase the Sr ratio to 0.70899.

TABLE C.1: Stratigraphic level, age and Sr isotopic ratio with 2σ standard error for the Goychay section (40.696275 N, 47.762389 E).

Sample ID	**Strat. level (m)**	**Ostracod used**	**Age (Ma)**	**Age error (Ma)**	**$^{87}Sr/^{86}Sr$**	**Error (x 10^{-6})**
GO1	77.5	Few fragments	2.5592	0.0042	0.708427	4.3
GO3	81	Few fragments	2.5565	0.0042	0.708415	8.0
GO4	93.6	4 valves	2.5468	0.0042	0.708419	9.2
GO11	184.3	Few fragments	2.4770	0.0042	0.708455	7.2
GO12	186.7	Few fragments	2.4752	0.0042	0.708490	1.5
GO12.1	187	7 valves	2.4749	0.0042	0.708512	5.3
GO13	191	2 valves + fragments	2.4718	0.0042	0.708505	5.2
GO13	191	Few fragments	2.4718	0.0042	0.708511	5.2
GO14	194.8	2 valves + fragments	2.4689	0.0042	0.708490	6.1
GO15	198	Few fragments	2.4665	0.0042	0.708304	9.0
GO15.1	199	5 valves	2.4657	0.0042	0.708492	4.9
GO15.1	199	5 valves	2.4657	0.0042	0.708492	4.9
GO17	204	7 valves	2.4618	0.0042	0.708489	5.9
GO17	204	1 valve + fragments	2.4618	0.0042	0.708493	4.9
GO18	231	1 valve + fragments	2.4411	0.0042	0.708482	6.1
GO20	242.2	6 valves	2.4325	0.0042	0.708536	5.8
GO27	336.4	Few fragments	2.3600	0.0042	0.708670	4.7
GO27	336.4	Few fragments	2.3600	0.0042	0.708670	4.8

Table C.1 Continued:

GO31	445.5	6 valves	2.2761	0.0042	0.708991	4.5
GO31.1	446.7	Few fragments	2.2752	0.0042	0.708774	3.9
GO31.2	449.25	Few fragments	2.2732	0.0042	0.708792	5.9
GO32.1	454.6	1 valve + fragments	2.2691	0.0042	0.708279	6.7
GO33	460	Few fragments	2.2649	0.0042	0.707804	6.5
GO35.2	509.8	Few fragments	2.2266	0.0042	0.708225	5.7
GO35.3	511.05	5 valves	2.2257	0.0042	0.708477	5.4
GO35.4	511.8	4 valves + fragments	2.2251	0.0042	0.708487	4.8
GO35.5	513.3	2 valves + fragments	2.2239	0.0042	0.708475	4.6
G036	516.3	Few fragments	2.2216	0.0042	0.708511	5.6
GO39	571.9	6 fragments	2.1788	0.0042	0.708099	5.5
GO43	651	3 valves + fragments	2.1270	0.0000	0.708489	4.6
GO45	700	Few fragments	2.0970	0.0107	0.708643	5.2
GO 45.1	703	7 valves	2.0950	0.0107	0.708694	4.1
GO46	703.5	2 valves + fragments	2.0950	0.0107	0.708717	4.3
GO47.1	758	Few fragments	2.0510	0.0109	0.708536	4.6
GO47.2	765	Few fragments	2.0450	0.0109	0.707716	4.9
GO56	849	6 fragments	1.9770	0.0112	0.708592	5.5
GO57	868.1	4 valves + fragments	1.9620	0.0113	0.708543	6.8
GO59	903	6 fragments	1.9362	0.0085	0.708247	7.5
GO70	1074.6	Few fragments	1.8255	0.0042	0.708082	5.7
GO75	1099	Few fragments	1.8097	0.0036	0.708021	5.8
GO96	1182.9	2 valves + fragments	1.7592	0.0024	0.708005	6.8
GO96	1182.9	1 valves + fragments	1.7592	0.0024	0.708010	7.4
G0104	1305.8	Few fragments	1.6890	0.0026	0.708018	4.3
G0104	1305.8	Few fragments	1.6890	0.0026	0.708017	7.5
G0108	1360.5	Few fragments	1.6577	0.0027	0.708059	7.1
GO120	1720	Few fragments	1.4523	0.0033	0.708224	5.1
GO126	1902.7	Few fragments	1.3479	0.0036	0.708324	5.3

TABLE C.2: Stratigraphic level, age and Sr isotopic ratio for the Karagoush Mountain section (40.240633 N, 49.54445 E; Page, 2004). Age for each sample was calculated in this study based on tentative tie-points provided by Page, 2004. No measurement errors for Sr isotopic ratios were provided by Page (2004).

Sample ID	**Strat. level (m)**	**Age (Ma)**	**$^{87}Sr/^{86}Sr$**
K006	6.5	2.00	0.708500
K013	15.8	1.98	0.708510
K018	22.2	1.97	0.708500
K026	32.3	1.95	0.708480
K029	35.3	1.94	0.708470
K031	37.1	1.94	0.708480
K066	69.6	1.87	0.708480
K070	73.5	1.86	0.708460
K083	84.7	1.83	0.708470
K100	99.6	1.80	0.708450
K106	103.9	1.79	0.708470
K108	105.6	1.79	0.708460
K116	112.3	1.77	0.708540
K120	115.6	1.77	0.708450
K137	129.8	1.74	0.708510
K138	130.6	1.73	0.708510
K152	152.2	1.69	0.708430
K155	155.8	1.68	0.708550
K157	158.2	1.67	0.708540
K163	165.4	1.66	0.708630
K164	166.6	1.66	0.708630
K168	172	1.64	0.708480
K172	176.2	1.63	0.708480
K194	201.6	1.58	0.708550
K199	207.9	1.57	0.708510
K212	223.3	1.53	0.708460
K223	236.3	1.50	0.708470
K225	238.7	1.50	0.708460
K234	248.8	1.48	0.708470
K243	257.9	1.46	0.708480
K244	258.9	1.45	0.708490
K250	265.2	1.44	0.708530
K251	265.5	1.44	0.708620

Table C.2 Continued:

K254	270.9	1.43	0.708450
K255	272.4	1.43	0.708440
K257	275.5	1.42	0.708470
K262	281.7	1.41	0.708470
K263	283.5	1.40	0.708590
K264	285.3	1.40	0.708470
K274	302	1.36	0.708530
K278	308.9	1.35	0.708470
K280	312.2	1.34	0.708590
K283	317.3	1.33	0.708470
K284	318.9	1.32	0.708560
K285	321.6	1.32	0.708490
K310	353.5	1.25	0.708480
K312	356.8	1.24	0.708480
K314	360.2	1.23	0.708470
K316	363.6	1.23	0.708480
K317	365.2	1.22	0.708470
K318	366.9	1.22	0.708490

TABLE C.3: Stratigraphic level, age and Sr isotopic ratio with 2σ standard error for the Guria sections.

Section	**Sample ID**	**Strat. level (m)**	**Ostracod used**	**Age (Ma)**	**$^{87}Sr/^{86}Sr$**	**Error (x10^{-6})**
Tsikhisperdi	KH038	0.25	5 valves + fragments	2.13	0.708510	8.7
Tsikhisperdi	KH040	2.15	5 valves + fragments	2.06	0.708550	6.1
Tsikhisperdi	KH042	3.45	Few fragments	2.01	0.708450	4.5
Tsikhisperdi	KH044	5	5 valves + fragments	1.96	0.708430	5.3
Tsikhisperdi	KH045	5.5	3 valves	1.94	0.708430	1.2
Tsikhisperdi	KH048	7.44	5 valves + fragments	1.87	0.708520	5.7
Tsikhisperdi	KH049	8.3	7 valves	1.84	0.708520	5.7
Khvarbeti	KH025	1.55	5 valves + fragments	1.76	0.708610	5.0
Khvarbeti	KH027	3.25	5 valves + fragments	1.75	0.708563	5.1
Khvarbeti	KH030	6.35	5 valves + fragments	1.74	0.708521	5.1
Khvarbeti	KH030	6.35	5 valves	1.74	0.708523	5.3
Khvarbeti	KH032	15	5 valves + fragments	1.69	0.708490	5.2
Khvarbeti	KH033	18	8 valves	1.68	0.708311	5.5
Khvarbeti	KH033	18	5 valves	1.68	0.708307	9.3
Khvarbeti	KH022	64	6 valves + fragments	1.45	0.708500	5.1
Khvarbeti	KH021	68	4 valves	1.43	0.708500	5.2
Khvarbeti	KH019	76	5 valves + fragments	1.39	0.708680	4.9
Khvarbeti	KH018	79.5	4 valves	1.37	0.708580	8.9
Khvarbeti	KH017	82	5 valves + fragments	1.36	0.708497	5.7
Khvarbeti	KH013	102	3 valves + fragments	1.26	0.708330	8.2
Khvarbeti	KH010	110	4 valves + fragments	1.22	0.708440	5.9
Khvarbeti	KH009	117.1	5 valves + fragments	1.18	0.708600	5.1
Khvarbeti	KH008	117.7	4 valves	1.18	0.708540	2.4
Khvarbeti	KH007	118	2 valves + fragments	1.18	0.708460	5.4
Khvarbeti	KH006	118.5	4 valves	1.18	0.708460	6.1
Khvarbeti	KH005	120	4 valves + fragments	1.17	0.708560	5.6
Khvarbeti	KH003	137	6 valves	1.08	0.708600	4.9
Khvarbeti	KH001	142	5 valves	1.06	0.708790	5.3

Appendix D

The content of this appendix belong to Chapter 6.

Model equations

The equations underlying the model for the different connectivity scenarios are presented here. Overview of the parameter, their description and values are presented in Table 4.1. The model is performed in a steady state, therefore volume remains constant.

Scenario A

In a steady state,

$$qBO = qOB + R_B + P_B - E_B \tag{D.1}$$

Sr concentration:

$$[Sr]_B = \frac{[Sr]_O * qOB + [Sr]_{RB} * R_B}{qOB + R_B} \tag{D.2}$$

Sr isotopic ratio:

$$\left(\frac{^{87}Sr}{^{86}Sr}\right)_B = \frac{\left(\frac{^{87}Sr}{^{86}Sr}\right)_O * [Sr]_O * qOB + \left(\frac{^{87}Sr}{^{86}Sr}\right)_{RB} * [Sr]_{RB} * R_B}{[Sr]_O * qOB + [Sr]_{RB} * R_B} \tag{D.3}$$

Salinity:

$$[S]_B = \frac{[S]_O * qOB}{qBO} \tag{D.4}$$

Scenario B

In a steady state,

$$E_B = R_B + P_B \tag{D.5}$$

Sr concentration:

$$[Sr]_{RB} = \frac{[Sr]_{Rb1} * Rb1 + [Sr]_{Rb2} * Rb2 + ... + [Sr]_{Rbn} * Rbn}{R_B} \tag{D.6}$$

Sr isotopic ratio:

$$\left(\frac{^{87}Sr}{^{86}Sr}\right)_{RB} = \frac{\left(\frac{^{87}Sr}{^{86}Sr}\right)_{Rb1} * [Sr]_{Rb1} * Rb1 + \left(\frac{^{87}Sr}{^{86}Sr}\right)_{Rb2} * [Sr]_{Rb2} * Rb2 + ... \\ ... + \left(\frac{^{87}Sr}{^{86}Sr}\right)_{Rbn} * [Sr]_{Rbn} * Rbn}{[Sr]_{RB} * R_B} \tag{D.7}$$

Salinity remains constant.

Scenario C

In a steady state,

$$E_B = R_B + P_B + qCB \tag{D.8}$$

Sr concentration:

$$[Sr]_B = \frac{[Sr]_C * qCB + [Sr]_{RB} * R_B}{qCB + R_B} \tag{D.9}$$

Sr isotopic ratio:

$$\left(\frac{^{87}Sr}{^{86}Sr}\right)_B = \frac{\left(\frac{^{87}Sr}{^{86}Sr}\right)_C * [Sr]_C * qCB + \left(\frac{^{87}Sr}{^{86}Sr}\right)_{RB} * [Sr]_{RB} * R_B}{[Sr]_C * qCB + [Sr]_{RB} * R_B} \tag{D.10}$$

Salinity remains constant.

Scenario D

In a steady state,

$$qBO = qOB + qCB + R_B + P_B - E_B \tag{D.11}$$

Sr concentration:

$$[Sr]_B = \frac{[Sr]_O * qOB + [Sr]_C * qCB + [Sr]_{RB} * R_B}{qOB + qCB + R_B} \tag{D.12}$$

Sr isotopic ratio:

$$\left(\frac{^{87}Sr}{^{86}Sr}\right)_B = \frac{\left(\frac{^{87}Sr}{^{86}Sr}\right)_O * [Sr]_O * qOB + \left(\frac{^{87}Sr}{^{86}Sr}\right)_C * [Sr]_C * qCB + \left(\frac{^{87}Sr}{^{86}Sr}\right)_{RB} * [Sr]_{RB} * R_B}{[Sr]_O * qOB + [Sr]_C * qCB + [Sr]_{RB} * R_B} \tag{D.13}$$

Salinity:

$$[S]_B = \frac{[S]_O * qOB + [S]_C * qCB}{qBO} \tag{D.14}$$

TABLE D.1: Core depth, age, Sr isotopic ratio with 2σ standard error and Dinocycts abundance for the DSDP 379A samples.

Core	**Sec**	**Top Depth (cm)**	**Bot Depth (cm)**	**Core Depth (m)**	**Age (ka)**	**Ost**	**Dino**	**$^{87}Sr/^{86}Sr$**	**Error (x10^{-6})**	***P. psilata* all variants**	**Low salinity dinos**	**All *Pyxidinopsis* TW**	***S. cruciformis***	***Spiniferites undiff.***	**Marine influence indicators**
4	1	127	129	27.27	28.72	2 frag	No analysis	0.708835	11.5						
4	5	86	88	32.87	34.60	None	No analysis								
6	1	3	5.5	45.54	47.94	2 + frag		0.708812	10.0	0.7511	0.0000	0.0000	0.2402	0.0000	0.0044
6	6	87.5	90	53.78	56.61	None	No analysis								
7	4	126	128.5	60.27	63.44	None	No analysis								
8	4	9	13	69.00	72.63	Few frag		0.708827	4.4	0.5975	0.0041	0.0041	0.2490	0.0539	0.0290
10	3	131	133	87.32	103.58	None	No analysis								
10	6	130	132.5	91.81	112.94	None	No analysis								
11	3	21	23.5	95.72	121.08	Few		0.709024	9.5	0.0755	0.0000	0.0000	0.0094	0.3491	0.5142
11	4	51.5	54	97.53	124.85	None	No analysis								
12	2	66.5	69	104.18	136.19	Some frag		0.709084	15.6	0.7837	0.0577	0.0048	0.0769	0.0433	0.0000
13	1	111	114	113.03	149.28	1+2 frag	No analysis	0.708820	6.4						
13	6	100	102.5	120.41	160.21	Abundunt		0.708834	26.5	0.2646	0.0493	0.0045	0.0179	0.0179	0.0045
14	6	131	133.5	129.03	172.97	Some frag		0.708581	6.1	0.3445	0.1092	0.0000	0.0840	0.1849	0.0168
16	4	65	68	145.17	196.84	None				0.6109	0.2840	0.0078	0.0000	0.0467	0.0000
16	4	135.5	138.5	145.87	197.89	None	No analysis								
17	1	15	17	149.66	203.50	3 frag		0.708582	33.1	0.0245	0.3333	0.0049	0.3676	0.1029	0.0098
18	2	43	45	160.94	220.19	None				0.1624	0.1181	0.0000	0.0849	0.4170	0.0000
19	2	27	29.5	170.28	234.01	None	No analysis								
19	4	129.5	133	174.31	239.98	None				0.0049	0.2087	0.0097	0.0340	0.0340	0.0049

Table D.1 continued

Core	**Sec**	**Top Depth (cm)**	**Bot Depth (cm)**	**Core Depth (m)**	**Age (ka)**	**Ost**	**Dino**	**$^{87}Sr/^{86}Sr$**	**Error (x10^{-6})**	***P. psilata* all variants**	**Low salinity dinos**	**All *Pyxidinopsis* TW**	***S. cruciformis***	***Spiniferites undiff.***	**Marine influence indicators**
19	6	5.5	8	176.06	242.57	None	No analysis								
20	3	90	92.5	181.91	251.22	None				0.6580	0.0433	0.0043	0.0952	0.0779	0.0346
21	6	20	23	195.56	271.43	3 + frag		0.708694	17.8	0.9591	0.0045	0.0136	0.0136	0.0000	0.0000
24	2	52.5	55	218.44	305.29	None	No analysis								
25	3	25.5	28	228.77	323.80	None	No analysis								
25	3	140	142.5	229.91	326.46	Some frag		0.708886	7.2	0.0137	0.0046	0.0000	0.0731	0.0457	0.7489
25	5	77.5	80	232.29	332.01	None	No analysis								
25	7	75.5	78	235.27	338.96	None	No analysis								
27	3	14	16.5	247.65	367.85	Some frag		0.708714	9.9	0.8152	0.0000	0.0000	0.0000	0.0000	0.0000
27	5	49	51.5	251.00	375.67	Some frag	No analysis	0.708845	37.6						
28	4	41	43	259.42	395.31					0.8093	0.0000	0.0000	0.1070	0.0605	0.0000
29	1	41	44	263.93	405.83	None				0.2357	0.0036	0.0000	0.1786	0.0571	0.0071
29	3	15	18	266.67	412.22	None				0.0369	0.0184	0.0046	0.6774	0.1797	0.0230
29	6	112	114.5	272.13	425.50	No analysis	None			0.0000	0.0000	0.0000	0.0000	1.0000	0.0000
30	2	1.5	5	274.53	431.69	None				0.0721	0.0337	0.0144	0.3990	0.2356	0.0481
31	1	71	73	283.22	454.09	Few frag	None	0.709044	7.5	0.0000	0.0769	0.0000	0.6923	0.0000	0.0769
31	5	125	129.5	289.77	470.98	Few frag	None			0.0000	0.0000	0.0000	0.3333	0.6667	0.0000
34	2	85	87	313.76	532.84	Some		0.708551	7.6	0.9420	0.0045	0.0000	0.0223	0.0089	0.0000
37	5	120.5	123	346.92	618.34	Abundunt		0.708609	6.5	0.8350	0.1359	0.0000	0.0000	0.0291	0.0000
38	6	116	119	358.03	646.98	Some	None	0.708937	10.1	0.0000	0.0000	0.0000	0.0000	0.0000	0.0000

Table D.1 continued

Core	**Sec**	**Top Depth (cm)**	**Bot Depth (cm)**	**Core Depth (m)**	**Age (ka)**	**Ost**	**Dino**	**$^{87}Sr/^{86}Sr$**	**Error (x10^{-6})**	***P. psilata* all variants**	**Low salinity dinos**	**All *Pyxidinopsis* TW**	***S. cruciformis***	***Spiniferites undiff.***	**Marine influence indicators**
40	2	111	113.5	370.82	679.97	Plenty	None	0.708673	6.7	0.1667	0.0000	0.0000	0.3333	0.1667	0.0000
43	1	61	64	387.95	724.13	Some	No analysis	0.708601	8.5						
43	5	7	10	393.40	738.20	Plenty	None	0.708587	9.1	0.6667	0.0000	0.0000	0.1667	0.0000	0.1667
45	4	100	104	411.52	785.49	None	No analysis								
46	4	30	32.5	420.31	811.49	Abundunt	No analysis	0.708570	6.1						
49	1	47.5	50	444.83	884.00	Plenty		0.708591	6.3	0.3382	0.0290	0.1981	0.2609	0.1353	0.0000
49	5	97	100	451.34	903.23	Abundunt	No analysis	0.708575	5.5						
51	4	137	140	469.24	956.17	Rare	No analysis	0.708369	7.6						
52	3	91	93.5	476.42	977.41	Few frag		0.708874	6.4	0.2816	0.1262	0.5291	0.0097	0.0388	0.0097
53	1	41	43.5	482.42	992.07	Few frag	No analysis	0.708439	9.0						
56	1	20	23.5	510.72	1039.61	Abundunt	No analysis	0.708475	5.8	0.8186	0.0233	0.0047	0.0093	0.0093	0.0000
56	1	20	23.5	510.72	1039.61	Abundunt	No analysis	0.708472	6.9						
58	4	72	76	534.74	1077.98	Some		0.708474	5.7	0.7251	0.0199	0.0279	0.0518	0.1275	0.0000
64	1	90	94	577.92	1132.50	Few frag		0.708709	6.1	0.8772	0.0044	0.0000	0.0526	0.0526	0.0000
67	2	86	89.5	607.87	1170.31	None	No analysis								
67	6	113.5	116	614.14	1177.97	Some frag		0.708381	6.3	0.6373	0.0539	0.0882	0.0196	0.1618	0.0000

Appendix E

The content of this appendix belong to Chapter 7.

Table E.1: Stratigraphic level, age and Sr isotopic ratio with 2σ standard error for the Hajiqabul section (N40.127033, E48.872699).

Sample ID	Strat. level (m)	Ostracod used	Age (Ma)	$^{87}Sr/^{86}Sr$	Error
DS 5.1	520.6	3 fragments	2.1	0.708293	5.2
DS 16.1	616	6 valves	2.1	0.708349	4.6
DS 18.1	647.6	4 valves	2.1	0.708510	4.6
DS 22.1	700	7 valves	2.0	0.708458	5.5
DS 25.1	740.4	7 valves	2.0	0.708264	6.0
DS 26.1	750	6 valves	2.0	0.708467	5.5
DS 41.1	955	3 valves +fragments	1.9	0.708720	4.8
DS 53.1	1120	8 valves	1.7	0.707730	5.0
DS 58.1	1180	6 valves	1.6	0.708487	4.3
DS 65.1	1245	6 valves	1.5	0.708693	4.4
DS 75.1	1335	7 valves	1.3	0.708662	5.1
DS 83.1	1415	2 valves + fragments	1.2	0.708624	5.7
DS 86.1	1439	Fragments	1.1	0.707801	13.8
DS 88.1	1465	8 valves	1.1	0.708387	4.3
DS 89.1	1490	8 valves	1.1	0.708456	4.3
DS 93.1	1564	7 valves	0.9	0.708486	4.7
DS 96.1	1590	7 valves	0.9	0.708396	4.6
DS 97.1	1701	7 valves	0.6	0.708438	4.3
DS 99.1	1714	7 valves	0.6	0.708251	5.7
DS 100.1	1719.7	7 valves	0.6	0.708353	4.5
DS 104.1	1741	7 valves	0.5	0.708549	4.4
DS 110.1	1770	7 valves	0.5	0.708654	4.9
DS 113.1	1842.5	7 valves	0.3	0.708268	4.8

Appendix F

The content of this appendix belong to Chapter 8.

Table F.1: Core depth, age and Sr isotopic ratio with 2σ standard error for the DSDP core 380A.

Site	**Hole**	**Core**	**Sec.**	**Top depth (cm)**	**Bot. depth (cm)**	**Core depth (m)**	**Age (Ma)**	**^{87}Sr/^{86}Sr**	**Error (x10^{-6}**
380	A	9	6	78.5	81	416.78	0.75	0.708569	8.70
380	A	34	3	136	140	640.86	between 1.8 and 4.2	0.708517	6.50
380	A	51	6	44	48	806.34	5.65	0.708584	7.32

TABLE F.2: Stratigraphic level, age and Sr isotopic ratio for the Zheleznyi Rog section (N45.115137, E36.760768).

Sample ID	**Strat. level (m)**	**Strat. level corresponding to Vasiliev et al., 2011**	**Age (Ma)**	**Ost species**	**$^{87}Sr/^{86}Sr$**	**Error (x10^{-6})**
ZR 281	1.6	137	5.85	*Caspiolla*	0.708572	11
ZR 288	3	134.5	5.83	*Caspiocypris alta*	0.708569	9
ZR 295	4.4	132.8	5.83	*Caspiocypris alta*	0.708563	8
ZR 300	5.4	132.5	5.82	*Caspiocypris alta*	0.708554	24
ZR 304	6.2	130.5	5.82	*Cyprideis torose*	0.708409	9
ZR 305.5	6.6	130.1	5.81	*Cyprideis torose*	0.708479	7
ZR 307	6.9	130.1	5.81	*Caspiocypris alta*	0.708585	9
ZR 311	7.7	129	5.81	*Caspiocypris alta*	0.708577	10
ZR 316	8.8	128	5.80	*Caspiocypris alta*	0.708593	7
ZR 321	9.9	127	5.80	*Caspiocypris alta*	0.708605	11
ZR 329	11.55	125	5.79	*Caspiocypris alta*	0.708586	8
ZR 330	11.8	124.5	5.79	*Caspiocypris alta*	0.708564	11

Appendix G

Table G1: Location of the water and modern sediment samples collected during this study. The list also include where the water or sediment samples were taken for other analysis; Sr: Sr isotopic ratio, DNA: Dinoflagellate phylogenetic, Ost: Ostracod micropaleontology, Paly: Palynology, Dino: Dinocysts, HM/MO: Heavy metal and microplastic. Samples for Sr isotopic analysis, Dinoflagellate phylogenetic, and Dinocysts are stored in School of Geographical Sciences, University of Bristol (PI: Prof. Rachel Flecker, ESR: Diksha Bista and Manuel Sala Perez), samples for ostracod micropaleontology are stored in the Department of Geology, University of Bucharest (PI: Prof. Marius Stoica, ESR: Lea Rausch), samples palynology are stored in Utrecht University (PI: Dr. Francesca Sangiorgi, ESR: Thomas M. Hoyle), samples for heavy metal and microplastic are stored in GiMaRIS (PI: Arjan Gittenberger, ESR: Anouk D'Hont). This table covers several pages and as such the header will not be repeated.

Station Name	River /Basin	Field ID	Collection Date	Sample depth (m)	Station Depth (m)	Lat [N]	long [E]	Temp	Sal (g/kg)	Water sample taken for		Sediment sample taken for				
										Sr	DNA	Sr	Ost	Paly	Dino	HM/MP
	Caspian	St. 001	27/04/16	0		40.29994	49.77321			Yes						
	Caspian	St. 002	30/04/16	0		40.78167	49.55417			Yes						
	Kura	St. 003	04/05/16	0		39.40502	49.36538			Yes						
	Kura	St. 004	05/05/16	0		40.12028	48.08528			Yes						
	Kura	St. 005	05/05/16	0		39.94694	48.34667			Yes						
	Dnieper	St. 007	14/05/16	0		46.68881	32.81876	18.2	0.31	Yes						
	Dnieper	St. 008	17/05/16	0		46.53733	32.53658			Yes						
	Dnieper	St. 009	16/05/16	0	4	46.54662	32.14368	17.5	0.5	Yes						
	Southern Bug	St. 010	17/05/16	0		46.74633	31.93933	19.7	3.2	Yes						
	Chorokhi	St. 011	01/10/16	0		41.60472	41.57611	14.2	0.12	Yes						
	Black Sea	St. 012	01/10/16	0		41.58222	41.56667	22.3	18.72	Yes						
	Chorokhi	St. 013	01/10/16	0		41.59	41.60194	15.2	0.07	Yes						
	Black Sea	St. 014	01/10/16	0		41.7725	41.75583	22.2	16.68	Yes						
	Natanebi	St. 015	01/10/16	0		41.91167	41.77833	16.5	0.05	Yes						
	Natanebi	St. 016	01/10/16	0		41.91222	41.76889	16.2	0.02	Yes						
	Enguri	St. 017	02/10/16	0		42.3932	41.56089	20.2	0.12	Yes						
	Black Sea	St. 018	03/10/16	0		42.08119	41.70482	21.7	18.68	Yes						Yes
	Paliastomi	St. 019	03/10/16	0		42.0929	41.70799	19.9	0.75	Yes	Yes					Yes
	Paliastomi	St. 020	03/10/16	0		42.12253	41.73241	19.1	1.39	Yes	Yes					Yes
	Pichori	St. 021	03/10/16	0		42.13711	41.75948	17.6	0.13	Yes						
	Black Sea	St. 022	04/10/16	0		42.12556	41.64944	21.7	17.16	Yes						
	Black Sea	St. 023	04/10/16	0		42.10861	41.67056	22.5	17.56	Yes						

Station Name	River /Basin	Field ID	Collection Date	Sample depth (m)	Station Depth (m)	Lat [N]	long [E]	Temp	Sal (g/kg)	Water sample taken for		Sediment sample taken for				
										Sr	DNA	Sr	Ost	Paly	Dino	HM/MP
	Black Sea	St. 024	04/10/16	0		42.0725	41.70722	22	17.62	Yes	Yes					
	Black Sea	St. 025	04/10/16	0		42.01722	41.75028	19.1	1.31	Yes						
	Black Sea	St. 026	04/10/16	0		42.03454	41.73816	22.7	17.62	Yes						
	Rioni Delta	St. 027	05/10/16	0		42.1975	41.66222	20.2	0.15	Yes						
	Supsa River	St. 028	05/10/16	0		42.02139	41.75333	19.3	0.77	Yes						
MN 167 CT03	Black Sea	St030 Surface	10/05/17	0	34	44.13043	28.77142	13	15.2	Yes	Yes	Yes	Yes		Yes	Yes
MN 167 CT03	Black Sea	St030 Bottom	10/05/17	34	34	44.13043	28.77142	8	18.13	Yes						
MN 167 PO01	Black Sea	St031 Surface	11/05/17	0	13	44.65598	29.04415	14.5	13.1	Yes	Yes	Yes	Yes		Yes	Yes
MN 167 PO01	Black Sea	St031 Bottom	11/05/17	13	13	44.65598	29.04415	11.5	16	Yes						
MN 167 PO02	Black Sea	St032 Surface	11/05/17	0	20	44.62003	29.10027	15	13	Yes	Yes	Yes	Yes		Yes	Yes
MN 167 PO02	Black Sea	St032 Bottom	11/05/17	20	20	44.62003	29.10027	9.8	17	Yes						

Station Name	River /Basin	Field ID	Collection Date	Sample depth (m)	Station Depth (m)	Lat [N]	long [E]	Temp	Sal (g/kg)	Water sample taken for		Sediment sample taken for				
										Sr	DNA	Sr	Ost	Paly	Dino	HM/MP
MN 167 PO04	Black Sea	St033 Surface	11/05/17	0	42.5	44.50848	29.34632	12.77	15.94	Yes		Yes	Yes			Yes
MN 167 PO04	Black Sea	St033 Bottom	11/05/17	42.5	42.5	44.50848	29.34632	6	18.5	Yes						
MN 167 SG01	Black Sea	St034 Surface	12/05/17	0	23.4	44.82365	29.65432	11.5	14.39	Yes	Yes	Yes	Yes		Yes	Yes
MN 167 SG01	Black Sea	St034 12m	12/05/17	12	23.4	44.82365	29.65432	6.47	18.22	Yes						
MN 167 SG01	Black Sea	St034 Bottom	12/05/17	23.4	23.4	44.82365	29.65432	6.32	18.36	Yes						
MN 167 SU01	Black Sea	St035 Surface	12/05/17	0	14.7	45.07112	29.7382	8.33	17.23	Yes	Yes	Yes	Yes		Yes	Yes
MN 167 SU01	Black Sea	St035 Bottom	12/05/17	14.7	14.7	45.07112	29.7382	6.95	17.6	Yes						
MN 167 SU03	Black Sea	St036 Surface	12/05/17	0	34.7	45.03992	30.04095	14.33	12.87	Yes	Yes	Yes	Yes		Yes	Yes

Station Name	River /Basin	Field ID	Collection Date	Sample depth (m)	Station Depth (m)	Lat [N]	long [E]	Temp	Sal (g/kg)	Water sample taken for		Sediment sample taken for				
										Sr	DNA	Sr	Ost	Paly	Dino	HM/MP
MN 167 SU03	Black Sea	St036 Bottom	12/05/17	34.7	34.7	45.03992	30.04095	5.9	18.29	Yes						
MN 167 SG04	Black Sea	St037 Surface	13/05/17	0	53.5	44.67305	29.81687	13.67	16.11	Yes	Yes	Yes	Yes		Yes	Yes
MN 167 SG04	Black Sea	St037 12m	13/05/17	12.5	53.5	44.67305	29.81687	13.7	16.17	Yes						
MN 167 SG04	Black Sea	St037 25m	13/05/17	24.7	53.5	44.67305	29.81687	7.81	18.11	Yes						
MN 167 SG04	Black Sea	St037 32m	13/05/17	32	53.5	44.67305	29.81687	6.12	18.28	Yes						
MN 167 SG04	Black Sea	St037 45m	13/05/17	45.5	53.5	44.67305	29.81687	6.45	18.4	Yes						
MN 167 SG04	Black Sea	St037 Bottom	13/05/17	53.5	53.5	44.67305	29.81687	6.48	18.4	Yes						
MN 167 SG05	Black Sea	St038 Surface	13/05/17	0	65.3	44.59153	30.1005	14.1	14.97	Yes	Yes	Yes	Yes		Yes	Yes
MN 167 SG05	Black Sea	St038 Bottom	13/05/17	65.3	65.3	44.59153	30.1005	6.4	18.41	Yes						

Station Name	River /Basin	Field ID	Collection Date	Sample depth (m)	Station Depth (m)	Lat [N]	long [E]	Temp	Sal (g/kg)	Water sample taken for		Sediment sample taken for				
										Sr	DNA	Sr	Ost	Paly	Dino	HM/MP
MN 167 SG14	Black Sea	St039 Surface	13/05/17	0	78	44.4674	30.31027	14.41	15.46	Yes	Yes	Yes	Yes		Yes	Yes
MN 167 SG14	Black Sea	St039 21m	13/05/17	21	78	44.4674	30.31027	7.59	17.63	Yes						
MN 167 SG14	Black Sea	St039 54m	13/05/17	54	78	44.4674	30.31027	6.75	18.45	Yes						
MN 167 SG14	Black Sea	St039 70m	13/05/17	70	78	44.4674	30.31027	7.69	18.78	Yes						
MN 167 SG14	Black Sea	St039 78m	13/05/17	78.1	78	44.4674	30.31027	7.73	18.79	Yes						
MN 167 EUXRO01	Black Sea	St040 Surface	13/05/17	0	80	44.70642	30.72617	13.22	17.24	Yes	Yes	Yes	Yes		Yes	Yes
MN 167 EUXRO01	Black Sea	St040 Bottom	13/05/17	80	80	44.70642	30.72617	7.81	18.76	Yes						
MN 167 SG06	Black Sea	St041 Surface	14/05/17	0	95.6	44.34152	30.52328	12.94	17.75	Yes	Yes	Yes	Yes		Yes	Yes
MN 167 SG06	Black Sea	St041 15m	14/05/17	15	95.6	44.34152	30.52328	12.08	18.14	Yes						
MN 167 SG06	Black Sea	St041 28m	14/05/17	28	95.6	44.34152	30.52328	8.42	18.22	Yes						

Station Name	River /Basin	Field ID	Collection Date	Sample depth (m)	Station Depth (m)	Lat [N]	long [E]	Temp	Sal (g/kg)	Water sample taken for		Sediment sample taken for				
										Sr	DNA	Sr	Ost	Paly	Dino	HM/MP
MN 167 SG06	Black Sea	St041 60m	14/05/17	60	95.6	44.34152	30.52328	7.32	18.53	Yes						
MN 167 SG06	Black Sea	St041 Bottom	14/05/17	95.6	95.6	44.34152	30.52328	8.24	19.11	Yes						
MN 167 EUXRO03	Black Sea	St042 Surface	14/05/17	0	74.2	43.97117	29.9535	14.01	16.21	Yes	Yes	Yes	Yes		Yes	Yes
MN 167 EUXRO03	Black Sea	St042 Bottom	14/05/17	74.2	74.2	43.97117	29.9535	7.71	18.71	Yes						
MN 167 CT06	Black Sea	St043 Surface	15/05/17	0	89.6	43.8526	30.05995	13.76	18.01	Yes	Yes	Yes	Yes		Yes	Yes
MN 167 CT06	Black Sea	St043 8m	15/05/17	8	89.6	43.8526	30.05995	13.12	16.69	Yes						
MN 167 CT06	Black Sea	St043 40m	15/05/17	40	89.6	43.8526	30.05995	8.86	18.35	Yes						
MN 167 CT06	Black Sea	St043 65m	15/05/17	64.5	89.6	43.8526	30.05995	8.09	18.4	Yes						
MN 167 CT06	Black Sea	St043 Bottom	15/05/17	89.6	89.6	43.8526	30.05995	7.7	18.65	Yes						

Station Name	River /Basin	Field ID	Collection Date	Sample depth (m)	Station Depth (m)	Lat [N]	long [E]	Temp	Sal (g/kg)	Water sample taken for		Sediment sample taken for				
										Sr	DNA	Sr	Ost	Paly	Dino	HM/MP
MN 167 MA03	Black Sea	St044 Surface	15/05/17	0	85.6	43.77132	29.8985	13.7?	17.5?	Yes	Yes	Yes	Yes		Yes	Yes
MN 167 MA03	Black Sea	St044 Bottom	15/05/17	85.6	85.6	43.77132	29.8985	7.9	18.7	Yes						
MN 167 CT05	Black Sea	St045 Surface	15/05/17	0	65.2	43.9771	29.51373	14.47	16.4	Yes	Yes	Yes	Yes		Yes	Yes
MN 167 CT05	Black Sea	St045 18m	15/05/17	18	65.2	43.9771	29.51373	9.44	17.67	Yes						
MN 167 CT05	Black Sea	St045 41m	15/05/17	41	65.2	43.9771	29.51373	7.53	18.48	Yes						
MN 167 CT05	Black Sea	St045 53m	15/05/17	53.4	65.2	43.9771	29.51373	6.65	18.46	Yes						
MN 167 CT05	Black Sea	St045 Bottom	15/05/17	65.2	65.2	43.9771	29.51373	6.67	18.46	Yes						
MN 167 MA04	Black Sea	St046 Surface	16/05/17	0	68.9	43.76843	29.40482	14.24	16.68	Yes	Yes	Yes	Yes		Yes	Yes
MN 167 MA04	Black Sea	St046 Bottom	16/05/17	68.9	68.9	43.76843	29.40482	7.82	18.76	Yes						

Station Name	River /Basin	Field ID	Collection Date	Sample depth (m)	Station Depth (m)	Lat [N]	long [E]	Temp	Sal (g/kg)	Water sample taken for		Sediment sample taken for				
										Sr	DNA	Sr	Ost	Paly	Dino	HM/MP
MN 167 MA08	Black Sea	St047 Surface	16/05/17	0	46.1	43.7728	28.73985	15.27	16.5	Yes	Yes	Yes	Yes		Yes	Yes
MN 167 MA08	Black Sea	St047 Bottom	16/05/17	46.1	46.1	43.7728	28.73985	8	18.67	Yes	Yes	Yes	Yes		Yes	Yes
MN 167 TZ17	Black Sea	St048 Surface	17/05/17	0	31.8	43.985	28.70167	15.87	16.46	Yes	Yes	Yes	Yes		Yes	Yes
MN 167 TZ17	Black Sea	St048 Bottom	17/05/17	31.8	31.8	43.985	28.70167	8.89	18.1	Yes						
MN 167 BG 506	Black Sea	St049 Surface	20/05/17	0	1280	42.49305	28.66172	15.47	18.47	Yes						
MN 167 BG 506	Black Sea	St049 500m	20/05/17	500	1280	42.49305	28.66172	8.88	22.03	Yes						
MN 167 BG 506	Black Sea	St049 1000m	20/05/17	1000	1280	42.49305	28.66172	8.96	22.28	Yes						
MN 167 BG 502	Black Sea	St050 Surface	21/05/17	0	45.6	42.5254	27.9772	15.21	17.7	Yes						
MN 167 BG 502	Black Sea	St050 Bottom	21/05/17	45.6	45.6	42.5254	27.9772	8.2	18.26	Yes						

Station Name	River /Basin	Field ID	Collection Date	Sample depth (m)	Station Depth (m)	Lat [N]	long [E]	Temp	Sal (g/kg)	Water sample taken for		Sediment sample taken for				
										Sr	DNA	Sr	Ost	Paly	Dino	HM/MP
MN 167 BG 303	Black Sea	St051 Surface	22/05/17	0	38.8	43.16688	28.31803	14.91	17.91	Yes						
MN 167 BG 303	Black Sea	St051 35m	22/05/17	35	38.8	43.16688	28.31803	8.79	18.36	Yes						
MN 167 BG 307	Black Sea	St052 Surface	22/05/17	0	1199.5	43.16897	28.98323			Yes						
MN 167 BG 307	Black Sea	St052 1000m	22/05/17	1000	1199.5	43.16897	28.98323			Yes						
MN 167 BG 203	Black Sea	St053 Surface	23/05/17	0	74.8	43.3675	28.81597	16.26	17.94	Yes						
MN 167 BG 203	Black Sea	St053 Bottom	23/05/17	74.8	74.8	43.3675	28.81597	7.8	18.58	Yes						
KZ St001	Caspian Sea	St054 Surface	16/06/17	0	8	44.56675	50.25877	21.6	4.5	Yes	Yes	Yes			Yes	Yes
KZ St001	Caspian Sea	St054 Bottom	16/06/17	8	8	44.56675	50.25877	21.6	4.6	Yes						
KZ St002	Caspian Sea	St055 Surface	16/06/17	0	10	44.62352	50.27237	21.7	4.6	Yes	Yes	Yes			Yes	Yes

Station Name	River /Basin	Field ID	Collection Date	Sample depth (m)	Station Depth (m)	Lat [N]	long [E]	Temp	Sal (g/kg)	Water sample taken for		Sediment sample taken for				
										Sr	DNA	Sr	Ost	Paly	Dino	HM/MP
KZ St002	Caspian Sea	St055 Bottom	16/06/17	8.5	10	44.62352	50.27237	18.9	5.2	Yes						
KZ St003	Caspian Sea	St056 Surface	16/06/17	0	12.4	44.67247	50.24539	22.2	4.5	Yes	Yes	Yes			Yes	Yes
KZ St003	Caspian Sea	St056 Bottom	16/06/17	8	12.5	44.67247	50.24539	20.7	5.04	Yes						
KZ St005	Caspian Sea	St057 Surface	16/06/17	0	8	44.72741	50.22056	22.3	3.8	Yes	Yes	Yes			Yes	Yes
KZ St005	Caspian Sea	St057 Bottom	16/06/17	7.3	8	44.72741	50.22056	22.1	5.1	Yes						
KZ St006	Caspian Sea	St058 Surface	16/06/17	0	8.7	44.70099	50.00237	22	3.9	Yes	Yes	Yes			Yes	Yes
KZ St006	Caspian Sea	St058 Bottom	16/06/17	8	8.7	44.70099	50.00237			Yes						
KZ St007	Caspian Sea	St059 Surface	16/06/17	0	19	44.50904	49.99442	21.9	4.3	Yes	Yes	Yes			Yes	Yes

Station Name	River /Basin	Field ID	Collection Date	Sample depth (m)	Station Depth (m)	Lat [N]	long [E]	Temp	Sal (g/kg)	Water sample taken for		Sediment sample taken for				
										Sr	DNA	Sr	Ost	Paly	Dino	HM/MP
KZ St007	Caspian Sea	St059 Bottom	16/06/17	19	19	44.50904	49.99442			Yes						
KZ St014	Caspian Sea	St060 Surface	17/06/17	0	20	43.79776	50.93914	17.24	11.1	Yes	Yes	Yes			Yes	
KZ St014	Caspian Sea	St060 Bottom	17/06/17	20	20	43.79776	50.93914			Yes						Yes
KZ St015	Caspian Sea	St061 Surface	17/06/17	0	31	43.8919	50.83564	18.02	10.9	Yes	Yes	Yes			Yes	
KZ St016	Caspian Sea	St062 Surface	17/06/17	0	25	44.13609	50.76331	17.23	11.2	Yes	Yes	Yes			Yes	Yes
KZ St016	Caspian Sea	St062 Bottom	17/06/17	20	25	44.13609	50.76331			Yes						
KZ St017	Caspian Sea	St063 Surface	17/06/17	0	20	44.2447	50.66578	16.8	11.3	Yes	Yes	Yes			Yes	Yes
KZ St018	Caspian Sea	St064 Surface	17/06/17	0	19	44.273	50.44154	15.2	8.9	Yes	Yes	Yes			Yes	Yes

Station Name	River /Basin	Field ID	Collection Date	Sample depth (m)	Station Depth (m)	Lat [N]	long [E]	Temp	Sal (g/kg)	Water sample taken for		Sediment sample taken for				
										Sr	DNA	Sr	Ost	Paly	Dino	HM/MP
KZ St018	Caspian Sea	St064 Bottom	17/06/17	19	19	44.273	50.44154			Yes						
KZ St019	Caspian Sea	St065 Surface	17/06/17	0	18.2	44.34685	50.18977	21.6	8.7	Yes	Yes	Yes			Yes	Yes
KZ St019	Caspian Sea	St065 Bottom	17/06/17	18	18.2	44.34685	50.18977			Yes						
KZ St021	Caspian Sea	St066 Surface	18/06/17	0	44.3	43.75634	50.75752	21.08	10.2	Yes	Yes	Yes			Yes	Yes
KZ St021	Caspian Sea	St066 Bottom	18/06/17	20	44.3	43.75634	50.75752			Yes						
KZ St022	Caspian Sea	St067 Surface	18/06/17	0	61.8	43.74141	50.67633	21.5	10.1	Yes	Yes	Yes			Yes	Yes
KZ St022	Caspian Sea	St067 20m	18/06/17	20	61.8	43.74141	50.67633			Yes						
KZ St023	Caspian Sea	St068 Surface	18/06/17	0	101	43.72398	50.57025	21.22	10.3	Yes	Yes	Yes			Yes	Yes
KZ St023	Caspian Sea	St068 20m	18/06/17	20	101	43.72398	50.57025			Yes						

Station Name	River /Basin	Field ID	Collection Date	Sample depth (m)	Station Depth (m)	Lat [N]	long [E]	Temp	Sal (g/kg)	Water sample taken for		Sediment sample taken for				
										Sr	DNA	Sr	Ost	Paly	Dino	HM/MP
KZ St024	Caspian Sea	St069 Surface	18/06/17	0	142	43.69947	50.46807	20.34	11.4	Yes	Yes	Yes			Yes	Yes
KZ St024	Caspian Sea	St069 20m	18/06/17	20	142	43.69947	50.46807			Yes						
KZ St025	Caspian Sea	St070 Surface	18/06/17	0	249	43.59659	50.2794	19.75	11.4	Yes	Yes	Yes			Yes	Yes
KZ St025	Caspian Sea	St070 20m	18/06/17	20	249	43.59659	50.2794			Yes						
KZ St026	Caspian Sea	St071 Surface	19/06/17	0	23.7	43.23659	51.25584	16.86	11.3	Yes	Yes	Yes			Yes	Yes
KZ St026	Caspian Sea	St071 Bottom	19/06/17	20	23.7	43.23659	51.25584			Yes						
KZ St027	Caspian Sea	St072 Surface	19/06/17	0	20.5	43.52945	51.17069	14.24	11.4	Yes	Yes	Yes			Yes	Yes
KZ St027	Caspian Sea	St072 Bottom	19/06/17	20	20.5	43.52945	51.17069			Yes						
KZ St028	Caspian Sea	St073 Surface	19/06/17	0	26.9	43.50589	51.08473	19.5	10.8	Yes	Yes	Yes			Yes	Yes

Station Name	River /Basin	Field ID	Collection Date	Sample depth (m)	Station Depth (m)	Lat [N]	long [E]	Temp	Sal (g/kg)	Water sample taken for		Sediment sample taken for				
										Sr	DNA	Sr	Ost	Paly	Dino	HM/MP
KZ St028	Caspian Sea	St073 20m	19/06/17	20	26.9	43.50589	51.08473			Yes						
KZ St029	Caspian Sea	St074 Surface	19/06/17	0	41.8	43.49924	51.01059	21.53	10.4	Yes	Yes	Yes			Yes	Yes
KZ St029	Caspian Sea	St074 20m	19/06/17	20	41.8	43.49924	51.01059			Yes						
KZ St030	Caspian Sea	St075 Surface	19/06/17	0	35.6	43.7827	50.77468	22.05	10.2	Yes	Yes	Yes			Yes	Yes
KZ St031	Caspian Sea	St076 Surface	20/06/17	0	14.4	43.7827	50.77468	21.86	9.1	Yes	Yes	Yes			Yes	Yes
KZ St031	Caspian Sea	St076 Bottom	20/06/17	14	14.4	44.61348	50.12604			Yes						
	Sea of Azov	St081	24/08/17	0		47.08833	39.24778	23.6		Yes						
	Don delta	St082	24/08/17	0		47.11028	39.31222	24.8		Yes						
103	Sea of Azov	St083		0						Yes						
106	Sea of Azov	St084		0						Yes						
	Don upstream	St085	26/08/17	0		47.1177	39.43064			Yes						

Station Name	River /Basin	Field ID	Collection Date	Sample depth (m)	Station Depth (m)	Lat [N]	long [E]	Temp	Sal (g/kg)	Water sample taken for		Sediment sample taken for				
										Sr	DNA	Sr	Ost	Paly	Dino	HM/MP
	Volga delat	St086A	29/08/17	0	1.3	45.59962	47.90989			Yes	Yes	Yes	Yes	Yes	Yes	Yes
	Volta delta	St086B	29/08/17	0	1.3	45.59962	47.90989			Yes	Yes	Yes	Yes	Yes	Yes	Yes
	Volga delat	St087A	29/08/17	0	1.1	45.68362	47.9031			Yes	Yes	Yes	Yes	Yes	Yes	Yes
	Volta delta	St087B	29/08/17	0	1.1	45.68362	47.9031			Yes	Yes	Yes	Yes	Yes	Yes	Yes
	Volga delat	St088A	29/08/17	0	1.3	45.74874	47.89408			Yes	Yes	Yes	Yes	Yes	Yes	Yes
	Volta delta	St088B	29/08/17	0	1.3	45.74874	47.89408			Yes	Yes	Yes	Yes	Yes	Yes	Yes
	Volga upstream	St089A	31/08/17	0	14.2	47.10806	47.3125	20.6		Yes				Yes		Yes
	Volga upstream	St089B	31/08/17	0	14.2	47.10806	47.3125	20.6		Yes				Yes		Yes
	Volga upstream	St090A	31/08/17	0	11	47.01861	47.4325	20.7		Yes				Yes		Yes
	Volga upstream	St090B	31/08/17	0	11	47.01861	47.4325	20.7		Yes				Yes		Yes
	Volga upstream	St091A	31/08/17	0	6.2	47.01889	47.44667	21.8		Yes						
	Volga upstream	St091B	31/08/17	0	6.2	47.01889	47.44667	21.8		Yes						

Station Name	River /Basin	Field ID	Collection Date	Sample depth (m)	Station Depth (m)	Lat [N]	long [E]	Temp	Sal (g/kg)	Water sample taken for		Sediment sample taken for				
										Sr	DNA	Sr	Ost	Paly	Dino	HM/MP
12	Don upstream	St092		0		47.22964 æ	40.0395			Yes						
15	Don upstream	St093		0		47.54776 æ	41.97201			Yes						
18		St094		0		48.4541	æ44.36181			Yes						
19	Volga upstream	St095		0		48.42905	44.94628			Yes						
20	Volga upstream	St096		0		48.06179 æ	46.12112			Yes						
23	Volga upstream	St097		0		49.5436	45.08047			Yes						
A1/A7?	Aral Sea	St005		12.5						Yes						
A2	Aral Sea	St002		0		45.08334	58.33631	25		Yes						
A3	Aral Sea	St002		5		45.08239	58.39014			Yes						
A4	Aral Sea	St002		10		45.08514	58.38756			Yes						
A6	Aral Sea	St002		20		45.08975	58.38261			Yes						
A9	Aral Sea	St002		33		45.08117	58.88314			Yes						
A28	Aral Sea	St005		18		45.10847	58.37219			Yes						
A43	Aral Sea	St008		12.5		45.07456	58.33446			Yes						
A45	Aral Sea	St008		18		45.07456	58.33446			Yes						
A46	Aral Sea	St009		5		45.09381	58.34044			Yes						
A46	Aral Sea	St010		7.5		45.09381	58.34044			Yes						
A47	Aral Sea	St010		12.5		45.08334	58.33631			Yes						
A49	Aral Sea	St010		2.5		45.08334	58.33631	27		Yes						

Station Name	River /Basin	Field ID	Collection Date	Sample depth (m)	Station Depth (m)	Lat [N]	long [E]	Temp	Sal (g/kg)	Water sample taken for		Sediment sample taken for				
										Sr	DNA	Sr	Ost	Paly	Dino	HM/MP
A53	Aral Sea	St013		5						Yes						
A553	Aral Sea	St016								Yes						
A59	Aral Sea	St020		10		45.10722	58.35983			Yes						
A61	Aral Sea	St022		5		45.10433	58.35492			Yes						
A62	Aral Sea	St023		5		45.09569	58.34628			Yes						
A63	Aral Sea	St024		5		45.09694	58.34881			Yes						
A64	Aral Sea	St025		5		45.09156	58.34144			Yes						
1	Aral Sea/Groundwater	Well 5-1-II				43.80611	58.76333			Yes						
2	Aral Sea/Groundwater	Well 804-2-II				43.925	58.68139			Yes						
3	Aral Sea/Groundwater	Well 807-1-II				43.90278	58.7025			Yes						
4	Aral Sea/Groundwater	Well 803-1-II				44.03361	58.62528			Yes						
5?	Aral Sea/Groundwater	Art - 1								Yes						
6	Aral Sea/Groundwater	Well 802-1-II				44.015	58.60694			Yes						

Station Name	River /Basin	Field ID	Collection Date	Sample depth (m)	Station Depth (m)	Lat [N]	long [E]	Temp	Sal (g/kg)	Water sample taken for		Sediment sample taken for				
										Sr	DNA	Sr	Ost	Paly	Dino	HM/MP
7	Aral Sea/Groundwater	Well 802-2-II				44.015	58.60694			Yes						
8	Aral Sea/Groundwater	Well 2-1-II				44.10056	58.65111			Yes						
9	Aral Sea/Groundwater	Well 1-1-II				44.15056	58.65917			Yes						
10	Aral Sea/Groundwater	Art - 2								Yes						
11	Aral Sea/Groundwater	Well 5-1-I				44.21472	58.49139			Yes						
18	Aral Sea/Groundwater	Well 3-1-III				44.01528	59.09139			Yes						
19	Aral Sea/Groundwater	Well 5-1-III				44.0325	59.09528			Yes						
23	Aral Sea/Groundwater	Well 2-1-III				43.90361	59.01861			Yes						

Station Name	River /Basin	Field ID	Collection Date	Sample depth (m)	Station Depth (m)	Lat [N]	long [E]	Temp	Sal (g/kg)	Water sample taken for		Sediment sample taken for				
										Sr	DNA	Sr	Ost	Paly	Dino	HM/MP
25	Aral Sea/Groundwater	Well 115-1				43.50417	58.98167			Yes						
26	Aral Sea/Groundwater	Well 115-2				43.50417	58.98167			Yes						
27	Aral Sea/Groundwater	Well 46-2				43.78472	59.02389			Yes						